Novel Applications of Mass Spectrometry to Organic Residues in Archaeology

Rachel Katherine Smith

PhD

University of York

Chemistry

September 2015

Abstract

Chemical analysis of archaeological artefacts is a well-established method for obtaining information on the artefacts and their use. In this thesis, the development and application of novel mass spectrometric methods to archaeological problems is presented.

Lipids, being the remains of foods cooked and stored in vessels, are one of the most common classes of molecule analysed, because unglazed vessels can preserve traces of lipids for thousands of years. Analysis is typically carried out by solvent extraction of the lipids followed by gas chromatography-mass spectrometry (GC-MS). However, this is time-consuming. For large ceramic assemblages, of which generally only a small proportion of extracts contain detectable levels of analytes, a medium-throughput screening technique to identify extracts for further analysis would be a great advantage. In addition, GC-based methods are not ideal for large heat-labile molecules such as intact triacylglycerides (TAGs). These molecules are the undegraded remains of the originally deposited fats and their detection is important because TAG distributions can be used to help identify animal species, and to differentiate between dairy and adipose fats. The first part of this thesis presents the development of a method for matrix-assisted laser desorption/ionisation (MALDI)-MS for archaeological lipid extracts, and its application to samples from two archaeological sites. The aim of this work was to develop a method that was better able to detect TAGs than GC-based methods, and that could be used to analyse many samples in a relatively short time.

The second part of this thesis presents the detection of opium alkaloids in a Cypriot base-ring juglet from the Late Bronze Age. Although these vessels have long been associated with opium due to their shape, which resembles an inverted poppy capsule, the work presented here is the first robust chemical demonstration of a link between these vessels and their purported use.

List of Contents

List of Figures

8

11

15

List of Tables

Acknowledgements

Firstly, I would like to thank my supervisors, Jane Thomas-Oates, Ed Bergström and Ol Craig for giving me the opportunity to carry out this PhD, and for supporting me throughout it. Special thanks go to Jane for her unfailing encouragement and enthusiasm (and for putting up with me talking too much!) and to Ed for all of the technical and practical advice. Thanks also to Rebecca Stacey for providing me with the opportunity to work at the British Museum, and for all of her additional support. I would like to thank the British Museum for allowing me to access some really exciting samples.

Thanks to everyone I have worked with at York, including Andy, Carwyn, Elena, Emily, Emma, Helen, James, Jo, Karl, Kirsty H, Kirsty S, Kyle, Lance, Lefkothea, Peter, Rachel, Salina and Tom from the JTO group. Particular mentions go to Emily for summer weekends spent working in the office during the thesis write-up period, to Rachel for being a fantastic summer project student, and to Andy and Salina for their support at the beginning of my PhD. In BioArCh, I would especially like to thank Matt for his technical help.

I must thank Toby for many lunches and for bravely volunteering to proof-read a chemistry thesis. I'm glad you now know what I've been doing for the past four years! I am also grateful to my friends Anne and Chris, for welcoming me as a spare member of their family and for always being there with wine when necessary!

Finally, love and thanks to my family, especially to my parents, without whose love, support and encouragement I would not have begun, let alone finished, my PhD.

These acknowledgements would not be complete without a mention of Phoebe, the best bear a human could ask for, who has been with me every step of the way.

Author's Declaration

I declare that the work presented in this thesis is my own, except where otherwise acknowledged, and that it has not been submitted previously for a degree at this or any other university.

Rachel Katherine Smith

1 INTRODUCTION: ORGANIC RESIDUE ANALYSIS IN ARCHAEOLOGY

1.1 INTRODUCTION

Molecular characterisation of archaeological artefacts and organic residues deposited on or in them is a crucial part of archaeological studies, since it is able to provide information about artefacts that cannot be gained simply by physical examination. Over the past 25 years there have been significant developments in the applications of analytical chemistry to the field of archaeology. This overview will present a history of the field, covering the techniques in use, the analytes detected and how the presence of these analytes can give us information about the past. The focus is primarily on the analysis of lipids in archaeological ceramics since lipid analysis is the main subject of this thesis. Knowledge of the preserved lipids can aid us in our understanding of the lives of people in the past, by giving us information about the commodities (particularly foods) to which they had access, and the way they processed these commodities.

Traditionally, pottery has been analysed by looking at the shape, style and decoration of the vessel to classify its use, by relating the form of the vessel to its function.[1] This technique has obvious limitations, especially since much excavated pottery is in fragmentary form and found as so-called *potsherds*. The realisation that unglazed ceramic can preserve traces, invisible to the eye, of the substances cooked or stored in the vessels over surprisingly long timescales, along with development of analytical instrumentation that is sensitive enough to analyse these residues, have revolutionised the field of archaeology. A review of the subject has recently been published in the journal *Mass Spectrometry Reviews*.[2]

1.2 CHROMATOGRAPHY

Chromatography is one of the primary methods in use in archaeological science, and so a description of its theory is included here.

Chromatography is a separation method, the use of which allows complex mixtures to be separated in order to allow the components to be detected without interference from other components.[3] The two main types of chromatography are gas

chromatography and liquid chromatography, which are used to separate mixtures of gas phase and liquid/solution phase analytes, respectively.[4]

The basic theory of chromatography is that the analyte mixture, carried by the *mobile phase*, travels through a column containing the *stationary phase*, which may be bound to the inside of the column or to the surface of particles of packing material in the column.[4] As the analyte mixture moves through the column it interacts with the stationary phase. The analytes are separated based on their relative affinities for the stationary and mobile phases, which can be represented by the equilibrium shown in Equation 1:[3]

$$A_{(mobile\ phase)} \rightleftharpoons A_{(stationary\ phase)} \qquad \text{Equation 1}$$
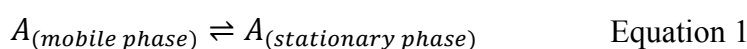
From this equilibrium, a partition coefficient, K, can be calculated (Equation 2):

$$K = \frac{[A_{(stationary\ phase)}]}{[A_{(mobile\ phase)}]} \qquad \text{Equation 2}$$

Analytes with a higher partition coefficient, K, interact strongly with the stationary phase and therefore spend more time in it because they have a higher affinity for it. From this it can be seen that analytes with different values for K will be separated by the column.

Both gas and liquid chromatographs can be coupled to mass spectrometers for analyte identification, but other detectors that allow detection without providing such specific information for identification are also used.

1.2.1   High Performance Liquid Chromatography

High performance liquid chromatography (HPLC) is a chromatographic method that allows separation of mixtures in solution. The analyte mixture solution is pumped through a column (usually 10 – 30 cm long and with an internal diameter of 2 – 5 mm)[3] packed with particles of a solid stationary phase, which is usually composed of small, spherical, porous particles made of silica.[4] The porosity of the particles gives them a very large surface area, which may be derivatised by covalently binding chemical groups onto the surface. The bound groups vary depending on the separation required – since different analytes have different affinities for different

chemical groups, a stationary phase which can effectively separate the analytes is chosen. The mobile phase in HPLC is a solvent, or a mixture of solvents. The composition of this solvent mixture may be varied throughout a chromatographic run to produce efficient separation of the analytes in an acceptable length of time.[3]

Normal phase HPLC (NP-HPLC) was the first type of HPLC to be developed.[3] In NP-HPLC the stationary phase is polar (e.g. underivatised silica) and the mobile phase is composed of organic solvents with a lower polarity than the stationary phase.

The more common type of HPLC now used is called reversed-phase HPLC (RP-HPLC).[3] As is indicated by the name, the polarities of the stationary and mobile phases in RP-HPLC are opposite to those in NP-HPLC. Therefore, in RP-HPLC, the stationary phase is non-polar (usually formed by derivatisation of the silica with hydrophobic alkyl chains, e.g. C_{18}) and the mobile phase is polar (usually a mixture of water with an organic solvent such as methanol).[4] This method separates analytes based on their interaction with the hydrophobic stationary phase. Therefore, they are separated based on their hydrophobicity, with more hydrophobic analytes being more strongly retained by the column than less hydrophobic ones, and thus eluting later. The proportion of organic solvent in the mobile phase is typically increased during the programme, making the mobile phase less polar and therefore increasing the partition of the more hydrophobic analytes into the mobile phase.

1.2.2   Gas Chromatography

In gas chromatography (GC) the mobile phase is a carrier gas, usually H_2 or He, in which the vaporised analytes are carried through the column.[4,5] For an analyte to be suitable for GC analysis it must have a high enough vapour pressure to allow it to be analysed in the gas phase.[4] Analytes are often derivatised before GC analysis to increase their volatility, making them more suitable for separation using this method.[4,6]

Most modern applications of GC use capillary GC, where the column is a tube of fused silica coated with polyimide (a plastic), typically 15 – 100 m in length and a few hundred μm in internal diameter.[4] These columns, more specifically known as wall-coated open tubular (WCOT) columns, have much narrower internal diameters

than the earlier packed columns used for GC.[3] The stationary phase is a liquid bonded to the inside of the column. Polyimide-coated fused silica has excellent properties for GC columns due to the inertness of the material and its flexibility and, therefore, durability.[7] The benefits of capillary columns over packed columns include better resolution and decreased analysis time, as well as lower limits of detection.[8]

The column is held inside an oven which is temperature programmable. At higher temperatures the vapour pressure of the analytes is increased, increasing their partition into the mobile phase and therefore causing them to elute earlier.[4] Usually a temperature programme, where the oven temperature increases throughout a chromatographic run, is employed. This allows early eluting analytes to be separated efficiently, whilst keeping the time of the analytical programme at an acceptable length (in the same way that mobile phase composition is modified in HPLC). Another reason for temperature control is that some analytes (those with relatively low vapour pressures) require high temperatures in order to elute from the column. Figure 1 shows a schematic of a gas chromatograph.
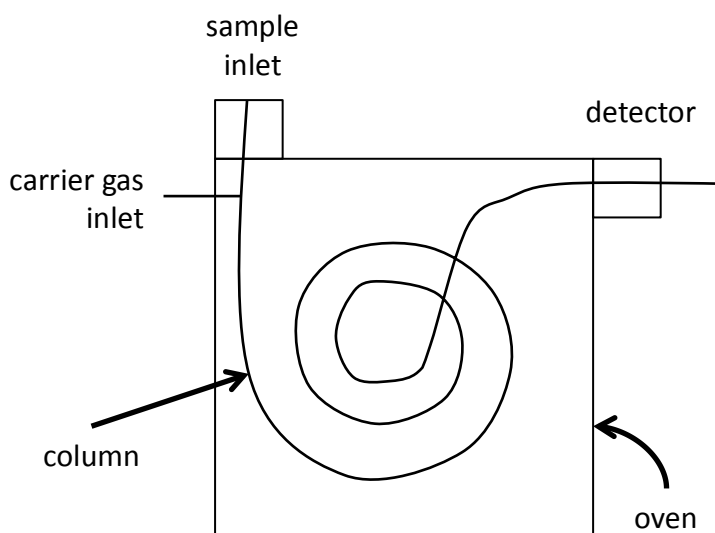
Figure 1. Schematic of a gas chromatograph.

There are various sample inlet methods for capillary GC, two of the most common being split/splitless injection and cool on-column injection (OCI).[9]

Split/splitless injection is typically used for samples that are relatively volatile.[4,9] The injector consists of a glass or quartz liner into which a liquid sample is injected. The injector is held at a high temperature, causing the sample to vaporise. A flow of carrier gas sweeps the vaporised analytes onto the column. Involatile components are not vaporised and so do not enter the column, and so split/splitless injection helps to protect the column. In splitless mode, the carrier gas flow is all directed onto the column. However, in split mode only a portion of it (typically 1%) goes to the column, with the rest going to waste. This allows control over how much of the sample enters the column, and is useful for samples with varying concentrations because the split ratio can be adjusted to allow more or less analyte onto the column. If the analyte has a low vapour pressure the processes that occur in split/splitless injection are inefficient and may result in the analyte not entering the column, as well as the heat causing the analyte to break down.[10] This can cause sample discrimination, particularly when a sample contains a range of analytes with widely varying boiling points.

In cool OCI, the analytes are injected directly onto the column, eliminating sample discrimination.[9] As the name suggests, the injector is not held at a high temperature, thus protecting thermally labile analytes.[4] The disadvantage of OCI is that involatile components of the mixture are also injected onto the column, which can reduce column performance over time.[9] This problem is overcome by the use of a retention gap.[4] This is a pre-column of de-activated fused silica inserted between the injector and column, which serves to protect the column.

GC is widely used in the analysis of lipids, including those extracted from archaeological ceramics, with lipid identification often carried out using mass spectrometry (GC-MS). Flame ionisation detection (FID) is used alongside mass spectrometry for lipid identification by comparison of retention times with standard compounds. This type of detector is particularly useful for quantitation, since it gives a signal that is proportional to the number of organic carbon atoms (excluding carbonyl and carboxyl carbons) in the molecules analysed.[4]

1.3 Lipids in Archaeological Artefacts

The analysis of lipid extracts of many thousands of potsherds have been reported in the literature, and they have been found to contain lipids from both animal and plant sources. These lipids come from foodstuffs and other commodities that the vessels have been used to cook or store.[11] Many of the residues are in the form of invisible absorbed deposits, but visible remains also exist. Some of these are charred food crusts on the surface of the potsherds.[12,13] However, not all are food-related. Examples of such residues include waterproof coatings[14] and the remains of substances burned as incense.[15,16] Lipids can also arise from the burial environment, with soil lipids deriving from animals and plants, as well as from fungi, bacteria and other living things in the soil.[17] Special care must therefore be taken to account for these lipids to avoid misinterpreting them as preserved archaeological lipids.
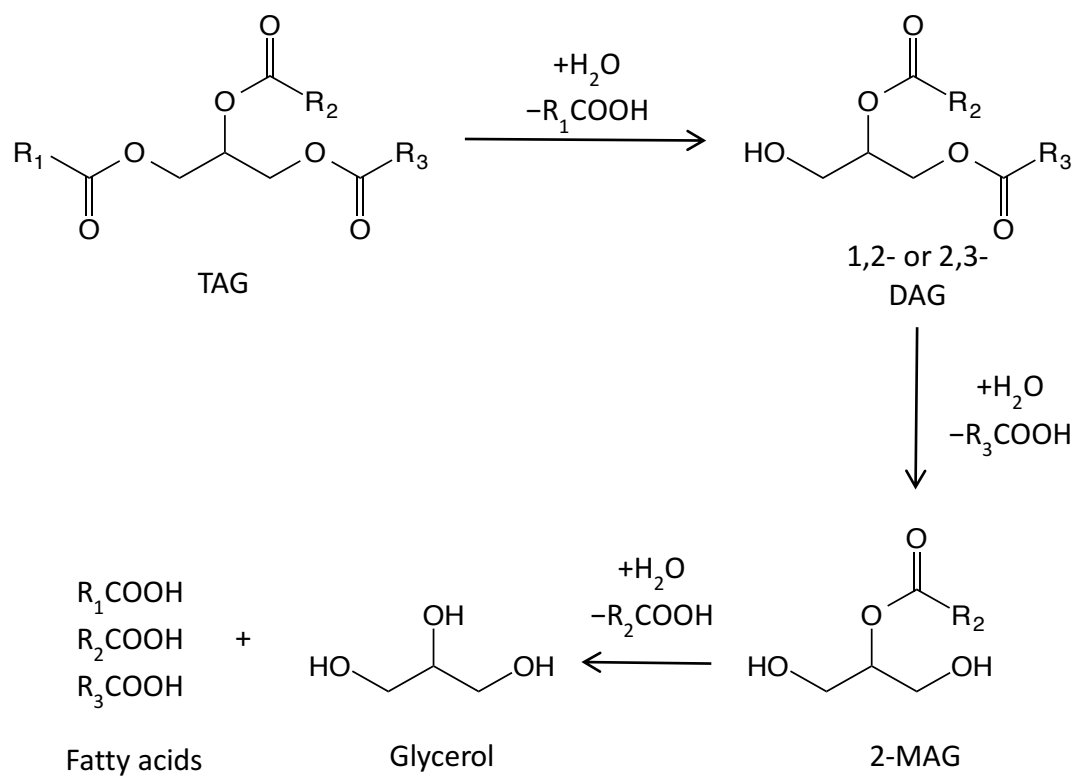
Figure 2. The hydrolytic breakdown of TAGs to DAGs, MAGs, fatty acids and glycerol.

Fresh animal and plant fats are predominantly composed of triacylglycerols (TAGs), formed from three fatty acid molecules esterified to a glycerol molecule, but they are usually highly degraded in archaeological artefacts.[18] TAGs degrade by the

successive hydrolysis of fatty acids from the glycerol backbone to give diacylglycerols (DAGs), monoacylglycerols (MAGs), free fatty acids (FAs) and glycerol, as shown in Figure 2. Fatty acids are usually lost from the 1- and 3- positions first, since this produces more stable DAGs and MAGs than if the 2- substituent was lost first.

The nomenclature used to describe acyl lipids is based on the number of carbon atoms and double bonds in the fatty acids.[19] Thus, $C_{16:0}$ denotes a fatty acid with 16 carbon atoms and zero double bonds. MAGs are designated by the letter M, DAGs by the letter D and TAGs by the letter T, with the number given in each of these cases corresponding to the total number of carbon atoms in the fatty acids, excluding the three in the glycerol moiety. This nomenclature does not indicate how the acyl carbons are distributed between the three fatty acids; for example, $T_{48:0}$ could be composed of three $C_{16:0}$ fatty acids, one each of $C_{14:0}$, $C_{16:0}$ and $C_{18:0}$, or other combinations. The position of double bonds is indicated by the Greek letters Δ (counting from the carboxyl carbon of the fatty acid) or ω (counting from the methyl end). The position of the fatty acids on the glycerol backbone is denoted by the term *sn*-. This is the stereospecific numbering system, in which *sn*-1 is used to denote the top carbon of the glycerol molecule, *sn*-2 the middle and *sn*-3 the bottom, when drawn as a Fischer projection with the glycerol carbons in a vertical line and the hydroxyl group on the middle carbon to the left, as shown in Figure 3.[20]

$$CH_2OP(O)(OH)_2$$
$$HO-C-H$$
$$CH_2OH$$
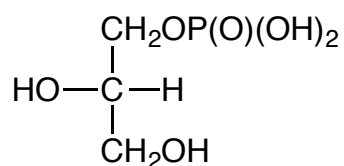
Figure 3. *sn*-Glycerol-1-phosphate, notated according to the stereospecific numbering system.

1.4   GAS CHROMATOGRAPHY FOR LIPID ANALYSIS IN ARCHAEOLOGY

The earliest use of GC for analysis of lipids extracted from archaeological ceramics was in 1976, by Condamin *et al*.[21] The samples used were Mediterranean amphorae whose ages were not stated, although it is implied that they are thousands of years old. The analysis involved saponification of lipids extracted from the ceramic and analysis of the resulting fatty acids, after methyl esterification to produce fatty acid

methyl esters, with comparison with the fatty acids found in pure modern olive oil. Whilst this was, at the time, the only way to analyse such lipids chromatographically, the saponification process degraded the lipid structures and resulted in loss of information relating to the presence and composition of intact complex lipids such as TAGs. Steps were taken to discount the presence of external contamination by analysing sections from the inside and outside surfaces of the vessels separately, as well as the sediment in contact with the potsherds. There was found to be much higher levels of lipid in the ceramic material from the inside surfaces than the outside and extremely low levels in the sediment, indicating that the absorbed residues were present in much greater concentrations than those due to contamination. Later work has shown that in most cases there are clear qualitative and quantitative differences between lipid extracts from potsherds and their associated soil.[22] This first analysis was carried out on lipids extracted from 100 g of potsherd powder, much more than is used in modern analyses, which typically involve extraction from only 1-2 g of ceramic.[2,22–25] This reduction in sample size required for modern analysis is due to the development of capillary GC columns.

It was several years after the publication of Condamin's paper when the next example of GC analysis of food residues in archaeological pottery was published. In 1985, Patrick *et al.* published an analysis of food residues adhering to the inside of potsherds (dated to less than 2000 years old) from the Southwestern Cape in South Africa (note that the analysed sample was a visible food residue rather than that absorbed into the ceramic material).[26] Lipids from the potsherds and from modern seal tissue were extracted and saponified to produce fatty acid methyl esters which were analysed by capillary GC. Based on the lipid composition, and especially on the ratio of $C_{18:1\omega9}$ (with the double bond in the ninth position from the methyl end of the fatty acid) to $C_{18:1\omega7}$, the authors concluded that the fat was of marine origin, perhaps seal, a conclusion which fits with the faunal remains at the site.[26]

Following these two early examples, it was not until the 1990s that the field of lipid analysis of archaeological ceramics by GC really took off. The breakthrough was in the application of high-temperature GC (HTGC), made possible because of advances in GC columns and injection techniques that had taken place in the late 1970s. Development of the silylation method for derivatisation of the columns to attach the

stationary phase allowed columns to be more inert and thermally stable,[27] enabling analysis at higher temperatures, and the on-column injection method was being recognised as more suitable for heat-labile and high boiling point samples.[28] This led to the ability to analyse TAGs directly from food items such as butter,[29,30] by using temperatures up to around 350 °C to enable elution of acyl lipids (MAGs, DAGs and TAGs). As well as the benefit of being able to gain information about intact lipid species, this method also reduced the sample preparation time since it meant that saponification became unnecessary.

Despite its wide use in food analysis from the late 1970s, the first report of HTGC for archaeological lipid samples was not until 1990.[23] This paper by Evershed *et al.* was a landmark study in archaeological science that precipitated a boom in the application of GC to archaeological lipids. For the first time, a range of lipids could be detected from a solvent extract of a potsherd, with the only sample pre-treatment required being derivatisation by trimethylsilylation of protic sites. The reduction in preparation time is particularly beneficial considering the large number of potsherds that are often recovered from archaeological sites. Since the first archaeological application of HTGC, it has become the standard technique for archaeological lipid analysis.

The initial work on the use of HTGC for archaeological lipids used on-column injection (OCI), and this sample introduction method is still considered optimum for the analysis of large biomolecules by HTGC.[31,24,32,33] The injection method is particularly important in the use of GC for TAGs because of their low volatility. In 1979 an evaluation of different injection methods for HTGC of TAGs was carried out, finding that cool OCI gave better results for TAGs than split or splitless injection.[34] Although it was found to be the best injection method, with OCI the response of the flame ionisation detector was lower than would be expected (calculated from comparison with the n-C_{15} alkane internal standard). However, split and splitless injection gave even lower responses, and higher standard deviation between injections, than OCI, with split injection giving the worst results of the three. Split injection also showed much more discrimination between TAGs of different mass than did on-column injection (i.e. the response factor decreased as TAG mass increased, and this happened to a much larger extent with split injection

than it did with OCI). In contrast to this work, a more recent study found that the injection method did not make a difference to the repeatability and accuracy of the results.[35] This seems odd since there are good reasons for why OCI should be a better injection method for TAGs than split/splitless injection. However, the TAGs analysed did only have a relatively small mass range, so the effects of analyte discrimination may have been less noticeable (a possibility that was noted by the authors). The authors also point out that although there did not seem to be a difference in analyte discrimination between sample introduction method, the results do not show that the recovery of TAGs from a sample is not affected. This point is important for the analysis of TAGs from archaeological artefacts since the absolute amounts of lipid retrieved are generally quite low, and therefore the selection of an injection method that maximises the amount of analyte put onto the column is important.

1.5 ARCHAEOLOGICAL BIOMARKERS

Since the 1990 work introducing the idea of using HTGC for the analysis of archaeological lipid samples, there has been much development in the basic principles of how and what lipid analysis can tell us about the lifestyles of past peoples. In 1993, Richard Evershed defined the concept of (lipid) archaeological biomarkers as compounds found in archaeological remains that, by comparison with compounds found in contemporary plants and animals, can provide information about past human activity.[36] Similar concepts existed in other fields such as organic geochemistry, but the archaeological biomarker concept is defined by the fact that it is concerned with the study of human activity. It has been noted that the concept can apply to any biological molecule (not just lipids),[11] though lipids are more resistant to decay than, for example carbohydrates, proteins and DNA,[37] and due to their hydrophobicity are less likely to leach away.[36]

1.5.1 Effect of Degradation

Before any discussion of specific biomarkers and what can be inferred from them, it is necessary to consider how the structures of the lipid components may be modified during use of the vessels and in the many years they have been deposited in the ground.

Despite the ability of ceramic material to preserve lipids over long periods of time, there is likely to be some level of lipid degradation. Application of the archaeological biomarker concept must therefore take into account the diagenetic processes (that is, the degradation that occurs over time, after the deposition of an object) that cause a change in lipid compositions preserved on the archaeological timescale, and so the interpretation of such residues must include knowledge of the degradative pathways of the compounds. Experiments carried out to determine the lipid capacity of modern replica potsherds, compared to the amount of lipid detected in archaeological samples, suggest that only 1 % of the initial lipid absorbed is preserved over the archaeological timescale.[18] Along with this reduction in preserved lipid, the composition also changes. For example, the degradation of TAGs tends to leave behind in the archaeological record primarily the saturated $C_{16:0}$ and $C_{18:0}$ fatty acids, since these are the primary fatty acids found in terrestrial animal fats, with unsaturated fatty acids not usually surviving in high concentrations, presumably due to oxidation at the double bond(s).[11] These hydroxy fatty acids are then either lost through leaching, due to their higher water solubility than their non-oxidised counterparts, or are covalently bound to the ceramic matrix and not extracted under solvent extraction conditions.[38] This change in composition means that, although there are differences in the lipid constituents of fresh fats from different organisms, on the archaeological timescale diagenesis makes these differences more difficult to distinguish. The degradation process is thought to occur by a mixture of biological and chemical actions,[18] and although the exact mechanisms of preservation are not fully understood, it is proposed that the absorption of lipid molecules into molecular-sized pores of the ceramic hinders microbial access to the lipids, reducing microbial degradation.[18,36]

Despite the degradation and loss of lipids over time, there are biomarkers that can be used to identify certain lipid sources, and these are outlined below.

1.5.2   Long-chain Ketones

GC analysis of lipid extracts from a selection of 9th – 13th century potsherds from Northamptonshire, UK showed that these samples contained relatively high levels of nonacosane (C_{29} alkane) as well as nonacosan-15-one and nonacosan-15-ol.[39] These compounds were known to be present in plant epicuticular leaf waxes, and analysis

of epicuticular leaf wax from cabbage (*Brassica oleracea*) revealed strikingly similar distributions to those in the potsherds.[39] Further work involving the cooking of cabbage in replica pots supported the idea that long-chain ketones absorb into the ceramic material,[40] and analysis of the $^{13}C/^{12}C$ ratios ($\delta^{13}C$ values) of the alkanes and ketones by GC-combustion-isotope ratio MS (discussed in section 1.6) produced good agreement between the potsherd extracts and leaf wax.[41]

$\delta^{13}C$ values are conserved within individual compounds, and are not affected by cooking or degradation since there is no exchange of carbon atoms in preserved compounds.[42] Different animal and plant species contain different ratios of ^{13}C and ^{12}C due to differences in biosynthesis and diet. Therefore, similar $\delta^{13}C$ values between an archaeological sample and a modern animal/plant extract can provide an indication of the source of the archaeological lipids. Since this was the case in the analysis of the long-chain ketones, the presence of these long-chain ketones in the potsherd extracts indicated that leafy vegetables had been cooked in the pots.[41]

Analysis of an early Bronze Age potsherd from Austria showed a series of ketones, from 29 to 35 carbon atoms long.[43] Based on the above evidence, the presence of these compounds could be taken to indicate leaf wax. However, $\delta^{13}C$ values of the C_{31}, C_{33} and C_{35} ketones showed values much closer to those of the $C_{16:0}$ and $C_{18:0}$ fatty acids found in the extracts, presumably from animal fats, than to those of leaf waxes, indicating that the ketones were from the same source as the fatty acids. Experiments involving heating TAGs and fatty acids in the presence of fired clay, to simulate cooking in the archaeological vessels, resulted in the formation of long-chain ketones.[43] The $\delta^{13}C$ values taken in conjunction with the experimental heating led to the conclusion that the longer-chain ketones in the archaeological vessels were formed by a decarboxylation and dehydration reaction between two fatty acids (Figure 4) rather than being preserved epicuticular leaf wax lipids.[43] This illustrates the care that must be taken when interpreting data from archaeological samples, because processing by the original users of the archaeological vessels, and degradation during burial, can have a significant effect on the structures of the preserved compounds.

$C_{16:0}$ fatty acid

$-CO_2$
$-H_2O$

$C_{18:0}$ fatty acid

$C_{33:0}$ ketone
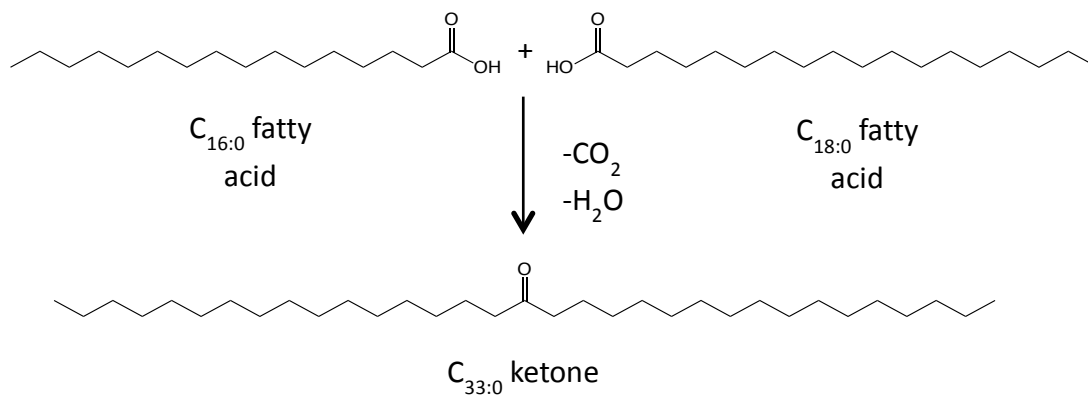
Figure 4. Reaction of two fatty acids to form a ketone. Redrawn from Evershed *et al.*[43]

1.5.3 ω-(o-Alkylphenyl)alkanoic Acids

In some cases animal and plant sources can be identified based on the presence of certain functional groups indicating the position of double bonds. The presence of C_{16}, C_{18} and C_{20} ω-(o-alkylphenyl)alkanoic acids has been used as evidence of the processing of marine products in pottery.[44–46] Marine animals contain the isoprenoid compounds 3,7,11,15-tetramethylhexadecanoic acid (phytanic acid), 4,8,12-trimethyltridecanoic acid (4,8,12-TMTD) and 2,6,10,14-tetramethylpentadecanoic acid (pristanic acid)[47] (Figure 5) and polyunsaturated fatty acids up to C_{22}.[48]

Phytanic acid

4,8,12-TMTD

Pristanic acid
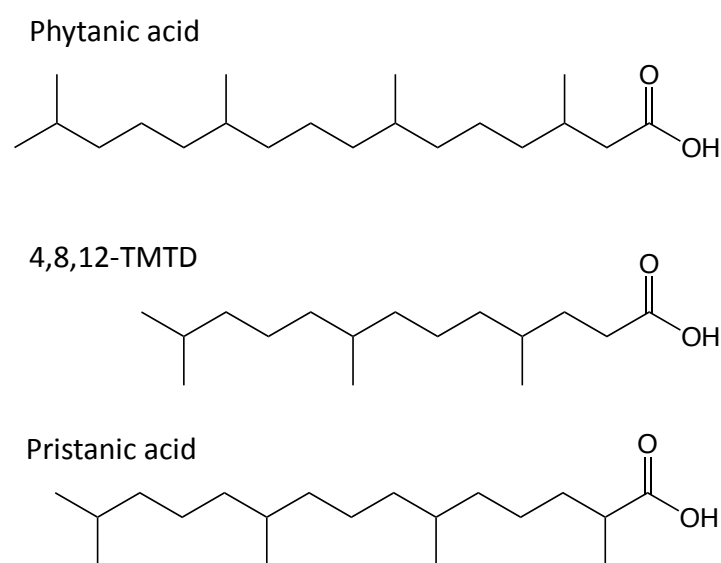
Figure 5. Some isoprenoid compounds found in marine animal fats.

On heating, triunsaturated fatty acids can undergo cyclisation, *via* an intra-molecular Diels-Alder reaction, and aromatisation to produce stable ω-(o-alkylphenyl)alkanoic acids,[49] as shown in Figure 6,[44] and experimental work has shown that this does indeed happen in ceramics at temperatures above 270 °C.[50] It is thought to be catalysed by metal ions in the ceramic, and when there are relatively low levels of oxygen (resulting in limited oxidative degradation). This indicates that the formation of the cyclic compounds happens once the fatty acids have been absorbed into the ceramic. However, the experimental work has also demonstrated that, with protracted heating (such as would occur with multiple uses of a pot), ω-(o-alkylphenyl)alkanoic acids can also form from mono- and di-unsaturated fatty acids (though not from saturated fatty acids). Taking this into account, it was concluded that ω-(o-alkylphenyl)alkanoic acids can be used to unambiguously

demonstrate the presence of marine fats, but only if C_{18} and C_{20} ω-(o-alkylphenyl)alkanoic acids (preferably with trace amounts of C_{22} as well) are present along with at least one of the isoprenoid fatty acids.[50]
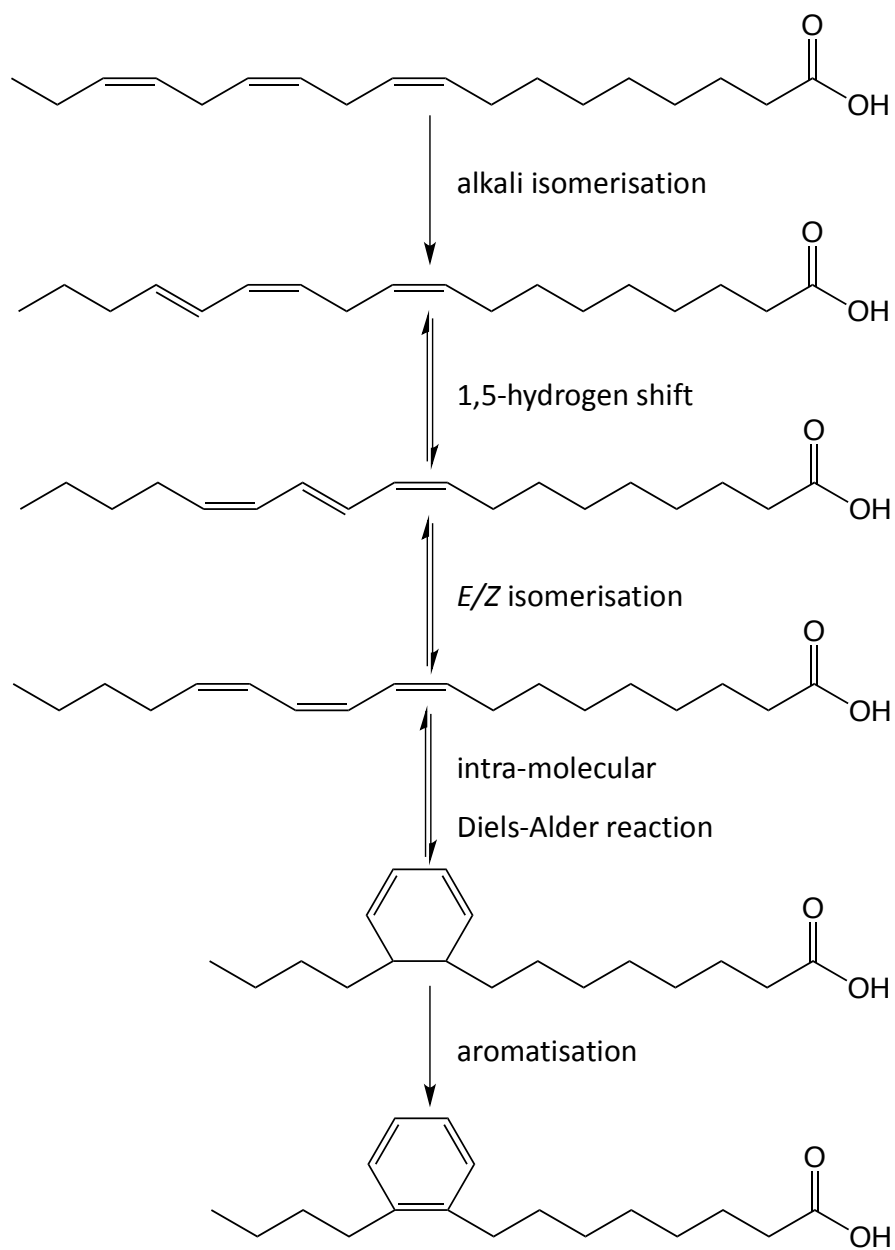
Figure 6. Formation of an ω-(o-alkylphenyl)alkanoic acid from a triunsaturated fatty acid. Other isomers can be formed when different hydrogen shifts occur. Redrawn (simplified) from Hansel et al.[44]

1.5.4 Steroids

Steroids can also be used to help differentiate between animal and plant sources of lipids, and are again detected using HTGC. Cholesterol is the most abundant sterol in animals, with campesterol and sitosterol being the two major sterols in plants (Figure 7).[36] These compounds are detected in archaeological lipid extracts and their presence is used to indicate a general animal and/or plant source for the lipids.[33,51] However, cholesterol has also been found at elevated levels in areas that have been subjected to manuring and therefore care must be taken to exclude contamination from the sediment surrounding the deposited potsherds as being the source of the steroids.[52,53] Cholesterol is found in human skin, so its presence in archaeological samples could be as a result of contamination from handling.[36] However, the hydrocarbon squalene is also found in human skin, at concentrations higher than those of cholesterol, so the presence of cholesterol in archaeological samples is generally not considered to be due to post-excavational handling unless squalene is also present.[36]
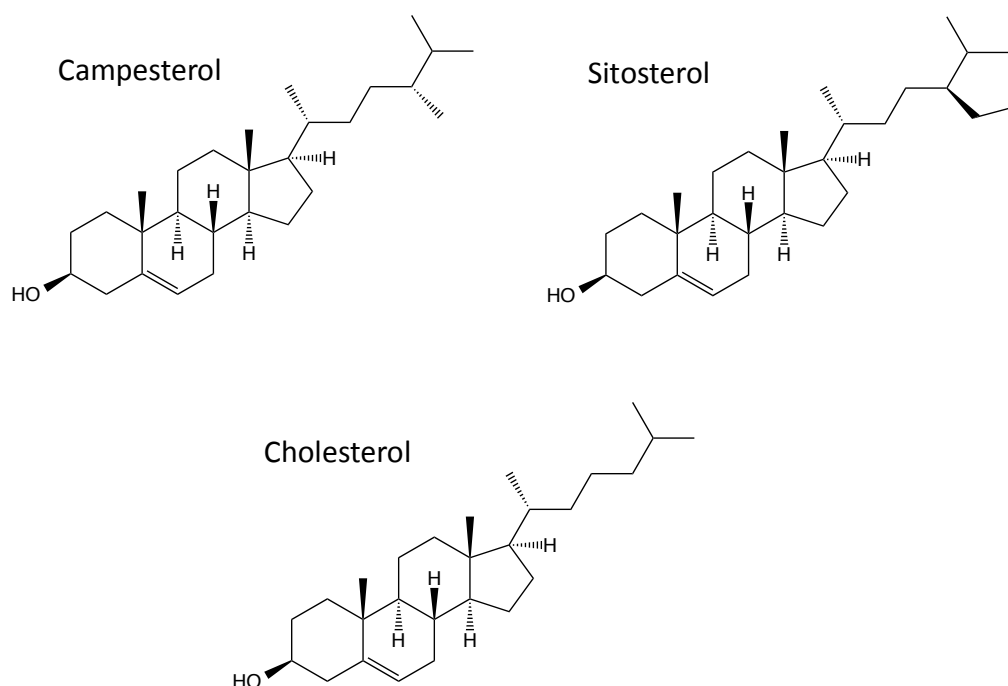
Figure 7. Structures of some steroids found in animals and plants.

1.5.5 Terpenoids

Resins and tars contain distinctive terpenoid components, and the presence of these and their diagenesis products, usually in the form of their cyclic skeletons, can be diagnostic of particular plant sources. Since resins and tars form watertight seals, they were often used to line or seal vessels. Therefore, their archaeological remains usually come in the form of visible residues in ceramics (in contrast to food residues which often only survive as absorbed, invisible residues), and their chemical components have been detected in archaeological samples using GC-MS. Coniferous resins can be recognised through the presence of tricyclic diterpenoid backbones, with the main diagenetic product being retene (Figure 8).[14,54] Birch bark tar is recognised from the presence of triterpenoids based on betulin (including lupeol and lupenone[55,56,16]) and pistacia resin is recognised from triterpenoids based on oleanoic acid (both shown in Figure 8).[56,15]

Retene   Betulin

Oleanoic acid
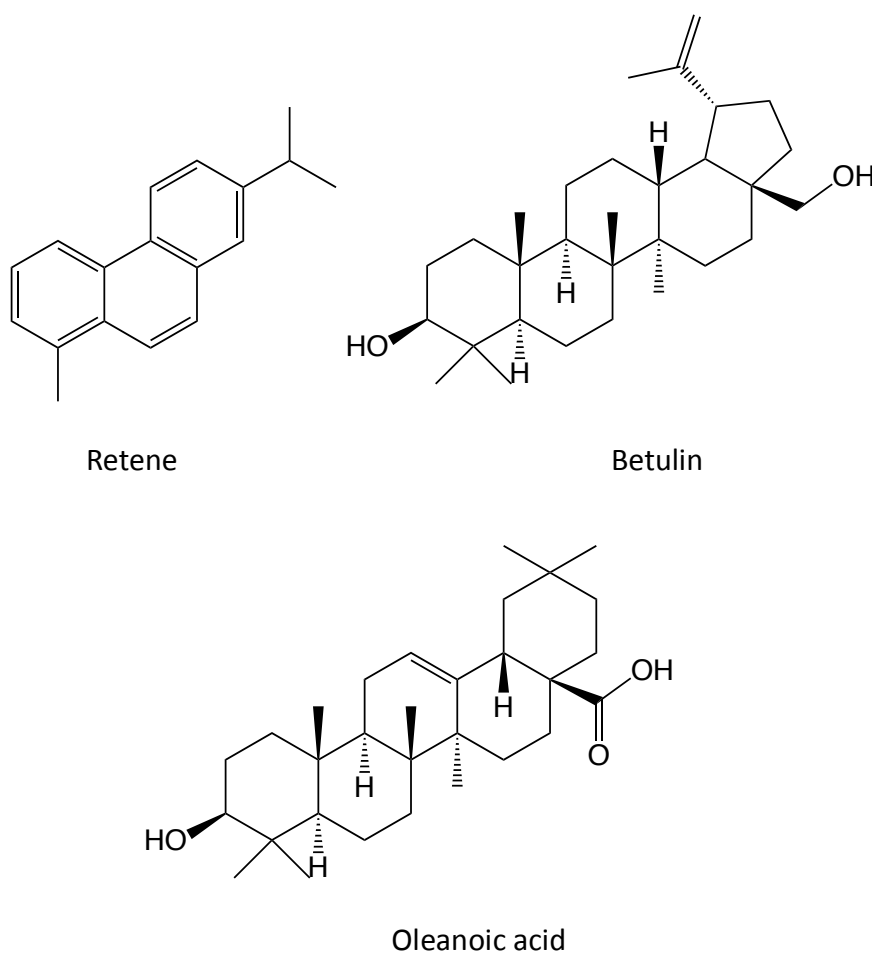
Figure 8. Structures of terpenoids found in resins and tars.

The presence of diterpenoid compounds in pitch found on Henry VIII's excavated flagship the *Mary Rose* (found in barrels and used as a waterproofing agent on the ship) has indicated a pine origin for the pitch.[14] Triterpenoids indicative of birch bark tar have been found in vessels known as *coupes-à-socles*, from Neolithic France.[16] These particular examples were excavated at a funerary site, and the triterpenoid structures showed evidence of degradation by combustion. These two pieces of evidence, together with the fact that these vessels are comparatively rare at domestic sites, has been taken to indicate that the vessels may have been used for the burning of birch bark tar as a type of incense.

1.5.6   Wax Esters

Beeswax can be detected through the presence of wax esters. It is composed of odd carbon-numbered alkanes (primarily $C_{25} - C_{33}$), free fatty acids (primarily $C_{24} - C_{34}$), monoesters ($C_{38} - C_{52}$, formed from C_{16} fatty acids esterified to alcohols of various chain lengths), diesters ($C_{56} - C_{66}$), hydroxymonoesters ($C_{40} - C_{50}$) and acid monoesters ($C_{32} - C_{44}$) (Figure 9).[57–59]
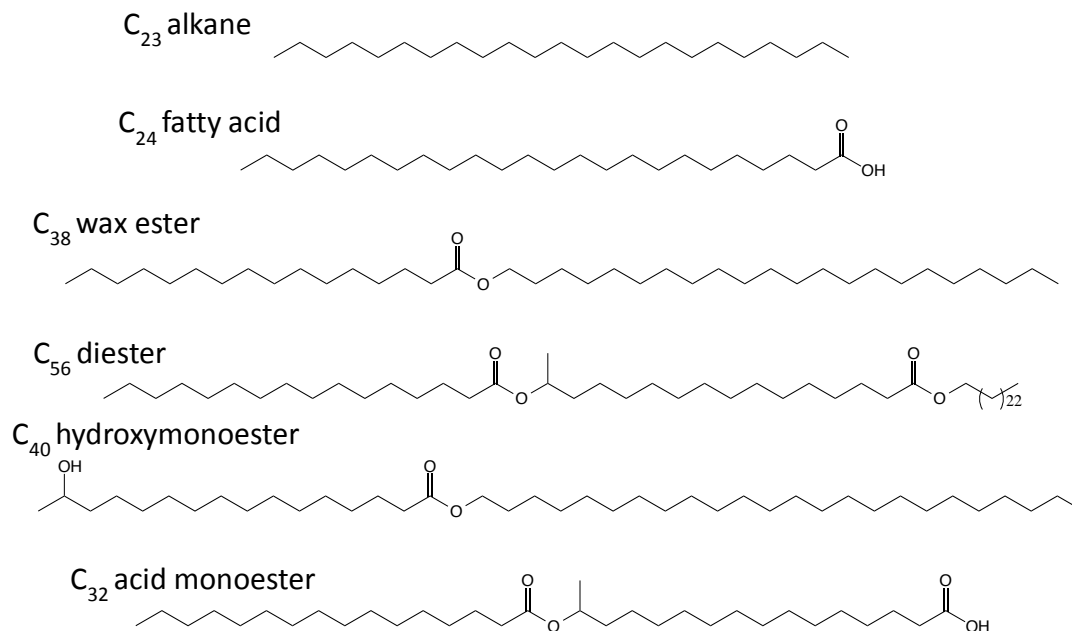
Figure 9. Components of beeswax. Drawn from information in Tulloch.[57]

Analysis of a Neolithic residue by HTGC(-MS) showed the presence of esters with a similar distribution to those in authentic beeswax, though the series of alkanes observed in the beeswax was present in only very low abundance in the Neolithic

sample.[59] However, the Neolithic sample was discoloured, indicating that it may have been heated or burned, and experiments showed that burnt beeswax had a similar physical appearance to the archaeological sample, with loss of alkanes when compared to unheated beeswax.[59] The presence of wax esters, odd carbon-numbered alkanes and long-chain even carbon-numbered fatty acids ($C_{22} - C_{34}$) in Roman medicine containers have been used to indicate the presence of beeswax.[60]

The presence of beeswax compounds has been used to provide chemical evidence to support a theory about the use of a type of vessel, based on their shape. So-called *combed ware* vessels are postulated to have been beehives due to their size, shape and because of grooves on their inside surfaces which are thought to have provided a surface for honeycombs to cling to. GC analysis of lipid extracts from combed ware potsherds has revealed the presence of a range of wax esters and hydroxymonoesters (both containing C_{16} fatty acids esterified to alcohols of different chain lengths) and odd carbon-numbered alkanes, as well as a series of even carbon-numbered alcohols.[61] These compounds indicate that beeswax was present in the vessels, and so their putative use seems likely to be correct. The distribution of free alcohols closely mirrors the distribution of the alcohols esterified to C_{16} fatty acids in the wax esters, indicating that these alcohols are formed on hydrolysis of the wax esters and hydroxy wax esters. Analysis of 100-year-old beeswax from a 19th century beehive in Crete[61] showed a very similar lipid distribution to authentic modern beeswax,[62] indicating that its composition is stable at least over that timescale.

1.5.7   Acyl Lipids

Although TAGs are the primary components of fresh animal fats, they degrade by the loss of fatty acids, and in most cases this means that archaeological lipid profiles are dominated by fatty acids, with small amounts of MAGs, DAGs and TAGs detectable.[18] The main fatty acid components of animal fat TAGs are $C_{16:0}$, $C_{18:0}$ and $C_{18:1}$, whereas plant oils tend to have higher proportions of unsaturated fatty acids such as $C_{18:1}$ and $C_{18:2}$.[63]

Experimental work has been carried out to try to understand the degradation processes. Experiments involving dosing potsherds with lipid followed by burial in mushroom compost at elevated temperatures of 30 °C to increase the rate of

degradation have shown that TAGs degrade to simpler lipid components and the total amount of lipid preserved in the potsherds decreases rapidly relative to unburied controls.[64] After only 10 days of burial under these conditions, the amount of intact TAG present had decreased by more than 95%, with the majority of that degradation occurring during the first five days. Complete hydrolysis of TAGs to fatty acids appears to proceed fairly rapidly after cleavage of the first fatty acid, with MAGs and DAGs not being detected in great concentrations at any point in the experiment. An important observation was that shorter fatty acids appear to hydrolyse more quickly than longer chains. Lighter TAGs ($T_{26} - T_{44}$) originally comprised 66 % of the total TAG content in potsherds which had been dosed with milk, but after 25 days of burial this had reduced to only 34 %. This has implications for the detection of milk products, since milk is characterised by the presence of short chain fatty acids ($C_4 - C_{14}$).[65] It has been suggested that the higher rate of hydrolysis of short chain fatty acids relative to longer chains is due to lower steric hindrance at the ester linkages of short chain fatty acyl moieties.[31] Coupled with this, once released as free fatty acids, the short chain homologues are more water-soluble than their longer chain counterparts and so are more likely to be leached away.

Despite the prevalence of $C_{16:0}$ and $C_{18:0}$ fatty acids in archaeological residues making the presence of these fatty acids relatively undiagnostic, there are some fatty acids found at low levels that can be used as indicators of specific animal fats. The presence of branched-chain fatty acids and odd carbon-numbered straight-chain fatty acids (specifically $C_{15:0}$, $C_{17:0}$ and $C_{19:0}$) has been taken as evidence of ruminant animal fat,[66] since these compounds are found at relatively high concentrations in ruminants due to their production by rumen bacteria.[67] The two primary branched fatty acids have methyl substitutions on the second from last (*iso-*) or third from last (*anteiso-*) carbon, counting from the carboxylic acid group end (Figure 10). The detection of a range of positional isomers in the $C_{18:1}$ fatty acid, with the double bond in the 9, 11, 13, 14, 15 or 16-position, has also been used to indicate ruminant fat, whilst monogastric animals have only one positional isomer.[66,67] The ratio of the $C_{17:0}$ branched fatty acid to the $C_{18:0}$ fatty acid has also been used to indicate a difference between ruminant dairy fats and ruminant/non-ruminant adipose fats, with dairy fats having a higher $C_{17:0}$:$C_{18:0}$ ratio.[68]

iso-C$_{17:0}$ branched fatty acid

anteiso-C$_{17:0}$ branched fatty acid
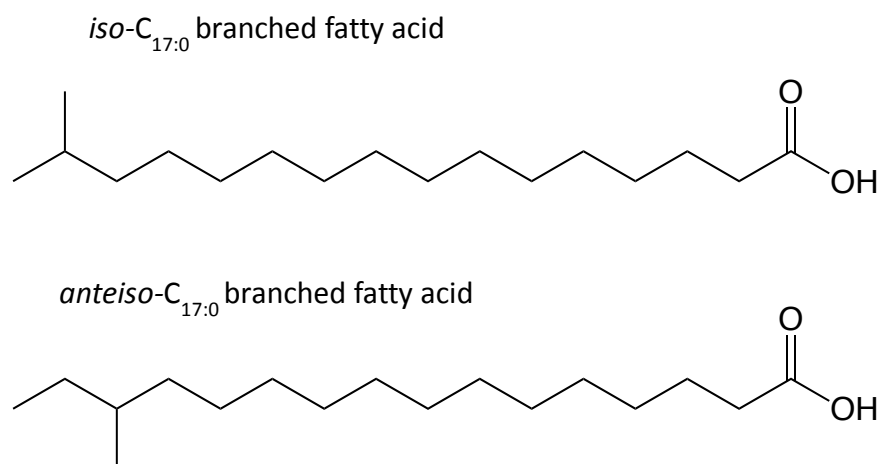
Figure 10. Structures of some branched fatty acids, which are characteristic of ruminant fats.

Despite the problems of diagenesis, variations in TAG distributions have been used to link lipids to different animal sources. A relatively broad TAG distribution ($T_{40} - T_{54}$) has been linked to ruminant fats, with the lightest TAGs ($T_{42} - T_{46}$) specifically indicating dairy fats,[65,68] and a narrower distribution ($T_{44} - T_{54}$), with low abundances of T_{44} and T_{46}, characterising non-ruminant adipose fats.[68] Vessels shown by GC-combustion-isotope ratio MS (discussed in section 1.6) that have been used for the processing of milk do show distributions of TAGs down to T_{42} and, in some cases, T_{40}.[65,69] These diagnostic TAG ranges obviously overlap, and therefore care must be taken when interpreting them, as factors such as conditions at one site compared to another can alter the degree of preservation of the lipids and have implications for interpretation. The possibility of mixing of different products within one pot, which is especially likely when a vessel has been re-used, must also be taken into account. For example, the cooking of ruminant fats could mask the fact that non-ruminants had also been processed in a vessel, since the TAG range used to assign ruminant fat is wider than that for non-ruminant fats.[68]

In order to overcome difficulties with identifying ruminants and non-ruminants, an alternative analytical method, gas chromatography-combustion-isotope ratio mass spectrometry, has been developed.

1.6 GAS CHROMATOGRAPHY-COMBUSTION-ISOTOPE RATIO MASS SPECTROMETRY (GC-C-IRMS)

Clearly, due to the changes in lipid distributions that occur due to diagenesis, the archaeological biomarker approach cannot reliably distinguish all sources of lipids. GC-c-IRMS has been used to help overcome this problem, and is now used extensively for the differentiation of ruminants and non-ruminants, and of ruminant adipose and milk fat, due to differences in the ratio of carbon isotopes present in the lipids of different origins.[65,42]

Different animals incorporate different ratios of ^{13}C and ^{12}C into their fatty acids due to differences in diet and metabolism. Metabolism is important because of the way animals incorporate dietary fatty acids. $C_{16:0}$ and $C_{18:0}$ fatty acids are absorbed from the diet as well as synthesised in animal tissues from dietary carbohydrate, with ruminants using different carbon sources to those used by monogastric animals.[70] In addition, the lactating ruminant mammary gland cannot produce the $C_{18:0}$ fatty acid, so this is exclusively absorbed from the diet.[71] Plant fatty acids contain lower levels of ^{13}C than do plant carbohydrates,[72] and these different sources of fatty acid carbon produce measurable differences in $^{13}C/^{12}C$ isotope ratios ($\delta^{13}C$ values) in monogastrics and ruminants, and in ruminant milk fat compared with ruminant adipose fat. Marine sources of fats can be distinguished because they have a higher abundance of ^{13}C than terrestrial sources.[73] This can also be seen in the fats of animals that have consumed marine diets.

GC-c-IRMS involves release and separation of the fatty acids, as methyl esters, followed by complete combustion to CO_2 and H_2O and analysis by MS to determine the $\delta^{13}C$ values.[74] This helps to overcome the problems of diagenesis affecting the structures of the lipids present in the samples, since isotope ratios within particular compounds are preserved throughout the degradation process.[42] Plotting the $\delta^{13}C$ values of the $C_{16:0}$ fatty acids against those of the $C_{18:0}$ fatty acids of various modern animals produces a graph such as that in Figure 11, demonstrating the separation that can be achieved between these samples.[73] The three primary groups that GC-c-IRMS are used to distinguish in terrestrial mammals (ruminant and non-ruminant adipose fat, and ruminant milk fat) are highlighted in Figure 11. Archaeological samples can be analysed and plotted on a graph like Figure 11 to determine the source of the

lipids. In Figure 11 it can be seen that there is a significant amount of overlap between some of the samples. Between two and nine individuals of each animal were analysed, all in triplicate, and the error bars represent the range of measurements, with the bars crossing at the mean value. The relatively large error bars show that, despite $\delta^{13}C$ apparently remaining stable during diagenesis, there is variation between individuals of a species with consequent overlap between different species.
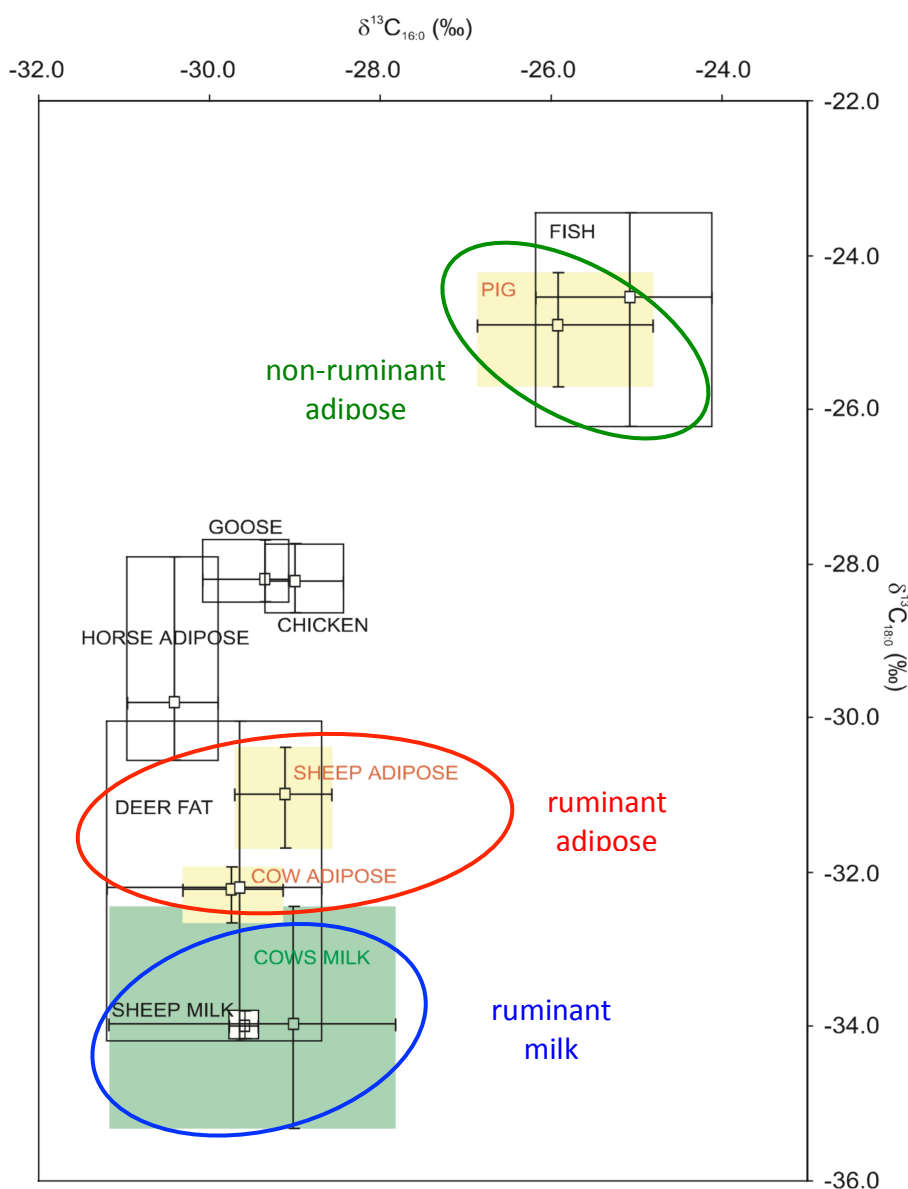
Figure 11. Plot of $\delta^{13}C_{16:0}$ vs. $\delta^{13}C_{18:0}$ for various animal fats, demonstrating the separation that can be achieved using GC-c-IRMS, as well as where there is overlap. The three main groups, of porcine adipose fat and ruminant adipose and milk fats, are marked. The error bars represent the ranges of biological and experimental replicates, since several of each animal were analysed, all in triplicate. Modified from Evershed *et al.*[73]

Like the archaeological biomarker concept, the application of GC-c-IRMS to archaeological samples has its roots in organic geochemistry, where it has been used to gain information about the origins of organic matter found in sediments.[75] The use of GC-c-IRMS in the context of archaeological analysis was first reported in 1994, when flash chromatography (for purification) was combined with isotope ratio monitoring GC-MS for analysis of the alkane fractions of lipid extracts from early medieval potsherds.[41] More work was published in 1997, when GC-c-IRMS was used to characterise two types of medieval vessel which were differently shaped.[66] By comparing isotope ratios in the lipids from the medieval vessels with those from modern animals of the type thought to have been the predominant domesticated species in the area at that time, one type of vessel was interpreted to have contained fat from monogastric animals (i.e. pig) and the other type fat from ruminants (i.e. cows or sheep). The technique was also used for the first demonstration of the detection of milk lipids extracted from archaeological potsherds, from samples from two sites: one late Saxon/early medieval and the other Iron Age/Romano-British.[65] It is in the case of milk that the importance of isotope ratio analysis can really be seen, because of the fact that the short-chain TAGs characteristic of milk are often completely degraded and unable to be detected in archaeological samples.[76]

Since the introduction of GC-c-IRMS, it has become widely used, in combination with lipid identification by GC and GC-MS, for analysis of archaeological lipids. Although the principles on which lipid sources are determined are different between GC and GC-c-IRMS, both techniques do rely on comparison with data from modern animals and plants in order to discriminate the source of the lipids. In biomarker analysis by GC-MS, the issues that need to be taken into account are lipid diagenesis and the fact that lipid distributions may be similar in different species of animal. However, with GC-c-IRMS typical isotope ratios for the different animals and plants are the relevant criteria. As can be seen in Figure 11, there is overlap between ratios for samples from different sources which complicates the interpretation. For example, the sheep milk signal is completely overlapped by the cow milk signal, meaning that it is only possible to assign the source broadly as ruminant milk, rather than saying which animal the milk came from. Recent analysis of wild deer using GC-c-IRMS has generated $\delta^{13}C$ values which, if found in an archaeological sample,

would fit the criteria for milk fats,[72] and so care must be taken when assigning lipid sources (Figure 11).

Mixing of different lipids (i.e. by cooking more than one commodity in the same vessel) also affects the $\delta^{13}C$ values obtained. Lipid mixtures give values that plot on a graph like that shown in Figure 11 somewhere between the constituent animals. Models are used to predict $\delta^{13}C$ values for mixing of different proportions of lipids from different sources, so that the percentage contributions from the different sources can be estimated from the experimental values.[77,78]

Although the application of GC-c-IRMS has undoubtedly contributed hugely to improving the amount of information we can gain about the sources of lipids in archaeological ceramic samples, the problems with overlapping signatures from, for example, milk from different ruminant species, has led to other avenues being explored. One of the focuses of research has been in improving the detection and structural characterisation of intact TAGs, using methods other than GC.

1.7   IMPROVING TAG DETECTION IN ARCHAEOLOGICAL SAMPLES

The detection of intact TAGs is one of the aims of the analysis of lipids from archaeological artefacts, since they are the undegraded remnants of the originally deposited lipids. Although HTGC has been used extensively for lipid analysis, including TAGs, it is not ideal for TAG analysis because the high temperatures required to elute them can cause them to break down. Therefore, one of the avenues that scientists working in archaeology have been pursuing is whether other techniques could be used to detect TAGs. HPLC and nanoelectrospray MS have both been reported to have been successful for such analyses.

1.7.1   HPLC for Lipid Analysis in Archaeology

There are numerous published examples of the use of HPLC for the analysis of lipids in general. Neutral lipids are most relevant for the study of archaeological samples since such samples consist mainly of intact TAGs and their breakdown products. Charged lipids, such as phospholipids, have not been reported in archaeological samples, presumably because they have long since degraded. For neutral lipids, the main difference between the analytes is the length of their fatty acid chains, and thus

it is the difference in hydrophobic character of the analytes that distinguishes them from each other. Because of this, RP-HPLC is the most suitable HPLC method for these analytes. However, despite the fact that HPLC is clearly suitable for the analysis of lipids, there are few examples of its application to archaeological lipids.

The first use of HPLC for the analysis of lipids in archaeological samples dates back nearly as far as the use of GC, with the first published work appearing in 1981.[79] Like the early work using GC for archaeological lipids, this work required the saponification of intact TAGs to produce fatty acids, which were derivatised to form *p*-bromophenacyl esters for detection by UV. However, before saponification, thin-layer chromatography (TLC) was carried out to separate free fatty acids from intact TAGs, so that information about how much TAG had survived intact in the archaeological sample could be gained. The amount of TAG remaining is a good measure of how well preserved an archaeological sample is, which is important to know because it has implications for the presence or otherwise of lipids such as fatty acids. The analysis was carried out on five examples of 1500-year old amphorae from the Mediterranean region as well as an oil lamp, all excavated in Rome, and required 1-2 g of ceramic powder from each sample (comparable to the requirements of modern GC-MS-based methods). The aim was to discover the contents of the vessels, and thus to shed light on the international trade and economy of Rome at the time. It was concluded that the vessels had contained vegetable oils, based on the presence of $C_{14:0}$, $C_{16:0}$, $C_{18:0}$, $C_{18:1}$, $C_{18:2}$ and $C_{20:0}$ fatty acids which are typical components of vegetable oils. Tentative conclusions were also drawn that the oil lamp contained rancid oil, due to the presence of 9,10-dihydroxystearic acid ($C_{18:0\ (2\ OH)}$). One of the amphora samples was thought to contain sesame oil due to relatively high amounts of $C_{18:2}$ and $C_{20:0}$ fatty acids, which are more common in sesame oil than in olive oil. Components were identified in the archaeological samples by retention time comparison with authentic standards. This makes it impossible to identify unambiguously all of the compounds in such complex mixtures as lipid extracts of archaeological pottery, which generally contain highly degraded fats. Mass spectrometric analysis of the lipid extracts would have been beneficial for this application, but because of the small amount of sample available it was not possible to carry out such analysis. This early study demonstrates proof of concept that HPLC can be used for analysis of lipids extracted from archaeological

ceramic samples. However, it was limited by the fact that the TAGs had to be saponified and that analyte identification by mass spectrometry could not be carried out, and so strong archaeological conclusions could not be drawn.

In the years following the 1981 publication, the applications of HPLC to archaeological samples do not seem to have been developed further. At this time the archaeological science field was in its infancy and, although the application of HTGC was still a few years away, GC methods were being applied to archaeological samples.[14,54] Once the use of HTGC for such samples was introduced, this was the method that was widely adopted and this seems to be the likely reason that HPLC was not applied further. More recently, however, there have been publications where HPLC has been applied specifically to detect TAGs.

Like all chromatographic methods, HPLC can be hyphenated to MS detectors for lipid identification. Atmospheric pressure chemical ionisation (APCI) has been shown to be a particularly effective ionisation method for gaining information about the fatty acid compositions of intact TAGs.[80] APCI mass spectra of TAGs give peaks corresponding to $[M+H]^+$, $[M-RCO_2]^+$ and $[RCO]^+$ and it has been observed that the $[M-RCO_2]^+$ peaks for loss of the fatty acid from the *sn*-2 position give smaller peaks than loss from the *sn*-1 (or *sn*-3) position (because it is less energetically favourable to lose a fatty acid from the *sn*-2 position).[80] Therefore, the ratio of the $[M-RCO_2]^+$ peak heights for losses of each of the fatty acids can be used to determine TAG positional isomers. The Evershed group, known for their many contributions to archaeological lipid analysis, have published papers on the application of HPLC-APCI-MS for determining positional isomers of TAGs in modern vegetable oils,[81] bovine milk fat[82] and animal fats.[83] However, they have only published one example of its application to archaeological samples, in which they determined the $C_{16:0}$:$C_{18:0}$ ratio in the *sn*-2 position of TAGs from archaeological lipid extracts which were believed to be of ruminant and non-ruminant origin based on previous lipid analyses. The ratio of $C_{16:0}$ to $C_{18:0}$ fatty acids in the *sn*-2 position of TAGs is known to vary between those from ruminants (ca. 60:40) and those from non-ruminants (ca. 95:5). Comparison of the ratios obtained from the archaeological samples with those of modern pig and cattle adipose fats found that there were differences in the archaeological samples that correlated fairly well with the modern samples.[31]

Measuring this ratio from archaeological samples should give a fairly reliable approximation of the ratio in the lipids that were originally deposited because, although lipids do degrade, the intact TAGs are the unchanged remains of those lipids. Short chain TAGs are more likely to be lost, but TAGs containing $C_{16:0}$ and $C_{18:0}$ fatty acids are likely to have been preserved in similar ratios to those of the originally deposited lipids.

Kimpe *et al.* have published several papers on the application of HPLC-APCI-MS, as well as GC-MS, to archaeological lipid analysis. This work focused on the site of Sagalassos in south-west Turkey, involving analysis of lipids extracted from potsherds of several different types of vessel. The main application of HPLC has been to improve the detection of intact TAGs compared to that obtainable using GC-MS, and the work has shown that it is possible to detect TAGs using HPLC-MS when they cannot be detected by HTGC,[84,85] as well as to quantify them.[84]

A comparison of HPLC-MS analysis of TAGs with GC-c-IRMS, as well as GC analysis to determine the $C_{16:0}$:$C_{18:0}$ ratio, has found good agreement between the three methods for identification of samples as being ruminant, non-ruminant or dairy.[86] This shows that TAG analysis can be used in place of GC-c-IRMS, although only when TAG preservation is relatively high.

Although there is a limited amount of literature on the use of HPLC-MS for archaeological lipid analysis, there has been a recent publication using a new type of HPLC stationary phase.[87] Core-shell particles have a solid silica core with a porous outer shell, and perform similarly to small (< 2 μm) fully porous particles such as those found in ultra-high performance LC (UHPLC) systems, without the need to operate at high pressures, and with shorter analysis times. In previously published work, it had been commented that chromatographic resolution had been sacrificed in order to obtain sufficiently low limits of detection.[33,84,85] Therefore, Saliu *et al.* used a core-shell HPLC column (with MS detection using electrospray ionisation) to analyse historical ointments from 18th century Spain and the contents of Ancient Egyptian vessels thought to be kohl containers, along with reference ointments produced following original recipes found in historical texts, reference lipids (animal fats and plant oils) and TAG standards.[87] The core-shell particles allowed better resolution of TAGs, whilst still using the solvent system that had given the best

detection limits in the previous work. Although this analysis was carried out on bulk material (i.e. ointment residues) rather than invisible lipids extracted from ceramic material, it illustrates the potential for newly-developed analytical methods to be applied to archaeological research.

1.7.2   Nanoelectrospray MS

Nanoelectrospray (nanoESI) is a variant of electrospray ionization (ESI – see section 2.2.3) that uses low solvent flow rates (in the nL/min range), resulting in low sample consumption and high sensitivity. These attributes clearly make it attractive for archaeological samples due to the limited amounts of lipid preserved, and it has been applied to the analysis of TAGs in lipid extracts of Neolithic potsherds from France.[24] In this work the authors have shown that nanoESI-MS is more sensitive for the detection of TAGs than HTGC - analysis of one archaeological sample by nanoESI-MS allowed the detection of T_{28}, whereas HTGC of the same sample only detected down to T_{40}. The implications of this are important, because the detection of lighter TAGs can be used to identify dairy fats (see section 1.5.7).

By the use of nanoESI-MS/MS it was possible to obtain information on the fatty acid composition of modern animal fats (both adipose and milk), and then apply this knowledge to some archaeological samples. The TAGs fragmented by loss of fatty acids and fatty acid lithium salts (since the samples had been doped with Li^+) to give $[M+Li−RCOOH]^+$ and $[M+Li−RCOOLi]^+$ ions, as well as the acylium ion, $[RCO]^+$, allowing the fatty acid compositions of the TAGs to be determined. By comparison of the fatty acid profiles of particular TAGs with those from modern animal fats it was possible to assign a lipid residue as probably that of goat milk rather than cow milk. For example, goat milk was found to be consistently higher in the $C_{10:0}$ fatty acid, across a range of TAGs ($T_{36:0}$, $T_{42:0}$ and $T_{44:0}$), and comparison of cow and goat milk with one of the archaeological samples showed the archaeological sample to have much more similar profiles to the goat milk profiles than to those of cow milk. Similarly, another archaeological sample was found to have fatty acid profiles closer to those of cow milk than goat milk. Plotting the fatty acid compositions of different TAGs from a range of sources (adipose and milk from different species) produced graphs with characteristic profiles for each TAG source. Comparison of such profiles with those obtained from well-preserved archaeological samples allowed

assignments to be made of the source of the archaeological lipids. This kind of in-depth study of TAG fatty acid distribution can reveal information about lipid sources that has not been obtainable before. These identifications to species level are obviously more specific than the information that is available from GC-c-IRMS, which can only broadly assign the sources of lipids as ruminant adipose, non-ruminant adipose or ruminant milk.

Although the species-specific identification of the lipids was carried out using an advanced analytical technique, this did not remove the need for HTGC analysis. A number of samples were analysed using HTGC (which was used as a screening method to determine the level of preservation of the lipids) and, from those, well-preserved samples were selected for the detailed nanoESI-MS(/MS) analysis. By applying the criteria already mentioned (section 1.5.7), where a wide distribution of TAGs ($T_{40} - T_{54}$) indicates a dairy source, a narrow distribution ($T_{46} - T_{54}$) indicates adipose fat, and a medium distribution ($T_{44} - T_{54}$) is ambiguous because it could be either adipose fat or very degraded dairy fat, the 21 samples were grouped into the different categories and just four were selected for nanoESI-MS analysis. Of those four, two had been initially categorised as dairy and, following nanoESI-MS/MS analysis, were further identified as cow and goat, respectively. The other two samples had a medium TAG distribution, and were identified respectively as subcutaneous fat probably from sheep, and degraded adipose fat with no information able to point to a specific source. Although the nanoESI-MS analysis has allowed specific determination of lipid sources in some cases, the fact that it could not pinpoint the exact source of the lipids in every one of the samples demonstrates the difficulty of this type of analysis, even with advanced analytical techniques. This is likely to be due to the complexity of the samples, with inherently complex lipid distributions (derived from biosynthesis and metabolism) being further complicated by potential mixing of different foodstuffs within vessels, and degradation over time.

As well as HTGC being used as a screening method to identify samples with well-preserved TAGs, it also provides useful information in its own right, since it is a good general method that allows identification of a wide range of molecules including the components of, for example, resins and beeswax, allowing those commodities to be distinguished from animal fat. It was noted by the authors that

50

some of the samples were exceptionally well preserved, which will have facilitated the nanoESI analysis. Such in-depth analysis is only possible when there are well-preserved TAGs present in the samples and thus it will not be suitable for samples from all archaeological sites. However, this work does show that the use of multi-technique strategies, including advanced MS methods, can improve the interpretation of archaeological lipid residues.

1.8 CONCLUSIONS

This review has shown how the development and application of analytical chemistry methods has contributed to the field of archaeology. A combination of techniques are widely used, including lipid detection and identification by HTGC-MS and analysis of stable isotopes, and these are able to provide information about the animal and plant sources of foods cooked and stored in vessels from antiquity. This, in turn, has helped archaeologists in their understanding of the lives of people in the past.

The published papers that report the application of these techniques to archaeological samples are too numerous to count. In many of the cases, the analysis of lipids in archaeological ceramics has been used to find out about the foods cooked in the vessels, which can tell us about what people in the past were eating. There are also examples in which analysis of vessels with unusual shapes has provided evidence of specialised uses for these vessels, for example the French *coupes-à-socles* (section 1.5.5) and the combed ware vessels (section 1.5.6). A more recent paper has even found that lipids can be preserved in stone vessels, not just ceramic ones.[32]

It is notable that the vast majority of the published papers do not stray from the established, GC-based, techniques. However, analytical chemistry is constantly developing and it is likely that there are newer techniques which could be successfully applied to archaeological samples. These have the potential to provide even more information than is currently available from the established techniques about the structural composition of lipids preserved in archaeological artefacts. An example of this is the success of the application of nanoESI-MS.

The current techniques are used together since they complement each other: GC for separation of the lipids, with MS used for identification in at least some samples, and FID used for others. GC is able to identify a wide range of lipids so, in combination

with the archaeological biomarker approach, it is able to identify some sources of lipids. It is also used to assess the amount of lipid present in the samples. Samples with a sufficient lipid content are then often subjected to GC-c-IRMS analysis to categorise the lipid as dairy, ruminant adipose or non-ruminant adipose. There has been some application of HPLC, which has been shown to be better able to detect intact TAGs. However, this method seems to have been somewhat underused, despite its potential. This is perhaps due to the GC-based methods being so widely used, with demonstrable success, that the archaeological community has not felt the need to explore other techniques to a great extent.

The successful application of nanoESI-MS has demonstrated that analytical techniques that are not currently applied to archaeological questions might be able to provide more details about the sources of the lipids. With this in mind, the application of other mass spectrometric methods would be beneficial to see if they can also provide more detailed information, to further complement the analytical techniques currently in use.

1.9   OVERALL AIMS OF THE THESIS

The overarching theme of this thesis is the application of mass spectrometry to archaeological residues. Within the thesis there are two branches of investigation. The first is to improve TAG detection by developing a method for matrix-assisted laser desorption/ionisation (MALDI)-MS analysis of archaeological lipid extracts. TAGs have been identified as a group of analytes for which the currently used method of HTGC is not optimal, and application of other analytical methods has already been shown to improve TAG detection. However, MALDI-MS has not been applied before and may provide additional benefits compared to the other methods. Development of a MALDI-MS method for archaeological lipid analysis is described in chapter 4, and compared with the conventional technique of HTGC. The method was then applied to samples from two different archaeological sites, from different time periods and different parts of the world, again with comparison to HTGC, and these data are described in chapters 5 and 6.

The second branch of the thesis, presented in chapter 7, is related to the overall theme of the research because it involves the detection of chemical residues in

archaeological pottery, with the aim of providing information about the use of the pots. However, rather than lipids, this branch is concerned with the detection of opium alkaloids in a particular type of vessel known as a base-ring juglet. These items were produced in Late Bronze Age Cyprus and have been associated with opium due to their shape. However, despite many attempts, convincing chemical evidence for opium has not been found in examples of these vessels. In the British Museum collection there are two examples of sealed base-ring juglets with contents inside. The work presented in chapter 7 involved the development of methods for extraction of alkaloids from the contents of one of the juglets, and for analysis of the alkaloids by HPLC-MS.

2 INTRODUCTION: MASS SPECTROMETRY

2.1 OVERVIEW

Mass spectrometry (MS) is the central technique used in this thesis, and for lipid analysis, and so a description of the various MS techniques used is included here. MS is an analytical method that essentially involves weighing molecules (in ionic form) and/or their fragments in order to determine their molecular mass, to gain information about their atomic composition and structure. A mass spectrometry system (shown schematically in Figure 12) consists of several components. In order to control and detect analytes in MS, magnetic and/or electric fields are used, and so the analytes must be charged in order to be affected by the fields. Therefore, the first component of a mass spectrometer is the ion source, where neutral analytes are ionised. The ions are then transferred into the mass analyser where they are separated based on their mass-to-charge ratios (*m/z* values), and then detected. A computer is used to run the software that controls the instrument and displays mass spectra. Because, in general, collisions of the ions with other species will cause them to fragment and/or be neutralised, most parts of a mass spectrometer are operated under vacuum.
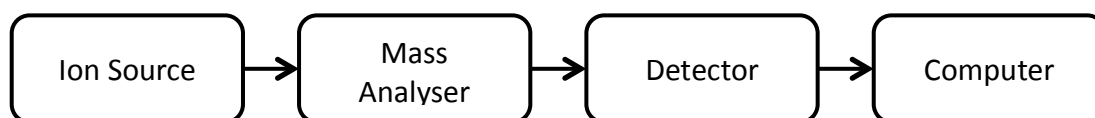
Figure 12. Schematic of the general components of a mass spectrometry system.

The first mass spectrometers were developed by J. J. Thomson, Francis Aston and Arthur Dempster in the early 20th century.[88] Since those early experiments, there have been many important developments in the technique and it is now an essential part of many branches of science.

The first ionisation method to be developed was electron ionisation. This method is now sometimes described as a 'hard' ionisation method because it imparts a lot of energy to the analytes, tending to cause them to fragment. This fragmentation is useful for providing information about the structure of the analyte, but often results in no intact analyte remaining so the molecular mass of the analyte cannot be determined. Therefore, in the second half of the 20th century there was much

research into the development of 'soft' ionisation methods that produce mainly ions of the intact molecule with little fragmentation. These techniques made possible the analysis by MS of larger molecules, including large biomolecules, for the first time. However, because of the lack of fragmentation induced by these methods, structural information cannot be obtained without providing extra energy to the ions generated, to cause them to fragment. One of the methods used for this is collision-induced dissociation (CID).[89] In CID, a gas such as N_2, He or Ar is introduced between the ion source and mass analyser (or between mass analysers in instruments that combine more than one analyser). Collisions between analyte ions and neutral gas molecules/atoms convert some of the ions' kinetic energy to internal energy, causing them to fragment.

The following sections describe the ion sources and mass analysers used in the work reported in this thesis.

2.2   ION SOURCES

2.2.1   Electron Ionisation (EI)

EI was first used by Dempster.[90] Today it is used primarily for small organic molecules, particularly when MS is coupled to GC.

In EI, a beam of electrons, formed by passing an electric current through a filament, are accelerated towards an anode. The gas phase analytes are introduced into the path of the electron beam. Figure 13 shows a diagram of an EI source. The electrons are travelling in a wave, and when the wavelength of the electrons is similar to the bond lengths in the analyte molecules, energy transfer between the electrons and the analytes occurs.[88] If there is enough energy, an electron can be removed from the analyte molecules, causing them to become radical cations. EI is less efficient for the production of negative ions than it is for positive ions.[88]
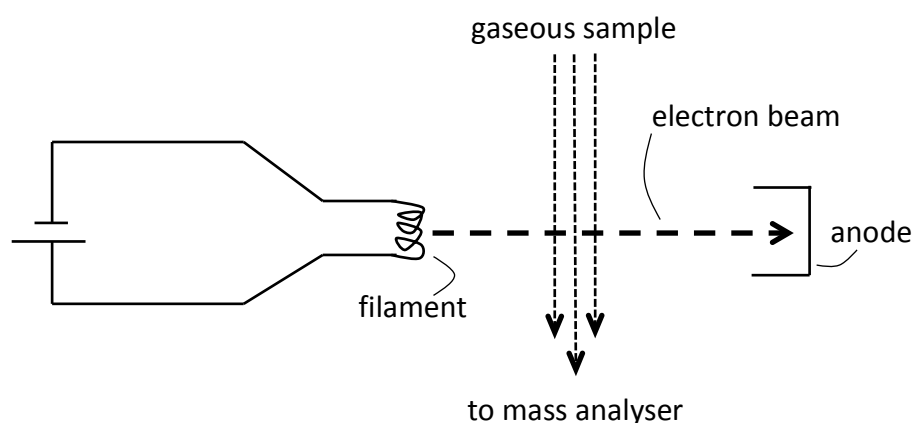
Figure 13. Schematic of an EI source.

In EI, the energy of the electrons is typically 70 eV, since this gives a wavelength of 1.4 Å,[88] close to the bond length of organic molecules. Experiments have shown that, at this energy, the number of ions produced for a given ion current and sample pressure is at a maximum, meaning that variability in filaments does not result in a loss of reproducibility.[88] EI introduces excess energy to the analytes and so usually results in extensive fragmentation. Also, because the analytes must be introduced in gaseous form, it is not generally suitable for large molecules with low vapour pressures. In order to volatilise large molecules, high temperatures are required and these may result in degradation of the analytes before they can be vaporised or

ionised. For this reason, other ionisation methods were developed that were more suitable for large molecules. The two most common of these are matrix-assisted laser desorption/ionisation and electrospray ionisation.

2.2.2 Matrix-Assisted Laser Desorption/Ionisation (MALDI)

MALDI is an ionisation method that combines the use of a matrix (usually a small organic molecule) with a laser to provide energy for the desorption and ionisation of non-volatile analytes.

The term 'matrix-assisted' in a laser desorption (LD) context was first used in 1985 by Karas and Hillenkamp, who were analysing amino acids using UV laser desorption MS. Because of their ability to absorb UV light, aromatic amino acids require a lower laser irradiance to produce ions than aliphatic amino acids do. However, Karas and Hillenkamp observed that when they analysed a mixture of tryptophan (aromatic) and alanine (aliphatic) at the laser irradiance that would normally give signals for tryptophan only, they observed signals for alanine too.[91] They extended this work to a range of other small organic molecules that absorb UV light, using them as matrices for the detection of molecules such as carbohydrates and peptides.[92] The results showed that compounds that could not be analysed using LD were able to be detected when a UV light-absorbing molecule was added as a matrix. They also found that, for analytes that could be analysed using LD, the addition of a matrix allowed signals for the analytes to be observed at lower laser irradiances and with greater S/N and reproducibility. In 1988 they reported the analysis of proteins with molecular weights up to 67 kDa using nicotinic acid (Figure 14a) as a matrix.[93]
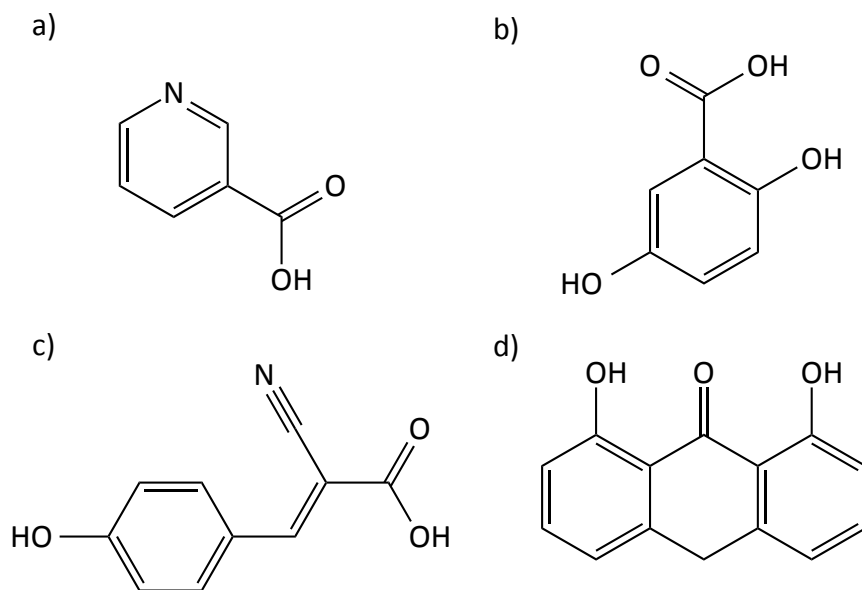
Figure 14. Some MALDI matrices. a) nicotinic acid, b) 2,5-dihydroxybenzoic acid (DHB), c) α-cyano-4-hydroxycinnamic acid (CHCA), d) dithranol.

Independently of Karas and Hillenkamp's work on using small organic molecules as matrices, in 1988 Tanaka *et al.* reported a method for analysing polymers and proteins up to 34 kDa. They used LD with a matrix of 'ultra fine metal powder' (specifically cobalt with a diameter of 300 Å) and glycerol.[94] This method was published just before Karas and Hillenkamp's 1988 protein analysis paper, and earned Tanaka a one quarter share of the 2002 Nobel Prize in Chemistry.

MALDI is one of the primary ionisation methods in use today, and is widely applied to the analysis of compounds including proteins, peptides, oligonucleotides, lipids and synthetic polymers. The methods used are very similar to Karas and Hillenkamp's original method, using a small organic molecule as the matrix. Figure 14 shows some MALDI matrices. Solutions of the matrix (typically a saturated solution) and sample are prepared and spotted onto a target (usually made from metal, though disposable plastic targets do exist) to produce analyte/matrix co-spots. The number of matrix molecules should be larger than that of analyte molecules, serving to isolate the analyte molecules from each other, and protecting them from the laser.[95] After the spots are dry, the target is placed into the mass spectrometer's vacuum chamber (except in the case of atmospheric pressure MALDI, which will not be discussed here). A pulsed UV laser (often a 337 nm N_2 laser or a frequency tripled or quadrupled Nd:YAG laser with wavelength 355 nm or 266 nm) is used to

irradiate the sample spot to produce a gas-phase plume of matrix and analyte molecules, resulting in the formation of analyte ions. These ions can then be accelerated into the MS. Figure 15 is a schematic showing the MALDI spot being irradiated and the formation of ions.
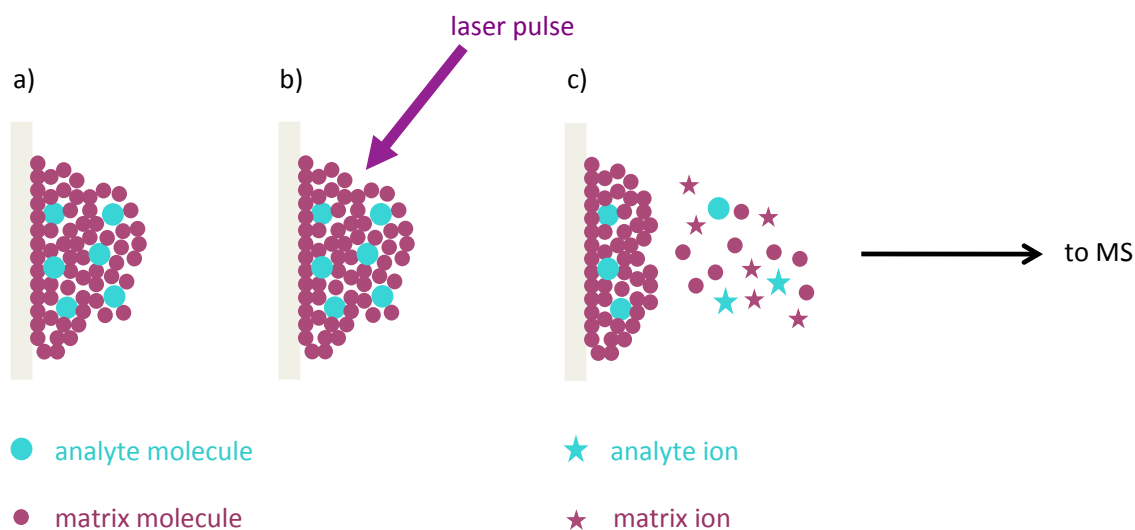
Figure 15. Schematic of the MALDI process. a) a MALDI spot; b) the spot is irradiated with a pulse of UV laser light; c) the laser energy causes the matrix to be ionised, and collisions between analyte molecules and charged matrix produce analyte ions.

Because the pulsed nature of the laser causes pulses of ions to be produced, MALDI is particularly suited for use with time-of-flight mass analysers (see section 2.3.3).

The exact mechanism for MALDI is still not fully understood. In fact, it is likely that there are several mechanisms because of the wide range of analyte classes that can be ionised using the technique.[96] However, it is thought that the laser energy causes the formation of charged matrix clusters, and that analyte ions can be formed through a number of processes including proton transfer with the matrix ions.[96] Cationised species (for example with Na^+ or K^+) are often observed in MALDI, and the ions produced are primarily singly-charged. Because most of the laser energy is absorbed by the matrix, MALDI is a soft ionisation technique and produces little analyte fragmentation.

MALDI is widely regarded to be more tolerant of contaminants (such as salts and buffers) than other ionisation techniques. However, the main challenge of MALDI is that it can suffer from poor shot-to-shot reproducibility.[97] Variables such as choice of

matrix, spotting method, pH of the solutions and rate at which the matrix/sample crystals are allowed to form have been shown to dramatically affect the *m/z* range of ions observed, the analyte classes that can be detected and the reproducibility of analysis.[98] Therefore, choosing the most appropriate sample preparation method is imperative in order to obtain the best results. The choice of method is not a trivial matter because the best approach varies between analytes.[99] In fact, even across one spot the spectra obtained can vary. Therefore, the sample is usually moved around randomly during data acquisition in order to produce spectra from across the area of the spot, which are summed to give an overall spectrum.

There are various ways of depositing the matrix and sample onto the target. The original method has become known as the 'dried-droplet' method, and involves mixing the two solutions before depositing the mixture onto the plate.[93] However, other methods have been reported involving spotting the matrix and sample in layers, letting each layer dry before spotting the next one on top. These include a 'thin layer' method, where the sample is spotted on top of the matrix, and a 'sandwich' method, where a layer of sample is spotted between two matrix layers.[99] Other methods have also been reported where layers of matrix and a matrix/sample mixture are spotted.[100]

Because in MALDI ions are generated only from the area on the sample spot that the laser irradiates, it is suitable for mass spectrometry imaging. MALDI imaging is frequently used for the analysis of tissue sections, allowing the spatial distribution of analytes such as proteins, peptides and small molecules to be determined.[101,102] The matrix is typically sprayed or spotted onto the surface of the thin section of sample to be analysed, and the laser is fired at the sample to produce MS data from discrete spots, thereby allowing pixels of MS data to be obtained. Spectra at different locations on the sample, or maps of each ion, can then be produced to show their spatial distributions within the sample.

It is known that the size and uniformity of the sample/matrix crystals have a dramatic impact on the results of MALDI-MS analysis. This was noted by Karas and Hillenkamp, who were able to correlate the success of their MALDI results with the visual appearance of the crystals as seen by optical microscopy.[92] MALDI imaging has been used to examine MALDI spots in order to try to understand the processes

underlying spot inhomogeneity and segregation of matrix and sample, in an attempt to improve the reproducibility of MALDI analysis. These experiments have shown that the matrix type, spotting method and concentration of matrix solution affect the distribution of the matrix in the sample spot, and that different analytes are sometimes found localised at different points in the spot.[97,103]

Because of the variation across and between MALDI spots, it is typically not defined as a quantitative analytical technique. However, in some cases, when used with care, MALDI can be semi-quantitative.[97,104]

2.2.3 Electrospray Ionisation (ESI)

Alongside MALDI, ESI is one of the main ionisation methods in use today. Based on work reported by Dole in the 1960s for the ionisation of polystyrene molecules (though not for MS analysis),[105] John Fenn and co-workers developed it for a range of other molecules including proteins,[106,107] earning Fenn one quarter of the 2002 Nobel Prize in Chemistry (alongside Tanaka, for his MALDI work). It is now used for a wide range of analytes, including large biomolecules such as proteins as well as small molecules. In ESI, the analyte is introduced into the source as a solution, making it ideally suited to coupling to liquid chromatography.

ESI is an atmospheric pressure ionisation method, because the ions are formed at atmospheric pressure before entering the vacuum system of the MS. Figure 16 shows a schematic of an ESI source. A solution of the analyte is pushed through a narrow capillary, which is held at a potential difference of between 3 kV and 6 kV relative to a counter electrode, to produce an electric field gradient. For direct infusion experiments the solvent flow rate is now usually in the low μL/min range (~1 – 20 μL/min), but higher flow rates directly from a liquid chromatograph can also be used. Charge builds up in the solvent surface at the tip of the capillary, deforming the shape of the droplet until the pressure of the accumulated charge is greater than the surface tension and droplets of charged solvent with analyte dissolved in them are released. The solvent capillary is generally placed inside another capillary of slightly larger diameter, through which a nebulising gas (usually N_2) is passed, to produce a coaxial gas flow that causes the emitted droplets to form a spray. A counter-current flow of gas (again, usually N_2), known as the dry gas, serves to encourage

evaporation of the solvent from the drops, producing gas-phase ions that can enter the vacuum system of the MS, to be analysed. The flow rates of the nebulising and dry gas, as well as the dry gas temperature, are chosen based on the solvent flow rate, with higher solvent flow rates requiring higher gas flow rates and temperature.
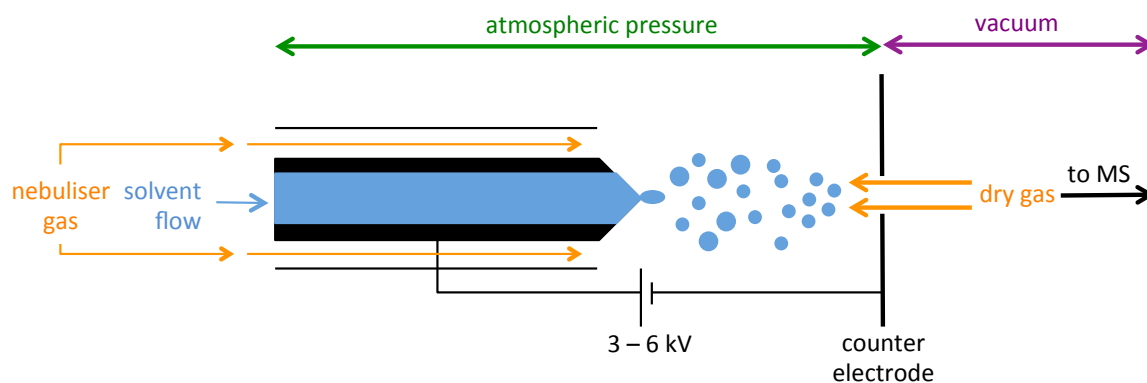
Figure 16. Schematic of an ESI source.

There are two models for how gas-phase ions are formed from the electrosprayed droplets: the charged residue model (CRM, Figure 17a) and the ion evaporation model (IEM, Figure 17b). The processes in the CRM were proposed by Dole in his original work.[105] As solvent evaporates from the droplets they reduce in size and their charge density increases. When the charge density reach a point known as the Rayleigh limit the droplets become unstable and explode into smaller droplets, which then continue to shrink due to solvent evaporation. The cycle of evaporation and explosion repeats until each droplet contains only one analyte molecule. The remaining solvent evaporates from these droplets, leaving charged gas-phase analyte molecules. The IEM was proposed by Iribarne and Thomson.[108] It begins with the same evaporation of solvent and consequent increase in charge density as in the CRM. However, in the IEM, when a droplet has sufficient charge density, gas-phase ions start to desorb directly from it.

a)

solvent evaporation   droplet explosion   solvent evaporation

b)

solvent evaporation   ion desorption

etc.
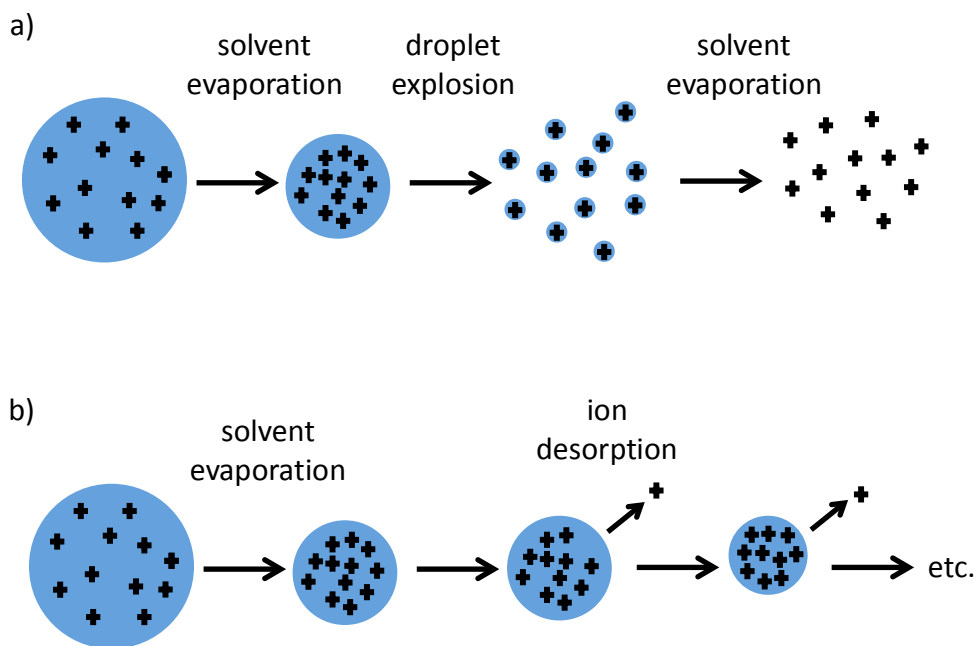
Figure 17. Models for gas-phase ion production in ESI. a) charged residue model (CRM); b) ion evaporation model (IEM).

ESI tends to produce either protonated or cationised molecules (in positive ion mode), which in the case of small molecules are usually singly charged. However, one of the features of ESI is its ability to form multiply charged ions from macromolecules. This means that it allows high-mass analytes to be detected using mass analysers that would not have m/z ranges high enough to detect them if they were singly charged. Because ions with a sequential range of charge states are produced, the mass of the analyte can be determined by considering all of the detected ions, since adjacent ions in the spectrum have a charge difference of $z = 1$.

A recent development in ESI is desorption ESI (DESI).[109] In DESI, instead of the analytes being dissolved in the sprayed solvent, as is the case in standard ESI, the analytes are on a surface. They can either have been deposited on the surface in advance of the analysis, or be inherently present on the object to be analysed. An ESI sprayer is directed onto the surface, near to the MS inlet. Charged solvent droplets impact onto the surface and desorb analyte molecules. The exact mechanisms have not been elucidated fully but several have been proposed. One is known as droplet micro-extraction or droplet pick-up, and involves the solvent droplets forming a film on the sample surface, with secondary droplets containing dissolved analyte being pushed off from the film by impacting primary droplets.[110] These secondary droplets

are subject to the same processes as ESI droplets to produce gas-phase ions. Other mechanisms involve charge transfer reactions between charged solvent molecules and analytes, either on the surface followed by desorption ('chemical sputtering') or in the gas phase after desorption.[110]

DESI was the first method in a now widely-expanding field known as ambient mass spectrometry.[111,112] Although there are now many ambient MS techniques, all based on different ionisation methods, the overriding feature of ambient MS is the fact that samples can be analysed directly from surfaces in the open atmosphere. This has great benefits in terms of minimal sample preparation and high throughput, and has found applications in many areas of science, such as forensics, food and pharmaceuticals. Many of the ambient MS methods are also suitable for imaging applications, by virtue of the ability to desorb analyte from across a 2D sample surface.

2.3 MASS ANALYSERS

2.3.1 3D Ion Traps

3D ion traps use electric fields to allow ions of a range of m/z to be trapped together in space, theoretically indefinitely, with detection of the ions when they are ejected from the trap. Because of their ability to trap ions and carry out fragmentation of the ions held within the trap, ion traps are particularly suitable for tandem mass spectrometry. Ions of a particular m/z can be held in the trap and fragmented by collision-induced dissociation, and the fragments detected after ejection from the trap. Multiple stages of mass spectrometry can be carried out by keeping fragment ions of a particular m/z from the MS^2 experiment and fragmenting those, and continuing the process up to MS^n.

The ion trap was invented by Wolfgang Paul in the early 1950s, for which he received a one quarter share of the 1989 Nobel Prize in Physics.[113] Therefore, ion traps are properly known as Paul traps to distinguish them from other devices that can be used to store ions. Although invented in the 1950s, it was not until the 1980s that developments in the ion trap produced a useful mass spectrometer. The first commercial ion trap, produced by Finnigan MAT, was announced in 1983.[114] They

are relatively low cost[115] and are bench-top instruments, making them very practical from a size perspective.

The ion trap is composed of three electrodes: one circular ring electrode and two electrically-connected end cap electrodes, as shown schematically in Figure 18, which shows a slice through all three electrodes. Figure 19 illustrates how the electrodes look in practice. Ions are injected through a hole in one of the end cap electrodes, along the z-axis (Figure 18), are trapped by an electric field formed within the space enclosed by the electrodes and, on ejection, exit through holes in the end cap electrodes. A detector is placed outside the end cap electrode opposite that through which the ions were injected, meaning that half of the ejected ions are detected. The distance between the centre of the trap and the ring electrode is defined as r_0, and that between the trap centre and each of the end cap electrodes is defined as z_0. The trap itself is very small, with the first commercial ion trap having $r_0 =$ 1 cm. This was reduced to 0.707 cm in later versions.[116]
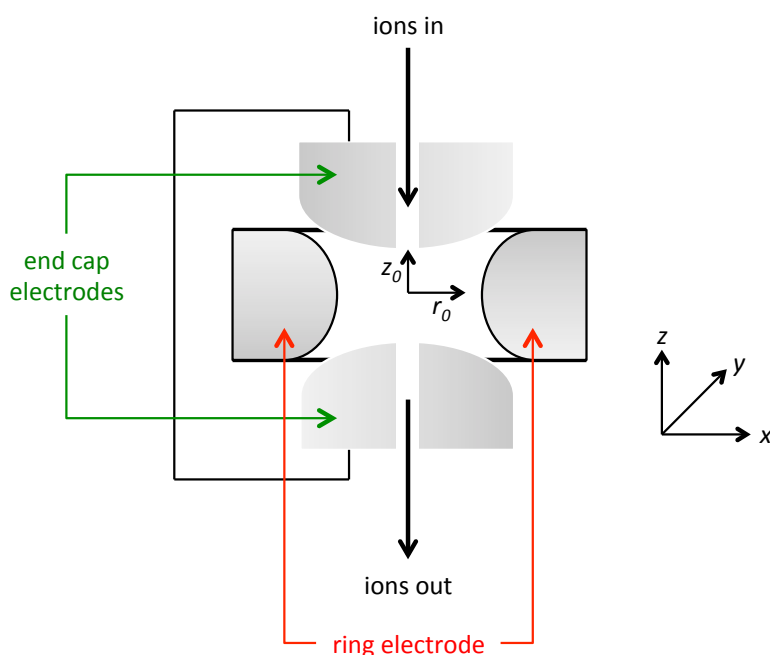
Figure 18. Schematic diagram of the electrode arrangement of an ion trap, sliced through all three electrodes as if an arc of the ring electrode had been protruding either side of the plane of the paper.
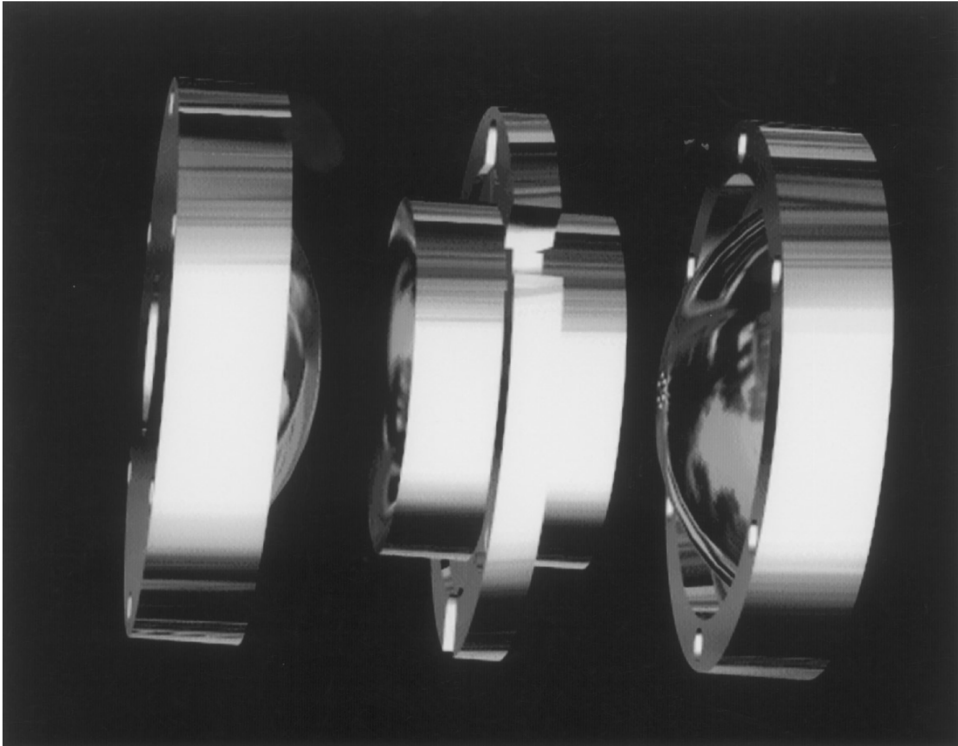
Figure 19. Image of the electrodes of an ion trap. Reproduced from Jonscher and Yates.[116]

The ions are trapped in a parabolic field created by the application of an electric potential to the ring electrode. The applied potential consists of an oscillating r.f. ($V\cos\omega t$) component, sometimes combined with a dc (U) component. The potential is saddle-shaped, and causes the ions to be trapped in the centre of the trap along one of the axes, since if their trajectories deviate from the centre along this axis the potential pushes them back. With this saddle-shaped potential they would not be confined along the other axis, since if they deviate from the centre along that axis they will be accelerated away. However, the oscillating nature of the r.f. potential means that the orientation of the saddle is constantly flipping, stopping the ions from falling down the slope of the saddle. Figure 20 shows the field in the two orientations to illustrate how an ion can be confined in the centre of the trap by the field.
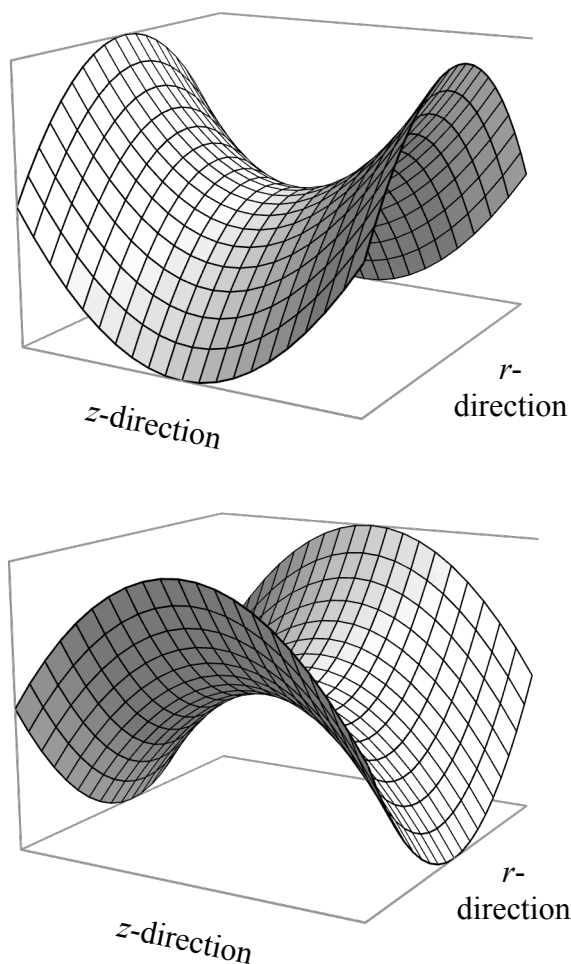
Figure 20. Oscillating parabolic field produced by the application of an r.f. potential to the ring electrode of an ion trap. The oscillating nature of the applied potential means that the ions are alternately focused in the z- and r- directions, trapping them in the centre.

When averaged over time this oscillating field cancels out, giving zero average potential. However, because the field is inhomogeneous (i.e. further from the centre of the trap the force on an ion is stronger) the potential experienced by an ion has a small average force to the weak field region (i.e. towards the centre of the trap). This is called a ponderomotive force and produces a pseudopotential well that allows the ion to be trapped. If the pseudopotential well did not exist then, although the ion would still be alternately focused and defocused in each direction, due to its initial velocity the ion would eventually hit one of the electrodes. The sign of the charge on the ion does not change the direction of the ponderomotive force, which is always towards the weak field region.

67

In order to be held stably in the trap, ions must not have a trajectory that exceeds the dimensions of the trap (along both the r and z axes). The motion of the ions in the trap is described by the Mathieu equations (Equation 3 and Equation 4):[88]

$$q_u = q_z = -2q_r = \frac{8zeV}{m(r_0^2 + 2z_0^2)\omega^2} \qquad \text{Equation 3}$$

and

$$a_u = a_z = -2a_r = \frac{-16zeU}{m(r_0^2 + 2z_0^2)\omega^2} \qquad \text{Equation 4}$$

where:

q_u and a_u are parameters describing the stability of the ions

z is the number of charges

e is the charge on an electron

m is the mass of the ion

r_0 and z_0 are the distances between the centre of the trap and the ring electrode and end cap electrodes, respectively

ω is the frequency of the fundamental r.f. applied to the ring electrode

V is the amplitude of the fundamental r.f. applied to the ring electrode

U is the amplitude of the dc applied to the ring electrode

It can thus be seen that the stability of the ions depends on the size of the trap, the m/z ratio of the ions, the amplitude of any applied dc and the amplitude and frequency of the applied r.f.

The values of q_u and a_u which result in stably-trapped ions along the z and r axes are defined by another parameter, β_u, which is a function of q_u and a_u. For ions to be stably trapped, β_u must have a value between 0 and 1. Plotting the values for q_u and a_u when $\beta_u = 0$ and $\beta_u = 1$, in the z and r directions, gives regions where ions will be stable in each of the two directions. Areas where stability along the two axes overlaps represent conditions in which an ion will be stable in the trap. Such a diagram is shown in Figure 21. The stability region for ions in the trap is shaded in red and labelled A. A second stability region is labelled B, but this region is not used because this would require the application of higher voltages than those required for region A. The stable region (A in Figure 21) is shown enlarged in Figure 22.
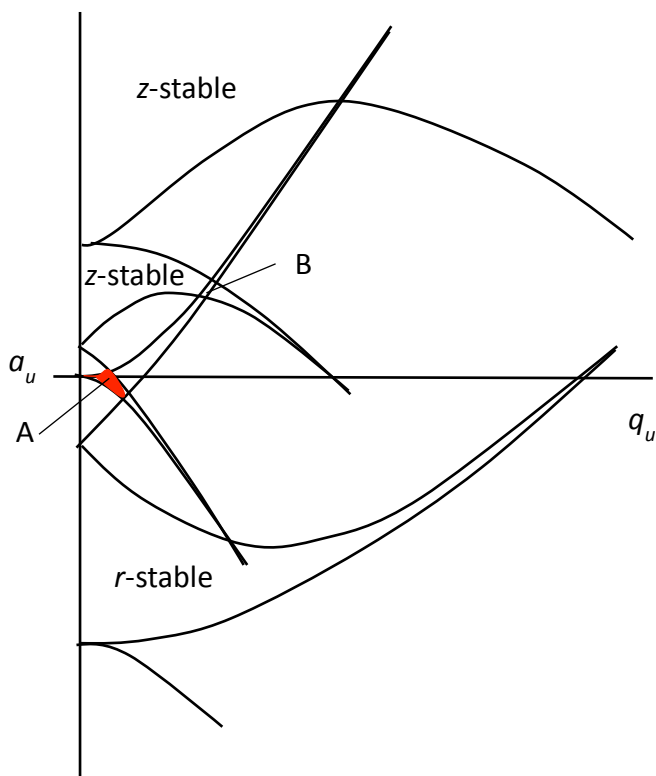
Figure 21. Stability diagram for a_u and q_u values in the r and z directions. The region of ion stability in the trap is labelled A. Sketched from March.[115]
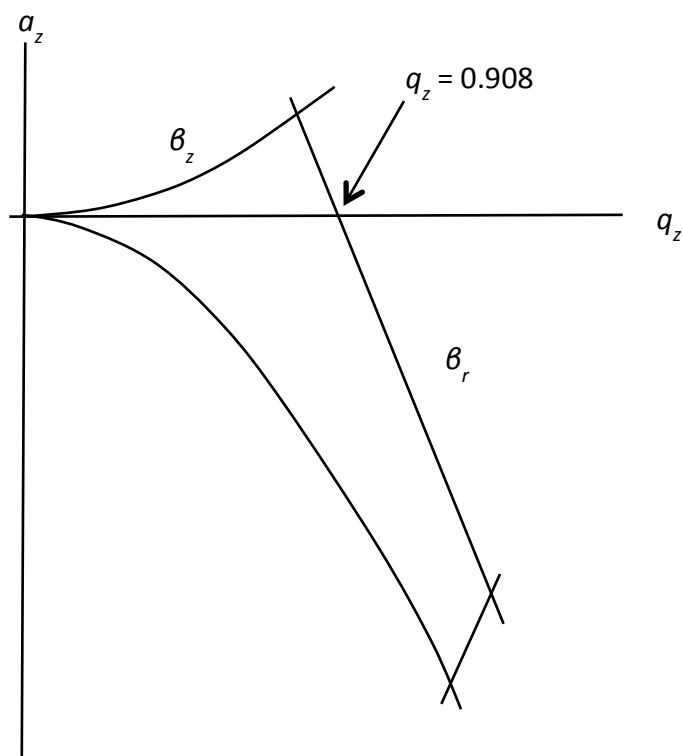
Figure 22. Ion stability region in an ion trap; corresponds to the region labelled 'A' in Figure 21. Sketched from March.[115]

As can be seen from the Mathieu equations, q_u depends on V, the oscillating r.f. potential, and a_u depends on U, the dc potential. It can also be seen that for a given ion, an increase in the amplitude of the applied potential will increase the value of q_u/a_u and for a given applied potential, ions with greater masses have smaller q_u/a_u values, i.e. the ability to trap an ion of a particular m/z depends on the applied potentials.

From Figure 22 it can be seen that when $a_u = 0$, the range of q_u values that result in trapped ions is the widest. For this reason, ion traps are generally operated without the application of a dc potential (when $U = 0$, $a_u = 0$). This is known as the 'mass-selective instability mode', was developed by Stafford in 1984, and was the innovation that allowed the ion trap to become a practical mass spectrometer through the trapping of ions of several m/z values together.[117] This lack of applied dc means that the ion trap is operated along the x axis of the graph shown in Figure 22, and the maximum value of q_z that results in a trapped ion is 0.908. This defines a low-mass cut-off for the ion trap (the value of m at which $q_z = 0.908$).

When ions are trapped, they have a trajectory the approximate shape of a figure-of-eight. This is shown in Figure 23, which is a simulation of the trajectory of an ion without initial velocity.[118] The line on the *x-y* plane is a projection of the ion motion, and shows that the ion moves in a plane in 3D space. If the ion had an initial velocity in a tangential direction, this motion would be superimposed on an elliptical orbit, and the projection would be an ellipse. However, simulating the trajectory of an ion with zero initial velocity allows better visualisation of the ion motion produced solely by the r.f. field. To cause ejection from the trap, the ion trajectory is made to increase along the *z*-axis, as shown in Figure 24 (again a simulation of an ion with no initial velocity),[118] and the ions travel through the holes in the end caps where they are detected by an electron multiplier.
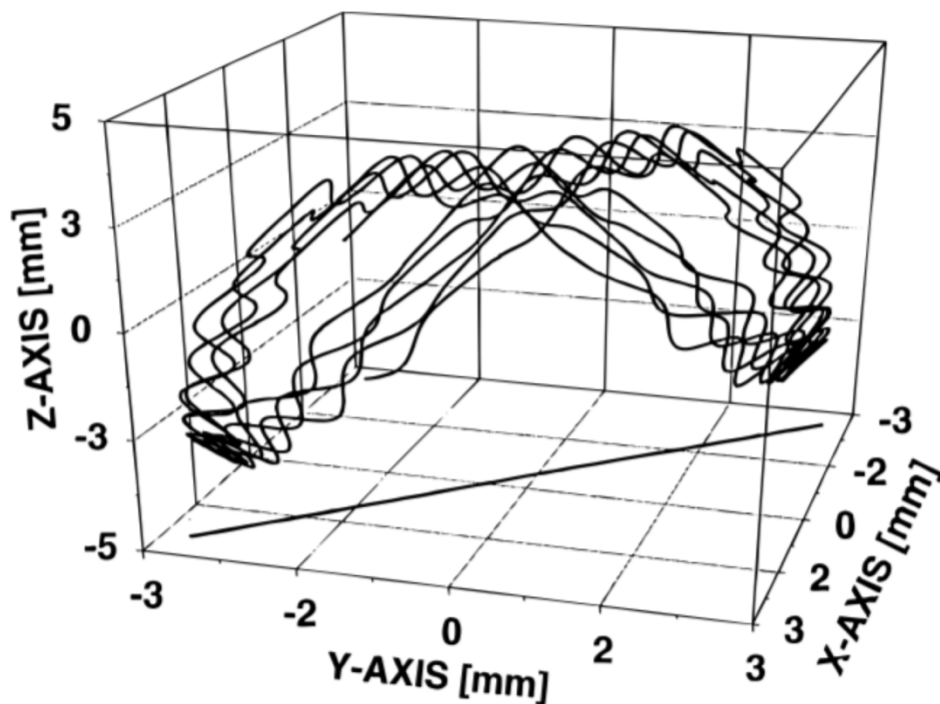
Figure 23. Simulation of the trajectory of a trapped ion with no initial velocity, travelling in a plane (shown by the projection onto the *x-y* plane) with a figure-of-eight motion. Reproduced from Nappi.[118]
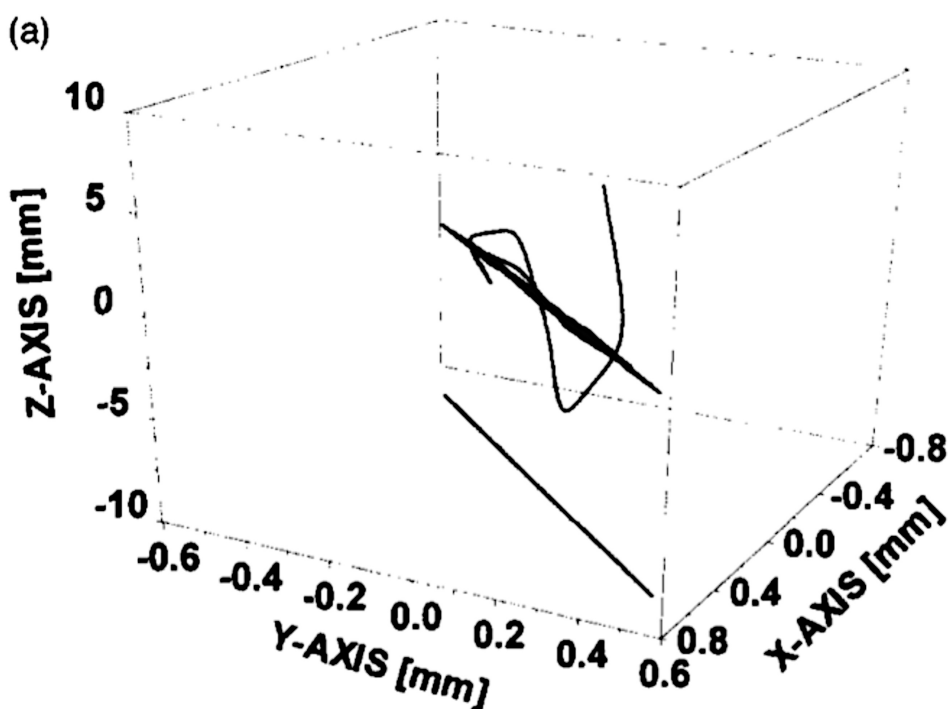
Figure 24. Simulation of the increase in the trajectory of an ion (with no initial velocity) along the Z-AXIS for ejection from the trap. Reproduced from Nappi.[118]

The trap is filled with helium at a pressure of ~ 1 mtorr. Collisions of the ions with He atoms cause loss of kinetic energy and cause the ion trajectories to be condensed into the centre of the trap.[116] This process is known as collisional cooling, and improves the resolution and sensitivity of the instrument for several reasons. Since it reduces the size of ion trajectories it stops the trajectories from increasing and allowing ions to travel through the holes in the end caps before they reach their stability limit, increasing the sensitivity.[117] Because He is light, collisions between ions and the He do not cause scattering of the ions so do not result in the ions discharging against the sides of the trap, which would reduce sensitivity. Furthermore, imperfections in the electric field, caused by tiny defects in the electrodes, should be at a minimum in the centre of the trap.[117] Thus, when ions are trapped very close to the trap centre they experience a more uniform field than they would if their trajectories were larger, which means that ions with the same *m/z* will reach their instability limit at as close as possible to the exact same time and be ejected together, increasing the mass resolution.

A trapped ion can be ejected from the trap, and thus detected, by increasing its value of q_z by increasing the amplitude of the applied r.f. potential. This is illustrated in Figure 25.[116] However, as Figure 25 shows, some ions have sufficiently high m/z ratios that they are not ejected from the trap even at the maximum r.f. amplitude that can be applied.
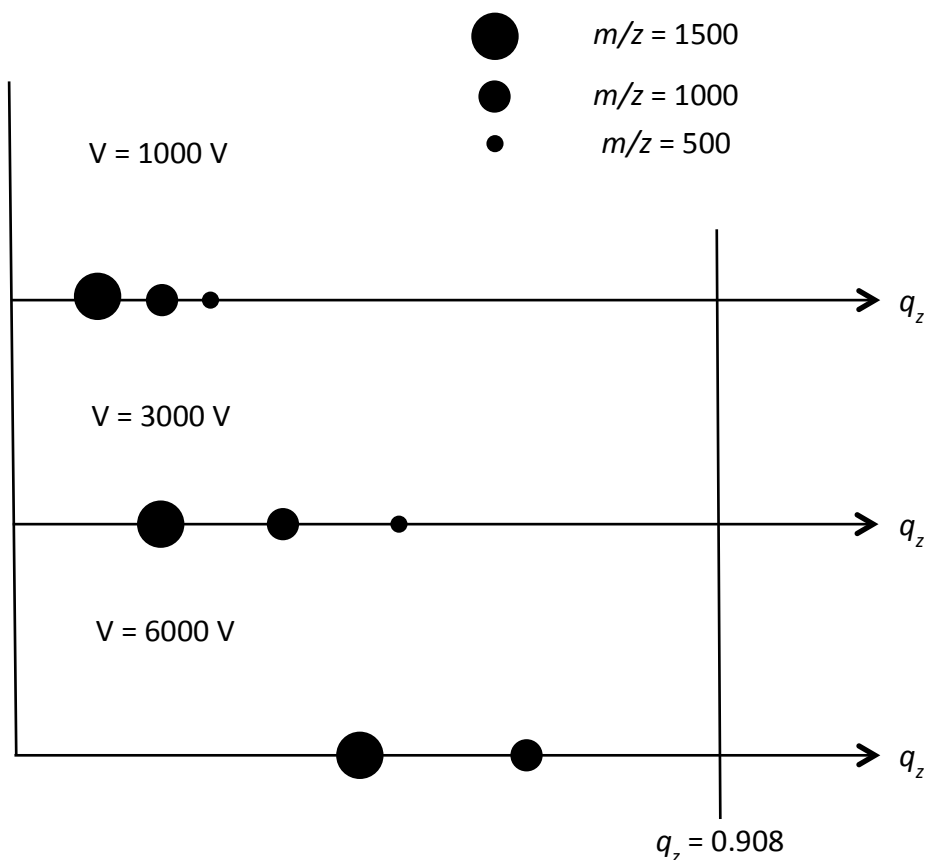
Figure 25. Ejection of ions from an ion trap by ramping the amplitude of the applied r.f. voltage.

In order to eject ions with higher m/z, a small supplementary ac voltage (of a few volts) can be applied across the endcaps.[119] This voltage, known as the tickle voltage, causes resonance with any ions which are oscillating at the same frequency as the tickle voltage. This resonance increases the kinetic energy of the ions, causing their trajectory to increase in the z-direction until they are ejected from the trap (resonance ejection). This can be thought of as producing a 'hole' along the q_z axis of the stability diagram, through which ions fall even though they have $q_z < 0.908$, as shown in Figure 26.[116] Typically, the ion trap is operated with the tickle voltage

turned on, and the amplitude of the fundamental r.f. is ramped to induce sequential resonance ejection of ions of different m/z ratios.
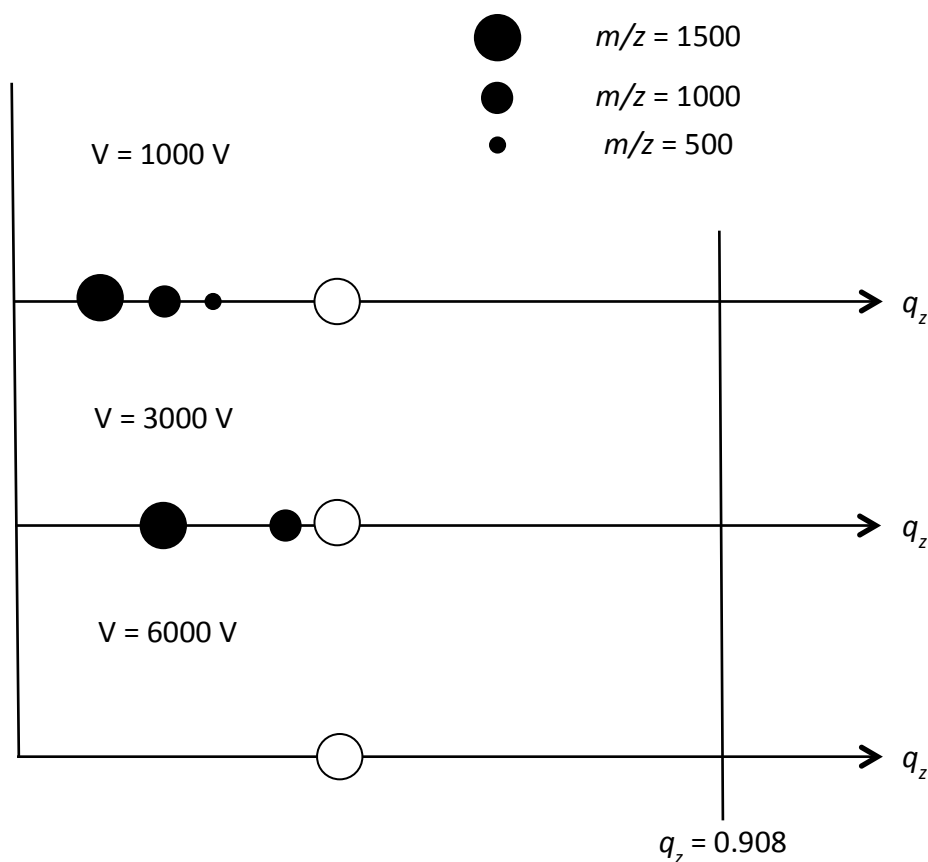
Figure 26. 'Holes' in the stability diagram caused by resonance excitation, allowing ions to be ejected from the trap when $q_z < 0.908$.

One great benefit of ion traps, alongside their relatively low cost and small size, is their ability to perform multiple stages of tandem MS. They can do this because they allow tandem mass spectrometry in time, rather than in space, i.e. all of the stages take place inside the same trapping volume but they happen sequentially. Ions are injected into the trap and those of a particular m/z are isolated by ejection of all other ions. The isolated ions can be caused to fragment by CID with the helium which is already present as the damping gas. The fragments can then be sequentially ejected, as described above, to produce a mass spectrum, or a fragment ion can be isolated and fragmented further. This process can be repeated several times for MS^n, and tandem mass spectrometry up to MS^{12} has been reported.[120]

Ions can be isolated by injecting the whole range of ions and ramping the amplitude of the applied r.f. in a reverse then forward scan (to eject first ions with m/z higher than the ions to be isolated, and then those with lower m/z).[116] However, since an ion trap can only hold a certain number of ions before space-charge effects adversely affect its performance, a more efficient way to isolate ions is to selectively inject ions of the m/z that are to be studied using tandem MS. This can be achieved by broadband excitation of ions, using SWIFT (stored waveform inverse Fourier transform). Notched SWIFT pulses, which can excite ions with a range of frequencies but that have a notch at the frequency of the ions to be isolated, are applied as the ions are injected and cause ejection of all ions except those that have the frequency of the notch.[121] This allows ions with a particular m/z to be selectively injected into the trap, thus maximising sensitivity. Two sets of pulses can be used to isolate a very narrow range of ions, with the first used to inject a small range of ions, and the second, narrower, notch used to isolate ions of just one m/z. Carrying out a two-stage process makes it easier to isolate a very small m/z range. The first step removes most of the ions contributing to the space-charge effects, causing the frequencies of the remaining ions to remain relatively constant and thus allowing greater resolution than would be possible with a single notch. The SWIFT technique can also be used to reduce matrix effects by causing ejection of matrix ions with selective injection of the analyte ions.[121]

Once isolated, ions are resonance excited by the application of an ac voltage to the endcaps.[122] This is analogous to that used for resonance ejection, but the applied ac has an amplitude such the ions are not excited to the extent that they exit the trap. The increased kinetic energy given to the ions by the applied ac means that they undergo CID when they collide with the helium damping gas. CID efficiency can be as high as 100%, though the energy of the collisions is low.[122] The fact that the CID is low energy is the reason why so many stages of tandem MS can be carried out in an ion trap. Indeed, it is often necessary to carry out several stages of tandem MS because the low energy nature of the CID means that the first stage (and even the second) can be uninformative. Following CID, the fragments are sequentially ejected or the process is repeated to carry out MS^3. This process can be continued up to MS^n.

2.3.2 Quadrupole Mass Analysers

The quadrupole mass analyser works according to the same underlying physics as the 3D ion trap. However, in a quadrupole ions of one (or a range of) m/z value(s) are transmitted through the instrument, as opposed to the ion trap which allows the trapping of ions of different m/z values in space. It is therefore a scanning mass analyser, where the instrument is set up to allow ions of sequential m/z to travel stably through the quadrupole; ions with non-stable m/z values will hit the sides of the quadrupole and be lost. This means that a quadrupole has a relatively low duty cycle, because a large proportion of the ions never reach the detector. The principle of the quadrupole was described in 1953 by the inventor of the ion trap, Wolfgang Paul, and Helmut Steinwedel.

The quadrupole is composed of four metal rods of ideally hyperbolic, but usually circular (due to the greater ease with which these can be manufactured), cross-section held parallel to each other and electrically connected in pairs (with the electrical connection being between rods opposite each other). Figure 27 is a schematic of the rod arrangement.[113] The rods are electrodes like in the ion trap, where one pair of rods is equivalent to the ion trap end caps, and the other pair is equivalent to the ring electrode. As in an ion trap, the distance from the space in the centre of the four rods to any one of the rods is defined as r_o. Ions are injected into one end of the quadrupole, travel through it and are detected by a detector placed at the far end (or transferred to another device in, for example, a quadrupole-time-of-flight or triple quadrupole instrument).

ions in
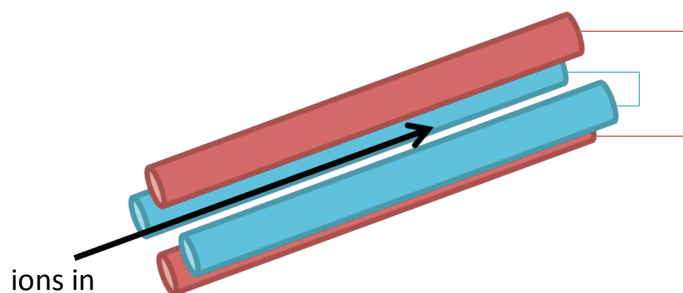
Figure 27. Schematic diagram of a quadrupole mass analyser, showing opposite rods electrically connected and the direction of ion injection.

An electric field is induced in the space between the rods by the application of an electric potential, Φ_0, formed from a combination of dc and r.f. potentials, i.e. $\Phi_0 = U + V\cos\omega t$. $+\Phi_0$ is applied to one pair of rods and $-\Phi_0$ to the other pair. Figure 28 shows a cross-section of the rods, with the potentials applied.[88]
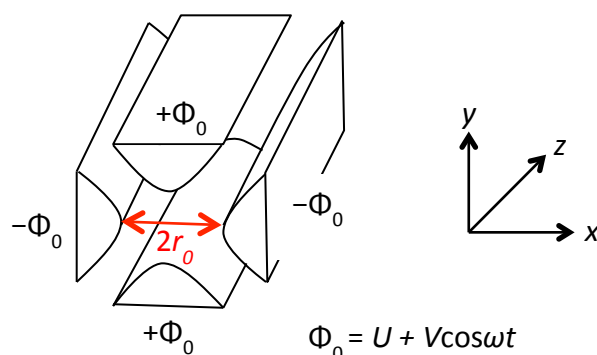
Figure 28. Schematic diagram of the cross-section of a quadrupole, showing the potentials on the rods.

Ions travel between the rods along the z-axis because they were injected into the quadrupole with a velocity in this direction, and will only be able to traverse the quadrupole if their trajectories in the x and y directions never exceed r_0. The applied field causes them to move in the x and y directions: for example, a positive ion will be attracted to a negatively charged rod, but because of the r.f. component of the applied potential the sign of the potential is constantly changing. When this happens the ion will change direction because it is now being repelled by that rod but

attracted by the oppositely charged pair of rods. If the ion has an *m/z* such that it does not hit a rod before it changes direction, it will have a stable trajectory and will be able to travel through the quadrupole. Since ions with different *m/z* values will have different trajectories in a given electric field, the electric field strength can be modified to select which ions can travel through without hitting one of the rods and being lost by discharging against it.

As in the ion trap, the Mathieu equations can be used to describe the motion of ions in a quadrupole (Equation 5 and Equation 6):[88]

$$q_u = q_x = -q_y = \frac{4zeV}{mr_0^2\omega^2} \qquad \text{Equation 5}$$

and

$$a_u = a_x = -a_y = \frac{8zeU}{mr_0^2\omega^2} \qquad \text{Equation 6}$$

From the Mathieu equations it can be seen that the stability of an ion in a quadrupole is dependent on *U*, *V* and its *m/z* value. All of the other terms are constant. Plotting the stable values of q_u and a_u in the *x* and *y* directions gives the diagram shown in Figure 29, where the red lines show the values stable along *y* and the blue lines show the values stable along *x*. Regions where the two plots overlap are where the trajectory of an ion will not exceed r_0 in either direction and so will be able to traverse the quadrupole, and the region labelled A is the region used in practice in a quadrupole. The stable areas are symmetrical about the q_u axis, so the stability is the same whether a_u, and therefore *U,* is positive or negative.
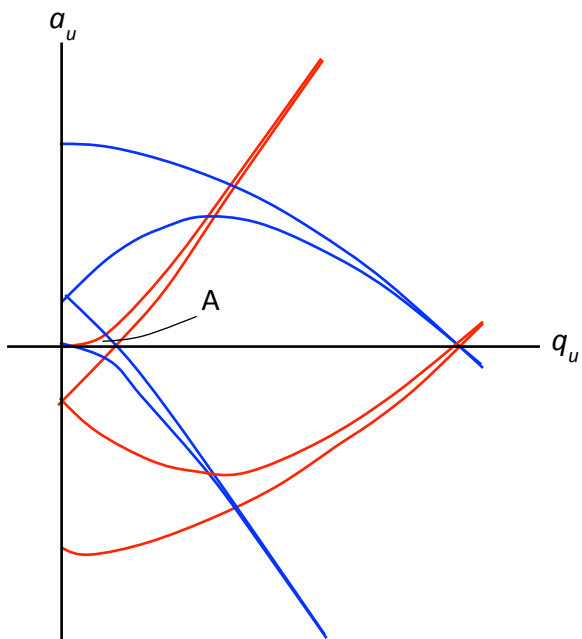
Figure 29. Sketch plot of the stable values of q_u and a_u along the x axis (blue lines) and y axis (red lines), with the overlapping regions showing areas where an ion will be stable along both axes. The stable area used in the quadrupole is labelled A.

Figure 30 shows the stable region labelled A in Figure 29. The line labelled $a/q = const.$ is a line of increasing dc and r.f. amplitude (the operating line), where the ratio between the two is kept constant. Ions of different m/z sit at points along this line (with ions of lower m/z being at higher a_u and q_u values, as shown by the Mathieu equations), and as the amplitudes of the applied dc and r.f. potentials are ramped, ions of different m/z are brought into the stable region.[123]
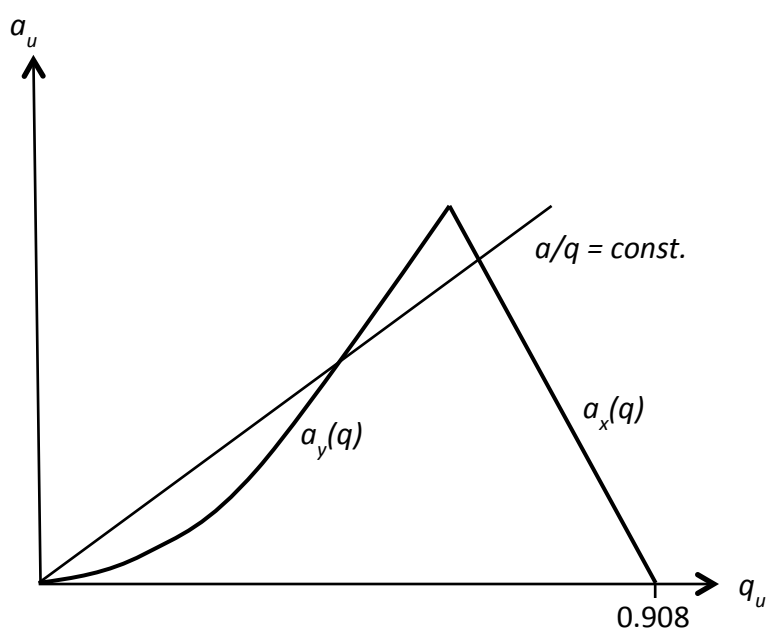
Figure 30. Stability diagram for an ion in a quadrupole. The a/q line is scanned to bring ions of different m/z values into the stable region. Sketched from Mathieson.[123]

The resolution of a quadrupole can be adjusted by changing the slope of the operating line. The steeper the slope, the closer the line passes to the vertex of the stability diagram, and so the smaller the range of stable m/z values and the greater the resolution. However, if the line is too steep it will not pass through the stable region at all, with the result that no ions are able to travel through the quadrupole.

2.3.2.1   *Quadrupoles as Ion Guides and Collision Cells*

Ion guides are used to focus ions and transmit them from one device to another. For example, in a quadrupole-time-of-flight instrument the quadrupole may be used to focus the ions produced in the ion source and guide them to the time-of-flight tube.

The r.f. applied to the electrodes in a quadrupole causes an oscillating saddle-shaped potential to form in the quadrupole, like in the ion trap, which has the effect of focusing the trajectory of the ions into the centre of the quadrupole. If a quadrupole is operated in r.f.-only mode, so no dc is applied to the rods (i.e. $U = 0$), the value of a_u will be 0, the quadrupole will be operated along the q axis shown in Figure 30 and the resolution will be zero. This means that all ions with $q_u < 0.908$ will be transmitted through the quadrupole and so the quadrupole can be used as an ion guide rather than as a mass spectrometer. The limiting q_u value means that there is a low-mass cut-off for the ion guide. However, ions with higher m/z are more difficult to focus and are therefore more likely to hit the rods and be lost. This limits the high-mass range of ions that can be transmitted. Increasing the value of V (the amplitude of the applied r.f.) will increase the ability to focus ions of higher m/z, but this increases the q_u value of all of the ions and so will increase the m/z value of the low-mass cut-off. Therefore, it is necessary to choose the value of V to compromise between the low and high m/z limits.

Hexapoles or octopoles can be used as ion guides instead of quadrupoles. These multipoles operate according to the same principles as quadrupoles except that they have six or eight electrodes, respectively, instead of the four in a quadrupole. The electrodes are electrically connected in two groups, with alternate rods being connected together. The pseudopotential well produced between the rods is given by Equation 7:

$$U(r) = \frac{n^2 z^2 e^2 V^2}{(4mr_0^2 \omega^2)} \left(\frac{r}{r_0}\right)^{2n-2} \qquad \text{Equation 7}$$

where:
2n is the number of rods
r is the radial distance from the centre of the rods

The potential is at a minimum in the centre of the multipole and increases as an ion moves closer to the rods. As can be seen from the equation, the potential varies with $(r/r_0)^2$ in a quadrupole but $(r/r_0)^6$ in an octopole. This means that, when an ion moves away from the centre of the multipole, in an octopole the potential does not start to increase as quickly as in a quadrupole, but closer to the rods the potential is much

steeper in an octopole than in a quadrupole. The result of this is that a quadrupole is better than an octopole at focusing ions right into the centre of the multipole, but an octopole can focus ions over a wider mass range. This makes octopoles particularly suitable as ion guides.

An r.f.-only quadrupole can be used as a collision cell for CID if it is filled with a collision gas (e.g. N_2 or Ar). In this case the quadrupole acts as both a collision cell and ion guide, causing fragmentation of the precursor ion and transfer of the fragments to a subsequent mass analyser.

2.3.2.2 Triple Quadrupole Mass Spectrometers

Triple quadrupole mass spectrometers are composed of three quadrupoles in series. The first and third quadrupoles act as mass analysers (with both dc and r.f. applied, denoted Q) and the second quadrupole is operated in r.f.-only mode, acting as a collision cell (denoted q). Triple quadrupole mass spectrometers are therefore often denoted QqQ. Triple quadrupoles can be used with either Q1 or Q3 in scan mode and the other two quadrupoles as ion guides to produce a mass spectrum. However, their main use is as tandem MS instruments.

QqQs can be operated in one of four tandem MS modes:

1. Product ion scan
2. Precursor ion scan
3. Neutral loss scan
4. Single/multiple reaction monitoring

The mode chosen depends on the information that is required in the experiment.

Product ion scanning is carried out to produce a mass spectrum of all of the fragments from a particular precursor ion, as shown in Figure 31. Q1 is set to allow only ions of one *m/z* value through. These ions are fragmented in q2 and Q3 is scanned to produce a spectrum of the fragments.
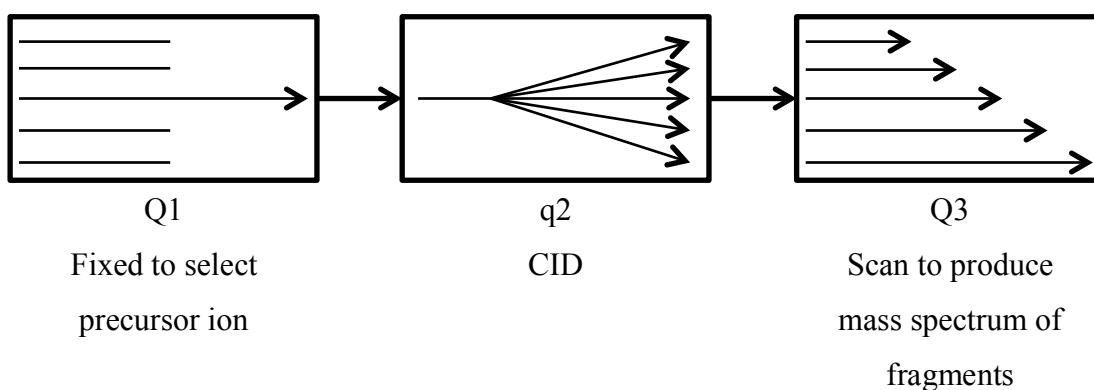
Figure 31. Operation of a triple quadrupole mass spectrometer in product ion scan mode.

Precursor ion scanning allows all of the ions that produce a particular fragment to be identified. As shown in Figure 32, in this mode it is Q3 that is fixed on the chosen fragment. A mass spectrum is produced from Q1, which is scanned through a range of m/z values to see which precursor ions produce the fragment with the m/z selected in Q3.
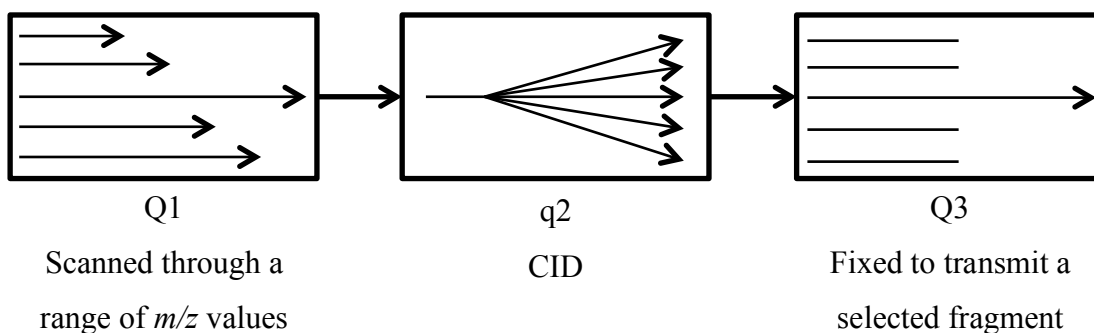
Figure 32. Operation of a triple quadrupole mass spectrometer in precursor ion scan mode.

In neutral loss scanning, it is the *m/z* difference between the precursor and product ion that is selected. Both Q1 and Q3 are scanned, with a constant offset between them. In Figure 33, Q1 scans the *m/z* range *a* to *b*, the neutral loss mass is set to *x* and so Q3 scans between $a - x$ and $b - x$. In this mode it is possible to detect ions which all have the same functional group, when the functional group is lost as a neutral.

Q1	q2	Q3
Scanned between	CID	Scanned between
m/z = a and *m/z = b*		*m/z = a − x* and
		m/z = b − x

Figure 33. Operation of a triple quadrupole mass spectrometer in neutral loss scan mode, with the neutral loss set to *x*.

Single/multiple reaction monitoring (SRM/MRM) allows detection of a particular analyte based on its precursor ion and one or more product ions. As shown in Figure 34, both Q1 and Q3 are fixed to transmit ions of selected *m/z* values. This method makes it possible to determine with great specificity and selectivity whether an analyte is present in a sample or not. Because of this specificity it is very sensitive, as effectively a lot of the noise which would be observed when the mass spectrometer scans is removed. It also has a very high duty cycle because all of the time is spent focused on the ions relevant for the selected transition.

Q1	q2	Q3
Fixed on a selected	CID	Fixed on a selected
precursor ion		fragment ion(s)

Figure 34. Operation of a triple quadrupole mass spectrometer in single/multiple reaction monitoring mode.

2.3.3   Time-of-Flight (TOF) Mass Analysers

The principle of a TOF is different to that of ion traps and quadrupoles. Rather than using electric fields to confine ions, a TOF differentiates ions of different m/z values based on their travel time through a field-free region. TOFs work because ions with the same kinetic energy but different m/z have different velocities in the absence of a field and can therefore be separated on the basis of differences in their flight times along a drift tube.

The general theory of operation of the TOF is relatively simple, and such an instrument was first described by W. E. Stephens in 1946.[124] The first commercial instrument was developed in the 1950s but problems with resolution and the need for electronics suitable for controlling the instrument and recording data on a short enough timescale meant that it was not until the 1980s that TOFs really took off.

A linear TOF-MS consists simply of a source, a flight tube and a detector, as shown in Figure 35. Since ions are separated based on differences in their flight times, they must be expelled from the source in packets. This makes TOFs particularly suited to use with pulsed ion sources such as MALDI. The ions are produced in the source and a pulse of ions is accelerated towards the field-free flight tube, where the ions are separated by their differing velocities before reaching the detector positioned at the far end of the flight tube.
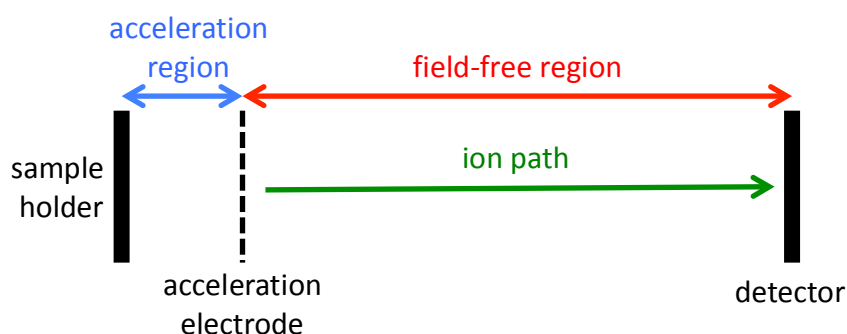
Figure 35. Schematic of a linear TOF mass analyser.

The equations below describe how ions with different m/z ratios have different velocities in the flight tube. An ion with mass, m, and charge, z, is accelerated from the source by the application of a potential, V, to give it kinetic energy, E_k, according to Equation 8 (where e is the charge of an electron and v is the velocity of the ion):

$$E_k = \frac{mv^2}{2} = zeV \qquad \text{Equation 8}$$

Equation 8 can be rearranged for v as shown in Equation 9:

$$v = \sqrt{\frac{2zeV}{m}} \qquad \text{Equation 9}$$

The length of time, t, an ion takes to travel in a straight line through a drift tube of length L is described by Equation 10:

$$t = \frac{L}{v} \qquad \text{Equation 10}$$

Substituting Equation 9 into Equation 10 gives Equation 11:

$$t^2 = \frac{m}{z}\left(\frac{L^2}{2eV}\right)$$

Equation 11

From Equation 11 it can be seen that measurement of t can be used to calculate the m/z of an ion, since the term in brackets is constant.

Although the mathematical theory of a TOF is quite simple, in practice it is more complicated and there were several technical issues that needed to be overcome in order to produce a TOF that can measure a mass spectrum with acceptable mass resolution. For all of the ions with a particular m/z to reach the detector at the same time they must have the same kinetic energy and travel the same distance (i.e. start in the same place). However, in practice there will always be a distribution of initial kinetic energies, and therefore velocities, and a spatial distribution of ions in the source which will result in a spread of times that ions of a particular m/z reach the detector, and therefore negatively affect the resolution. Developments in TOF design have sought to reduce these distributions, or at least their effects, to improve mass resolution. TOFs are often used with MALDI ion sources because in MALDI the ions are produced in a pulse and with a limited spatial distribution since they form from a surface. However, even using a source such as MALDI, the pulse is not sufficiently well defined to give high resolution and mass accuracy in the TOF so steps must be taken to correct for these distributions.

In 1955, Wiley and McLaren introduced a TOF that was designed to correct for both kinetic energy distribution and spatial distribution (using an EI source).[125] The spatial distribution of ions in the source results in ions that are closer to the detector receiving less kinetic energy from the extraction potential than those further from the detector, and therefore having lower velocities. The lower velocity ions are overtaken by the higher velocity ions at a point known as the space-focus plane. Wiley and McLaren's TOF used two extraction regions in order to correct for the spatial distribution, with the strengths of the two fields adjusted to bring the space-focus plane to the same place as the detector.[125,126] To correct for kinetic energy distribution they introduced a time delay between the production of ions and their extraction from the source. This was called time-lag focusing and meant that, before

the extraction pulse was turned on, the ions rearranged themselves in the source according to their initial velocities. This resulted in the ions with higher initial velocities travelling further towards the detector during the delay, and thus gaining less kinetic energy from the extraction pulse than those with lower initial velocities. In this way the initial kinetic energy distribution was reduced. These approaches helped to increase mass resolution but only over a relatively small mass range (they were able to give useful resolution only up to *m/z* 300), and the time delay required was mass dependent.[126,127] However, they did lay the foundations for further improvements which are present in the commercial instruments of today.

In modern TOFs the kinetic energy spread is usually corrected for by making ions with higher kinetic energy take a longer flight path. The most successful method, used in most commercial TOFs now, is the reflectron. Introduced in 1973, the reflectron is composed of a series of ring-shaped electrodes which act to slow down the ions, eventually stopping them and then accelerating them back out with their trajectory reversed.[128] As shown in Figure 36, the reflectron is positioned at the far end of the flight tube. The instrument is designed so that ions enter the reflectron at a slight angle, so that when they are reflected they do not retrace their exact path and the detector can be positioned so as not to interfere with the source. Ions with higher kinetic energy penetrate more deeply into the reflectron before being turned towards the detector than those with lower kinetic energy. This acts to increase the flight path length of ions with higher kinetic energies compared to those with lower kinetic energies, and with careful selection of the voltages on the reflectron electrodes this can allow ions of the same *m/z* to reach the detector at the same time, regardless of their initial kinetic energy. This method is able to correct for kinetic energy differences over a much larger *m/z* range than time-lag focusing could, though the optimum potential for the reflectron is still mass dependent, and was one of the most important factors in making TOFs viable practical mass spectrometers. It has the added advantage of increasing the length of the flight tube without increasing the length of the instrument.
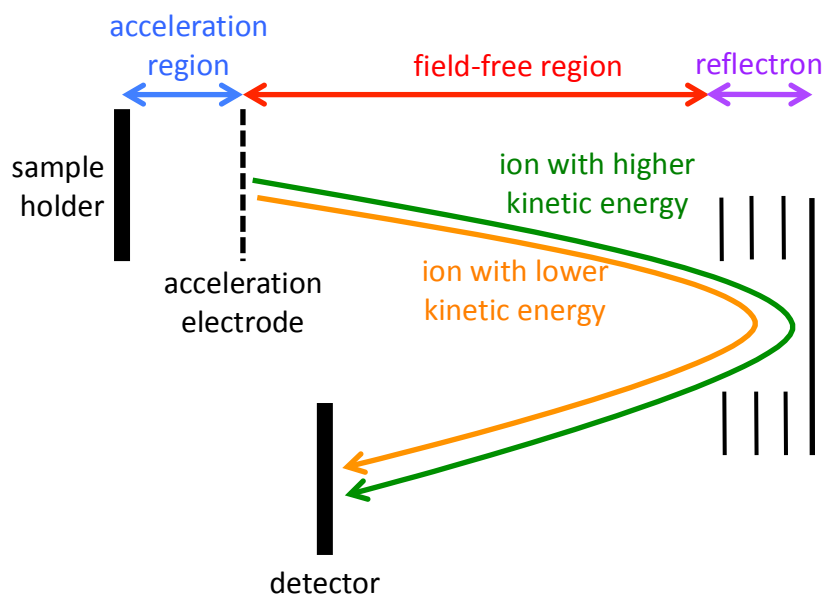
Figure 36. Schematic of a reflectron TOF mass analyser.

The advent of the reflectron, which corrected for kinetic energy distributions in a less mass-dependent fashion, meant that time-lag focusing fell out of favour and continuous extraction fields were used on many instruments (with pulsed ion sources, since the ions do of course still need to leave the source in a packet).[126] However, in the mid-1990s it was discovered that, when MALDI was the ionisation method, using a form of delayed extraction gave greater improvements in mass resolution than would be expected based on the results from Wiley and McLaren's work, with resolution approaching that of a reflectron TOF obtainable on a linear TOF.[129,130] This effect is thought to be due to a decrease in the range of initial ion velocities compared to when continuous extraction is used. In a MALDI plume, collisions resulting in kinetic energy exchange occur, causing changes in ion velocity. If there is a delay in the application of the extraction voltage then the ions do not have so much energy for exchange in the early collisions, and so the range of kinetic energies is not as wide as if the extraction voltage was applied continuously.[129] This became known as delayed pulse extraction, with the delay time used being of the order of a few hundred ns.[130] As with time-lag focusing, the optimum extraction voltage and time delay are mass dependent, with larger m/z values requiring higher voltage amplitudes or longer delays.[129] For a given m/z value, if a shorter delay time is used a higher voltage is required.[129]

One of the benefits of TOFs is that all of the ions are transmitted, with theoretically all of the ions reaching the detector, giving them a high duty cycle. They are also able to detect ions with a very wide mass range (theoretically unlimited upper mass), although the reflectron TOF does have a lower upper limit than linear TOFs.

2.3.4 Tandem MS in TOF Mass Analysers and the Bruker ultraflex III TOF/TOF MS

The internal energy of an ion affects its lifetime, since internal energy causes ions to fragment and those with a higher internal energy will fragment more quickly. If an ion's lifetime is more than the time it takes to travel through the flight tube, it will reach the detector unfragmented and its *m/z* value can be determined. However, if an ion fragments before reaching the detector it is possible to detect the precursor ion and the fragments, with the place in the TOF where the fragmentation occurs affecting how the precursor and its fragments can be detected.

If the fragmentation occurs in the source, before the ions are accelerated out, it is known as in-source decay (ISD). Since the acceleration provides all ions with the same kinetic energy, once the ions leave the source they will have different velocities, dependent on their *m/z* values.[88] This means that the precursor ions and their in-source fragments can be detected separately in both linear and reflectron TOFs. It is, however, not possible to determine which fragment ions come from which precursor. ISD has been used to gain peptide sequence information, since if a pure peptide is analysed all fragments will come from that peptide and so the precursor is already known.[131]

If the fragmentation occurs after the ions have left the source it is known as post-source decay (PSD). In TOF mass spectrometers, ions spend a relatively long time travelling through the flight tube, allowing time for PSD to occur. The activation energy for fragmentation is thought to be provided by collisions between ions and matrix molecules in the MALDI plume, and later collisions with residual gas in the flight tube.[132] In PSD, the precursor and fragments have the same velocity, and therefore different kinetic energies, determined by the mass of the fragments relative to that of the precursor. The fact that the velocities of the precursor and fragments are the same means that in a linear TOF the precursors and fragments all

reach the detector at the same time and are not distinguished. In contrast, in a reflectron TOF they can be separated because their different kinetic energies mean that they penetrate into the reflectron to different extents, with the lighter ions spending less time in the reflectron and consequently reaching the detector sooner than heavier ions. However, because the optimum potential for the reflectron is mass dependent, not all of the fragments will be detected with good mass resolution at any given reflectron potential. Therefore, one way to record all of the fragments is to cover the full *m/z* range by recording it over several smaller *m/z* portions with adjustments of the reflectron potential.[132] This can be time-consuming, with a total time reported of ~30 min per spectrum, made from 10-12 segments.[132] When carrying out PSD experiments, the precursor ions (and their fragments already formed, since they will be travelling at the same velocity) can be selected by a deflection gate between the source and the reflectron. The deflection gate is formed of an electrode that has a potential applied to it, stopping ions from passing. Ions are selected by briefly turning off the voltage at the time that the ions reach the gate, allowing them to pass, and then turning it back on to deflect later ions.[88]

In order to overcome some of the limitations of PSD in TOFs, such as the fact that the reflectron voltage must be stepped and that resolution and mass accuracy for the fragments can be poor,[88] TOF/TOF mass spectrometers have been developed. The Bruker ultraflex III is one such instrument.[133,134]

2.3.4.1 Bruker ultraflex III TOF/TOF MS

The Bruker ultraflex III is a mass spectrometer that combines a MALDI source with a tandem TOF mass analyser, as shown in Figure 37.

The first TOF is a short linear TOF (from the source to the LIFT cell in Figure 37), and the second (after the LIFT cell) is a reflectron TOF. Ions are accelerated into the first TOF and, when MS/MS is carried out, precursor ions and fragments are reaccelerated in the LIFT cell as they enter the second TOF. The ultraflex was designed specifically for proteomics experiments, allowing protein identification by producing peptide mass fingerprints, from enzymatically digested proteins, that can be used for database searching to identify the proteins.[134] MS/MS can be carried out on the peptides to gain structural information and improve protein identification, with both CID and laser-induced dissociation (LID) available for MS/MS.[134] LID involves unimolecular decay of ions, i.e. no collision gas is introduced. However, if more fragmentation information than can be obtained from LID-MS/MS is required, CID-MS/MS can be carried out. In this mode, a collision gas is introduced into the CID cell, which is positioned beyond the extraction region, to allow high-energy collisions to occur.[134]
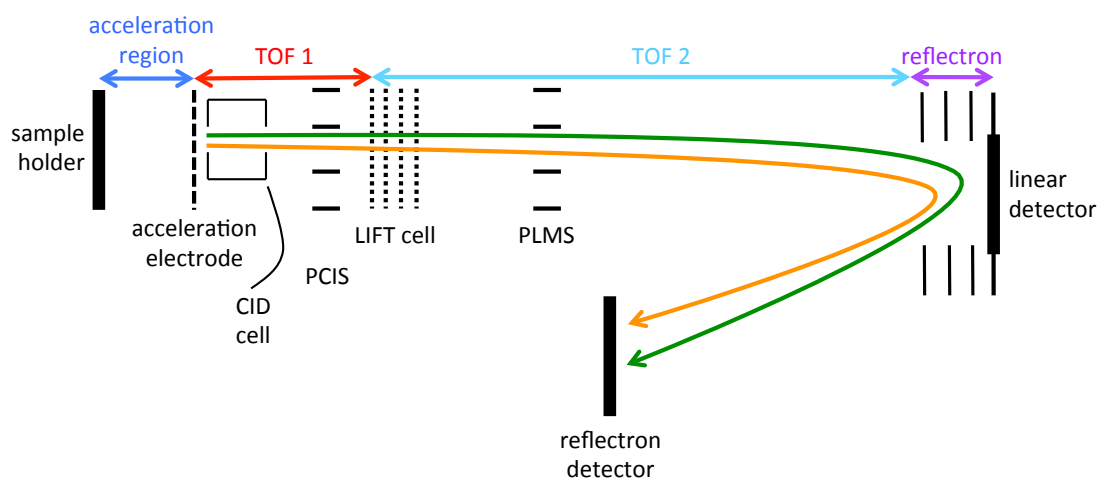
Figure 37. Schematic of the Bruker ultraflex III TOF/TOF MS.

In the ultraflex, ions are formed by MALDI and enter the flight tube after delayed pulse extraction. In MS mode, it can be used as either a linear or reflectron TOF, since there is both a linear detector and a reflector detector.[134] Using it as a linear TOF maximises sensitivity, since it allows precursor ions as well as their PSD

fragments to be detected at once so they all contribute to the signal. It also allows high *m/z* ions to be detected because there is no high mass limit on a linear TOF, whereas a reflectron TOF does have a high mass limit related the voltages that can be applied.

In LID-MS/MS mode, a high laser fluence is used to generate large numbers of precursor ions, which are accelerated with a relatively low voltage of 8 kV. This gives them a relatively long flight time (10 – 20 μs), during which they fragment.[134] The precursor ion is selected by the precursor ion selector (PCIS), which is a series of deflector plates that are switched on except at the time when the selected ions enter the deflection field. As soon as the selected ions leave the deflector the field is switched back on, allowing only those ions to pass.

The selected precursor and its fragment ions can be separated by the reflectron since they have the same velocity but different kinetic energies. However, the reflector can only focus ions with a difference in their kinetic energies of up to 30%.[133] This means that fragment ions with kinetic energy less than 70% that of the precursor are not detected. To overcome this problem, the ions are accelerated again, in the LIFT cell, to raise the energy of all of the ions so that the proportional difference between them is reduced. In the LIFT cell, the ions are accelerated with a voltage of 19 kV, giving them 19 keV of energy in addition to the energy they already had from the first acceleration (maximum 8 keV, dependent on the mass of the fragment). Therefore, after acceleration in the LIFT cell, the energy of the ions ranges from 19 keV to 27 keV, a difference of just under 30%, meaning that all ions are transmittable.

One final feature of the ultraflex increases the sensitivity of the instrument by reducing background ions. The post lift metastable suppressor (PLMS) is an ion deflector like the PCIS. It is used to deflect remaining precursor ions after the LIFT cell but before the reflector, to prevent PSD fragments formed after the LIFT cell contributing to chemical noise.[134]

2.3.5 Fourier Transform Ion Cyclotron Resonance MS (FTICR-MS)

FTICR-MS is a technique capable of very high mass accuracy and mass resolution. It works on the principle that when the trajectory of an ion is curved by a magnetic

field, if the velocity of the ion is low and the magnetic field is strong then the radius of the ion's trajectory becomes such that the ion is trapped in a circular motion. The frequency at which an ion travels in this circular trajectory is proportional to its *m/z* ratio, and so the *m/z* ratio can be determined by measuring the frequency.

FTICR-MS is an ion trapping technique where the ions are trapped in a Penning trap. The first Penning trap was built by Hans G. Dehmelt who, along with Wolfgang Paul, won a one quarter share of the 1989 Nobel Prize in Physics for their work on ion trapping. The first use of FTICR-MS was described in 1974 by Comisarow and Marshall.[135,136]

FTICR-MS involves trapping the ions inside a Penning trap, referred to as the FTICR cell. The cell is a box, with dimensions of a few cm, composed of three pairs of plates (trapping plates, excitation plates and detector plates) located in a magnetic field (Figure 38). The magnetic field is formed by a superconducting magnet, with typical field strengths currently routinely commercially available between 7 T and 15 T.[i] The largest field strength magnet used to date is 21 T, in a Bruker FTICR instrument.[ii] Various cell configurations exist, with shapes including cubic, cylindrical and cuboidal.[137] The ions are injected into the cell along the axis of the magnetic field and trapped radially by the magnetic field into a circular motion (known as the cyclotron motion). A small voltage (~1 V) is applied to the trapping plates, which are positioned at either end of the cell, perpendicular to the axis of the magnetic field, to stop the ions from leaving the cell along the magnetic field axis.[137] This causes a potential well between the trapping plates,[138] allowing ions to be trapped for extended periods of time.

---

[i] https://www.bruker.com/products/mass-spectrometry-and-separations/esimaldi-ftms/solarix/technical-details.html, accessed 4th September 2015

[ii] https://www.bruker.com/industries/clinical/news/single-view/article/worlds-highest-field-21-tesla-magnet-for-ft-icr-mass-spectrometry-installed-at-national-high-magn.html, accessed 4th September 2015
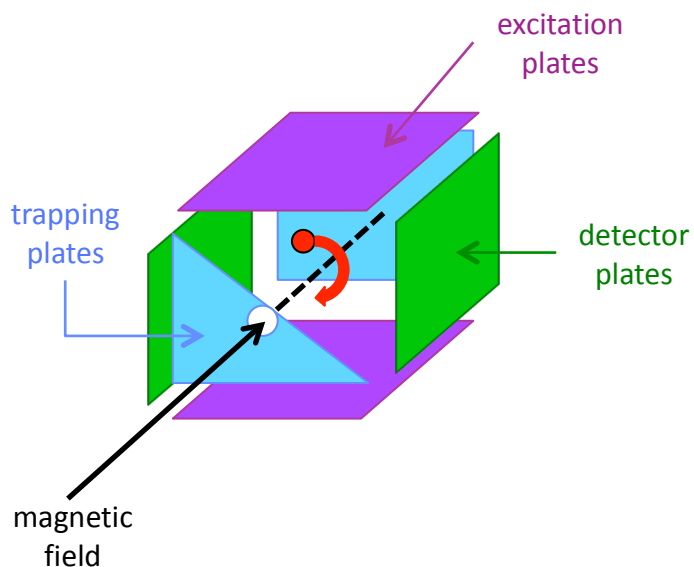
Figure 38. Diagram of an FTICR cell.

An ion travelling in cyclotron motion has a velocity and radius given in Equation 12:[88]

$$zB = \frac{mv}{r}$$

Equation 12

where:

z is the charge on the ion
v is the ion's velocity
B is the magnetic field strength
m is the mass of the ion
r is the radius of the trajectory

The cyclotron frequency, v, of the ion on its circular orbit is given by Equation 13:

$$v = \frac{v}{2\pi r}$$

Equation 13

Substituting Equation 12 into Equation 13 gives Equation 14:

$$v = \frac{zB}{m2\pi}$$

Equation 14

Equation 14 shows that an ion's cyclotron frequency is inversely proportional to its *m/z* ratio and the magnetic field strength. Since the magnetic field strength within an FTICR cell is kept constant, this means that measurement of the frequency can be used to calculate *m/z*. Importantly, the cyclotron frequency is independent of the ion's velocity. This is one of the reasons that such high resolution is possible in an FTICR instrument, since kinetic energy distributions, and hence velocity distributions, of the ions do not affect the measurement of *m/z*.[138]

Although the velocity, *v*, of an ion does not affect its cyclotron frequency, according to Equation 13 the velocity does affect the radius of the cyclotron orbit. Since the cyclotron frequency of an ion of a given *m/z* is constant, ions of that *m/z* with higher velocities, and therefore higher kinetic energies, have a larger radius of orbit. This fact is exploited in order to increase the radius of an ion's orbit to allow it to be detected within the FTICR cell.

The detector plates are a pair of electrically-connected electrodes that are positioned parallel to the direction of the magnetic field. When a cation passes close to a detector plate it attracts electrons to the plate, inducing a current. Because there are two plates and the ion induces a current in first one plate then the other as it travels round its orbit, an overall alternating current (the image current) is produced.[138] Detection of this current can be used to determine the cyclotron frequency and thus the *m/z* of the ion.

When injected into the FTICR cell, ions have a radius of the order of hundreds of μm,[137] small compared with the dimensions of the cell. Because the radius is small the ions do not pass near enough to the detector plates to induce a detectable current. In addition, although all the ions of a single *m/z* have the same cyclotron frequency, they are not all in phase: since an ion can start its path at any point on the circular trajectory the ions are spread out along this path and are not travelling in a coherent package.[137] This means that, statistically, the current induced by an ion in one plate will be cancelled out by a current induced in the other plate by an ion with the same *m/z* that is positioned 180° further round the orbit.

In order to increase the radius of the ions and make them have a coherent phase, resonant excitation is used. This is carried out by applying a small r.f. voltage (~1 V)

with the same frequency as that of the cyclotron motion to the third pair of plates, the excitation plates. This increases the kinetic energy of the ions and causes their radius to increase (Equation 13). All ions of one *m/z* are excited together and brought into phase. This means that the ions travel in a packet of appropriate radius, and so an image current can be produced in the detector plates.

During an FTICR experiment, all of the ions in the cell are excited simultaneously by applying a rapid sweep of the r.f. frequency, causing the ions' cyclotron orbits to increase so that ions of each *m/z* induce an image current. The radius that the ions have after excitation is a function of the r.f. voltage amplitude and the magnetic field strength, and is independent of *m/z*.[137] This means that ions of all *m/z* values in the trap can be excited to the same radius by applying an r.f. voltage of increasing frequency but constant amplitude. Once all of the ions are excited, an image current is induced in the detector plates that is a composite of the image currents from each *m/z* present. Fourier transformation is applied to this composite image current to give a frequency spectrum, which can then be converted into a mass spectrum through the use of a calibration. The image signal is known as a transient, and the longer the transient is recorded, the higher the resolution obtainable.[138] However, over time the amplitude of the transient reduces because collisions between the ions and neutral molecules within the cell mean that the ion packets lose their coherence. For this reason, ultra high vacuum is used in an FTICR cell, to maximise the duration of the transient.[138]

Besides cyclotron motion, the ions undergo so-called magnetron motion. This is caused by the interaction of the magnetic field with the trapping electric field, and causes the centre around which the cyclotron motion is based to move around the centre of the cell (Figure 39).[138] When the ions have been excited, their cyclotron radius is larger than the magnetron radius so the cyclotron motion can be detected (i.e. in Figure 39 the magnetron radius is larger than the cyclotron radius, but after excitation the cyclotron radius is the larger). Magnetron motion has much lower frequencies than cyclotron motion, and the frequency measured practically in FTICR is the difference between the cyclotron frequency and the magnetron frequency, rather than the cyclotron frequency alone. Magnetron motion serves no useful purpose, and can have negative effects through the formation of side bands in the mass spectrum and reduction in mass accuracy.[138] Therefore, its radius should be minimised by injecting the ions as close to the axis of the magnetic field through the centre of the cell as possible.
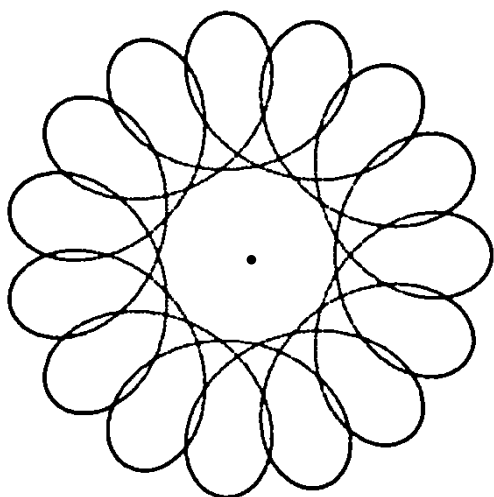
Figure 39. Diagram showing cyclotron and magnetron motion. An ion moves in cyclotron motion (the orbit with the smaller radius), but the point around which the cyclotron motion turns moves according to magnetron motion (the orbit with the larger radius, which orbits around the dot in the centre).[iii]

In FTICR-MS, very narrow peaks can be produced, meaning that they are high resolution instruments. Precise measurement of the cyclotron frequency allows very high mass accuracy to be obtained. Because the measured frequency is the difference

---

[iii] Created using http://www.artbylogic.com/parametricart/spirograph/spirograph.htm#

between cyclotron frequency and magnetron frequency, calibration must be carried out to determine accurate *m/z* ratios from measured frequencies. FTICR instruments are capable of measuring *m/z* values to less than 1 ppm, allowing exact mass determination to be carried out.

2.4 ELECTRON MULTIPLIER DETECTOR

Except for in the FTICR-MS, which has already been discussed, the MS detector used in all of the instruments in this thesis is the electron multiplier (EM), or a variant of it.

There are various designs of EM but the basic premise is that ions strike an electrode called a conversion dynode, which is held at a high potential (±3 kV to ±30 kV) with charge opposite to that of the ions.[88] When an ion strikes the conversion dynode it causes the emission of secondary particles, including ions, electrons and neutrals. In the type of EM known as a discrete dynode EM, beyond the conversion dynode are a series of further dynodes held at decreasing potentials. Secondary particles striking a dynode cause electrons to be emitted from that dynode. The electrons emitted are accelerated to the next dynode because it has a lower potential, and when they strike each dynode further electrons are emitted. In this way, a cascade of electrons is created, which induces an electric current at the end of the EM. This current is amplified and detected to give a signal corresponding to the arrival of the original ions.

As well as discrete dynode EM, there is a slightly different design of EM called a continuous dynode EM.[88] This is made from a curved tube of lead-doped glass, which emits secondary particles when struck by ions. In order to obtain a continuous accelerating field when there is effectively only one electrode, a voltage is applied between the two ends of the dynode. Electrons emitted by the conversion dynode enter the continuous dynode EM and, because of the shape of the dynode, strike the walls multiple times as they travel through, causing the emission of more electrons. An electric current is induced by the electrons in an anode at the end of the continuous dynode, which is measured to give a signal.

A variant of the continuous dynode EM is the microchannel plate (MCP) detector. This is used in most TOF instruments because it has a very fast response time, which is necessary for TOFs because they need to measure the timing of the signal very accurately and precisely.[88] The MCP is a plate with parallel cylindrical channels in it, that are coated with a semiconductor that emits secondary electrons. A potential difference is applied between the front of the plate (the input) and the back (the output) to produce continuous dynodes. MCPs can receive signals over a larger area than other (point) EM detectors.

2.5 CONCLUSIONS

Each of the techniques described in this chapter were used in the work described in this thesis. An understanding of the techniques is necessary in order to select methods that are suitable for the analysis to be carried out. Important factors include the selection of suitable of ionisation methods for the types of molecules to be analysed and the choice of mass analyser to provide the most useful information. For example, in cases where very low limits of detection are required and the identity of the analytes is known (and standards are available), SRM/MRM on a triple quadrupole mass analyser may be considered a suitable method. On the other hand, if very high mass accuracy is required, an FT-ICR instrument may be chosen. Other factors include the availability of instrumentation and, when developing methods intended to be used by other researchers in the future, their general availability to the researchers to whom the methods are being directed.

In the next chapter, the methods used in the work carried out are described. Subsequent chapters describe the results, including the development of the methods.

3 EXPERIMENTAL

This chapter describes all of the sample preparation and analytical methods that were used in the work described in this thesis. It is separated into sections by chapter.

All solvents used were either HPLC or analytical reagent grade.

3.1 METHODS FOR WORK DESCRIBED IN CHAPTER 4. RESULTS: DEVELOPMENT AND APPLICATION OF MALDI-MS FOR ARCHAEOLOGICAL LIPID ANALYSIS

3.1.1 Standard Lipid Mixes

Three different mixtures of authentic lipid standards (Sigma Aldrich) were prepared in hexane and diluted in hexane as necessary, as follows:

3.1.1.1 *Standard Lipid Mix A*

This mixture contained approximately 0.1 mg/mL each (accurately weighed out) of azelaic acid ($C_{9:0}$ dicarboxylic acid), palmitic acid ($C_{16:0}$ fatty acid), stearic acid (C-$_{18:0}$ fatty acid), cholesterol, tetratriacontane ($C_{34:0}$ alkane), DL-α-palmitin ($M_{16:0}$), glyceryl trimyristate ($T_{42:0}$), glyceryl tripalmitate ($T_{48:0}$) and glyceryl tristearate ($T_{54:0}$).

3.1.1.2 *Standard Lipid Mix B*

This mixture contained approximately 0.01 mg/mL each (accurately weighed out) of 1,2-diplamitoyl-*rac*-glycerol ($D_{32:0}$), 1,3-dilinoleoyl-*rac*-glycerol ($D_{36:4}$), glyceryl tridodecanoate ($T_{36:0}$), 1,2-distearoyl-3-palmitoyl-*rac*-glycerol ($T_{52:0}$) and the three TAGs used in standard lipid mix A ($T_{42:0}$, $T_{48:0}$, $T_{54:0}$).

3.1.1.3 *Standard Lipid Mix C*

This mixture contained approximately 0.01 mg/mL each (accurately weighed out) of azelaic acid, palmitic acid, stearic acid, cholesterol, $M_{16:0}$ $D_{32:0}$, $D_{36:4}$, $T_{36:0}$, $T_{42:0}$, $T_{48:0}$, $T_{52:0}$ and $T_{54:0}$.

3.1.2 Lipid Extraction from Potsherds

Lipids were extracted following an in-house protocol that is standard in BioArCh at the University of York, based on published methods (for example, that by Evershed *et al*[23]). Before use, all glassware was heated to 450 °C for 6 h to destroy organic matter. Drill bits were washed three times in dichloromethane (DCM), with ultrasonication.

Using a modelling drill (Dremel) the immediate internal surface of the potsherd (and accompanying soil if present) was removed and discarded. Approximately 1 g of powder was drilled from the resulting exposed interior surface of the potsherd onto a sheet of aluminium foil and transferred into a glass vial. 2:1 (v:v) DCM:methanol (approx. 5 mL) was added and the mixture was ultrasonicated in an ultrasonic bath, without heating, for 15 minutes followed by centrifugation at 3500 rpm from 5 min. The supernatant was decanted into a separate vial. The sonication and centrifugation steps were repeated twice and the extracts combined to give a total volume of approx. 15 mL. The volume of solvent was reduced to approx. 2 mL under a stream of N_2 with gentle heat (37.5 ºC). The extract was split roughly equally between three small vials (in order to allow different analyses to be carried out on each portion) and dried completely under a stream of nitrogen before storage at -20 ºC.

A solvent blank was prepared alongside each batch of samples. This was processed in exactly the same way as the other samples except that no potsherd powder was added to the vial.

3.1.3 Preparation for MALDI-MS Analysis

The MALDI-MS method was developed based on published literature.[139–142] Development of the method is described in chapter 4, with the final method as follows. One portion of each extract was dissolved in 100 μL hexane for analysis. A solution of 2,5-dihydroxybenzoic acid (DHB, 10 mg/mL) was prepared in acetonitrile. 1 μL of this solution was applied to spots of a Bruker AnchorChip™ MALDI target plate and left to dry in air. When dry, 1 μL acetone was spotted on top to recrystallise the DHB. When the acetone had evaporated, 1 μL lipid sample solution in hexane was spotted on top and left to dry in air. Samples were spotted in duplicate.

3.1.4 MALDI-MS Analysis

Samples were analysed in the positive mode using a Bruker ultraflex III MALDI-TOF/TOF MS with a smartbeam™ (frequency-tripled Nd:YAG, 355 nm) laser. Mass spectra were typically recorded over the *m/z* range 300 – 2000. Calibration was carried out using Bruker Peptide Calibration Standard II because this covered the mass range of the TAGs typically detected. Several spectra were summed in steps of 800 shots to give a total of typically 2400 shots which were combined into one spectrum, because this was found to give good results. The laser power was varied over the range 40-60 %. Data processing was performed using flexAnalysis 3.3 software. Product ion experiments were performed by manually selecting the precursor ion (with no collision gas), with the laser power varied over the range 60-100 %.

3.1.5 Fractionation

In order to try to improve lipid detection, fractionation was carried out on selected samples by solid-phase extraction (SPE), using silica SPE cartridges (500 mg, 6 mL, Agilent SampliQ).

The method used was modified from that published by Mirabaud *et al.*[24] Cartridges were conditioned with 2 mL of hexane, 2 mL of DCM:MeOH (2:1 v:v) then 8 mL of hexane. After sample loading, the fractions were sequentially eluted as detailed in Table 1.

Table 1. Solvents used for elution of each fraction in SPE of lipid extracts.

Fraction	Components	Solvent
A	Hydrocarbons	Hexane (1 mL)
B	DAGs, TAGs	DCM (2 mL)
C	Sterols, alcohols	2:1 DCM:methanol (1.5 mL)
D	Fatty acids	1:1 DCM:methanol (4 mL)

The fractions were dried under a gentle stream of nitrogen and analysed by MALDI-MS, as described in sections 3.1.3 and 3.1.4.

3.1.6 Preparation for OCI-HTGC-MS Analysis

Following the standard protocol used in BioArCh, *N,O*-bis(trimethylsilyl) trifluoroacetamide (BSTFA) containing 1 % trimethylchlorosilane (100 μL) was added to the dry lipid extract and heated at 70 ºC for 1 h. Excess BSTFA was removed under a gentle stream of nitrogen and the extract redissolved in 100 μL hexane (containing 10 ng C_{34} alkane as an internal standard) for analysis.

3.1.7 OCI-HTGC-MS Analysis

The GC column and temperature programme used are standard in BioArCh, and the settings for the on-column injector were chosen based on published literature.[9,35] OCI-HTGC-MS analysis was carried out using an Agilent 7890 GC coupled to an Agilent 5975 C single quadrupole MS. An Agilent DB-1HT capillary column (15 m × 0.32 mm, film thickness 0.10 μm) was used, with a retention gap of deactivated fused silica (1 m × 0.32 mm) placed between the injector and column to protect the column.[9] The oven was set to an initial temperature of 50 ºC for 2 min, followed by an increase to 350 ºC at 10 ºC/min with the final temperature held for 15 min (total run time 47 min). Samples were manually injected on-column using a fused silica needle. The injector was programmed to follow the same temperature sequence as the column. The carrier gas was He with a flow rate of 3 mL/min. The MS interface was at 280 °C. Data were acquired over the *m/z* range 50 – 800 after a solvent delay of 2 min.

3.2 METHODS FOR WORK DESCRIBED IN CHAPTER 5. RESULTS: APPLICATION OF MALDI-MS TO ARCHAEOLOGICAL SAMPLES FROM DURRINGTON WALLS

3.2.1 Lipid Extraction from Potsherds

Lipids were extracted using the same protocol as for the work presented in chapter 4, described in section 3.1.2. For samples prepared by Lisa-Marie Shillito for HTGC-FID analysis, an internal standard of C_{34} alkane was added as a solution in hexane to the drilled powder.

3.2.2 Preparation for MALDI-MS Analysis

Samples were prepared as for the work presented in chapter 4, described in section 3.1.3.

3.2.3 MALDI-MS Analysis

Samples were analysed as for the work presented in chapter 4, described in section 3.1.4. Selected samples were, in addition, analysed using a Bruker solariX FTICR MS with a 9.4 T magnet and a MALDI source with a smartbeam™ (frequency-tripled Nd:YAG, 355 nm) laser. Calibration was carried out using the same peptide mixture as for the ultraflex (Bruker Peptide Calibration Standard II). Data processing for data from the solariX was performed using DataAnalysis 4.0 software.

3.2.4 Fractionation

Fractionation was carried out as for the work presented in chapter 4, described in section 3.1.5.

3.2.5 Preparation for OCI-HTGC-MS Analysis

Samples were prepared as for the work presented in chapter 4, described in section 3.1.6.

3.2.6 OCI-HTGC-MS Analysis

Samples were prepared as for the work presented in chapter 4, described in section 3.1.7.

3.2.7 Preparation for HTGC-FID Analysis

This work was carried out by Lisa-Marie Shillito and published in Craig *et al.*[143] Samples were prepared in the same way as for OCI-HTGC-MS analysis (section 3.1.6) except that the internal standard was C_{36} alkane.

3.2.8 HTGC-FID Analysis

This work was carried out by Lisa-Marie Shillito and published in Craig *et al.*[143] The method used is standard in BioArCh.

HTGC-FID analysis was carried out using an Agilent 7890A GC coupled to an FID with an Agilent 7693 autosampler. The column and temperature programme used were the same as those for the OCI-HTGC-MS analysis (section 3.1.7) and 1 μL was injected in splitless mode. No retention gap was used. The injector was held at 300 ºC and the carrier gas was H_2 with a flow rate of 1.5 mL/min.

3.3 METHODS FOR WORK DESCRIBED IN CHAPTER 6. RESULTS: LIPID ANALYSIS OF CHLORITE COOKING VESSELS FROM ANCIENT MERV, TURKMENISTAN

3.3.1 Lipid Extraction

Lipids were extracted following an in-house protocol that is standard in the Department of Conservation and Scientific Research at The British Museum. This method differs slightly from that used in BioArCh so is described separately, but is expected to give similar results to those obtained using the BioArCh method. All glassware was acid washed and rinsed with DCM before use. Drill bits were ultrasonicated in DCM three times before use.

Using a modelling drill, the immediate internal surface (and accompanying soil, if present) was abraded and discarded, followed by approximately 1 g of powder being drilled from the now exposed interior surface of the potsherd onto a sheet of aluminium foil and transferred from there into a glass vial. An internal standard of C_{34} alkane solution (10 μL, 1 mg/mL in DCM) was added to the dry powder. 2:1 (v:v) DCM:methanol (approx. 10 mL) was added and the mixture was ultrasonicated in an ultrasonic bath, without heating, for 10 minutes. The mixture was transferred to a glass centrifuge tube and centrifuged at 3000 rpm for 5 min. The supernatant was transferred into a clean vial using a glass Pasteur pipette. 2:1 (v:v) DCM:methanol (approx. 10 mL) was added to the centrifuge tube to re-suspend the potsherd powder and the mixture was transferred back to the original vial. The sonication and centrifugation steps were repeated and the extracts combined to give a total volume of approx. 20 mL. The extract was dried completely

under a stream of N_2 with gentle heat (37.5 ºC) before being redissolved in 1 mL DCM. Solutions were stored at -20 ºC.

An extraction blank was prepared alongside each batch of samples.

3.3.2 Preparation for HTGC-MS Analysis

The methods used for HTGC-MS preparation and analysis are standard in the Department of Conservation and Scientific Research at The British Museum. 25 % of each extract was used for HTGC-MS analysis. 250 µL of the extract in DCM was transferred to a clean glass vial and dried under a stream of nitrogen. BSTFA containing 1 % trimethylchlorosilane (100 µL) was added to the dry extract and heated at 70 ºC for 1 h in order to trimethylsilylate protic sites to increase volatility and improve chromatographic behaviour. Samples were injected, as described in section 3.3.3, without further manipulation.

3.3.3 HTGC-MS Analysis

HTGC-MS analysis was carried out using an Agilent 6890N GC, with an Agilent 7683B autosampler, coupled to an Agilent 5975C single quadrupole MS. An SGE HT-5 capillary column (12 m × 0.22 mm, film thickness 0.10 µm) with a deactivated fused silica retention gap (1 m × 0.53 mm) was used and 1 µL aliquots of sample solution were injected on-column. The oven was set to an initial temperature of 50 ºC for 2 min, followed by an increase to 370 ºC at 10 ºC/min with the final temperature held for 15 min (total run time 49 min). The injector was set to follow the same temperature programme as the oven. The carrier gas was He with a flow rate of 1.5 mL/min. The MS interface was at 350 ºC. Data were acquired in scan mode (*m/z* 50 – 750) after a solvent delay of 4.5 min. The lipid yield was quantified by integrating the peak areas and converting the total peak area to mass of lipid by comparison with the internal standard, and reporting a yield relative to the mass of potsherd powder extracted.

3.3.4 Preparation for MALDI-MS Analysis

25 % of each extract was dried under a gentle stream of nitrogen and redissolved in 100 µL hexane for analysis. Samples were spotted as reported for previous chapters, described in section 3.1.3.

3.3.5 MALDI-MS Analysis

Samples were analysed as reported for previous chapters, described in section 3.1.4.

3.4 METHODS FOR WORK DESCRIBED IN CHAPTER 7. RESULTS: DETECTION OF OPIUM ALKALOIDS IN A CYPRIOT BASE-RING JUGLET

3.4.1 Solvents and Standards

HPLC grade and LC-MS grade water and methanol, and HPLC grade acetonitrile and DCM, were purchased from VWR Chemicals. HPLC grade hexane was purchased from Fisher Scientific. Papaverine hydrochloride (solid) and morphine solution (100 μg/mL in methanol) were purchased from Sigma Aldrich. Thebaine solution (1 mg/mL in methanol) was purchased from Thames Restek UK Ltd. A generic co-codamol tablet (30 mg codeine, 500 mg paracetamol) was obtained and a solution containing 1 mg/mL codeine (and consequently 16.7 mg/mL paracetamol) in methanol was prepared from it. A stock solution of papaverine (1 mg/mL) was made up in methanol and the solutions were stored at 5 °C (papaverine and codeine) or -80 °C (morphine and thebaine, due to the need to keep these compounds locked away). Working solutions were made by dilution of the stock solutions.

Solutions of papaverine and thebaine were prepared for quantitation purposes. Papaverine solutions in the range 1 ng/mL to 3000 ng/mL (giving masses of 5 pg – 15 ng injected into the HPLC), and thebaine solutions in the range 1 ng/mL – 500 ng/mL (5 pg – 2.5 ng injected), were prepared.

3.4.2 Oil Samples

Two types of cold pressed organic poppyseed oil (Oshadhi and Fandler) and olive oil were purchased. 1 mL samples of different types of oil were spiked with working papaverine solutions, to generate samples with which to validate extraction procedures.

3.4.3 Extraction and Purification

The extraction and purification methods were developed from those described by Guo *et al.*[144]

DCM was added to samples when necessary to solubilise/suspend the sample. Alkaloids were extracted by adding 4 mL HCl (0.1 M) to the sample, vortex mixing for a few seconds followed by ultrasonicating for 15 min in an ultrasonic water bath at ambient conditions. 1 mL hexane was added, followed by vortex mixing for a few seconds and centrifugation to separate the layers, and the organic (DCM and hexane) layers were removed. The aqueous layer was subjected to SPE.

SPE was carried out using Strata C18-E (50 mg/1 mL) cartridges (Phenomenex). Each cartridge was conditioned with 1.5 mL methanol followed by 1.5 mL water. After loading the aqueous sample the cartridge was washed with 1 mL water and the alkaloids eluted with 1 mL methanol. The alkaloid-containing extract was dried under a stream of N_2 and redissolved in water:acetonitrile (9:1, v/v) for analysis by HPLC-MS. The volume of solvent used was the same as that of the original oil sample. Archaeological samples were redissolved in 100 μL solvent.

Blank extractions were carried out alongside the samples, involving adding all of the reagents but not the sample to a sample tube and carrying out the full extraction and purification process.

3.4.4 LC-MS Analysis

The HPLC method was modified from that described by Guo *et al.*[144] HPLC-MS analysis was carried out with a Dionex UltiMate 3000 HPLC fitted with a Dionex Acclaim 120 C18 column (3 μm, 120 Å, 2.1 x 150 mm) coupled to a Bruker HCTultra ETD II ion trap MS, a Bruker solariX XR 9.4T FTICR MS or an Applied Biosystems/MDS Sciex API 3000 triple quadrupole MS. All mass spectrometers were operated in positive ion mode with electrospray ionisation (the triple quadrupole fitted with Sciex's TurboIonSpray source). The mobile phase was composed of water (solvent A) and acetonitrile (solvent B). The mobile phase flow rate was 220 μL/min and the gradient was as follows: 10 % B initially, increasing linearly to 90 % B over 5 min. A further increase to 95 % B took place over 0.1 min followed by holding for 2 min. B was then returned to 10 % over 0.1 min and held for 5 min to allow column equilibration. The column compartment was held at 40 °C and the injection volume was 5 μL.

On the ion trap and FTICR mass spectrometers, extracted ion chromatograms for each analyte were produced. On the triple quadrupole MS, SRM was used in order to obtain the lowest limits of detection possible, and to allow quantitation. Suitable transitions were identified from the literature[144–150] and the instrument parameters were optimised by direct infusion of a solution of 10 ng/mL of each analyte in methanol. Table 2 shows the transitions and optimised parameters for each analyte. The ion trap was used for method development experiments before moving onto the triple quadrupole in order to gain optimal sensitivity, and the FTICR was used to obtain full scan data with high mass accuracy in order to try and detect compounds for which standards could not be obtained. Extracted ion chromatograms were produced from the full scan data, with *m/z* values for [M+H]$^+$ extracted to 3 decimal places ± 0.001.

Table 2. SRM transitions for analysis of the alkaloids, together with optimised triple quadrupole instrument parameters.

Analyte	Transition / *m/z*	Declustering Potential / V	Focusing Potential / V	Entrance Potential / V	Collision Energy / eV	Collision Cell Exit Potential / V
Morphine	286 → 165	80	80	15	50	12
Codeine	300 → 215	35	200	15	35	15
Thebaine	312 → 281	22	150	10	17	22
Papaverine	340 → 202	45	280	15	36	15

3.4.5 Artificial Ageing

Poppyseed oil samples (100 μL each) were artificially aged by heating, sealed in glass Kilner® jars under various conditions, at 60 °C in a GC oven, as described in Table 3. Samples were aged either at 100 % relative humidity (achieved by placing a small vial of deionised water in the jar) or at ambient humidity; in a thin layer on a glass slide or as a pool in a 1 mL vial; with or without approx. 40 – 50 mg of ceramic powder added to simulate the juglet in which the archaeological material had been discovered. The ceramic powder was prepared by crushing a portion of open-fired pot and heating the powder at 450 °C for 6 h to destroy organic matter. Samples

were extracted after varying amounts of time in the oven: 17 days, 8.5 months, 10.5 months and 11 months.

Table 3. Properties of each of the samples prepared for artificial ageing of poppyseed oil. Each sample is represented by a tick.

Heating time	High Humidity				Low Humidity			
	Thin layer, with ceramic	Thin layer, without ceramic	Pool, with ceramic	Pool, without ceramic	Thin layer, with ceramic	Thin layer, without ceramic	Pool, with ceramic	Pool, without ceramic
17 days (10 samples)								✓
8.5 months		lost		✓		✓		✓
10.5 months	✓	lost	✓	✓	✓	✓	✓	✓
11 months					✓	✓	✓	✓

3.4.6   Archaeological Sample

Samples of the residue sealed inside a base-ring juglet (BM Reg. No.: 1981,1218.53) were taken using a dissection microprobe with bent needle inserted though a hole drilled into the base. The thick, brown, oily contents were smeared onto the insides of six small glass vials. Each portion weighed approximately 40 – 80 mg.

4 RESULTS: DEVELOPMENT AND APPLICATION OF MALDI-MS FOR ARCHAEOLOGICAL LIPID ANALYSIS[iv]

4.1 OVERVIEW

It is important in the analysis of lipid extracts of archaeological pottery to be able to detect the full range of lipids present in the samples. HTGC and HTGC-MS are well established for lipid analyses in the archaeological science field, but gas chromatography is not ideally suited to large molecules such as intact TAGs because they are heat labile and likely to break down at the high temperatures required to elute them.[151] Another disadvantage is the cycle time, which is approximately 45 - 50 minutes for a typical HTGC programme[23,32,143] plus around 10 minutes equilibration time, resulting in approximately one hour per sample. Since many hundreds of potsherds can be excavated from one archaeological site, a method that could increase throughput and improve the detection of TAGs would be a great advantage.

Modern mass spectrometric methods hold great promise for the analysis of archaeological lipids due to their ability to detect much larger molecules than GC-based methods. Nanoelectrospray has already been shown to be more suitable for the detection and characterisation of intact TAGs in archaeological samples than HTGC[24] and it would be beneficial to investigate other mass spectrometric methods to see if there are other methods that may be able to contribute to the archaeological science field.

4.2 AIMS

The aims of this chapter were to develop MALDI-MS for archaeological lipid analysis in advance of its application to archaeological samples reported in the following chapters. MALDI-MS is widely reported for the analysis of TAGs in animal and plant fats (for example in their use as food products)[139–142] so its extension to archaeological samples seems a logical step. Development of the method has thus been the focus of the work described in this chapter. This has

---

[iv] N.B. In general, in the text, *m/z* values are rounded down to give an integer value.

involved optimisation of the MALDI-MS conditions and application to lipid extracts from a selection of modern animal fats and extracts of replica pots which had been heated with milk in them and buried for varying lengths of time.

4.3   MALDI METHOD DEVELOPMENT USING STANDARDS

4.3.1   MALDI Target Plate and Matrix Choice

The instrument used for all of the experiments reported in this chapter was a Bruker ultraflex III TOF/TOF MS, which has a MALDI ion source.

There are a variety of different target plates available for use with Bruker MALDI interfaces. Three of these were tested for analysis of the samples in this work: polished steel, a ground aluminium plate and AnchorChip™ plates. AnchorChip™ plates have a hydrophilic patch on each spot that is surrounded by a hydrophobic ring. This hydrophilic patch is called an 'anchor', and is designed to concentrate the sample into a smaller area and in a specific place within the target spot (making it particularly suitable for automated MALDI-MS data acquisition).[152] The polished steel plate was found to be unsuitable for this work because the solvents required for dissolving lipids (e.g. hexane or DCM) have too low a surface tension to produce discrete spots on this surface, but samples were able to be spotted on the ground aluminium and AnchorChip™ plates.

Several matrices have been reported for the MALDI analysis of lipids, including 2,5-dihydroxybenzoic acid (DHB),[142] α-cyano-4-hydroxycinnamic acid (CHCA)[140] and dithranol.[153] For TAG analysis, DHB is one of the most commonly used matrices, and a published comparison of matrices for analysis of TAG standards and in food oils found that DHB gave better results than CHCA and dithranol.[139] DHB and CHCA were tested in the work presented here.

A mixture of authentic lipid standards, denoted standard lipid mix A to distinguish it from other lipid mixtures described in this thesis, was prepared in hexane. The mixture contained equal masses of azelaic acid ($C_{9:0}$ dicarboxylic acid), palmitic acid ($C_{16:0}$ fatty acid), stearic acid ($C_{18:0}$ fatty acid), DL-α-palmitin ($M_{16:0}$), cholesterol, tetratriacontane ($C_{34:0}$ alkane), glyceryl trimyristate ($T_{42:0}$), glyceryl tripalmitate ($T_{48:0}$) and glyceryl tristearate ($T_{54:0}$). It was analysed on the ground aluminium and

AnchorChip™ plates, using DHB or CHCA as matrices (Figure 40). 0.1 µg (~0.1 −
0.5 nmol) of each lipid was deposited on each spot.
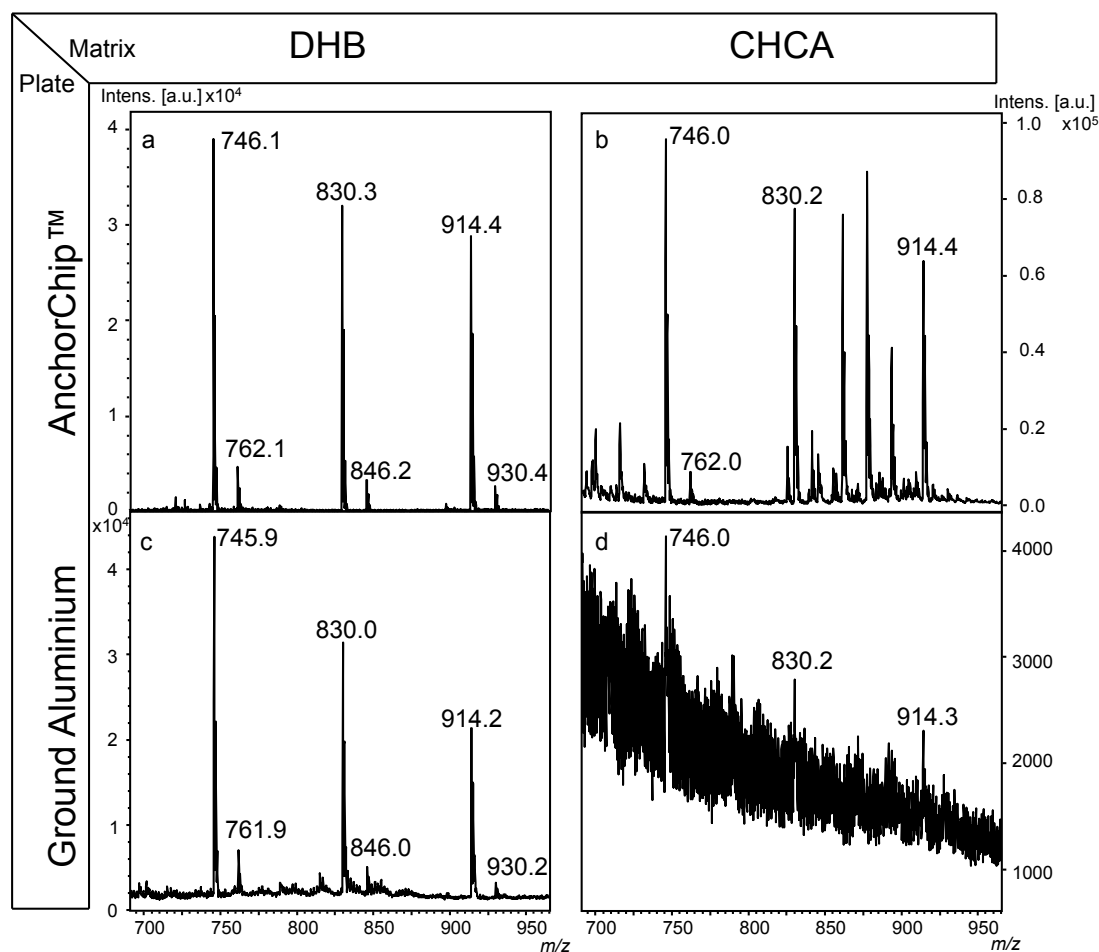
Figure 40. MALDI mass spectra showing the standard lipid mix on two types of
MALDI target plate with two different matrices. m/z 746 is $[T_{42:0} + Na]^+$, m/z 830 is
$[T_{48:0} + Na]^+$ and m/z 914 is $[T_{54:0} + Na]^+$. The corresponding $[M + K]^+$ peaks are at
m/z 762, 846 and 930, respectively. a) DHB on AnchorChip, b) DHB on ground
aluminium plate, c) CHCA on AnchorChip, d) CHCA on ground aluminium plate.

In MALDI the solvents would usually be chosen to dissolve both the matrix and the

sample, in order to produce a matrix/sample co-spot by recrystallising the matrix

when the sample is spotted on top (although there are multiple ways to produce the

co-spot). However, in the case of TAG analysis with DHB this is not possible due to

differences in the solubility of these two types of molecule. It has been shown that

DHB performs well as a matrix for TAG analysis when spotted on the plate in

acetone.[139] However, when this was attempted discrete spots could not be produced.

Instead, the DHB solution was prepared in acetonitrile (10 mg/mL), and after the

DHB spot had dried, 1 µL acetone was spotted on top and allowed to dry in order to

recrystallise the DHB. The sample in hexane (1 μL) was then spotted on top. Spotting the acetone on top of the dried DHB spot seems to give matrix crystals that produce good results for TAGs. Tests showed that TAGs are not soluble in acetone.

CHCA solution was prepared in 1:1 acetonitrile:water (10 mg/mL) and 1 μL spotted on the plate. For proper comparison with the DHB matrix, 1 μL aetone was spotted on half of the CHCA spots and allowed to dry. 1 μL sample in hexane was then added.

For HTGC analysis typically carried out at York, hexane is used as the solvent in which samples are dissolved for analysis (see chapter 3). This is the reason that standard lipid mix A was prepared in this solvent. The high volatility of hexane makes it very difficult to spot the small volumes required for MALDI-MS analysis because the solvent tends to evaporate in the pipette before it can be deposited onto the plate. To overcome this problem, a gel-loading pipette tip was used, which has a very narrow tip so that the solvent does not evaporate from it so quickly.

In the analysis of standard lipid mix A (Figure 40) TAGs were observed, mainly as $[M+Na]^+$ ions with small $[M+K]^+$ peaks also present in some cases. Both of the plates and matrices produced spectra showing TAGs, but the DHB matrix clearly gave much better signal-to-noise than CHCA, and of the two plates, the signal-to-noise on the AnchorChip™ plate was superior to that on the ground aluminium plate. Therefore, the AnchorChip™ plate and DHB were used for all further analyses. None of the other lipids were detected, showing that MALDI-MS is selective for TAGs over fatty acids, MAGs and alkanes. This is to be expected since MALDI-MS is generally less suitable for low molecular weight analytes because of interference from matrix ions. There have, however, been reports of the analysis by MALDI-MS of lower molecular weight lipids using specific matrices. For example, the porphyrin-based matrix *meso*-tetrakis(pentafluorophenyl)porphyrin (MTPFPP) has been used for fatty acid analysis.[154–156] MTPFPP has a molecular weight of 974 Da so matrix ions are not produced in the fatty acid *m/z* region and interference is not an issue as it is with conventional matrices. However, the LOD for fatty acids when using this matrix is in the μg region,[157] making it of limited use for archaeological samples where there is typically only μg of lipid present in total. The basic matrix 9-aminoacridine (9-AA) has also been used for carboxylic acid analysis, including

the $C_{16:0}$ fatty acid, in negative ion mode.[158] However, although these matrices are useful for fatty acid analysis, the methods used are not suitable for detection of TAGs as well, so it is difficult to detect the full range of lipids expected in archaeological samples using a single MALDI-MS method.

4.3.2   Limit of Detection

Standard lipid mix B (containing equal masses of the diacylglycerides 1,2-diplamitoyl-*rac*-glycerol ($D_{32:0}$) and 1,3-dilinoleoyl-*rac*-glycerol ($D_{36:4}$) (where the term '*rac*' indicates that the compound is a racemic mixture), and triacylglycerols glyceryl tridodecanoate ($T_{36:0}$), glyceryl trimyristate ($T_{42:0}$), glyceryl tripalmitate ($T_{48:0}$), 1,2-distearoyl-3-palmitoyl-*rac*-glycerol ($T_{52:0}$) and glyceryl tristearate ($T_{54:0}$)) in hexane was analysed by MALDI-MS at four different concentrations, giving amounts of approximately 20 pmol, 2 pmol, 0.2 pmol and 20 fmol of each lipid per MALDI spot. Figure 41 shows MALDI mass spectra of the three most concentrated lipid samples. Standard lipid mix B was prepared to contain DAGs (including an unsaturated DAG) as well as TAGs, since DAGs were not included in standard lipid mix A.
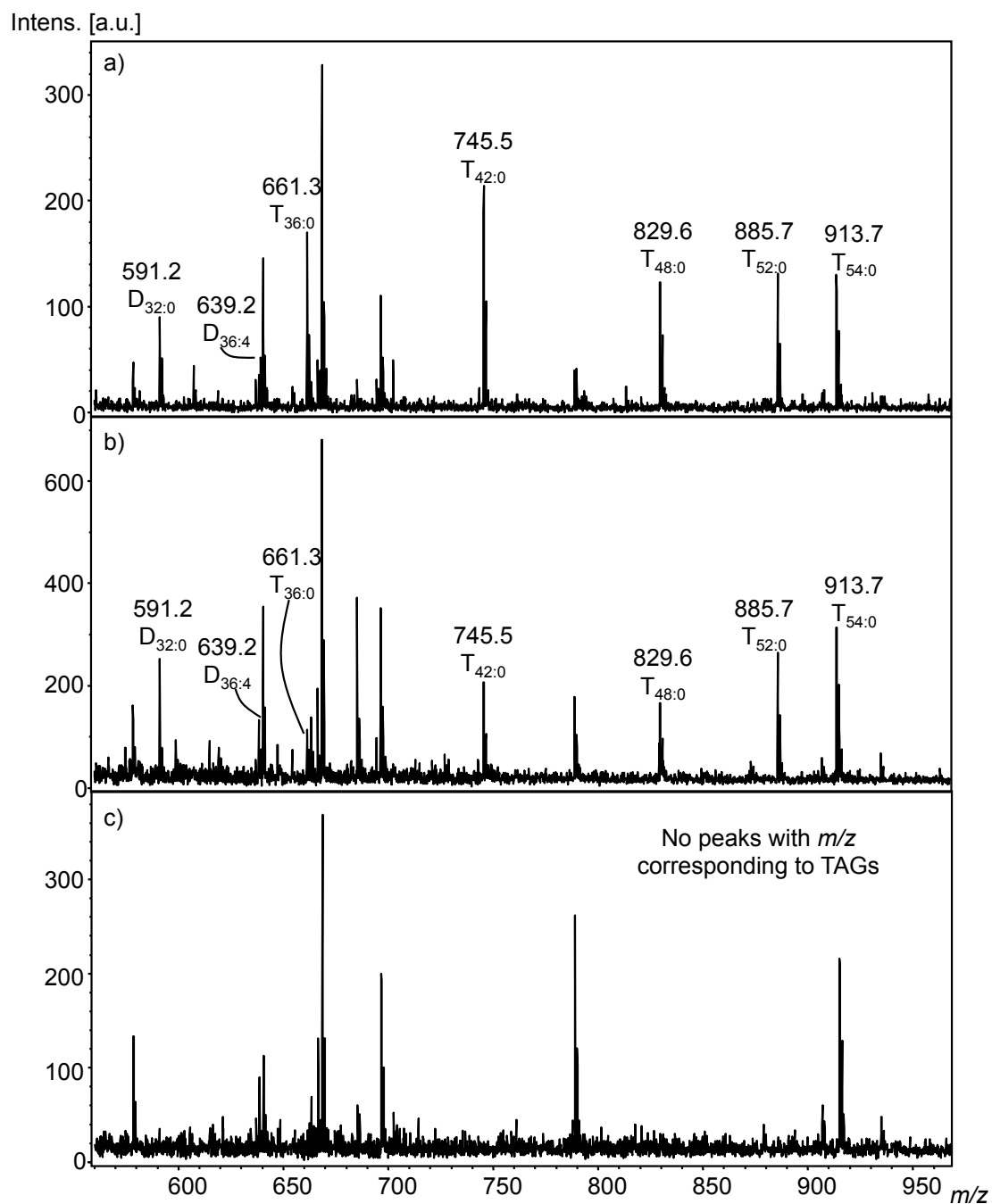
Figure 41. MALDI mass spectra of lipid mix B with different amounts of lipid spotted. a) 20 pmol each lipid per spot; b) 2 pmol each per spot; c) 0.2 pmol each per spot.

As can be seen in Figure 41, TAGs and DAGs were clearly detected in the two spots with higher amounts of lipid (a and b), with visual inspection of the spectra indicating slightly lower signal-to-noise (S/N) in the spectrum of the spot with less analyte of those two (b). Although there is some difference in the relative intensities of each peak within a spectrum, this does not appear to be consistent between

117

spectra, as demonstrated by the intensity of the peak at *m/z* 745, which is the most intense TAG peak in Figure 41a but is not in Figure 41b. It has been reported that MALDI-MS signal decreases with increasing TAG mass.[139] However, this trend was not observed here. Of the two DAGs analysed, $D_{32:0}$ has a similar S/N to the TAGs, while $D_{36:4}$ has a lower S/N than the other lipids in the sample. This may be partly due to an intense peak at *m/z* 640.4 interfering with the signal from the lipid (this peak does not correspond to a TAG or DAG, and is also present in all of the spectra, indicating that it is due to contamination, either of the sample plate or solvents). It may also indicate that the sensitivity of MALDI-MS for unsaturated acyl lipids is lower than that for saturated ones. However, published work has indicated that this is not the case. In fact, one paper reports that the signal of a fully saturated TAG is suppressed when added to a sample of oil containing polyunsaturated TAGs, when compared to the saturated TAG on its own.[140] The authors attribute this to the unsaturated TAGs having a higher affinity for Na^+ than the saturated TAG.

The sample with approximately 0.2 pmol each lipid per spot was below the limit of detection, because no peaks corresponding to the lipids were detected, as was the sample with 20 fmol per spot (data not shown). This shows that the limit of detection for a mixture of pure lipids by MALDI-MS using this method is between 2 pmol and 0.2 pmol component per spot. It might be supposed that for crude total lipid samples extracted from archaeological artefacts, the LOD would be higher due to the presence of sample-derived contaminants that could interfere with the ionisation of the lipids. A value for a typical total lipid extract (calculated as the mean across many samples) from archaeological potsherds has been reported to be 100 µg/g of pottery.[18] In the analysis carried out here, lipids are typically extracted from 1 g of ceramic material, that portion split into three and 1/100 of one extract spotted onto the plate. This would give ~0.3 µg of lipid on the spot. Clearly, most of this lipid will be degraded and not in the form of intact TAGs, but if it was 100 % intact TAG this would equate to around 400 pmol (calculated using a molecular mass of 807 g mol^{-1}, as for T48:0). Therefore, even if only 1 % of the surviving lipid is in the form of intact TAGs, the amount of TAG present is above the limit of detection in many cases. Most published papers do not state what proportion of the lipid detected in archaeological potsherds is in the form of intact TAGs so it is not possible to determine a typical value for this. However, one of the early publications of the

application of HTGC-MS to archaeological potsherds found that, in samples in which TAGs were detected, individual TAGs were almost always present at levels over 1 %, with the total TAG content therefore being more than this.[22] Of course, the amount of TAG preserved will be dependent on the general level of preservation in the samples, but these results show that MALDI-MS, when carried out as optimised, is likely to have good enough limits of detection (LODs) to be used for detecting TAGs in archaeological potsherd extracts.

Analysis of standard lipid mix B shows that both DAGs and TAGs can be detected using MALDI-MS. This is in agreement with the literature, where detection of DAGs[159] and both DAGs and TAGs in one method[160] have been reported.

4.3.3   Addition of Cations to Prepared Samples

Based on the observation that TAGs were detected mainly as $[M+Na]^+$ ions, with small amounts of $[M+K]^+$, experiments were carried out to determine if the fact that there was more $[M+Na]^+$ was due to a higher affinity of the TAGs for sodium than potassium, or if it was because there is more sodium than potassium present in the prepared sample spots. The source of these cations in MALDI mass spectra (when none have been deliberately added to the samples) is the solvents, which gain the metals from the glassware that they are stored in. To test the relative affinity of the TAGs for sodium and potassium, equimolar amounts of the two metals were added to the samples on the plate in the form of sodium acetate and potassium acetate (10 nmol each metal per spot).

When no cations were added, the usual method of spotting DHB was in acetonitrile (1 µL, 10 mg/mL) and allowing to dry, followed by acetone (1 µL) and allowing that to dry, followed by the sample in hexane (1 µL). When cations were added, the acetates were added in two ways: by dissolution of the matrix in a solution containing the acetate mixture or by spotting the acetate mixture in a separate layer. When the cations were added in a separate layer, several tests were carried out with them spotted between each of the other layers to see which gave the best results.

Standard lipid mix B was analysed by MALDI-MS with approximately 20 pmol of each lipid per MALDI spot, using each of the four cation spotting methods (Figure 42).
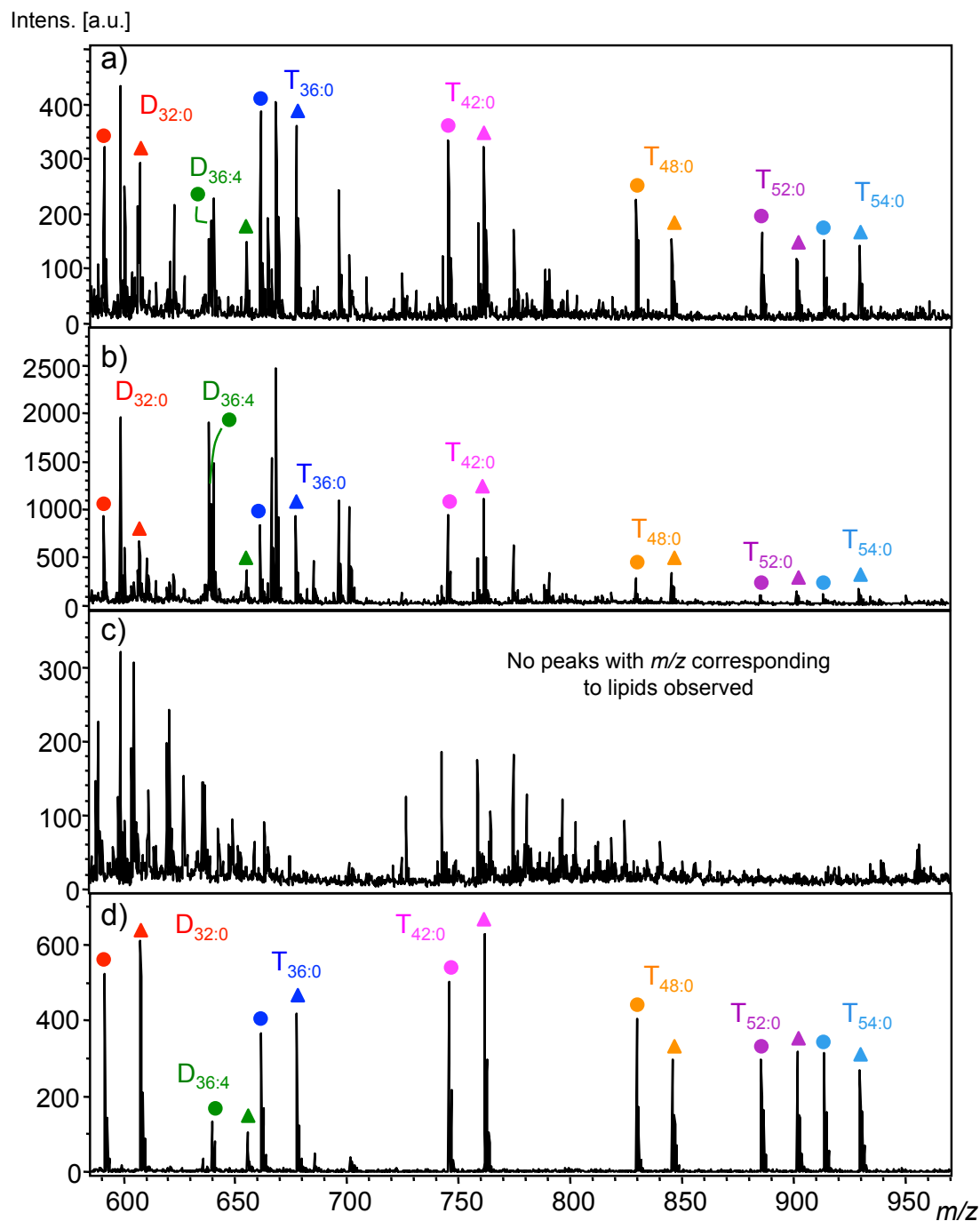
Figure 42. MALDI mass spectra of lipid mix B with 20 pmol of each lipid spotted. a) DHB in acetonitrile, followed by acetone, followed by cation solution, followed by lipid sample; b) DHB in acetonitrile, followed by acetone, followed by lipid sample, followed by cation solution; c) DHB in acetonitrile, followed by cation solution, followed by acetone, followed by lipid sample; d) DHB in cation solution, followed by acetone, followed by lipid sample. Circles denote [M+Na]$^+$ TAG signals and triangles denote [M+K]$^+$.

As can be seen from Figure 42, three of the four methods gave peaks corresponding

to both [M+Na]$^+$ and [M+K]$^+$ ions of each of the lipids in the mixture. The only

method that did not give good results was when the cations were spotted on top of the matrix layer (Figure 42c). In this case, a noisy spectrum was produced with no peaks corresponding to the lipids. It is very clear from Figure 42 that the method which gave the best S/N was that in which the DHB was dissolved in solvent containing the cations (Figure 42d). Here the S/N is excellent, and each lipid gives both $[M+Na]^+$ and $[M+K]^+$. It can be seen from the spectra that when the cations are added in equimolar amounts, the potassiated and sodiated species have peaks with similar intensities (although the intensity of the peaks does vary between the different analytes, and this difference varies between the different spotting methods). This indicates that the affinity of the lipids for each of these two cations is similar. It seems likely that the high intensity of the $[M+Na]^+$ peak in most samples is due to a higher level of sodium than potassium in the solvents that are the source of the cations during analysis.

Although adding salts to MALDI spots can be used to promote ionisation, it is often not necessary because of the fact that metals are found in the solvents used for sample preparation. Comparison of Figure 41a with Figure 42d shows that in the best example of a spectrum where the standards were spotted with added cations, the S/N was better than in those spotted without added cations. However, the addition of an extra component onto the spot increases the likelihood of introducing small amounts of contaminants which may affect the quality of the spectrum obtained. Since TAGs can be observed with good S/N without the addition of any salts, and archaeological lipid extracts are likely to contain various sample-derived contaminants already, it was decided not to add salts to the lipid extracts when they were analysed. In samples where the detection of TAGs is poor when they are first analysed, it could, however, be beneficial to add sodium acetate to try and improve TAG detection.

4.3.4   Tandem Mass Spectrometry

Sodiated TAG species are known to fragment by loss of fatty acids or fatty acid sodium salts,[139] which means that the fatty acid composition of TAGs can be determined using tandem mass spectrometry. MS/MS of the three TAGs in standard lipid mix A was carried out. As an example, Figure 43 shows a tandem mass spectrum of the peak at m/z 830.3, $[T_{48:0}+Na]^+$, with product ion peaks at m/z 551.9 and 573.9 corresponding to the $[D_{32:0}+H]^+$ and $[D_{32:0}+Na]^+$ fragments, respectively.
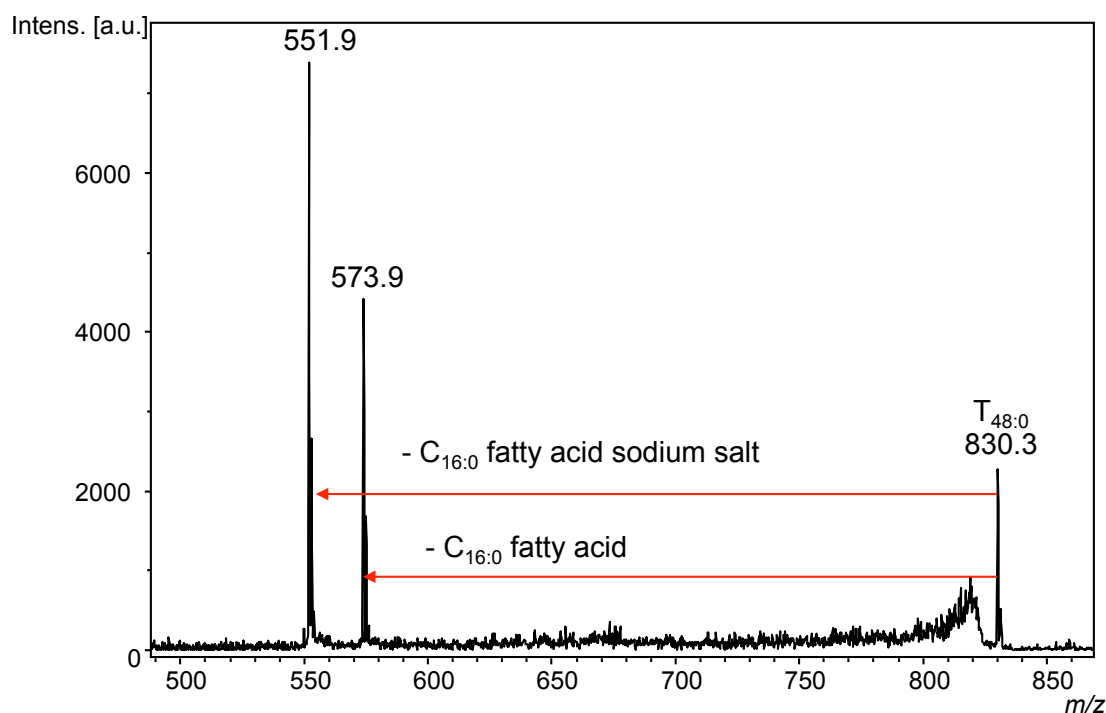
Figure 43. Product ion spectrum of the peak at m/z 830 ($[T_{48:0} + Na]^+$) illustrating fragmentation of a TAG by loss of fatty acids and fatty acid sodium salts.

Since each of the TAGs in standard lipid mix A has only one type of fatty acid attached (i.e. all three fatty acids attached to the glycerol backbone are the same) they give simple tandem mass spectra with only two product ion peaks: that for loss of the fatty acid and that for loss of the fatty acid sodium salt. For TAGs with more than one different fatty acid attached, the tandem mass spectra contain more peaks.[161]

4.4 MODERN ANIMAL FATS

In order to test the MALDI-MS method on more complex samples than authentic lipid standards, total lipid extracts (TLEs) from modern fresh bovine and porcine adipose tissues and bovine milk (prepared by Cynthianne Debono Spiteri)[162] were analysed by MALDI-MS.

Although the standard method in BioArCh for analysis of lipids extracted from archaeological ceramics is to dissolve them in hexane, 2:1 DCM:methanol is the solvent mixture used for extraction of the lipids in almost all published methods. Therefore, 2:1 DCM:methanol and hexane were both tested as the solvent for dissolving TLEs for MALDI-MS analysis. Portions of the modern animal fat TLEs were dissolved in hexane or in 2:1 DCM:methanol, and analysed by MALDI-MS using DHB as the matrix.

When prepared in 2:1 DCM:methanol, the spectra obtained were dominated by peaks at m/z 760 and 782 (data not shown), assigned as the M^+ and $[M-H+Na]^+$ of the phosphatidylcholine (PC) lipid 2-oleoyl-1-palmitoyl-sn-glycero-3-phosphocholine (PC$_{34:1}$). Peaks corresponding to TAG $[M+Na]^+$ ions in these spectra were of very low intensity compared to the peaks at m/z 760 and 782. PCs are reported to suppress ionisation of TAGs and methods, using SPE, have been developed to separate them in order to detect TAGs in samples containing both of the types of molecules.[163] However, the samples spotted in hexane gave slightly better quality TAG peaks than those spotted in 2:1 DCM:methanol, so hexane was used for future analyses. This is to be expected since hexane has a lower polarity than DCM, and TAGs are less polar than phospholipids. Therefore, TAGs are relatively more soluble in hexane than phospholipids are. In any case, there are no reports of phospholipid detection in archaeological lipid extracts, presumably because they are much more susceptible to degradation than TAGs, so the suppression of TAGs by PCs is unlikely to cause problems in MALDI-MS analysis of archaeological samples. Figure 44 shows the MALDI mass spectra for each of the three modern animal fat TLEs.

123
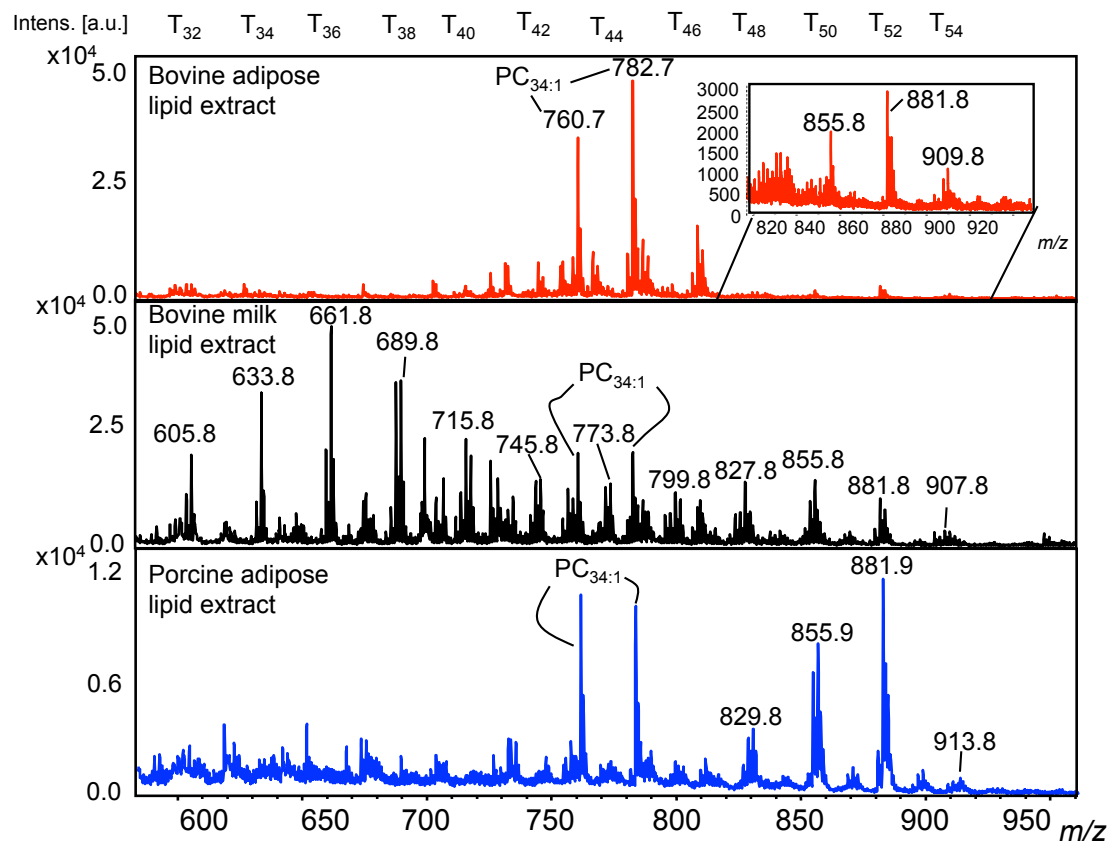
Figure 44. MALDI mass spectra of extracts from modern animal animal fats (hexane, DHB matrix).

All three modern animal fat extracts show a range of TAGs, with saturated and (poly)unsaturated TAGs observed, as well as the two phospholipid peaks. The milk fat shows the widest range of TAGs, from T_{32} to T_{54}, whereas the adipose fats show a much narrower distribution ($T_{50} - T_{54}$ for bovine adipose fat and $T_{48} - T_{54}$ for porcine adipose fat), as would be expected.[142] Table 4 shows the expected m/z values for $[M+Na]^+$ of TAGs in the range $T_{28:0} - T_{54:0}$. Each unsaturation (double bond) reduces the m/z by 2 units.

Table 4. m/z values corresponding to $[M+Na]^+$ ions of fully saturated TAGs from $T_{28:0}$ to $T_{54:0}$ (rounded down to integer values). Each level of unsaturation (double bond) reduces the m/z by 2 units.

TAG	$[M+Na]^+$ m/z	TAG	$[M+Na]^+$ m/z	TAG	$[M+Na]^+$ m/z
$T_{54:0}$	913	$T_{44:0}$	773	$T_{34:0}$	633
$T_{52:0}$	885	$T_{42:0}$	745	$T_{32:0}$	605
$T_{50:0}$	857	$T_{40:0}$	717	$T_{30:0}$	577
$T_{48:0}$	829	$T_{38:0}$	689	$T_{28:0}$	549
$T_{46:0}$	801	$T_{36:0}$	661		

Tandem MS was carried out on some of the unsaturated TAGs observed in the milk TLE (Table 5). Signals indicating the loss of a range of even carbon-numbered fatty acids from $C_{14:0}$ to $C_{22:0}$ were observed. For a singly unsaturated TAG (such as $T_{48:1}$ in Table 5) one of the fatty acids is singly unsaturated, and for a doubly unsaturated TAG (such as $T_{50:2}$ and $T_{52:2}$ in Table 5) either two of the fatty acids are singly unsaturated or one of them is doubly unsaturated. For this reason, doubly unsaturated fatty acids cannot be present in the $T_{48:1}$ TAG. As can be seen from Table 5, more than three different fatty acids are observed to be lost from each TAG. These represent the different combinations of fatty acids that could make up the TAG, though of course each individual TAG molecule contains only three. For example, the $T_{48:1}$ TAG is a mixture of three different molecular structures: (C_{14},C_{14},C_{20}), (C_{14},C_{16},C_{18}) or (C_{16},C_{16},C_{16}), with one of the fatty acids in each case being singly unsaturated. Fatty acids larger or smaller than these were not observed and this may be because they are not present in the TAGs, but it could also be that they are present at such low levels that they are below the LOD of the method. The size of the lowest and highest mass fatty acids observed increased as the TAG mass increased, which is

logical because for a small fatty acid to be part of a large TAG, a very large fatty acid would also need to be present. For example, loss of C_{14} is not observed from $T_{52:2}$ while it was observed from $T_{48:1}$ and $T_{50:2}$, but loss of C_{20} is observed only from $T_{52:2}$ and not from the lighter TAGs. The maximum chain length of fatty acids typically observed in the fats of terrestrial animals is C_{18},[142,67,164] meaning that medium-large sized TAGs cannot be produced with short fatty acids. Some fatty acids longer that C_{18} were observed (Table 5) but the signals for these were very weak.

The detection of a range of fatty acids from TAGs in an animal fat TLE shows the power of MALDI-MS/MS for determining the structures of TAGs using a relatively rapid method with easy to interpret data. The intact TAG carbon numbers can be easily identified from the *m/z* values of the TAGs, and information about their fatty acid composition can be obtained by tandem MS, with *m/z* values corresponding to loss of fatty acids from the glycerol backbone. This is in contrast to HTGC-MS which takes much longer and produces more complex data that take significant time to interpret.

Table 5. Peaks observed in tandem mass spectra of $T_{48:1}$, $T_{50:2}$ and $T_{52:2}$ from bovine milk TLE.

Neutral Loss	Expected *m/z* from $T_{48:1}$ (*m/z 827*)	Seen? Y/N	Expected *m/z* from $T_{50:2}$ (*m/z 853*)	Seen? Y/N	Expected *m/z* from $T_{52:2}$ (*m/z 881*)	Seen? Y/N
$C_{14:1}$ acid	601	Y	627	?	655	N
$C_{14:1}$ sodium salt	579	Y	605	?	577	N
$C_{14:0}$ acid	599	Y	625	Y	653	N
$C_{14:0}$ sodium salt	577	Y	603	Y	575	N
$C_{16:2}$ acid	N/A	N/A	601	?	629	N
$C_{16:2}$ sodium salt	N/A	N/A	579	X	607	N
$C_{16:1}$ acid	573	Y	599	Y	627	Y
$C_{16:1}$ sodium salt	551	Y	577	Y	605	Y
$C_{16:0}$ acid	571	Y	597	Y	625	Y
$C_{16:0}$ sodium salt	549	Y	575	Y	603	Y
$C_{18:2}$ acid	N/A	N/A	573	Y	601	Y
$C_{18:2}$ sodium salt	N/A	N/A	551	Y	579	Y
$C_{18:1}$ acid	545	Y	571	Y	599	Y
$C_{18:1}$ sodium salt	523	Y	549	Y	577	Y
$C_{18:0}$ acid	543	Y	569	Y	597	Y
$C_{18:0}$ sodium salt	521	Y	547	Y	575	Y
$C_{20:2}$ acid	N/A	N/A	545	N	573	Y
$C_{20:2}$ sodium salt	N/A	N/A	523	Y	551	Y
$C_{20:1}$ acid	517	?	543	N	571	N
$C_{20:1}$ sodium salt	495	Y	521	N	549	Y
$C_{20:0}$ acid	513	N	541	N	569	N
$C_{20:0}$ sodium salt	491	N	519	Y	547	N
$C_{22:2}$ acid	N/A	N/A	517	N	545	Y
$C_{22:2}$ sodium salt	N/A	N/A	495	N	523	Y
$C_{22:1}$ acid	487	N	515	N	543	N
$C_{22:1}$ sodium salt	465	N	493	N	521	Y

4.5 EXPERIMENTALLY BURIED POTS

After the successful application to modern animal fats, the MALDI-MS method was applied to samples that are more similar to archaeological samples than fresh modern fat extracts. Unglazed open-fired pots, of a similar material to Neolithic potsherds, had previously (in 1997) had milk boiled in them, been broken into pieces and buried at the Palace Leas plots at Newcastle University's Cockle Park experimental farm (O. Craig, personal communication). This was carried out in order to provide material for studying the decay of lipids absorbed into ceramic, under conditions similar to those that archaeological potsherds have been subjected to, albeit for a much shorter period of time. Pieces of pot were excavated after one year and two years. Additional samples were buried after the first year and excavated after two months. Pieces of pot were also kept unburied for comparison. Since their excavation, the potsherds have been stored primarily at −20 °C, though they have been through several lab moves and been extracted by several researchers so they have been through a number of freeze-thaw cycles (and not necessarily the same number of cycles for each potsherd). Lipids were freshly extracted from the unburied, two month, one year and two year potsherds and subjected to MALDI-MS analysis in order to test how well MALDI-MS could detect TAGs extracted from a more complex matrix than fresh animal fats, and with some level of degradation. Pots in which milk had been cooked were selected because milk is characterised by the presence of short-chain TAGs. These are known to degrade rapidly compared to TAGs with longer chains,[64] so partially degraded milk TAGs are a good choice of analyte to test how well the MALDI-MS method works. Potsherds from the rim, body and base of the vessels were analysed. An example spectrum of an unburied control (rim potsherd) is shown in Figure 45.
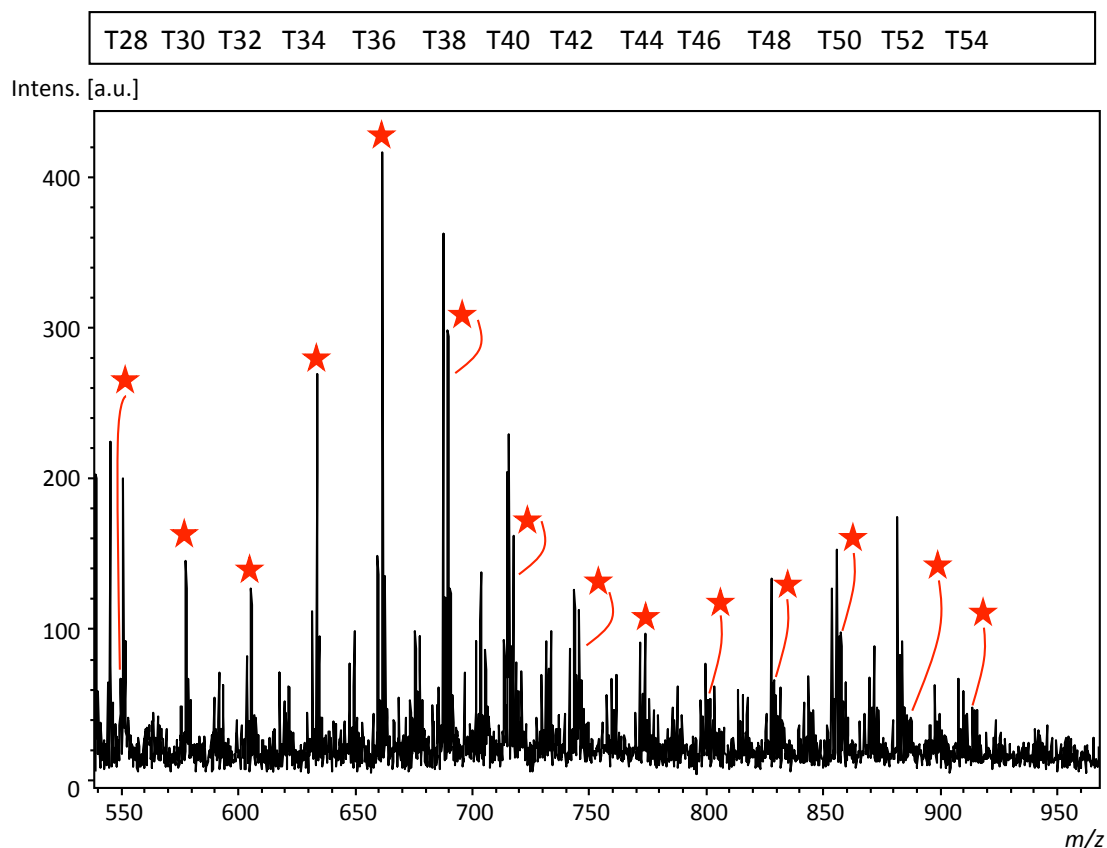
Figure 45. MALDI mass spectrum of an unburied control rim potsherd from a pot that had had milk cooked in it in 1997, and has been largely frozen since. TAGs from T28 to T54 are observed, but are not individually labelled because of the complexity of the mixture. Stars mark the saturated TAGs.

In the spectrum of the unburied control rim potsherd extract (Figure 45), TAGs in the range T_{28} - T_{54} are observed with good S/N, and there is a variety of levels of unsaturation in the fatty acid chains (saturated TAGs are marked in the spectrum with stars, and peaks with *m/z* values 2 lower correspond to singly unsaturated TAGs).

MALDI-MS is not generally a quantitative method, and analysis of a mixture of TAG standards from $T_{30:0}$ to $T_{66:0}$ has shown that there is a signal drop-off as TAG mass increases.[139] This signal drop-off is particularly steep in the milk TAG range $(T_{30:0} - T_{54:0})$ and so in order to quantitate the TAGs, the reduction in signal as TAG mass increases would need to be factored in. Nevertheless, in Figure 45 there appears to be a bimodal distribution of TAGs, with local maxima at T_{36} and T_{50}. This implies that the different TAGs are present at different concentrations. Figure 46 shows graphically the TAG peak height distribution in the unburied control rim potsherd extract (Figure 45) compared to that of the lipid extract of fresh milk (Figure 44), where the peak heights have been normalised to the highest peak in each spectrum ($T_{36:0}$ in each case). In general the peak height distributions are in agreement between the two samples, indicating that the milk lipids have absorbed into the ceramic in similar proportions to those occurring in fresh milk. Despite the fact that it is not a fully quantitative method, MALDI-MS has been reported for TAG quantitation.[165] However, that work was carried out on TAGs in the range $T_{50} - T_{56}$, where there appears to be only a small difference in signal with increasing TAG mass.
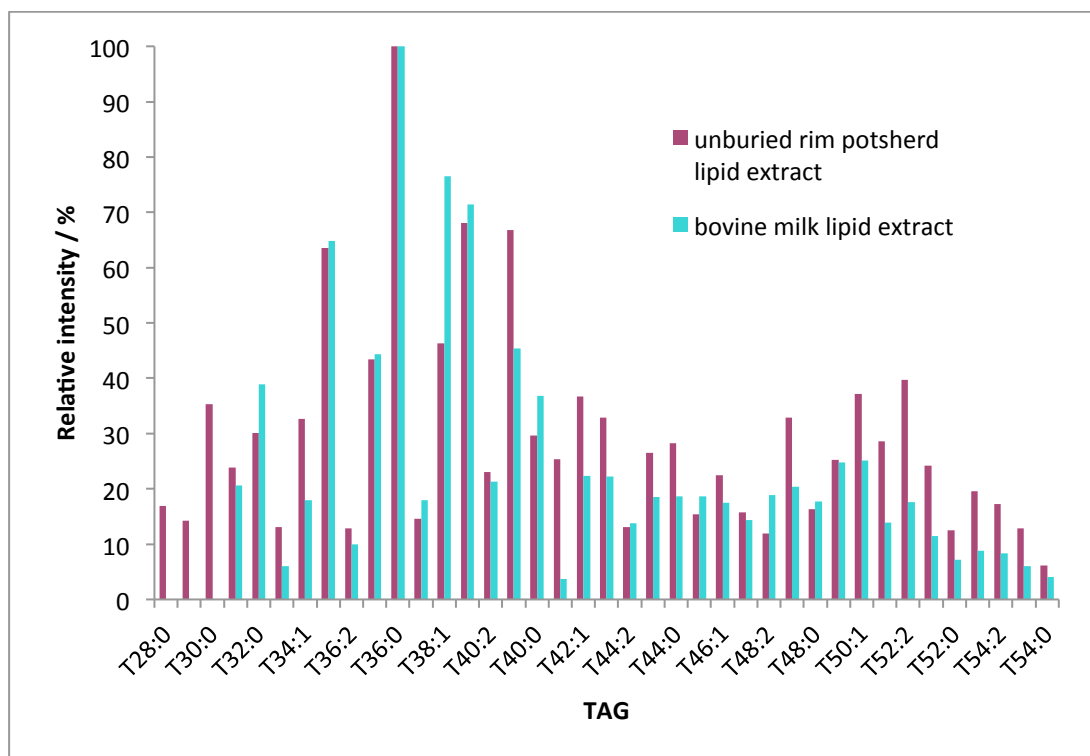
Figure 46. Relative intensities of TAG peaks in the MALDI mass spectra of the unburied control rim potsherd extract and the lipid extract of fresh milk, showing that the peak height distributions are similar in the two samples.

Figure 47 shows spectra of lipids extracted from rim potsherds that have been buried for 1 year and 2 years. In these samples, the range of TAGs observed has only slightly changed compared with the unburied control, though the S/N has decreased, consistent with there being some degradation. The only change in the carbon number range of TAGs observed is that T_{28} has been lost. However, this ion was observed only with relatively low S/N in the unburied control so degradation may have taken it below the LOD. Also, there was a contaminant peak at *m/z* 550 (present in many of the samples analysed) that may have interfered with the signal for T_{28}. The main difference between the unburied and buried samples is the fact that there has been a reduction in the number of unsaturated TAGs detected. In the extract of the unburied rim potsherd, singly unsaturated TAGs from $T_{30:1}$ to $T_{54:1}$, doubly unsaturated TAGs from $T_{34:2}$ to $T_{54:2}$, plus $T_{54:3}$, were observed. After one year of burial this had decreased to singly unsaturated TAGs $T_{30:1}$, $T_{32:1}$, $T_{36:1}$ and $T_{42:1} - T_{52:1}$, and doubly unsaturated TAGs $T_{48:2} - T_{52:2}$. A similar pattern is observed with potsherds from the body of the vessel, with TAGs in the range $T_{28} - T_{54}$ observed in the unburied control and the two month sample, but by two years the range has reduced to between T_{30} and T_{54}, with a reduction in S/N and a concurrent reduction in the number of unsaturated TAGs detected. The one year sample showed a range of TAGs from T_{48} to T_{52} and these were of extremely low S/N. However, this may be attributed to the fact that the potsherd was small due to being extracted by other researchers so only 0.61 g of ceramic could be drilled from it (compared to ~1 g for the other samples), which may also coincide with a larger number of freeze-thaw cycles causing degradation. Potsherds from the base of the vessel had TAGs in the range T_{28} to T_{54} in the unburied control, and this had not changed after one year of burial (there was no two year sample of base potsherd available). Figure 48 summarises the TAGs detected in the experimental burial samples.
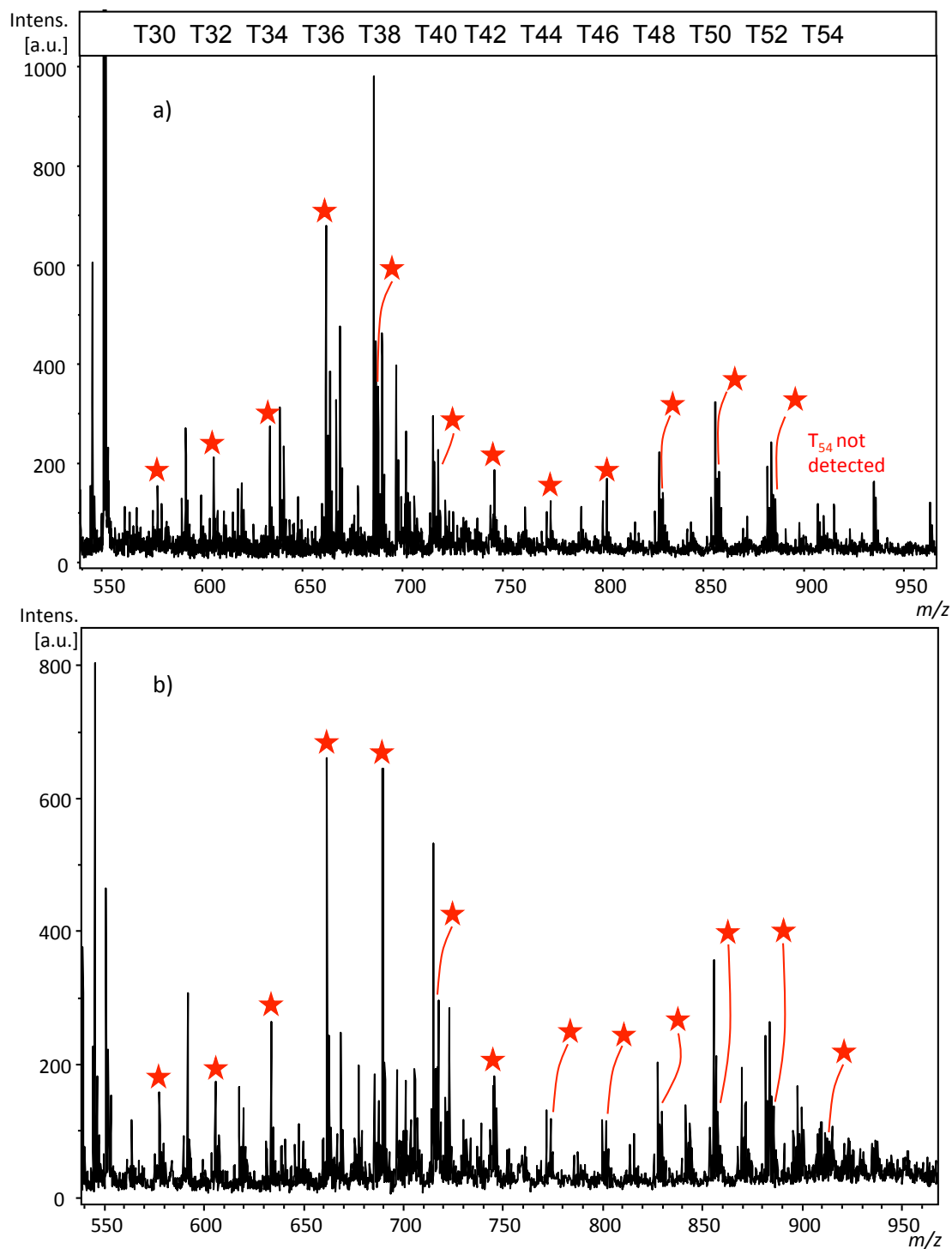
Figure 47. MALDI mass spectra of lipid extracts of experimental rim potsherds containing milk residues. a) buried for 1 year; b) buried for 2 years.

Acyl carbon number		T_{28}	T_{30}	T_{32}	T_{34}	T_{36}	T_{38}	T_{40}	T_{42}	T_{44}	T_{46}	T_{48}	T_{50}	T_{52}	T_{54}
Sample															
Rim potsherds	Unburied				& $T_{54:3}$										
	1 year burial														
	2 year burial												& $T_{54:3}$		
Body potsherds	Unburied					& $T_{54:3}$									
	2 month burial														
	2 year burial														
Base potsherds	Unburied				& $T_{54:3}$										
	1 year burial														
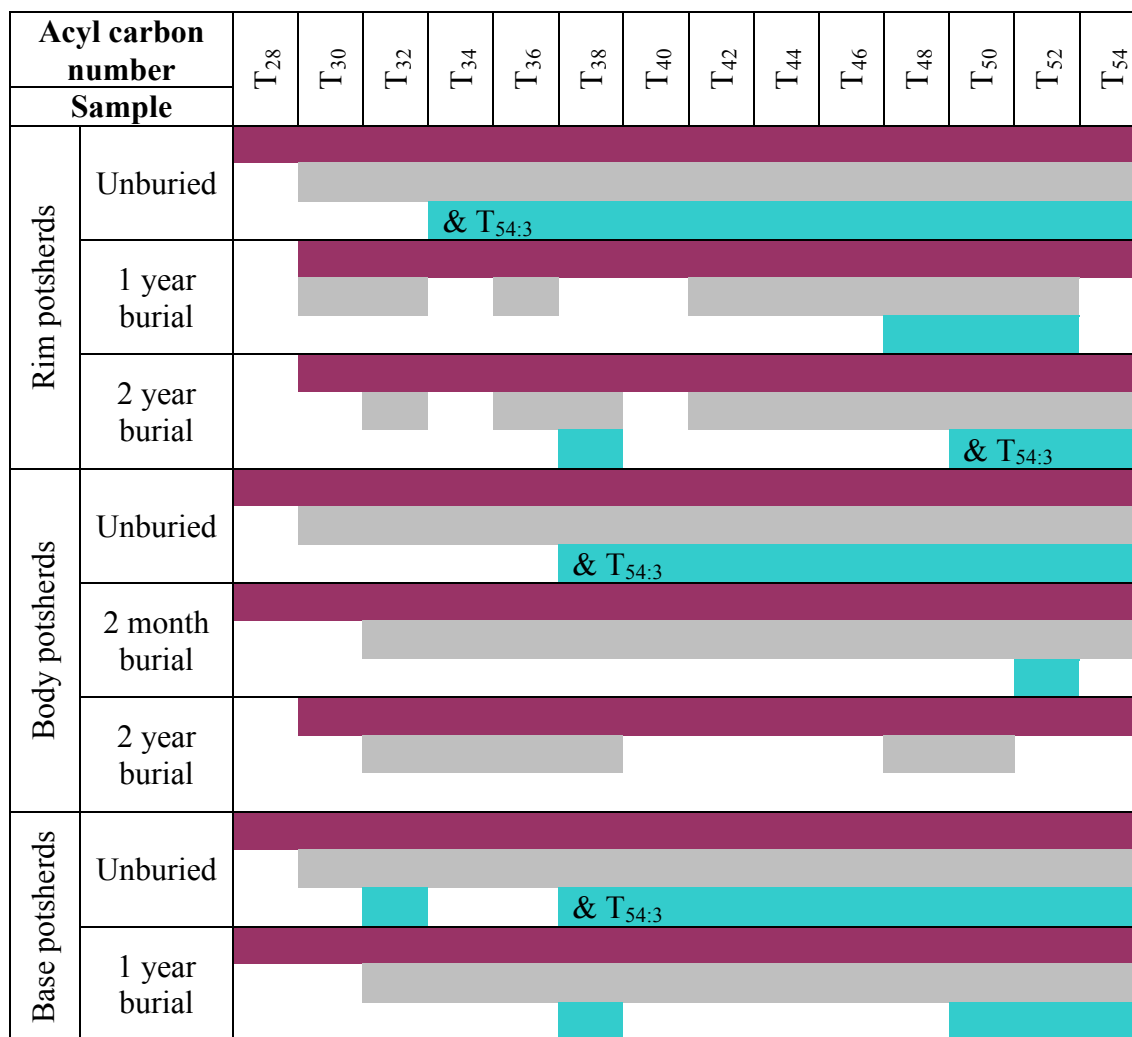
Figure 48. Summary of the TAGs detected in the experimental burial samples. The upper bar in each case (purple) represents fully saturated TAGs, the middle bar (grey) singly unsaturated TAGs and the lower bar (turquoise) doubly unsaturated TAGs. TAGs with three double bonds are written in where relevant.

Published degradation studies, involving burying pieces of pottery dosed with TAG standards, milk and olive oil in mushroom compost and incubating at 30 °C to accelerate decay, followed by analysis using HTGC-MS, have shown that the initial stages of degradation are rapid (over only a few months).[64] This initial decay is proposed to be microbe mediated, with further degradation occurring by abiotic means over a longer period of time.[66,18] For the milk-dosed samples, incubation was carried out for 95 days and by the end of the experiment the lower mass TAGs could no longer be detected (size of smallest detectable TAG increasing from T_{24} to T_{38} over the 95 days).[64] The results of the present MALDI-MS analysis show that almost the full range of TAGs can still be detected by MALDI-MS after two years of burial, compared with an unburied control. Obviously two years is not directly comparable with the ~4000 years over which Neolithic potsherds have been buried, nor necessarily with 95 days of accelerated degradation (though this is hard to compare), but if the initial degradative processes indeed occur over a period of a few months it might be expected that these would be complete within two years. The detection by MALDI-MS of light TAGs after two years of burial may indicate that the loss of short-chain TAGs that is observed to have taken place in archaeological samples may not occur as quickly as was thought. Based on these results it would be beneficial to analyse some experimental potsherds that have been buried for longer than two years. However, samples of this nature obviously take time to prepare so are not within the scope of this project. In fact, when the samples analysed here were prepared, further samples were excavated after four and eight years.

Tandem mass spectrometry was carried out on some of the lighter TAGs detected in the buried milk samples, in order to try to gain some structural information on the lighter TAG species. Since $C_{16:0}$ and $C_{18:0}$ are the most common fatty acids in animal fats, $T_{48:0}$ to $T_{54:0}$ TAGs generally contain some combination of $C_{16:0}$ and $C_{18:0}$, and these are the neutral losses observed when tandem mass spectrometry is carried out on precursor ions in this range. Milk is known to contain fatty acids as short as $C_{4:0}$,[166,167] so with lighter TAGs the possible combinations of fatty acids increases – for example with a $T_{30:0}$ TAG there could be three $C_{10:0}$ fatty acids, or $C_{16:0}$, $C_{10:0}$ and $C_{4:0}$, or many other combinations. An example tandem mass spectrum is shown in Figure 49. There are some peaks which could be due to loss of fatty acids or fatty acid sodium salts; however, the S/N is much poorer than that in tandem mass spectra

of heavier TAGs. This is probably due to the fact that when a precursor ion is selected it is obviously a combination of all TAGs with a particular number of acyl carbons, which can be constituted as several different molecular species with different combinations of fatty acids. With the higher mass TAGs there are fewer likely combinations, with most individual TAGs containing some $C_{16:0}$ and $C_{18:0}$ fatty acids. Therefore, fragments corresponding to losses of these fatty acids are observed clearly. However, in the case of lighter TAGs, the number of individual molecules containing any one fatty acid is likely to be lower, and therefore a fragment ion corresponding to that neutral loss is likely to be of lower intensity and harder to detect. Similarly, it may be the case for the higher mass TAGs that there are some individual molecules with an unusual combination of fatty acids, but because these are present at low levels they may not be detected when tandem mass spectrometry is carried out.
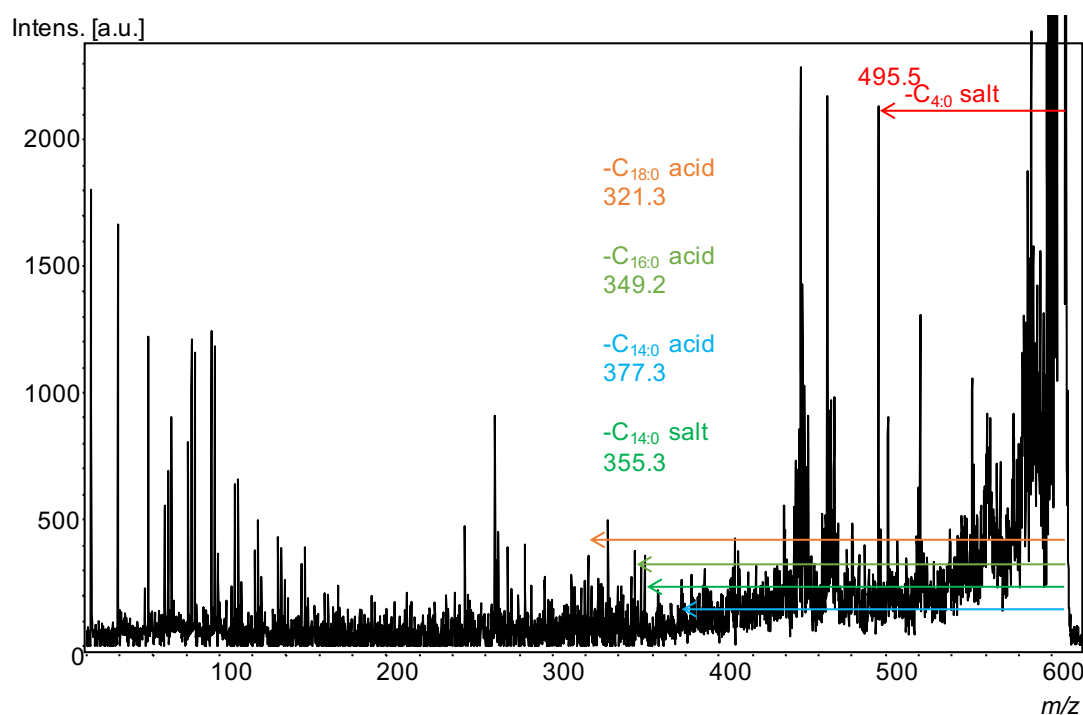
Figure 49. Tandem mass spectrum of the ion at m/z 605 ($T_{32:0}$) in the lipid extract of a rim potsherd buried for 2 years.

4.6 FRACTIONATION

The data in this section were obtained by Rachel Heap, a British Mass Spectrometry Society Summer Studentship student. Her project was designed by the author of this

thesis, who also wrote the successful proposal for the funding and supervised the project.

Published work on the use of nanoESI-MS for the analysis of TAGs in lipid extracts of archaeological ceramics has indicated that in order to obtain good results it is necessary to fractionate the TAGs by SPE to separate them from other components of the samples such as fatty acids, sterols, alcohols and hydrocarbons.[24]

MALDI-MS is generally considered to be more tolerant of contaminants than ESI is, so fractionation may not be necessary when using MALDI-MS for analysis. Therefore, in order to see if there was any merit in fractionation of lipids prior to MALDI-MS analysis, an SPE method was developed and applied to the lipid standards and some experimental burial samples. The aim of the fractionation was to separate TAGs from other lipids in an attempt to improve the S/N. However, increasing sample preparation, for example by carrying out fractionation, will always result in some sample loss and therefore fractionation could in fact reduce S/N rather than improve it.

4.6.1 Method Development Using Standards

The published SPE method, described by Mirabaud *et al.* for their nanoESI-MS analysis,[24] was used as a starting point for the method described here. Standard lipid mix C, containing equal masses of azelaic acid, palmitic acid, stearic acid, cholesterol, $M_{16:0}$, $D_{32:0}$, $D_{36:4}$, $T_{36:0}$, $T_{42:0}$, $T_{48:0}$, $T_{52:0}$ and $T_{54:0}$, was prepared at a concentration of ~30 μg/mL total lipid for optimisation of the fractionation method. Since the mean amount of lipid extracted from archaeological pottery has been found to be 100 μg/g of ceramic,[18] and in the analysis of archaeological lipids used here the extract used for analysis is typically a one third portion of an extract from 1 g of ceramic material, i.e. ~30 μg lipid (although the amount spotted onto the MALDI plate is typically 1/100th of this), 30 μg/mL was chosen as a concentration which would be equivalent if 1 mL of standard lipid mix C was fractionated.

Silica SPE cartridges (500 mg, 6 mL, Agilent SampliQ) were purchased and fractionation of standard lipid mix C was carried out according to Mirabaud's protocol. The SPE cartridges used had the same type and mass of stationary phase as those used by Mirabaud. However, they were from a different manufacturer and

therefore may have some differences, such as in particle size and how the stationary phase is packed, which could affect their performance. Cartridges were conditioned with 2 mL of hexane, 2 mL of DCM:MeOH (2:1 v:v) then 4 mL of hexane. After sample loading, the fractions were sequentially eluted: 1 mL of hexane for hydrocarbons, 1 mL of DCM for DAGs and TAGs, 1.5 mL of DCM:MeOH (2:1 v:v) for sterols and alcohols and 4 mL of DCM:MeOH (1:1 v:v) for fatty acids. Standard lipid mix C does not contain any hydrocarbons or alcohols but these were not required for the method optimisation since the main focus of the work is TAGs. The fractions were analysed by both HTGC and MALDI-MS, since MALDI-MS is selective for DAGs/TAGs and the two complementary methods are required to detect all of the components of standard lipid mix C.

Unfortunately, the published method was found not to be reproducible. Although HTGC analysis showed the sterols and fatty acids to elute in the expected fractions, the TAGs eluted in both the hexane and DCM fractions. In order to overcome this, the volume of hexane used for the final stage of conditioning was increased to 8 mL. 1 mL of hexane was then used to elute the first fraction (which in the case of the standard should not contain any lipids, though in lipid extracts would contain hydrocarbons) and the volume of DCM used to elute the DAGs and TAGs was increased to 2 mL. Using this method, the DAGs and TAGs were found to elute only in the DCM fraction. Comparison of the MALDI mass spectrum of the unfractionated lipid mix with that of the fractionated TAGs shows that although all of the TAGs are detected in both samples, there are a number of extra peaks in the fractionated standard which affect the S/N. This can be attributed to the increased sample handling introducing contaminants. However, a standard is by definition a relatively clean sample and so is expected to give good results on analysis. Therefore, fractionation may in this case introduce more components than it removes. By contrast, the archaeological samples are relatively dirty and so fractionation may still be beneficial for these samples.

4.6.2 Application to Experimentally Buried Samples

Following optimisation of the fractionation method using standard lipid mix C, it was applied to lipid extracts of the experimentally buried pots. These were analysed by MALDI-MS only, since the aim of the work was to detect the TAGs by

MALDI-MS and so once the method had been optimised it was not necessary to use HTGC to detect other lipids. For the unburied and two month experimental burial body potsherds, TAGs were detected in both the unfractionated and fractionated samples with similar S/N (Figure 50 for the two month sample), so fractionation was not found to be beneficial in these cases. However, for the two year experimental burial, in which TAGs were detected in the unfractionated sample but at low S/N, the S/N improved markedly after fractionation, particularly for TAGs in the range T_{40} – T_{54} (Figure 51). Tandem mass spectrometry was carried out on peaks at m/z 829 ($T_{48:0}$) and m/z 857 ($T_{50:0}$) and peaks for loss of $C_{16:0}$ fatty acids, and $C_{16:0}$ and $C_{18:0}$ fatty acids, respectively, were observed. It was not possible to carry out tandem MS on these TAGs in the unfractionated sample due to their low S/N, so fractionation was beneficial here. Although the unfractionated experimentally buried potsherds had all been analysed by MALDI-MS before their selection for fractionation, they were respotted prior to fractionation so that they could be analysed in their fractionated and unfractionated forms at the same time, for a proper comparison.
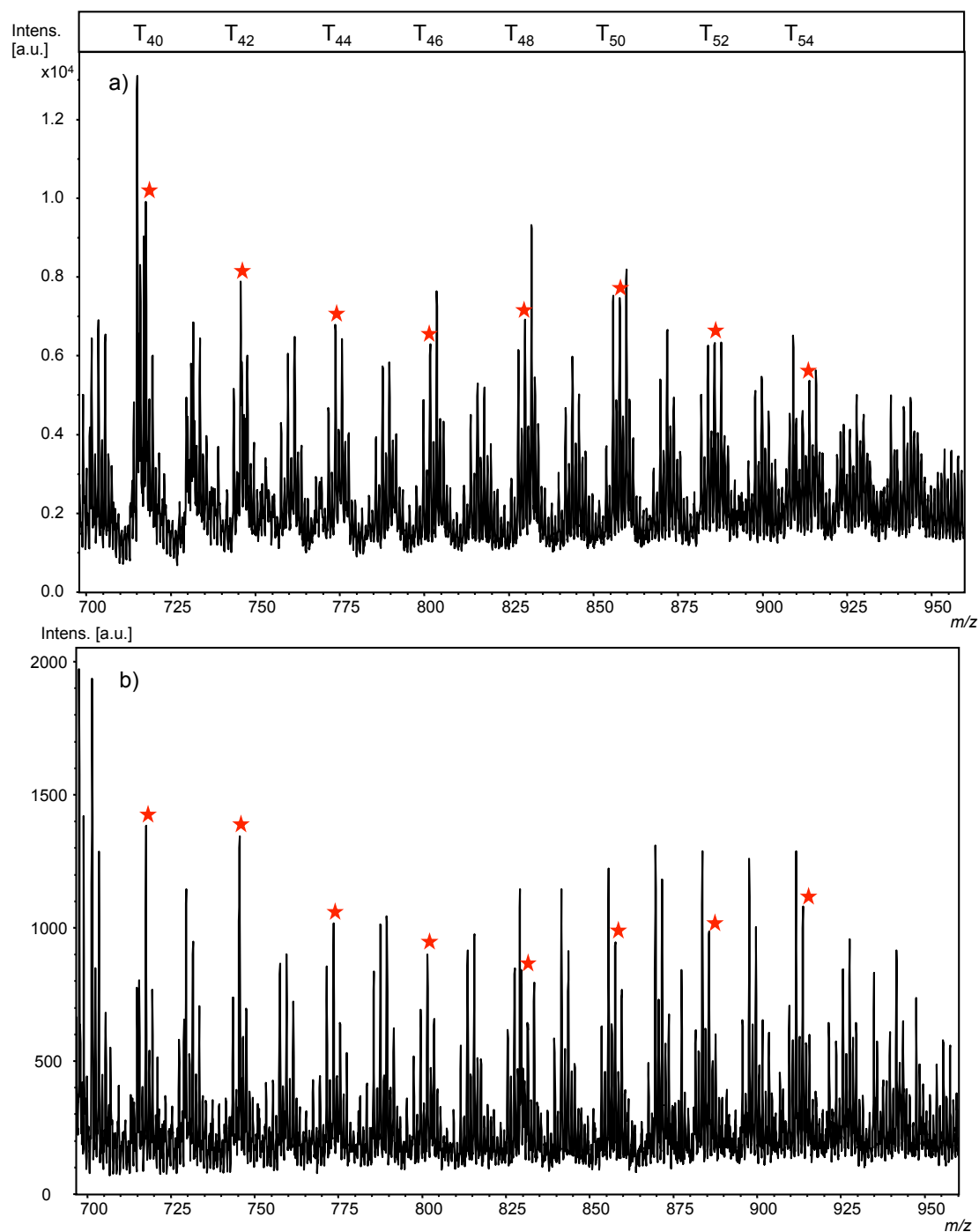
Figure 50. Lipid extract of a two month experimentally buried body potsherd. a) Total lipid extract; b) After fractionation (TAG fraction). S/N for TAGs in the range $T_{40} - T_{54}$ is similar before and after fractionation. Data were obtained by Rachel Heap.
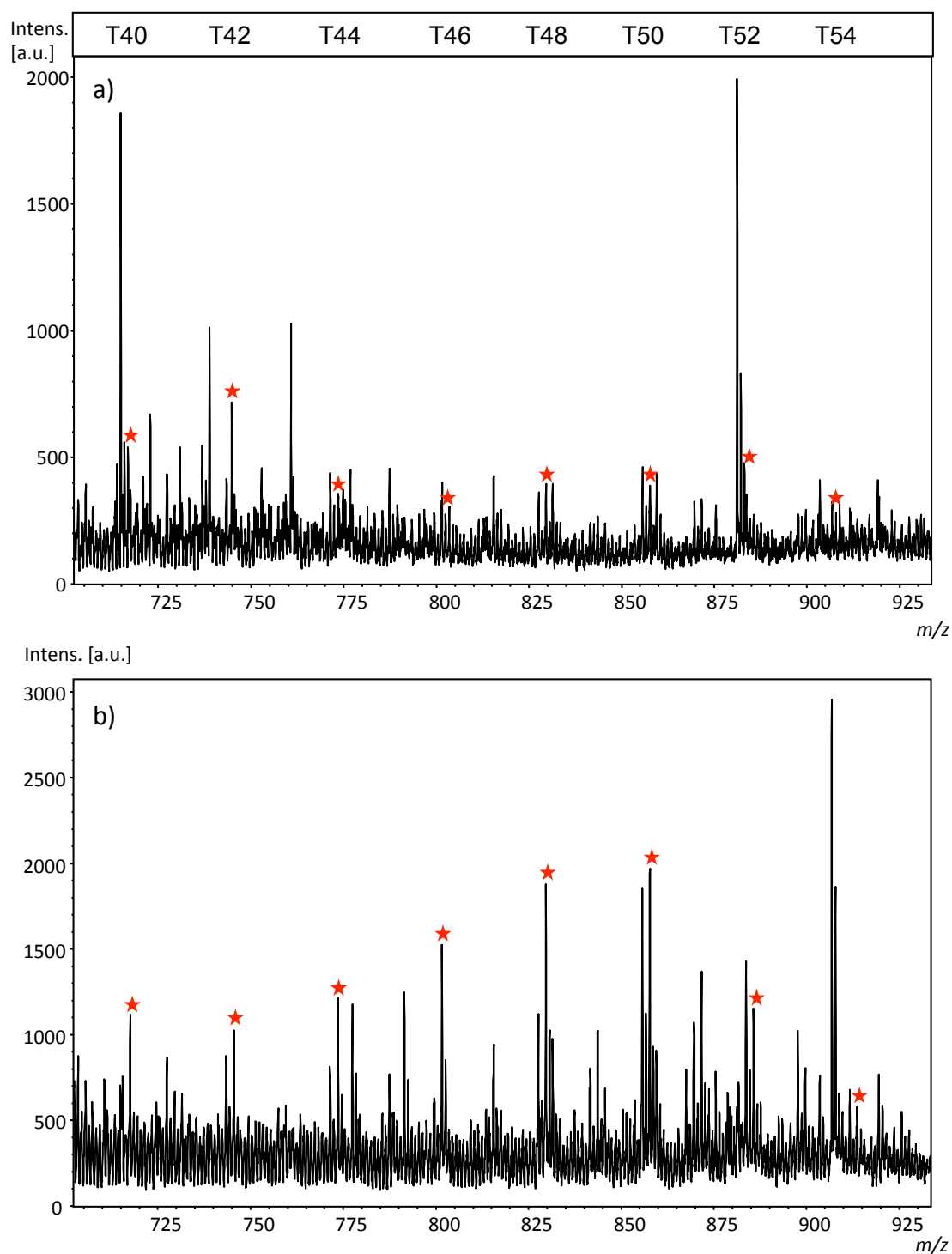
Figure 51. Lipid extract of a two year experimentally buried body potsherd. a) Total lipid extract; b) After fractionation (TAG fraction). S/N for TAGs in the range $T_{40} - T_{54}$ has increased following fractionation. Data were obtained by Rachel Heap.

4.6.3 Application to an Ethnographic Milk Pot

The method was also applied to the lipid extract of an ethnographic pot from India that had been used to cook milk. Analysis by MALDI-MS of an unfractionated lipid

extract did show TAGs but these were of very low S/N and there was a large contaminant peak at *m/z* 829.4 (Figure 52a). This is almost the same *m/z* as $T_{48:0}$ (*m/z* 829.9), which was not observed in the spectrum, probably because its detection was being interfered with by the contaminant. Fractionation of the sample improved the S/N of the TAGs and allowed detection of $T_{48:0}$ (Figure 52b).
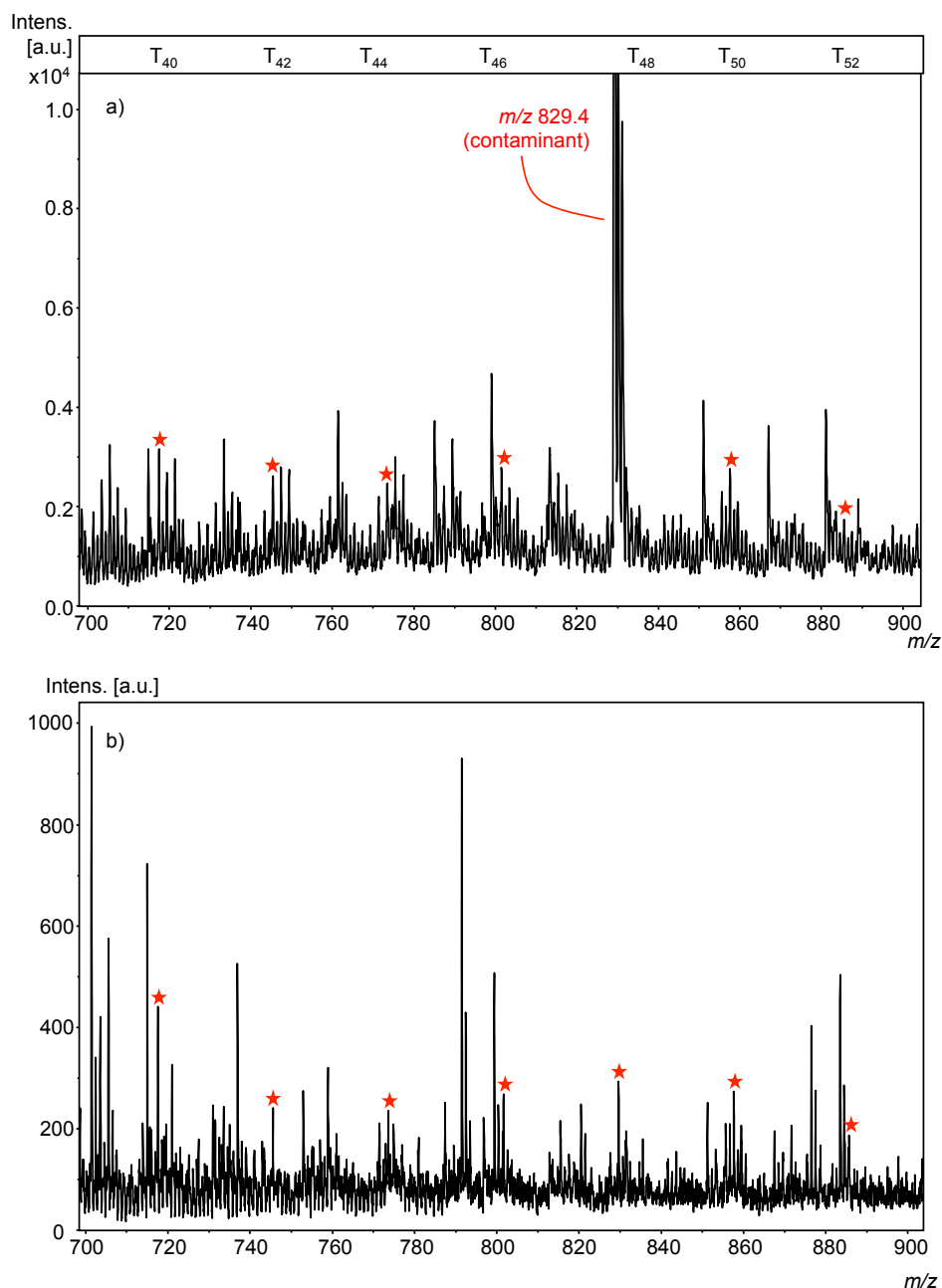
Figure 52. Lipid extract of an ethnographic Indian pot used to cook milk. a) Total lipid extract; b) After fractionation (TAG fraction). Fractionation resulted in the removal of a contaminating species with *m/z* 829.4, allowing the $T_{48:0}$ TAG to be detected (*m/z* = 829.9). Data were obtained by Rachel Heap.

4.6.4 Fractionation Overview

The overall results of the fractionation experiments were that in some cases it produced improved S/N relative to unfractionated extracts, which is clearly beneficial. However, in other cases it resulted in very little difference. Since one of the aims of this work was to reduce the time taken for analysis of archaeological lipids relative to using conventional techniques, adding a lengthy sample preparation step undermines this ideal, particularly if it results in no real benefit. Therefore, it was concluded that fractionation should only be carried out after analysis by MALDI-MS of total lipid extracts, and then only on samples for which sufficient signal was not obtained on analysis of the crude extracts. In these cases, the extra sample preparation time would be well spent if it did result in improved S/N, but time would not be wasted on fractionating all samples.

4.7 COMPARISON OF MALDI-MS WITH HTGC-MS

Since HTGC is the conventional method used for analysing lipids from archaeological samples, any new method proposed for analysis of such samples must be benchmarked against it. For optimum results when analysing TAGs by HTGC, on-column injection (OCI), as opposed to split/splitless injection, must be used. In split/splitless injection the injector is hot and the sample is introduced to the column by being vaporised and swept in to the column by the carrier gas. TAGs are not very volatile so this process is inefficient for these analytes, and the heat can break them down since they are heat-labile. In OCI, the sample is injected directly onto the column, which is cool initially, with its temperature increasing according the temperature programme of the method. However, the analysis of archaeological lipids by HTGC carried out at BioArCh at the University of York is done using splitless injection, so it was necessary to set up on-column injection for HTGC-MS analysis in order to carry out a proper comparison of MALDI-MS with HTGC-MS.

The GC was fitted with an on-column injector and a non-polar (Agilent DB-1HT) column (15 m × 0.32 mm, film thickness 0.10 μm) with a retention gap of deactivated fused silica (1 m × 0.32 mm) placed between the injector and column to protect the column. The column used was the same as that used for the HTGC work in BioArCh, and is designed to be suitable for use up to 400 °C. The injector was

programmed to follow the same temperature programme as the column: 50 °C for 2 min, followed by an increase to 350 °C at 10 °C/min and the final temperature held for 15 min (total run time 47 min).

Samples were derivatised using N,O-bis(trimethylsilyl)trifluoroacetamide (BSTFA) to trimethylsilylate protic sites, dissolved in 100 μL hexane containing 10 ng C_{34} alkane as an internal standard and manually injected using a fused silica needle. Although TAGs lack protic sites and so are not derivatised by BSTFA, other components of the standards and of archaeological lipid extracts, such as fatty acids, MAGs, DAGs and sterols, are derivatised. Trimethylsilylation increases the volatility of the analytes, thereby improving their GC response.

Since electron ionisation (EI) is used in HTGC-MS, there is no molecular ion peak because the amount of energy imparted to the molecule during ionisation causes extensive fragmentation. TAGs are therefore detected in HTGC-MS data by the presence of $[M-RCOO]^+$, corresponding to loss of a fatty acid acyloxy group from the TAG, $[RCO]^+$ for the acylium ion of a fatty acid and $[RCO+74]^+$ for an acyl group with the glycerol backbone. For example, Figure 53 shows the mass spectrum of $T_{42:0}$ TAG standard (glyceryl trimyristate, containing three $C_{14:0}$ fatty acids) from the HTGC-MS analysis of standard lipid mix A.
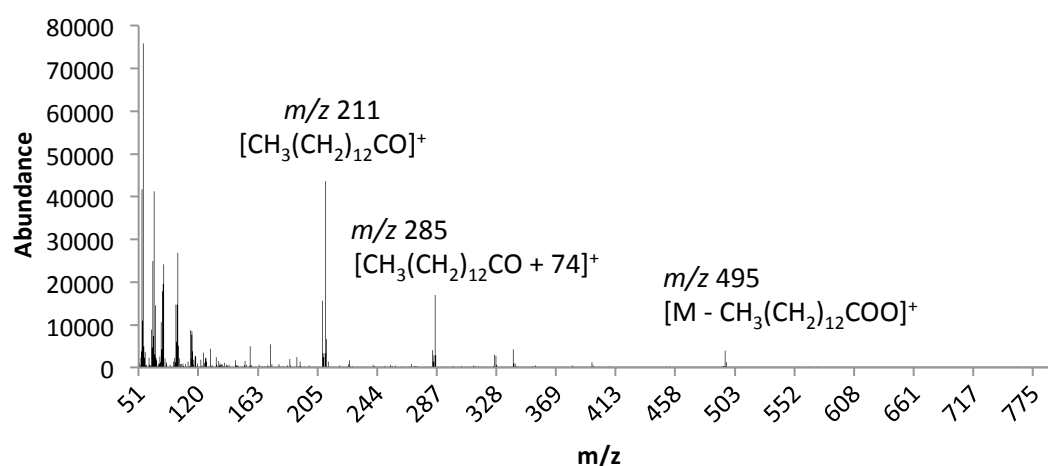
Figure 53. Mass spectrum of $T_{42:0}$ TAG standard from OCI-HTGC-MS of Standard Lipid Mix A, with the main peaks used for identification labelled.

4.7.1 Analysis of Modern Animal Fats

The three modern animal fats were analysed by OCI-HTGC-MS for comparison with MALDI-MS. In the bovine milk TLE, TAGs in the range T_{28} to T_{54} were detected using OCI-HTGC-MS, in contrast to $T_{32} - T_{54}$ with MALDI-MS. In bovine adipose TLE, TAGs in the range $T_{50} - T_{54}$ were detected by OCI-HTGC-MS, which is the same range as that detected by MALDI-MS. In this sample the peaks in the chromatogram were all of low S/N, which is assumed to be because of degradation during storage, though all of the modern animal fats were the same age and stored under the same conditions (at -20 °C). A possible explanation is that the bovine adipose fat may have been defrosted more times than the other modern animal fats, so that its storage conditions were not the same as for the other samples. In the porcine adipose TLE, TAGs from T_{46} to T_{54} were detected by OCI-HTGC-MS, and TAGs from T_{48} to T_{54} by MALDI-MS. A range of saturated and unsaturated TAGs were detected using both methods. These results show that in MALDI-MS the range of TAGs detected was the same or slightly smaller than that detected by OCI-HTGC-MS. However, in all of the chromatograms the T_{54} peaks were broad and of low S/N, and in general the higher the TAG mass the broader was the peak, whereas in MALDI-MS analysis TAGs are still well detected even up to T_{54}. This peak broadening is not unexpected in HTGC, since the longer an analyte stays on the column, the larger the effect of longitudinal diffusion, causing later-eluting analytes to have broader peaks. In addition to this, the later-eluting species are subjected to higher temperatures so are more likely to degrade, reducing the amount of analyte reaching the detector.

The effect of peak broadening of higher mass TAGs can be seen in Figure 54, which is the TAG region of a chromatogram of lipid standards, containing equal masses of $T_{42:0}$, $T_{48:0}$ and $T_{54:0}$. Table 6 gives the relative areas of the three peaks, after adjusting for the number of moles, showing how the area decreases with increasing TAG mass. The peak for $T_{54:0}$ is also markedly broader and of lower S/N that the other two peaks, illustrating how there is a reduction in performance for longer-retained species.
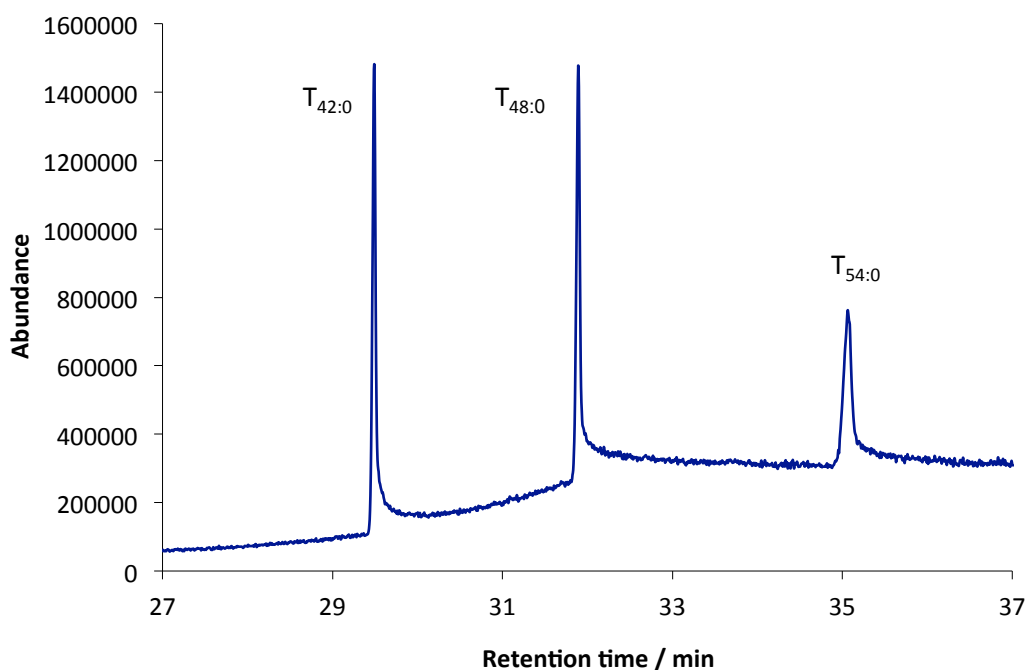
Figure 54. TAG region (27 min – 37 min) of a partial gas chromatogram of lipid standards, containing equal amounts of $T_{42:0}$, $T_{48:0}$ and $T_{54:0}$.

Table 6. Relative peak areas per mole of analyte for equal amounts of three authentic TAG standards analysed by OCI-HTGC-MS (Figure 54).

TAG	Relative Area
$T_{42:0}$	1.00
$T_{48:0}$	0.80
$T_{54:0}$	0.79

4.7.2   Analysis of Experimentally Buried Samples

Five of the experimental burial samples were selected for OCI-HTGC-MS analysis for comparison with MALDI-MS, with the aim of covering a range of burial periods.

The chosen samples were body potsherds buried for two months and two years respectively, rim potsherds buried for one year and two years respectively, and a base potsherd buried for one year. Figure 55 shows the TAG region of a chromatogram of the base potsherd which had been buried for one year, as an example. The peaks are labelled with the carbon number of the TAG, and unsaturated TAGs elute just before their saturated counterparts due to their slightly higher polarity and thus lower retention. The lack of molecular ion peaks in the EI-MS data means that it is not always simple to determine which TAG is which from the data. Of course, retention times can be taken in combination with MS data, with the TAGs eluting in size order and the largest TAGs having longest retention times. However, interpretation of such data takes time. This illustrates one of the advantages of MALDI-MS: the ease and speed with which data analysis can be carried out, since the identity of a TAG can be determined simply from its *m/z* value.
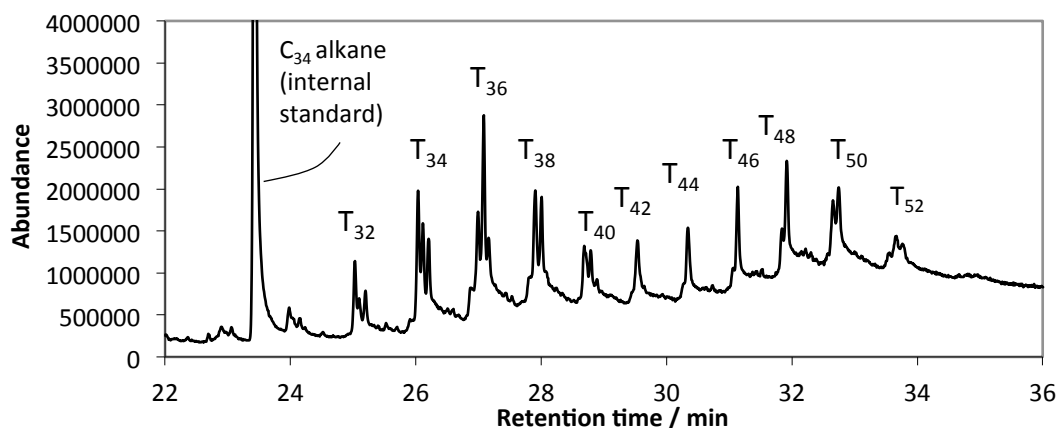
Figure 55. TAG region (22 – 36 min) of a partial gas chromatogram of a one-year experimentally buried base potsherd that had been used to cook milk. TAGs from T_{32} to T_{52} are detected.

Figure 56 is the mass spectrum of the peak at t_R = 32.8 min in the chromatogram of the one year burial base potsherd, corresponding to $T_{50:0}$. There are six peaks, some of which are at low S/N and difficult to see relative to other peaks in the spectrum, that help to identify the TAG. This illustrates the complexity of the HTGC-MS data compared to MALDI-MS data.

Another point illustrated by the chromatogram (Figure 55) is that saturated and unsaturated TAGs are not fully resolved in HTGC-MS, whereas in MALDI-MS they are well resolved, having an *m/z* difference of 2 units. Figure 57 shows the MALDI mass spectrum of the one year base potsherd experimental burial for comparison with the OCI-HTGC-MS. Even carbon-numbered TAGs in the range T_{28} to T_{54} were detected with good S/N, the saturated examples being marked with stars. Singly unsaturated TAGs were observed for TAGs in the range $T_{30:1}$ to $T_{54:1}$, with $T_{54:2}$ also observed. The peaks for the unsaturated TAGs are clearly resolved from their saturated counterparts, and the data are easily interpreted by looking at the *m/z* value, which corresponds to $[M+Na]^+$.
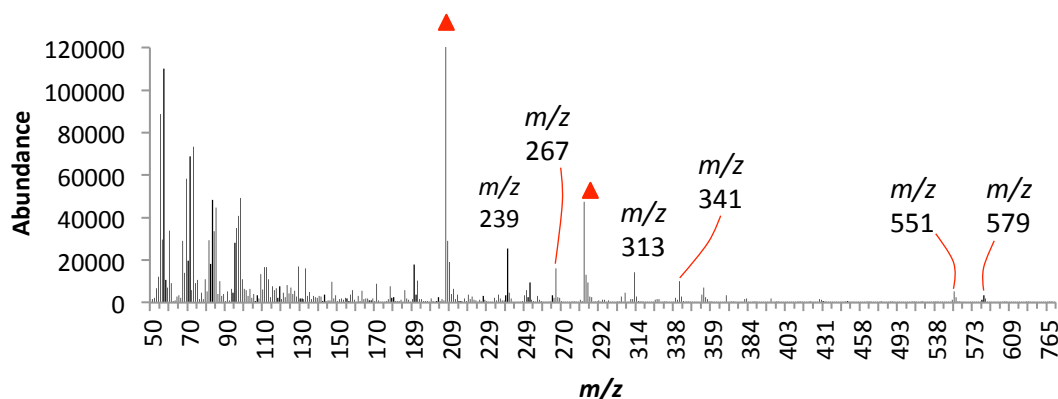
Figure 56. Mass spectrum of the peak corresponding to $T_{50:0}$ (t_R = 32.8 min) in the one-year experimentally buried base potsherd chromatogram (Figure 55). The peaks at *m/z* 239 and 267 correspond to $[RCO]^+$ for the $C_{16:0}$ and $C_{18:0}$ fatty acids, respectively. The peaks at *m/z* 313 and 341 correspond to $[RCO+74]^+$ for the $C_{16:0}$ and $C_{18:0}$ fatty acids, respectively. The peaks at *m/z* 551 and 579 correspond to [M-$RCOO]^+$ for loss of the $C_{18:0}$ and $C_{16:0}$ fatty acids, respectively. Peaks marked with triangles are associated with column bleed.
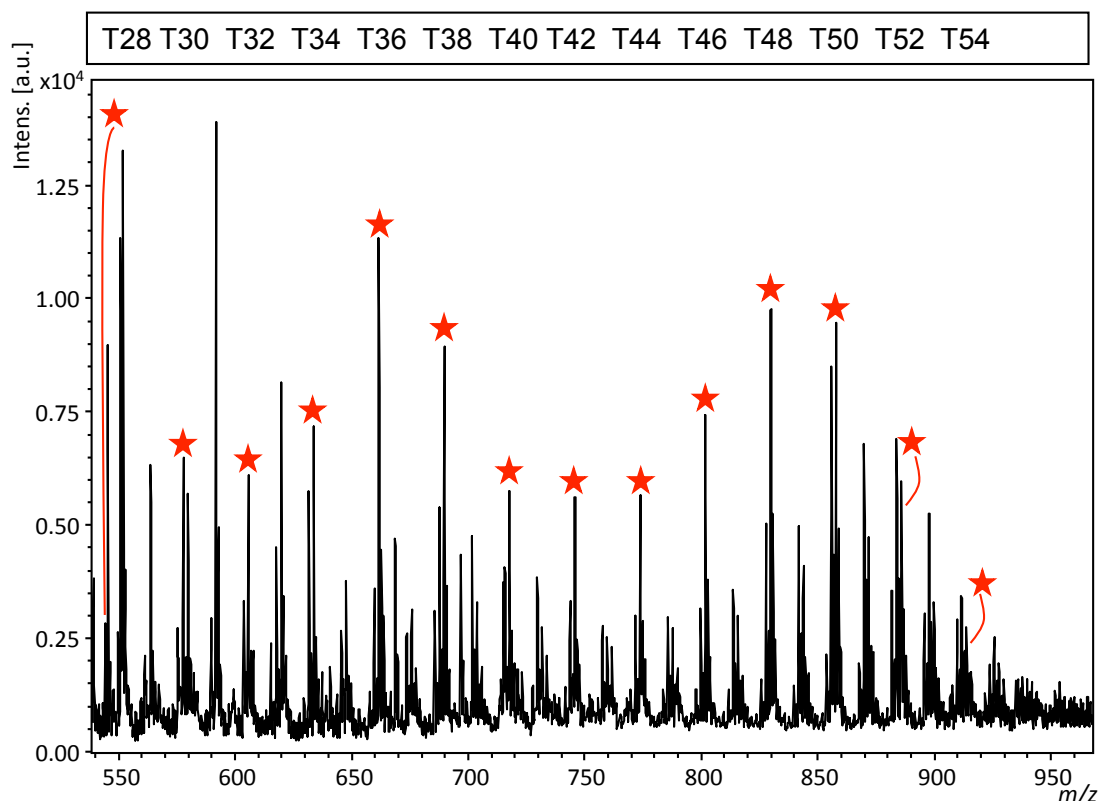
Figure 57. MALDI mass spectrum of a one-year experimentally buried base potsherd that had been used to cook milk. TAGs from T_{28} to T_{54} are detected. Stars denote saturated TAGs.

TAGs smaller than T_{32} were not detected using HTGC-MS in the one year base potsherd experimental burial, although it looks from the chromatogram (Figure 55) as if the sequence of TAGs may continue below T_{32}, with peaks at $t_R \approx 23$ min and $t_R \approx 24$ min. However, analysis of the MS data shows that these peaks correspond to DAGs, rather than TAGs. This was the case in several of the samples, and care must be taken that peaks corresponding to DAGs are not misassigned as TAGs. The low mass TAGs co-elute with DAGs, making these TAGs impossible to detect in some cases. This is another advantage of MALDI-MS. Since MALDI-MS is selective for TAGs over other lipids, this problem does not occur (and in any case, TAGs and DAGs have different masses, although a DAG with one odd carbon-numbered fatty acid does have the same mass as a TAG with three even carbon-numbered fatty acids) and TAGs down to T_{28} were detected in several samples using MALDI-MS. Although DAGs were detected by MALDI-MS in standards, they were not detected using this method in any of the experimental burial samples, presumably due to their low abundance. T_{54} was also not detected in the one year base potsherd using

HTGC-MS, although it was using MALDI-MS. In the chromatogram there does appear to be a very small peak at the expected retention time for T_{54}. However, this is hardly above the baseline and the MS data did not contain any peaks corresponding to T_{54} ions so it could not be identified.

Table 7 shows the range of TAGs detected in each of the five potsherd burial samples using each method. Except for the two month body potsherd, where the range of detected TAGs was the same for the two methods, MALDI-MS was able to detect TAGs of a wider mass range. The lightest TAG detected by MALDI-MS in each of the samples was lighter than that detected by OCI-HTGC-MS, and in most cases the heaviest TAG detected by MALDI-MS was heavier than that detected by OCI-HTGC-MS. In all of the chromatograms, the T_{54} samples were of very low S/N and hardly detectable. In MALDI-MS the peaks for T_{54} also tended to be of low S/N. However, these peaks were detectable in each sample, which was not always the case when using HTGC-MS.

Table 7. Range of TAGs detected in a selection of experimentally buried samples by both OCI-HTGC-MS and MALDI-MS.

Sample	OCI-HTGC-MS	MALDI-MS
Body – 2 month	$T_{28} - T_{54}$	$T_{28} - T_{54}$
Body – 2 year	$T_{32} - T_{54}$	$T_{30} - T_{54}$
Rim – 1 year	$T_{32} - T_{46}$ (T_{48} and T_{50} possibly detected)	$T_{30} - T_{54}$
Rim – 2 year	$T_{32} - T_{52}$	$T_{30} - T_{54}$
Base – 1 year	$T_{32} - T_{52}$	$T_{28} - T_{54}$

As well as the ability to interpret MALDI-MS data more quickly than HTGC-MS data, MALDI-MS data acquisition is much faster. The HTGC-MS method (which is a standard method in use across many labs with very little variation) takes almost one hour, whereas one sample can be analysed by MALDI-MS in a few seconds. Even with subsequent MS/MS analysis, all of the data for one sample can be obtained by MALDI-MS in less than five minutes. The process can also be automated (as can HTGC, of course, with the use of an autosampler). Automatic MALDI-MS data acquisition works particularly well when using an AnchorChip™

plate, since the sample spots are concentrated on the anchor in the centre of each target spot, meaning that more reproducible data can be obtained.

The sample preparation for MALDI-MS is no more onerous than that for HTGC-MS. Although both matrix and sample must be spotted on the MALDI plate, and in the method used here there is an additional step of spotting acetone, sample preparation for HTGC-MS typically involves trimethylsilylation which is time-consuming (involving an hour of heating followed by drying and redissolving) and adds another step to the preparation process.

4.8 CONCLUSIONS

The overall aims of this work were to explore the potential use of MALDI-MS for the analysis of lipid extracts from archaeological potsherds. Standard lipids, and lipid extracts of modern animal fats and experimentally buried potsherds, have been used to develop the method and demonstrate its feasibility for application to archaeological samples, and the advantages of doing so.

The method has been shown to be successful for the detection of TAGs from samples of increasing complexity and levels of degradation, and the analysis of experimentally buried potsherds has been able to provide information about the ability of MALDI-MS to detect a range of TAGs extracted from a ceramic matrix after relatively short-term burial. It shows that MALDI-MS is capable of detecting a wide range of TAGs, but that S/N decreases after a period of burial when compared to unburied controls. This shows that degradation starts to occur over relatively short periods of time, but that short-chain TAGs are not completely lost over these short periods, consistent with data from other methods.

A fractionation method was developed to separate TAGs from other species present and it was tested to determine whether it could improve TAG detection. Although the MALDI-MS method had been shown to be specific for TAGs and so this step may be unnecessary, published work had indicated that it does improve results when nanoESI is used, so the method development was undertaken. It was found that it may improve TAG detection in samples for which TAGs are not well-detected in crude extracts. However, it is recommended that fractionation is only carried out after analysis of the TLEs and identification of samples where it may bring

advantages, since it does result in a significant increase in sample preparation time and is not beneficial for all samples.

The MALDI-MS method has been shown to be able to detect TAGs when HTGC cannot, making it an important addition to the techniques available for interpretation of archaeological ceramic remains. It is specific for TAGs, making it complementary to HTGC-MS, which is better for the detection of smaller lipids. The fact that MALDI-MS is specific for TAGs means that the problem of co-detection of DAGs with smaller TAGs is not an issue, as it is with HTGC-MS.

In addition to the fact that MALDI-MS is more suitable for TAG analysis than HTGC-MS, it is much faster, making it suitable for use as a screening method to identify samples for further in-depth analysis by HTGC-MS. Since TAGs are the primary components of fresh animal fats, but their levels decrease as the samples become more degraded, the detection of TAGs by MALDI-MS in the first instance can provide an indication that a particular sample is well preserved, allowing such samples to be prioritised for further analysis. Since a large number of potsherds can be excavated from any one archaeological site, this prioritisation can enable best use of the available analytical resources. Subsequent chapters will present case study applications of the methods developed in this chapter to archaeological samples.

5 RESULTS: APPLICATION OF MALDI-MS TO ARCHAEOLOGICAL SAMPLES FROM DURRINGTON WALLS

5.1 INTRODUCTION

Following the development of the MALDI-MS method for analysis of archaeological lipid analysis, real archaeological samples were required to test its applicability. The Neolithic site of Durrington Walls in Wiltshire, UK was part of a large project in BioArCh at the University of York, so many samples were available from this site, making it ideal as a case study for the MALDI-MS method.

5.1.1 Background to Durrington Walls

Durrington Walls is one of Britain's largest henge monuments, with a diameter of nearly 500 m.[168] Although the term 'henge' is popularly thought to mean a ring of standing stones, it actually refers to an earthen enclosure composed of a circular bank with an internal ditch.[168] It is interesting to note that the famous Stonehenge monument is in fact not a henge at all, having a bank with an *external* ditch.

Durrington Walls (51.1925° N 1.7867° W) is located in Wiltshire, UK, around 14 km north of Salisbury, 3 km north-east of Stonehenge and close to the River Avon.[169] Figure 58 shows the location of Durrington Walls relative to Stonehenge and Salisbury. It was first discovered in the early nineteenth century by Sir Richard Colt Hoare[170] and has been excavated several times since: in 1959 by Stuart Piggott, 1966-7 by Geoffrey Wainwright (in advance of the A345 road being built through the eastern half of the monument)[170], and most recently between 2004 and 2007 by Mike Parker Pearson and the Stonehenge Riverside Project as part of a large investigation into Stonehenge and the surrounding area.[169]
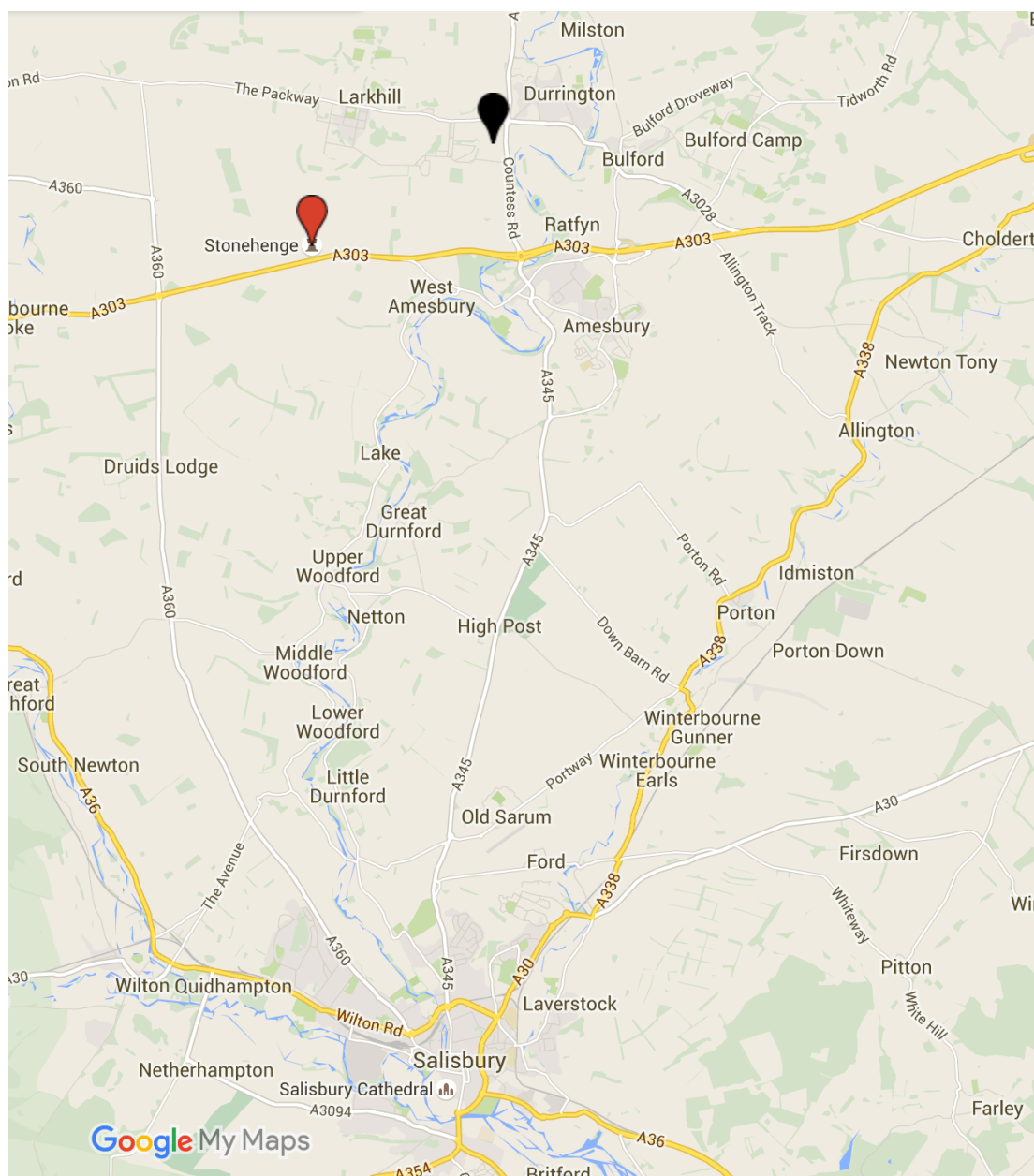
Figure 58. Map showing the location of Durrington Walls (black marker) relative to Stonehenge (red marker), the river Avon and Salisbury. Map data ©2015 Google.

An article in 1929 described Durrington Walls with the use of aerial photographs, though no excavation was carried out at this time.[171] Radiocarbon dates obtained from charcoal excavated from under the bank of the henge in 1952 placed the construction of the earthworks in 2620 – 2630 calibrated years BC.[172] At the time this was considered 'archaeologically unacceptable' due to the presence of two fragments of Beaker pottery, which did not appear in Britain until later.[172,173] Later radiocarbon dating (from material excavated in the 1960s) gave widely varying dates

154

and so was able to place the construction of Durrington Walls only broadly in the mid-third millennium BC.[169] The most recent radiocarbon dating at Durrington Walls was carried out on material excavated from the remains of houses at the site. The houses were constructed before the henge bank and ditch and are estimated to have been used for a maximum 55 years, with their construction starting between 2535 cal. years BC and 2475 cal. years BC.[143]

Within the henge the remains, in the form of post holes, of two timber circles were discovered. Both of these circles are in the eastern half of the henge and lay in the path of the road, so were excavated in 1966-7. The larger of the two structures (the Southern Circle) had three phases of construction, and a large quantity of pottery was discovered in the post holes, mainly Grooved Ware (see later) but also some Beaker pottery. The Northern Circle was similar to the Southern Circle but built on a smaller scale. It had an avenue leading to it from the south. Figure 59 shows Durrington Walls with the position of the Northern and Southern Circles marked. The Southern Circle was reconstructed for the TV programme Time Team in 2005, as shown in Figure 60.
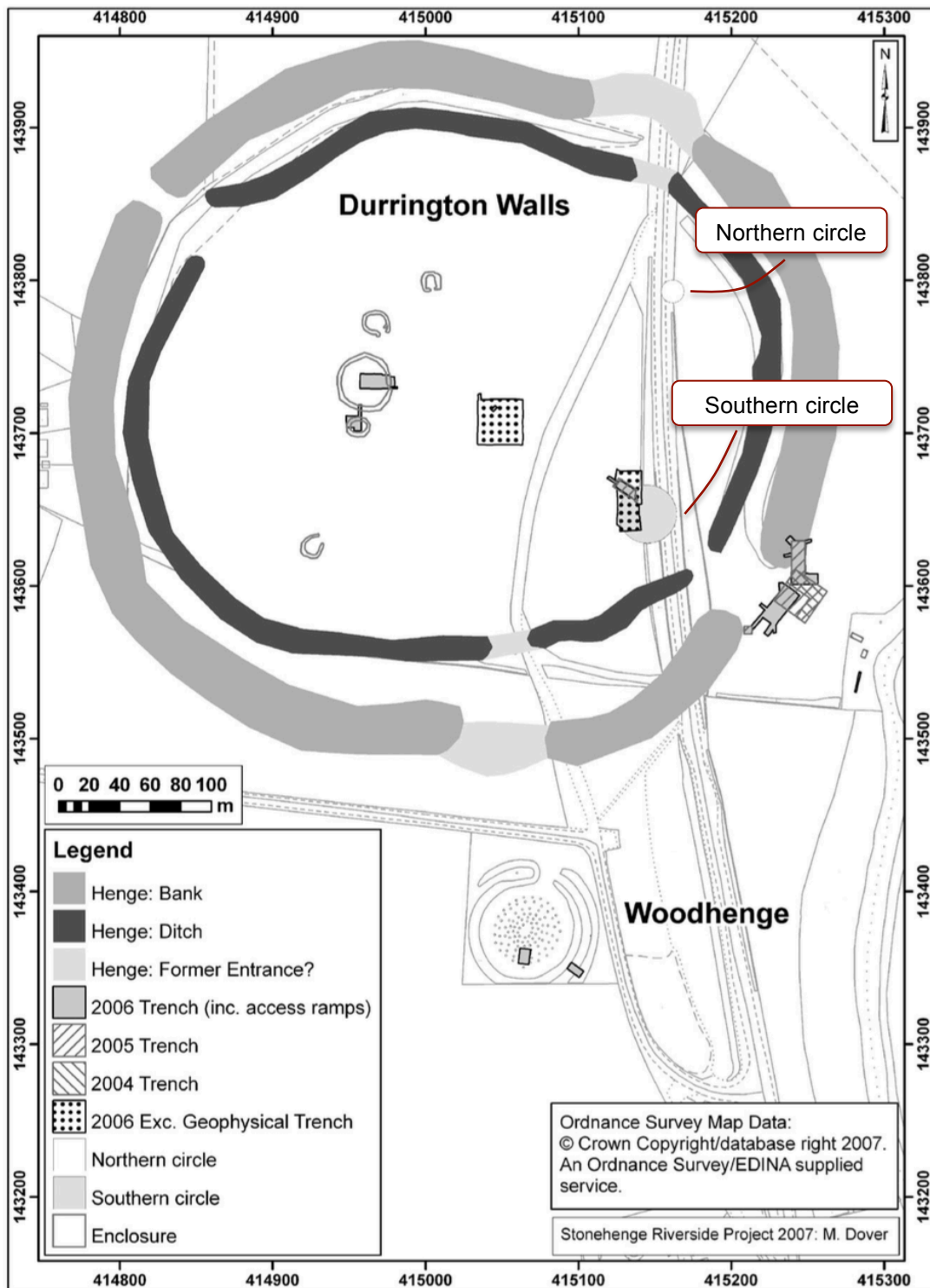
Figure 59. Diagram of Durrington Walls showing the location of, amongst other features, the Northern and Southern Circles. Modified from Parker Pearson *et al*.[169]

Figure 60. Full-size reconstruction of the Southern Circle at Durrington Walls, constructed in 2005 for the TV programme Time Team. Reproduced from Parker Pearson et al.[168]

One of the aims of the Stonehenge Riverside Project was to try to discover whether Durrington Walls had an avenue leading to the River Avon, as Stonehenge does, which could provide evidence for a connection between Durrington Walls and Stonehenge via their avenues and the river.[168] During the excavations, which did indeed discover an avenue leading from the Southern Circle inside Durrington Walls to the river, the remains of several houses were discovered. It was from these houses that the most recent radiocarbon dates were obtained.[143] These dates are similar to the dates for the building of Stonehenge Stage 2 (the period when the sarsen circle and trilithons were erected)[174] and Durrington Walls has been proposed as the most likely place for the builders of Stonehenge to have lived.

The idea for a path linking Stonehenge and Durrington Walls stemmed from the theory that Stonehenge was associated with dead ancestors whilst Durrington Walls was a place for the living, and that ceremonial processions could have taken place between the two monuments via their avenues and the river, perhaps taking the dead on a journey from the world of the living to the land of the dead.[175] Stonehenge contains many human cremation burials, whereas Durrington Walls was found to

157

have a large amount of Grooved Ware pottery and animal bones (some 50 000 in total, with only a few human bones[169]), and the structures of the monuments have also been used to add weight to this theory. The inspiration for the idea came from a comparison with Madagascar, where, according to tradition, for many people the body is seen to be soft and wet at birth, and over time hardens and dries, even into death. In Madagascar this means that houses are made from wood, but stone is used for tombs, and it was thought that the same could have applied to Durrington Walls and Stonehenge.[175] Whilst making a comparison between Neolithic Britain and contemporary Madagascan folk traditions may seem like a big leap, it is conceivable that two completely separate societies could have similar views about the relationships between certain materials and stages of life, especially when the archaeological evidence seems to support the theory.

Further evidence for a processional route between Durrington Walls and Stonehenge comes from the fact that the Southern Circle at Durrington Walls faces the midwinter sunrise and the avenue is on the line of the midsummer sunset, which is complementary to the arrangement at Stonehenge, where the stone circles face the midsummer sunrise and the avenue is on the line of the midwinter sunset (Figure 61).[168] The thought is that processions could travel from Durrington Walls to Stonehenge at midwinter and in the opposite direction at midsummer. Whilst it might be expected that the positions of the sun at the two solstices would be opposite each other and therefore it would be impossible to tell on which solstice the features are aligned, the fact that Durrington Walls is built on a slope means that the sun appears to set further south than it would on the flat. This, taken with the fact that the avenue is positioned across the contour of the valley, rather than following it, indicates that its alignment was deliberate.[169]
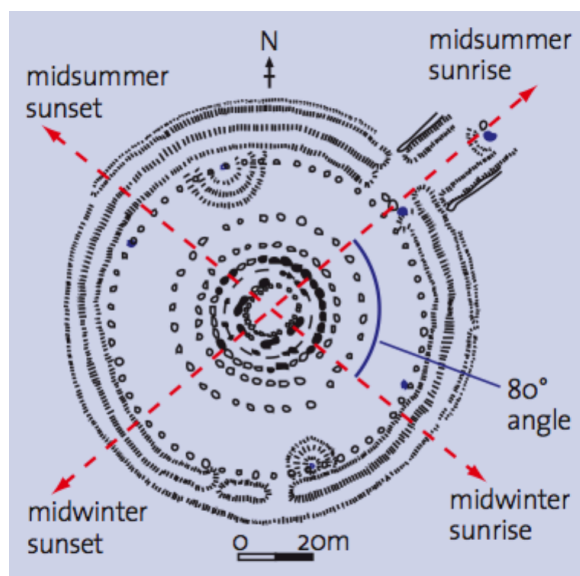
Figure 61. Diagram of Stonehenge showing the directions of sunrise and sunset at the solstices. Reproduced from the Royal Astronomical Society factsheet *Stonehenge and Ancient Astronomy*.[v]

The houses discovered around the region of the avenue are remarkable in that never before on mainland Britain have a large collection of such houses of this age been found.[168] Seven houses were discovered, with clay floors with a central hearth and walls made from wattle and daub. In the areas around the houses there are accumulations of waste material, including animal bones, and at other excavations around the henge there have been found similar deposits which has been taken to indicate that there may have been many more houses and that Durrington Walls was a large settlement. There is also evidence that it was no ordinary domestic settlement. The bones at the site are almost exclusively from pigs and cows,[176] and none of them come from neonates, suggesting that Durrington Walls was not a site where animals were born and raised.[143] Marks on the bones from butchery, and the fact that many of the pig bones were burnt at the ends, suggests that pig carcasses may have been spit-roasted, perhaps for large gatherings of people for feasting.[176] This, taken with the alignments of the circles on the midwinter solstice, has been

---

used as evidence that some kind of event may have taken place at Durrington Walls at midwinter.[168]

5.1.2 Grooved Ware Pottery

Grooved Ware, of which a large number of potsherds have been found at Durrington Walls, was a style of pottery produced in the Late Neolithic period and is characterised by the vessels having flat bottoms, straight sides and grooved decoration around the outside.[177] An image of a reconstructed Grooved Ware pot is shown in Figure 62. Grooved Ware originated in the north of Scotland (probably in Orkney) some time before 3000 cal. years BC and spread throughout Britain.[177] In England and Wales it is thought to have been in use in the period 2900-2100 cal. years BC. It was followed by Beaker pottery, which came to Britain from continental Europe. Grooved Ware has been characterised into four styles, based on the decorative features: Rinyo, Clacton, Woodlands and Durrington Walls (though there is some debate that Woodlands is a development of Clacton, and the two are in fact one style).[177] Huge numbers of Grooved Ware potsherds have been discovered, with some archaeological sites in Scotland being found to contain as many as 10 000 examples.[177] Grooved Ware deposits are often found near rivers or the coast, and near monuments. It has been argued that many of the deposits look like they have been deliberately placed, sometimes with along with animal bones. There appears to be a connection between Grooved Ware deposits and barrows (Late Neolithic and Bronze Age burial mounds), which were built later. In Wiltshire, for example, around 75% of Grooved Ware deposits have been reported to be under or near to barrows, and most of the others are in places which have been interpreted as ceremonial or ritual sites.[177] This has been taken to imply that certain places were considered important over long periods of time. Of course, most archaeological excavation takes place at sites where features can be observed on the surface of the land and so it could be argued that this observed link is a function of bias in site selection. However, activities such as quarrying and building also result in ground disturbance that is recorded by archaeologists and so if Grooved Ware was more widely deposited this would probably have been observed.[177]

Figure 62. Reconstructed Grooved Ware vessel, showing the characteristic markings on the outside. Image courtesy of Salisbury and South Wiltshire Museum.

5.1.3 Rationale for Analysis

Chemical analysis of Grooved Ware potsherds from Durrington Walls was one of the subjects of the Feeding Stonehenge Project, led by Mike Parker Pearson at University College London and involving researchers from the University of York as well as other institutions. The aim of the project was to study the lives of the prehistoric people in the area around Stonehenge, with part of the work involving gaining information on the foods people were eating by analysing lipids extracted from the ceramic assemblage found at Durrington Walls. The residues were analysed and the results compared with the samples' location at the site to try to gain information about the spatial distribution of various activities there, using GC(-MS) and GC-c-IRMS.[143] Previous analysis of Grooved Ware from Durrington Walls had found generally good TAG preservation in potsherds from the site, including some low molecular weight TAGs (down to T_{42}).[178] However, the analysis carried out using HTGC at York for the Feeding Stonehenge project revealed that a disappointing number of potsherds contained detectable TAGs. Therefore, it was suggested that these could be suitable samples for applying MALDI-MS in the hope of improving the detection limits for intact TAGs in these samples.

5.2 RESULTS AND DISCUSSION

A total of 44 potsherds from Durrington Walls were selected and subjected to lipid extraction and MALDI-MS analysis. All except three of the samples had previously

161

been analysed by HTGC[vi] as part of the Feeding Stonehenge project.[143] The choice of potsherds for MALDI-MS analysis was intended to cover a range of lipid distributions based on HTGC analysis in order to:

- test whether MALDI-MS could be used to detect TAGs in archaeological sample extracts in which HTGC was unable to do so.
- compare the MALDI-MS and HTGC results for samples in which TAGs were detected by HTGC.

Therefore, it was important that some but not all of the samples had detectable TAGs based on HTGC analysis. All of the selected samples at least contained detectable fatty acids (which are the final breakdown product of TAGs), most contained MAGs and DAGs and a few contained steroids. However, only seven contained detectable intact TAGs, and when there were detectable TAGs, the peaks were of very low S/N. The HTGC analysis had been carried out using splitless injection so samples were selected, after MALDI-MS analysis, for analysis using OCI-HTGC-MS to compare TAG detection between the two techniques when the optimum HTGC technique is used.

Lipids were freshly extracted from the potsherds before MALDI-MS analysis (so it is important to note that the extract used for MALDI-MS analysis was not exactly the same as that used for the previous HTGC analysis, although the same protocols were used). The extraction was carried out according to the standard lipid extraction protocol used in BioArCh (see section 3.1.2). Briefly, approximately 1 g of ceramic was removed from the inside surface of each potsherd using a modelling drill and lipids were extracted from the powder using three portions of 2:1 (v:v) DCM:methanol with ultrasonication in an ultrasonic bath. The portions were combined, split into three roughly equal portions and dried under a stream of nitrogen. One portion from each sample was dissolved in 100 μL hexane and 1 μL was spotted onto a Bruker AnchorChip™ plate with DHB matrix for analysis by MALDI-MS on a Bruker ultraflex III TOF/TOF MS. Thus, the lipids detected were those from approx. 3 mg of potsherd powder. No internal standard was used (which

---

[vi] Carried out by Lisa-Marie Shillito, as described in sections 3.2.7 and 3.2.8.

would normally be included for HTGC analysis) since the aim was not to quantitate but to look qualitatively for TAGs. Blank extractions, which involved carrying out the extraction method in the same way as for a sample except that no potsherd powder was added, were carried out alongside the samples to control for reagent and method contamination.

Analysis of the extraction blanks by MALDI-MS did not reveal TAGs, indicating that there is no detectable TAG contamination deriving from the solvents or sample handling, and that the TAGs detected in the samples are due to lipids deriving solely from the potsherds.

Figure 63 shows an example MALDI mass spectrum from one of the samples (pottery residue number (PRN) 5051). The spectrum shows a distribution of saturated TAGs in the range $T_{48:0} - T_{54:0}$, with monounsaturated TAGs in the range $T_{50:1} - T_{54:1}$ also present. This is a sample in which TAGs were detected using HTGC, and Figure 64 shows the chromatogram from the same potsherd, obtained as part of the Feeding Stonehenge Project (Lisa-Marie Shillito). The peaks in the TAG region of Figure 64 are very weak and there are only three of them, demonstrating that for TAG detection the MALDI-MS method is an improvement over the methods currently in use in BioArCh. This chromatogram is quite typical of the HTGC data that was obtained for Durrington Walls samples and illustrates why samples from this site were selected for TAG analysis by MALDI-MS.

In the HTGC, the peaks do not show any differentiation between saturated and unsaturated TAGs, whereas there are three unsaturated TAGs detected using MALDI-MS. The detection of these unsaturated TAGs validates one of the advantages of MALDI-MS over HTGC for the analysis of TAGs. As demonstrated in chapter 4, on HTGC-MS analysis TAGs with the same number of carbons but different levels of unsaturation are not fully resolved, which is particularly problematic when the peaks are so small that it is very difficult to see the difference between saturated and unsaturated TAGs. In contrast, with MALDI-MS the difference of 2 *m/z* units between a fully saturated TAG and its monounsaturated counterpart can readily be distinguished.
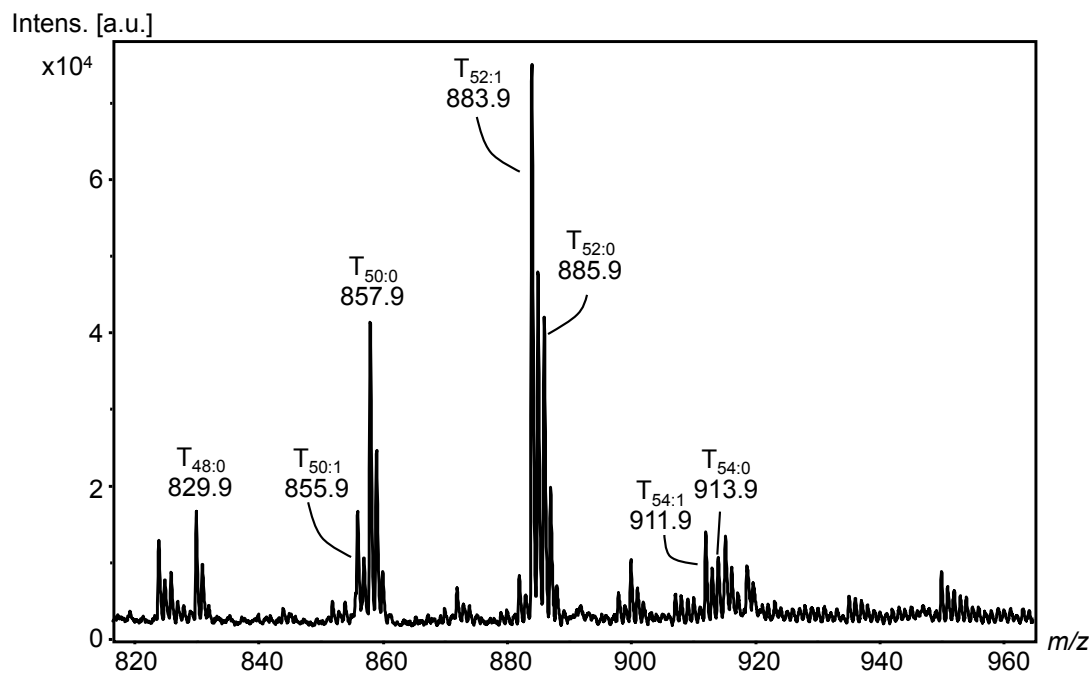
Figure 63. MALDI mass spectrum of PRN 5051, showing a range of saturated and unsaturated TAGs.
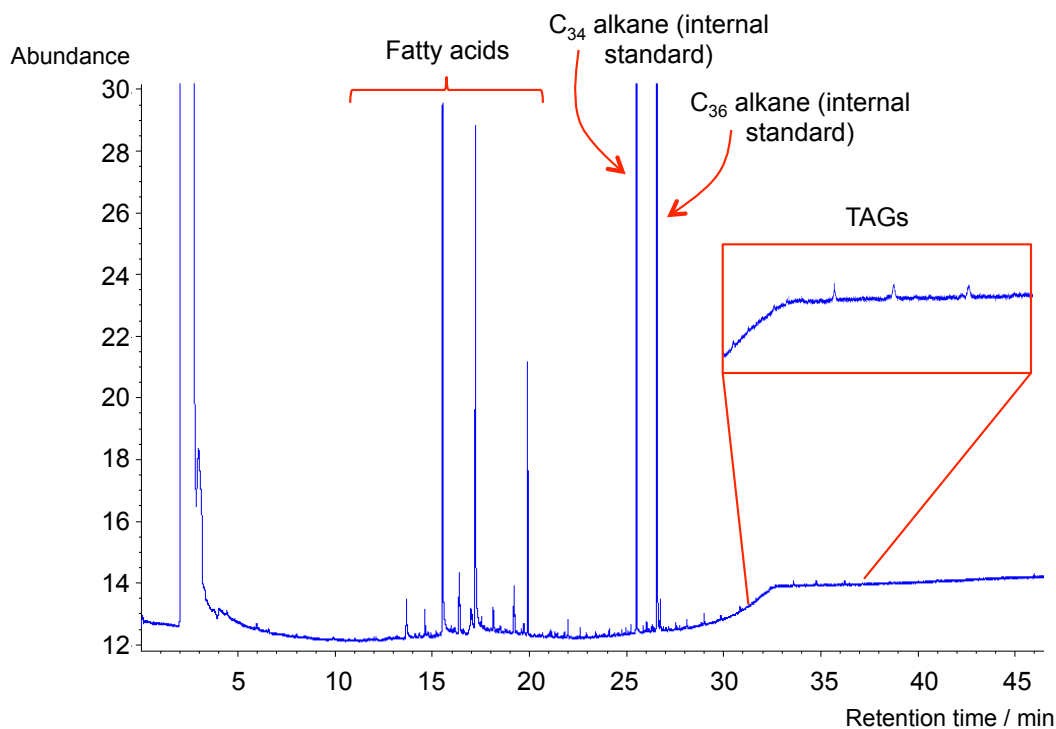
Figure 64. High temperature gas chromatogram of PRN 5051, showing very small peaks for TAGs, and giving no information about whether the TAGs are saturated or not (data obtained by Lisa-Marie Shillito). The internal standard peaks are off-scale.

Table 8 summarises whether TAGs were observed by MALDI-MS in extracts of
each of the potsherds, along with the lipid species observed on the previous HTGC
analysis. As can be seen from Table 8, 31 of the 44 potsherds contained TAGs
detectable by MALDI-MS (70%). This is in contrast to only 7 of the 41 samples
analysed by HTGC having detectable TAGs using that method (17%), showing that
MALDI-MS is able to detect TAGs in archaeological samples where HTGC fails.
This is an important validation of the method development reported in Chapter 4
because it shows that the method is applicable to archaeological samples and can
make a real contribution to the archaeological science field. TAGs are the primary
components of animal fats and so represent the undegraded remains of the foods that
were cooked in the pots. Various publications have reported the successful
application of methods other than HTGC to archaeological lipid extracts in order to
try and improve the detection of TAGs (particularly HPLC and
nanoelectrospray),[84,24] demonstrating the importance of these compounds for
interpretation of archaeological lipid residues. In Table 8, PRN 3298 is marked with
an asterisk because the TAGs were detected after fractionation and not in the
unfractionated extract (see section 5.2.5).

Table 8. Durrington Walls potsherds and the lipids detected in each one by HTGC, and whether TAGs were detected by MALDI-MS. (PRN = pottery residue number)

PRN	Fatty Acids	Steroids	MAGs	DAGs	TAGs	TAGs by MALDI
1285	No HTGC analysis					Y
1301	Y	N	Y	Y	N	Y
1311	Y	Y	Y	Y	N	Y
1325	Y	N	N	N	N	N
1343	Y	Y	Y	Y	N	N
1619	Y	N	Y	Y	N	N
1645	Y	N	Y	Y	N	Y
1651	Y	N	Y	N	N	Y
1653	Y	N	Y	Y	N	N
1665	Y	N	Y	N	N	N
1698	Y	N	Y	Y	Y	N
1735	Y	Y	Y	Y	N	Y
1889	Y	N	Y	Y	N	Y
2052	Y	N	Y	N	N	Y
2062	Y	N	Y	Y	N	Y
2144	Y	N	Y	Y	Y	Y
2156	Y	Y	Y	Y	Y	Y
2175	Y	N	Y	Y	Y	Y
2319	Y	N	Y	Y	Y	Y
2417	Y	N	N	N	N	N
2764	Y	Y	N	N	N	Y
2849	Y	N	Y	N	N	Y
2876	Y	N	Y	Y	N	Y
2902	Y	Y	Y	Y	N	Y
2998	Y	N	Y	Y	N	Y
3142	Y	Y	Y	Y	N	Y
3266	Y	N	Y	Y	N	Y
3298	Y	N	Y	N	N	Y*
3323	Y	N	Y	Y	N	Y
3341	Y	N	Y	N	N	N
3981	Y	Y	N	Y	N	N
3999	Y	N	Y	Y	N	Y
4481	Y	N	Y	Y	N	Y
4704	Y	N	N	N	N	Y
5008	Y	Y	N	Y	N	Y
5039	Y	Y	Y	N	N	N
5051	Y	Y	Y	Y	Y	Y
5053	Y	Y	Y	Y	Y	Y
5062	Y	Y	Y	Y	N	N
5074	No HTGC analysis					Y
5075	Y	N	N	N	N	Y
5536	Y	N	Y	N	N	N
5537	Y	N	Y	N	N	N
10235	No HTGC analysis					Y

As can be seen from Table 8, all except one of the samples in which TAGs were detected by HTGC also showed TAGs on MALDI-MS analysis. The MALDI mass spectrum of the one sample that did not show detectable TAGs on MALDI-MS analysis, PRN 1698, is shown in Figure 65. The mass spectrum has many peaks in the TAG region with *m/z* values that do not correspond to TAG [M+Na]$^+$ ions, with a series of peaks in the *m/z* range ca. 700 – 1200 separated by 14 *m/z* units. This is suggested to be due to polymer contamination. There were some low intensity signals which did have *m/z* values corresponding to TAG [M+Na]$^+$ ions, but due to the large number of other peaks these could not be assigned conclusively as TAGs.
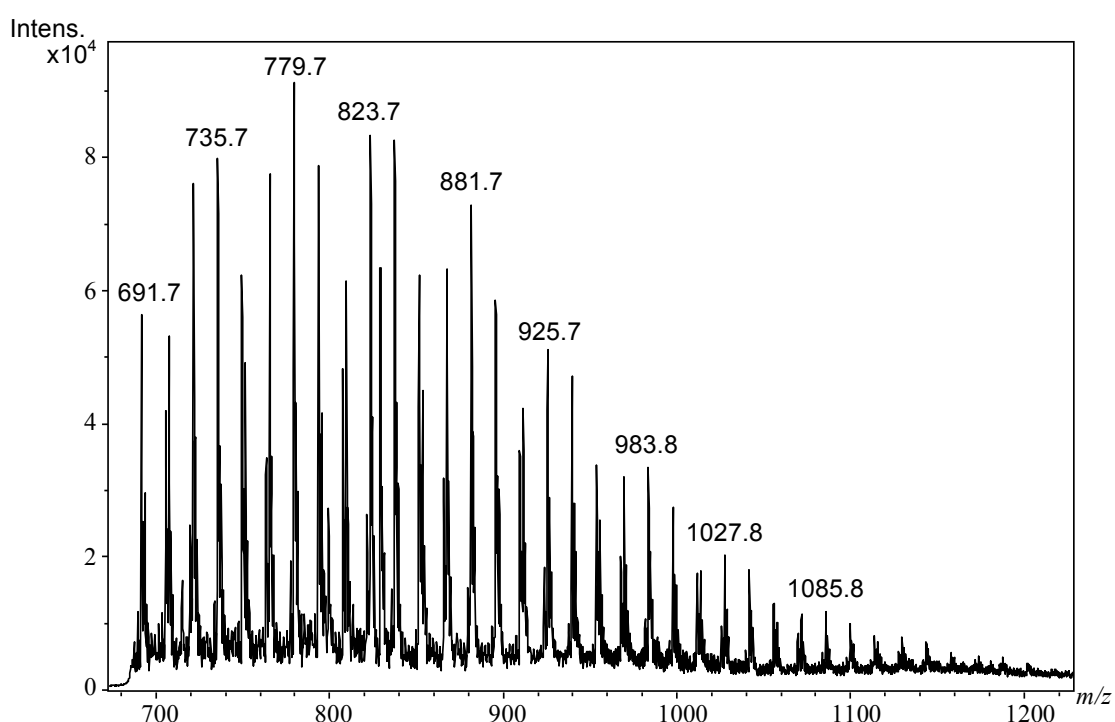
Figure 65. MALDI mass spectrum from extract of PRN 1698, showing a range of peaks with *m/z* values which do not correspond to those for TAG species.

TAGs detected / PRN	$T_{46:0}$	$T_{48:0}$	$T_{50:0}$	$T_{52:0}$	$T_{54:0}$	$T_{46:1}$	$T_{48:1}$	$T_{50:1}$	$T_{52:1}$	$T_{54:1}$
1285	■	■	■	■				□		
1301		■	■	■						
1311			■	■						
1325										
1343										
1619										
1645		■	■	■					□	□
1651		■	■							
1653										
1665										
1698										
1735			■	■	■					
1889			■	■	■					
2052		■	■	■				□	□	
2062		■	■	■	■		& $T_{50:2}$, $T_{50:3}$			
2144			■	■						
2156	■	■	■	■	■				□	
2175		■	■	■	■				□	□
2319	■	■	■	■	■		& $T_{48:2}$, $T_{48:3}$, $T_{50:2}$, $T_{50:3}$, $T_{52:2}$			
2417										
2764	■	■	■	■	■				□	
2849		■	■	■	■				□	
2876			■	■	■				□	
2902		■	■	■	■					
2998	■	■	■	■	■			□	□	□
3142		■	■	■	■			□	□	
3266				■	■					
3298			■	■	■		& $T_{50:2}$			
3323		■	■	■						
3341										
3981										
3999		■	■	■				□		
4481		■	■	■	■		& $T_{52:2}$			
4704		■	■	■	■					
5008		■	■	■	■			& $T_{52:2}$		
5039										
5051		■	■	■	■		& $T_{52:2}$			
5053			■	■	■					
5062										
5074		■	■	■	■			□		
5075		■	■	■	■				□	
5536										
5537										
10235		■	■	■	■			□		

5.2.1 Ranges of TAGs Detected

The MALDI mass spectra were examined to determine the range of TAGs that were detected in each sample (Figure 66). The graph has labels for even carbon number TAGs only, but odd carbon number TAGs between them were always present.

As can be seen from Figure 66, there is variation in the range of TAGs detected in the extracts of the different samples. The lightest TAG observed in any sample is T_{46} and the heaviest is T_{54} (which was observed in most samples). Unsaturated TAGs were observed in fewer of the samples than saturated TAGs, and the mass ranges of unsaturated TAGs were smaller. The signals for the lighter TAGs were always of lower S/N than those for the heavier ones, except for T_{54} which was always of low S/N. It was not possible to carry out tandem mass spectrometry of these low S/N peaks, which means it has not been possible to obtain information on the fatty acid constituents of the lighter TAGs. This is unfortunate because it is the fatty acid composition of the lighter TAGs that is likely to be most informative, since heavier TAGs have to be composed primarily of $C_{16:0}$ and $C_{18:0}$ fatty acids, these being the most common in animal fats (Chapters 1 and 4).

Figure 66 (on facing page). Graph showing the range of TAGs detected by MALDI-MS in lipid extracts from Durrington Walls. The left hand bars (purple) refer to saturated TAGs and the right hand bars (grey) refer to singly unsaturated TAGs. TAGs with more unsaturation are noted when they occur.

Work published by the Evershed group has linked TAG distributions to the animal sources of the lipids, with TAGs in the range $T_{40} - T_{54}$ indicating ruminant fats (specifically dairy fats in the range $T_{40} - T_{46}$) and a narrower range, from $T_{44} - T_{54}$, indicating non-ruminant fats (see section 1.5.7).[65,68] Clearly, since no TAGs smaller than T_{46} were detected in samples from Durrington Walls in the analysis carried out here (though previous analysis had found T_{42} and T_{44} TAGs[178]), following these criteria the TAG ranges in samples from this site cannot be used to identify differences in the source of the fats cooked in the different pots. This is a function of degradation, since lighter TAGs are known to degrade more quickly than heavier TAGs, with the shorter chain fatty acids that make up these lighter TAGs preferentially lost (see section 1.5.7), and so TAG ranges can only be used to indicate animal sources of the fats in samples that are exceptionally well preserved. Therefore, it is difficult to know if the lack of detection of TAGs lighter than T_{46} is because they were never present or because of degradation.

As part of the Feeding Stonehenge Project, GC-c-IRMS was applied to the lipid extracts. $^{13}C/^{12}C$ ratios of the $C_{18:0}$ and $C_{16:0}$ fatty acids were measured, and differences in the ratios were used to identify whether the lipids were primarily from ruminant adipose, ruminant dairy or non-ruminant adipose (porcine) sources (work carried out by Lisa-Marie Shillito). Table 9 is a comparison of the GC-c-IRMS interpretation of the residues with the TAG range as determined by MALDI-MS. There does not seem to be any correlation between TAG range and lipid source as determined by GC-c-IRMS. Due to short-chain TAGs being characteristic of milk lipids, a wide TAG range can be used to indicate the presence of milk (see section 1.5.7). However, of the three samples with the widest range of TAGs ($T_{46} - T_{54}$), one was assigned as dairy based on GC-c-IRMS, one was ruminant adipose and one had not been analysed by GC-c-IRMS. Although these samples had the widest TAG ranges of the samples analysed here, the lightest TAG detected (T_{46}) is not small enough to be indicative of milk, since it is TAGs in the range $T_{40} - T_{46}$ that have been used to indicate dairy fats in previous analyses.[65] Other samples interpreted as containing dairy fats based on the GC-c-IRMS analysis had either no TAGs detected or had T_{48} or T_{52} as their smallest detected TAG. From these results it seems that the majority of Durrington Walls samples are too degraded to be able to infer much from their TAG distributions. This illustrates how it is important to use a

range of techniques to gain maximum information about the lipids in archaeological ceramics.

Table 9. TAG range determined by MALDI-MS in each of the Durrington Walls samples, with the source of the lipids assigned from interpretation of GC-c-IRMS data (GC-c-IRMS analysis and interpretation by Lisa-Marie Shillito – for complete dataset see Craig et al.[143])

PRN	GC-c-IRMS	TAG Range	PRN	GC-c-IRMS	TAG Range
1285	N/A	T_{46}-T_{52}	2876	Ruminant	T_{50}-T_{54}
1301	Porcine	T_{48}-T_{52}	2902	Ruminant	T_{48}-T_{54}
1311	Porcine	T_{50}-T_{52}	2998	N/A	T_{46}-T_{54}
1325	Dairy	No TAGs	3142	Ruminant	T_{48}-T_{54}
1343	Porcine	No TAGs	3266	Dairy	T_{52}-T_{54}
1619	Ruminant	No TAGs	3298	Dairy	T_{48}-T_{54}
1645	Ruminant	T_{48}-T_{54}	3323	Ruminant	No TAGs
1651	Ruminant	T_{48}-T_{52}	3341	Ruminant	No TAGs
1653	Ruminant	No TAGs	3981	Dairy	No TAGs
1665	Ruminant	No TAGs	3999	Ruminant	T_{48}-T_{52}
1698	Ruminant	No TAGs	4481	Ruminant	T_{48}-T_{54}
1735	Ruminant	T_{50}-T_{54}	4704	Ruminant	T_{48}-T_{54}
1889	Ruminant	T_{50}-T_{54}	5008	Ruminant	T_{48}-T_{54}
2052	Porcine	T_{48} only	5039	Dairy	No TAGs
2062	Porcine	T_{48}-T_{52}	5051	Porcine	T_{48}-T_{54}
2144	Porcine	T_{50}-T_{52}	5053	N/A	T_{50}-T_{54}
2156	Dairy	T_{46}-T_{54}	5062	N/A	No TAGs
2175	Ruminant	T_{48}-T_{54}	5074	N/A	T_{48}-T_{54}
2319	Porcine	T_{46}-T_{52}	5075	Porcine	T_{48}-T_{54}
2417	N/A	No TAGs	5536	Ruminant	No TAGs
2764	Ruminant	T_{46}-T_{54}	5537	Ruminant	No TAGs
2849	Porcine	T_{48}-T_{54}	10235	N/A	T_{48}-T_{54}

When GC-c-IRMS is not carried out, it is usually because there is not enough lipid present, since this technique needs relatively high levels of the free $C_{16:0}$ and $C_{18:0}$

fatty acids. Carrying out MALDI-MS analysis as the first step could indicate whether the lipids are well preserved enough to allow GC-c-IRMS analysis. This is usually done using HTGC, but MALDI-MS is much quicker so it can increase throughput, and efficiency of subsequent steps. Although MALDI-MS is used to detect intact TAGs rather than free fatty acids, in archaeological samples with good TAG preservation there are always observed to be reasonably high levels of free fatty acids too.

5.2.2   Tandem Mass Spectrometric Analysis

Product ion spectra were obtained on the ultraflex MALDI-TOF/TOF-MS to demonstrate that the species observed were indeed TAGs and to gain information about the fatty acids present on the glycerol backbone.

Figure 67 shows a MALDI mass spectrum of PRN 2175, with the product ion spectrum of the species at m/z 857, corresponding to the $T_{50:0}$ TAG. A $T_{50:0}$ TAG would be expected to contain two $C_{16:0}$ fatty acids and one $C_{18:0}$ fatty acid; although other combinations of fatty acids would also give a total of 50 acyl carbons, since $C_{16:0}$ and $C_{18:0}$ fatty acids are the most common in animal tissues the majority of TAG species are likely to contain these fatty acids. The product ion spectrum does indeed show peaks at m/z 573 and 551 (corresponding to loss of the $C_{18:0}$ fatty acid and fatty acid sodium salt, respectively) and m/z 601 and 579 (corresponding to the loss of the $C_{16:0}$ fatty acid and fatty acid sodium salt).

172
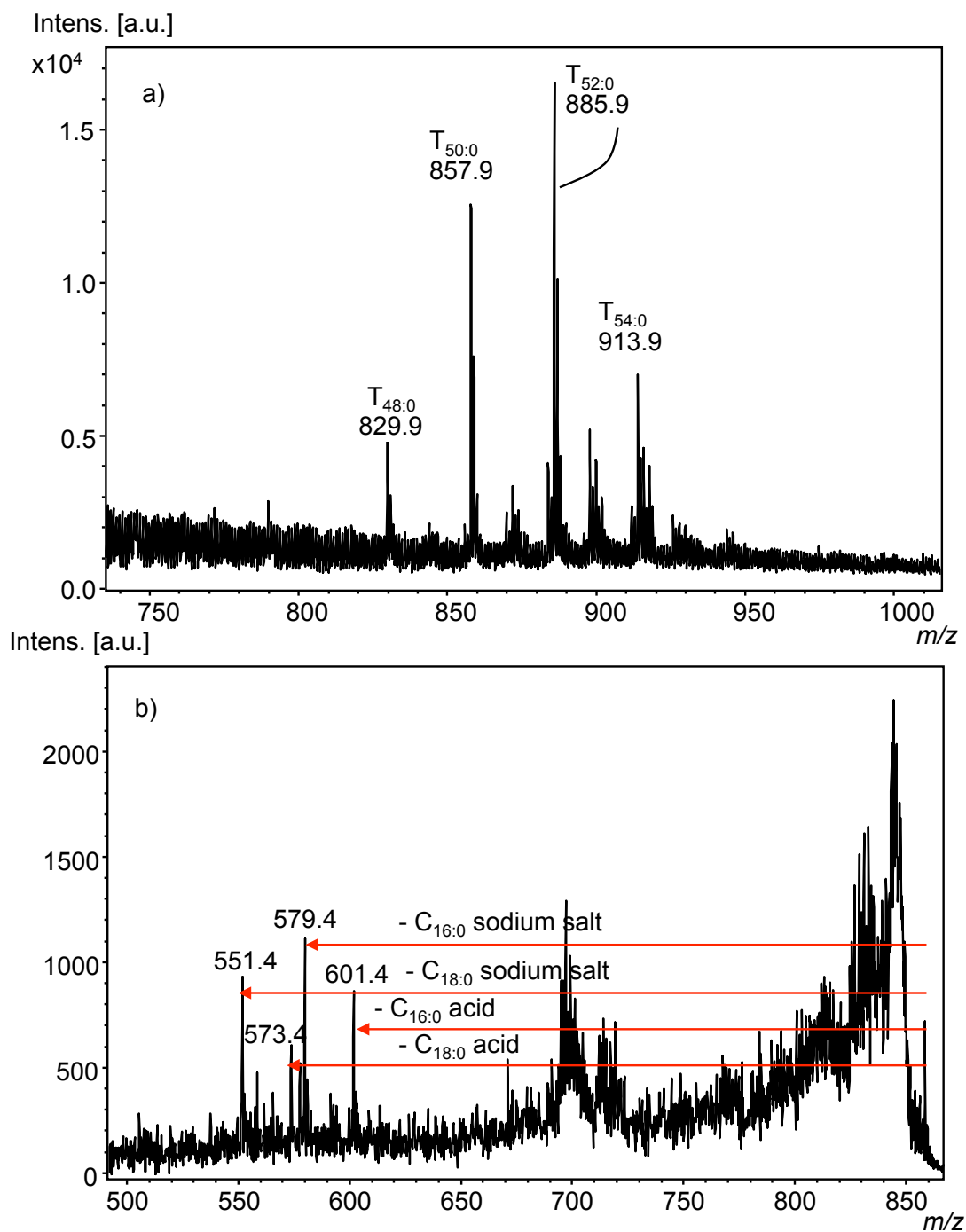
Figure 67. a) MALDI mass spectrum and b) product ion spectrum of extract of PRN 2175, illustrating loss of $C_{16:0}$ and $C_{18:0}$ fatty acids from the species at m/z 857 corresponding to $[T_{50:0} + Na]^+$.

Another, slightly more complicated, example of a product ion spectrum is shown in Figure 68. In this example (from PRN 5051, mass spectrum shown in Figure 63) the precursor ion is at m/z 883, corresponding to the $T_{52:1}$ TAG. The tandem mass spectrum is complicated by the fact that the double bond could occur in any one of the three fatty acids, which, in the case of a TAG with 52 acyl carbons, are likely to be two C_{18} and one C_{16} fatty acids. Again, the expected peaks are observed, with peaks at m/z 599 and 577 (corresponding to the loss of a $C_{18:0}$ fatty acid and fatty acid sodium salt), m/z 601 and 579 (corresponding to the loss of a $C_{18:1}$ fatty acid and fatty acid sodium salt) and m/z 627 and 605 (corresponding to the loss of a $C_{16:0}$ fatty acid and fatty acid sodium salt). No peaks due to the loss of the $C_{16:1}$ fatty acid or its sodium salt were observed.
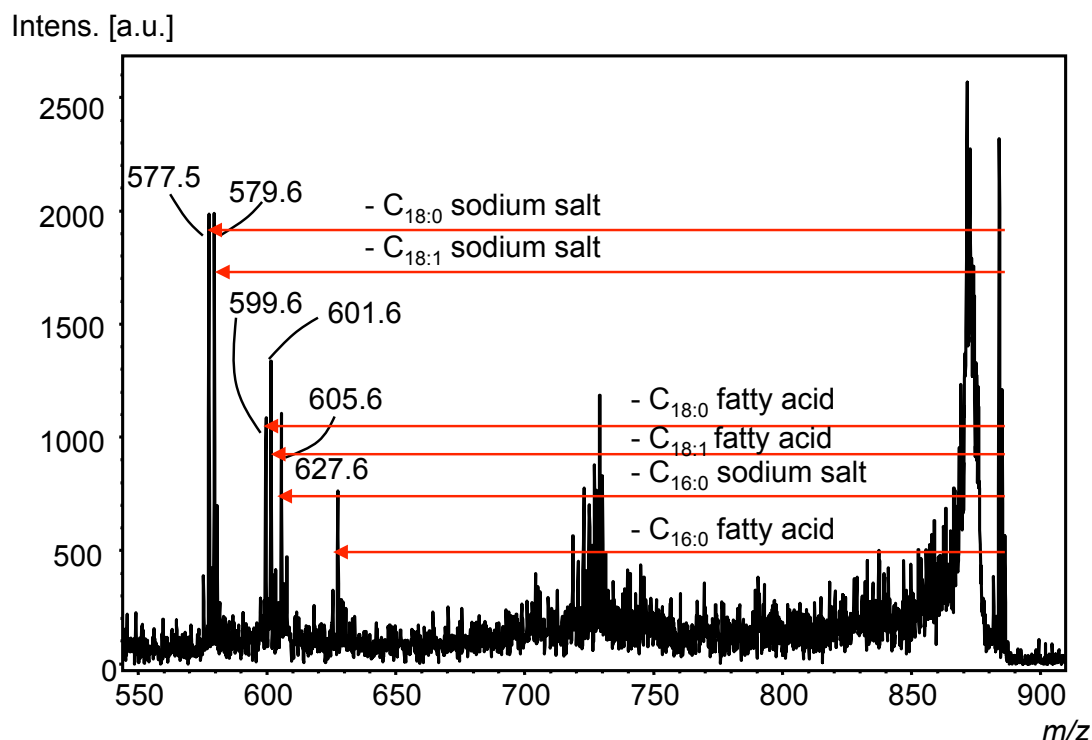
Figure 68. Product ion spectrum of the species with m/z 883 from extract of PRN 5051, corresponding to $[T_{52:1} + Na]^+$, illustrating the range of fatty acids which can make up a monounsaturated TAG.

The ability to carry out tandem mass spectrometry to elucidate the fatty acids which comprise a particular TAG is another advantage of MALDI-MS over GC. There are several different isobaric species possible for any TAG, because the acyl carbons can be distributed between the fatty acids in more than one way. These isobars have the same GC retention times so they cannot be distinguished, and of course have the

same mass. Interpretation of the GC-MS data can provide information about the fatty acids present due to the presence of $[RCO]^+$ and $[M-RCOO]^+$ peaks, but the peaks are often very weak and difficult to interpret. Tandem mass spectrometry can give a clear demonstration of the fatty acids present and with higher throughput than can HTGC-MS.

5.2.3   Fourier Transform Ion Cyclotron Resonance MS Analysis

Some samples were also analysed using a Bruker solariX FTICR mass spectrometer for accurate mass determination, to gather further evidence that the species observed were TAGs and to see if this could give better S/N than the ultraflex.

Figure 69 shows the MALDI-FTICR mass spectrum of the extract from PRN 5051. This spectrum gives slightly better S/N and is able to detect TAGs in this sample down to $T_{46:0}$, when the smallest TAG detected using the ultraflex was T_{48} (possibly with some unsaturation) (Figure 63). Being able to record *m/z* values with high mass accuracy allowed the assignment of more of the peaks than had been possible when using the ultraflex. For example, on the FTICR MS peaks corresponding to T_{48} with between one and three double bonds were assigned as TAGs based on their accurate *m/z* values, whereas this could not be done with certainty on the ultraflex. Table 10 shows the TAGs detected in PRN 5051 using FTICR-MS, with the calculated and measured *m/z* values and the associated errors. For all of the assigned peaks, comparison of the calculated *m/z* values for the assigned TAGs and the measured values gave errors of less than 2 ppm.
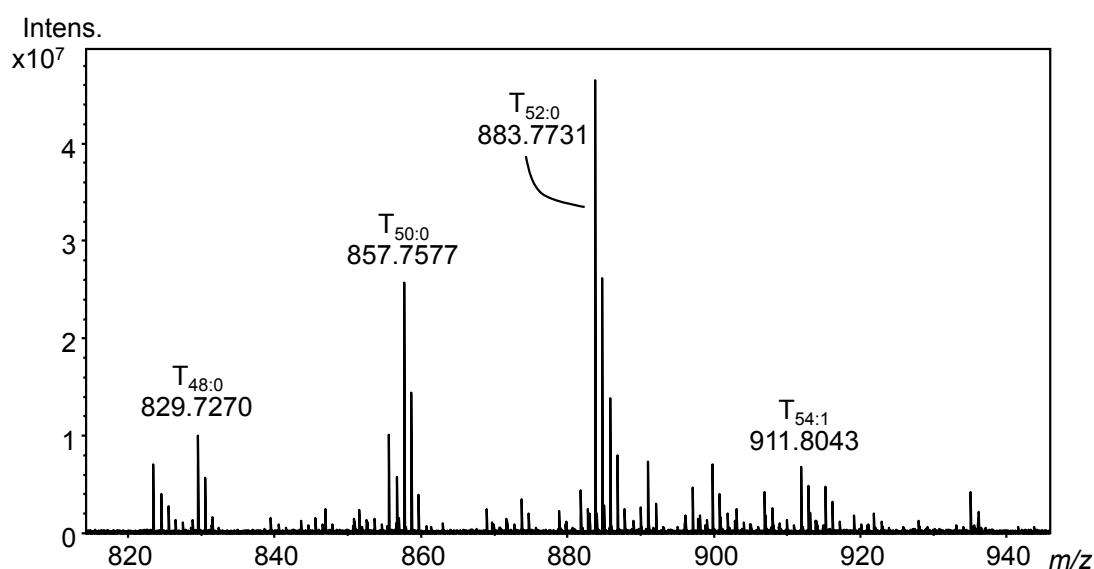
Figure 69. MALDI-FTICR mass spectrum of extract of PRN 5051, showing the same peaks as those seen in the MALDI-TOF mass spectrum, with exact masses consistent with these species being TAGs.

176

Table 10. TAGs detected in the FTICR mass spectrum of PRN 5051, with their calculated and measured *m/z* values, and the error.

TAG	Formula	Calculated *m/z*	Measured *m/z*	Error / ppm
$T_{54:0}$ + Na	$C_{57}H_{110}O_6Na$	913.81946	913.82057	-1.22
$T_{54:1}$ + Na	$C_{57}H_{108}O_6Na$	911.80381	911.80435	-0.59
$T_{52:0}$ + Na	$C_{55}H_{106}O_6Na$	885.78816	855.78922	-1.19
$T_{52:1}$ + Na	$C_{55}H_{104}O_6Na$	883.77251	883.77314	-0.71
$T_{52:2}$ + Na	$C_{55}H_{102}O_6Na$	881.75686	881.75751	-0.74
$T_{50:0}$ + Na	$C_{53}H_{102}O_6Na$	857.75686	857.75770	-0.98
$T_{50:1}$ + Na	$C_{53}H_{100}O_6Na$	855.74121	855.74167	-0.53
$T_{50:2}$ + Na	$C_{53}H_{98}O_6Na$	853.72556	853.72667	-1.29
$T_{50:3}$ + Na	$C_{53}H_{96}O_6Na$	851.70991	851.71100	-1.28
$T_{48:0}$ + Na	$C_{51}H_{98}O_6Na$	829.72556	829.72697	-1.69
$T_{48:1}$ + Na	$C_{51}H_{96}O_6Na$	827.70991	827.71152	-1.94
$T_{48:2}$ + Na	$C_{51}H_{94}O_6Na$	825.69426	825.69529	-1.25
$T_{48:3}$ + Na	$C_{51}H_{92}O_6Na$	823.67861	823.67909	-0.58
$T_{46:0}$ + Na	$C_{49}H_{94}O_6Na$	801.69426	801.69474	-0.60

5.2.4   Comparison of MALDI-MS with GC

Because all of the Feeding Stonehenge HTGC work was done using splitless GC injection, in order for proper comparison of MALDI-MS with HTGC for these samples they needed to be analysed using OCI-HTGC. Eight of the samples were selected for OCI-HTGC-MS analysis. All of them had detectable TAGs on MALDI-MS analysis (except for PRN 1698) but only four of them had TAGs detected on splitless HTGC analysis, with a further one having a tentative detection of TAGs (Table 11). All of the samples had very weak TAG peaks in the splitless HTGC analysis, if TAGs were detected at all.

One of the three portions of each extract was used for OCI-HTGC-MS analysis. Samples were trimethylsilylated using BSTFA and dissolved in 100 µL hexane containing 10 ng C_{34} alkane (internal standard), with 1 µL of this solution injected.

Table 11. Table indicating whether TAGs were detected using splitless HTGC and MALDI-MS in samples selected for OCI-HTGC-MS analysis.

PRN	TAGs on Splitless HTGC?	TAGs on MALDI-MS?
1698	✓	
5051	✓	✓
2998		✓
4481		✓
2062	?	✓
2319	✓	✓
3142		✓
2175	✓	✓

On-column injection for HTGC did improve TAG detection relative to splitless injection, as would be expected. PRN 2175 gave a particularly good chromatogram with very well defined peaks for TAGs in the range $T_{48} - T_{54}$ (Figure 70), which is the same range as that detected by MALDI-MS (Figure 67). In contrast, the splitless injection chromatogram is shown in Figure 71, and gives very poor peaks for TAGs. However, although OCI-HTGC-MS gives good peaks for the even carbon numbered TAGs, it only gives very small peaks for the odd carbon numbered TAGs, whereas they are detected much more clearly in the MALDI mass spectrum.

178
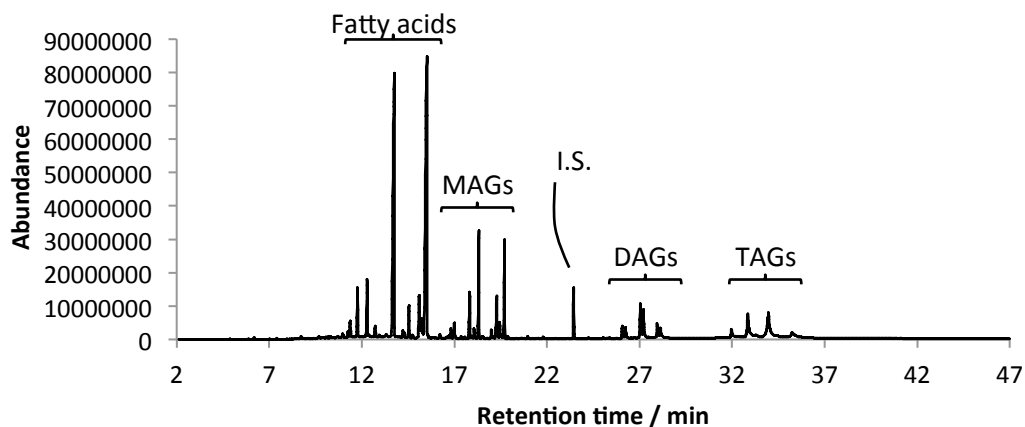
Figure 70. OCI-HTGC-MS chromatogram of extract of PRN 2175 showing much better TAG signals than the splitless injection HTGC (Figure 71).
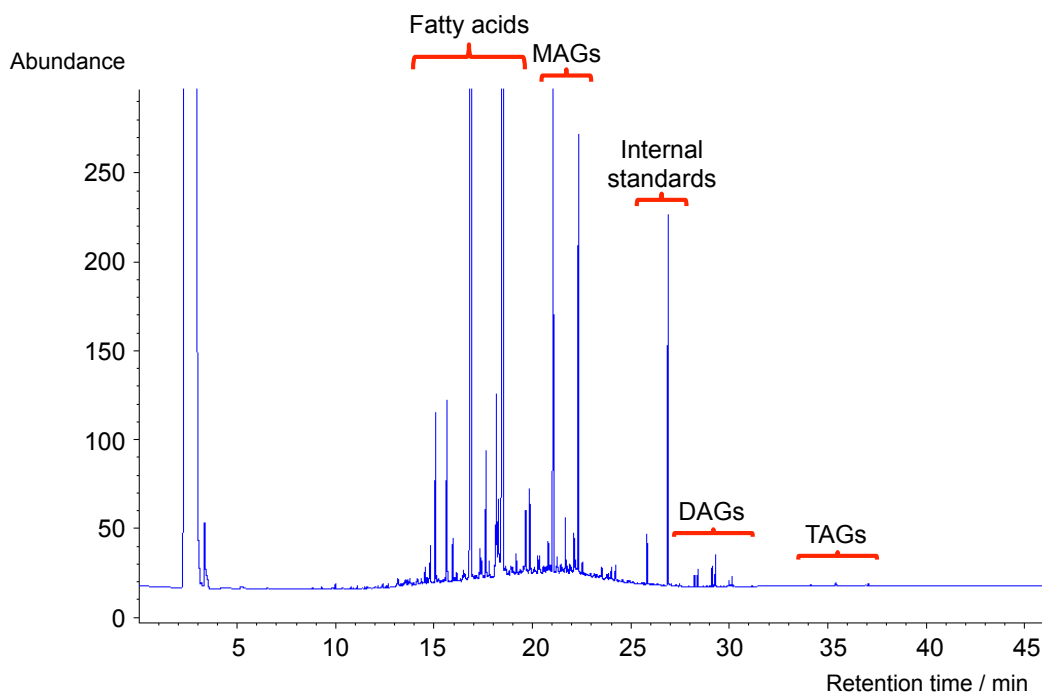
Figure 71. Splitless injection high temperature gas chromatogram of extract of PRN 2175, showing very poor TAG detection (data obtained by Lisa-Marie Shillito). The two largest fatty acid peaks are off-scale.

179

Although PRN 2175 gave very good TAG detection on OCI-HTGC-MS, this was not the case with all of the samples. The chromatogram of the extract of PRN 2319 (Figure 72), is much more typical of the data obtained when OCI-HTGC-MS was carried out. Here, only three TAGs are detected, all fully saturated, and there is no evidence of any odd carbon number TAGs. In contrast, the MALDI mass spectrum shows TAGs from T_{46} to T_{54}, including odd carbon numbered TAGs and several monounsaturated and polyunsaturated examples (Figure 73). Tandem MS was carried out on some of the TAGs, and Figure 74 and Figure 75 are the spectra of m/z 857 ($T_{50:0}$) and m/z 843 ($T_{49:0}$), respectively, showing fatty acid losses from the TAGs.
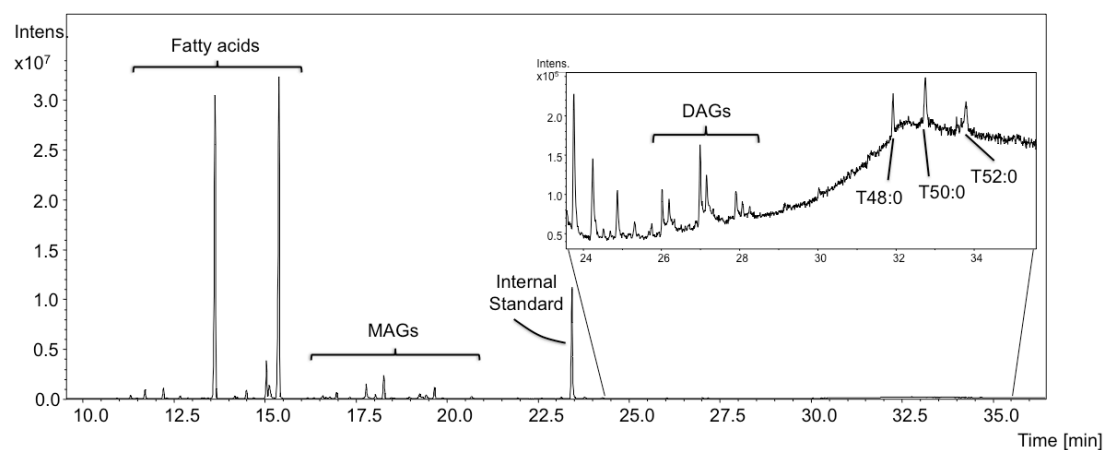
Figure 72. OCI high temperature gas chromatogram of extract of PRN 2319, showing poor TAG detection.
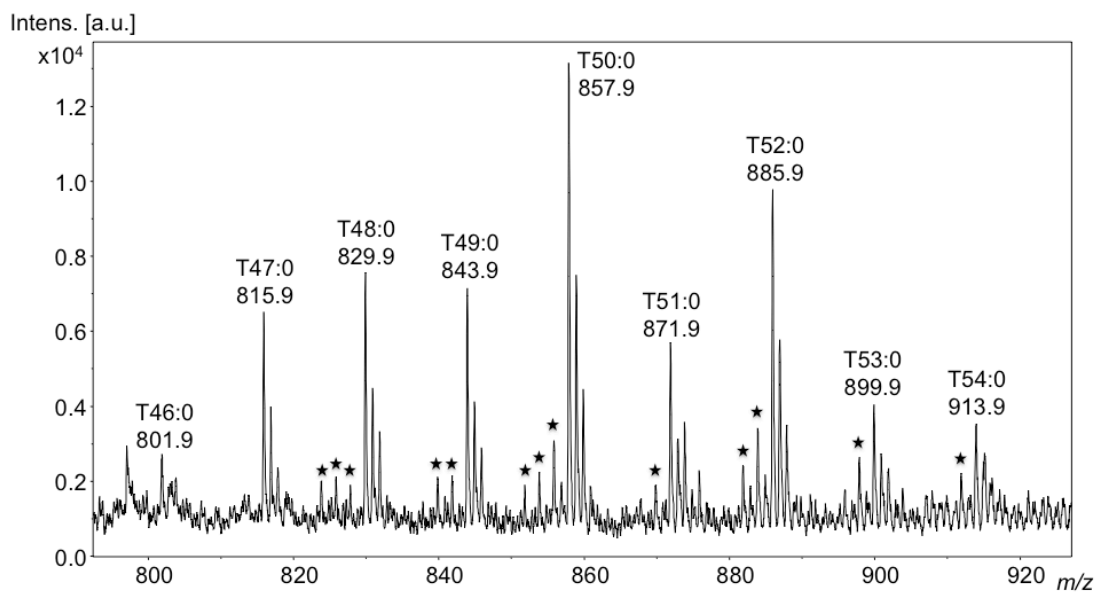
Figure 73. MALDI mass spectrum of extract of PRN 2319, showing both even and odd carbon numbered TAGs in the range $T_{46} - T_{54}$ with several unsaturated TAGs detected (unsaturated TAGs are marked with stars).
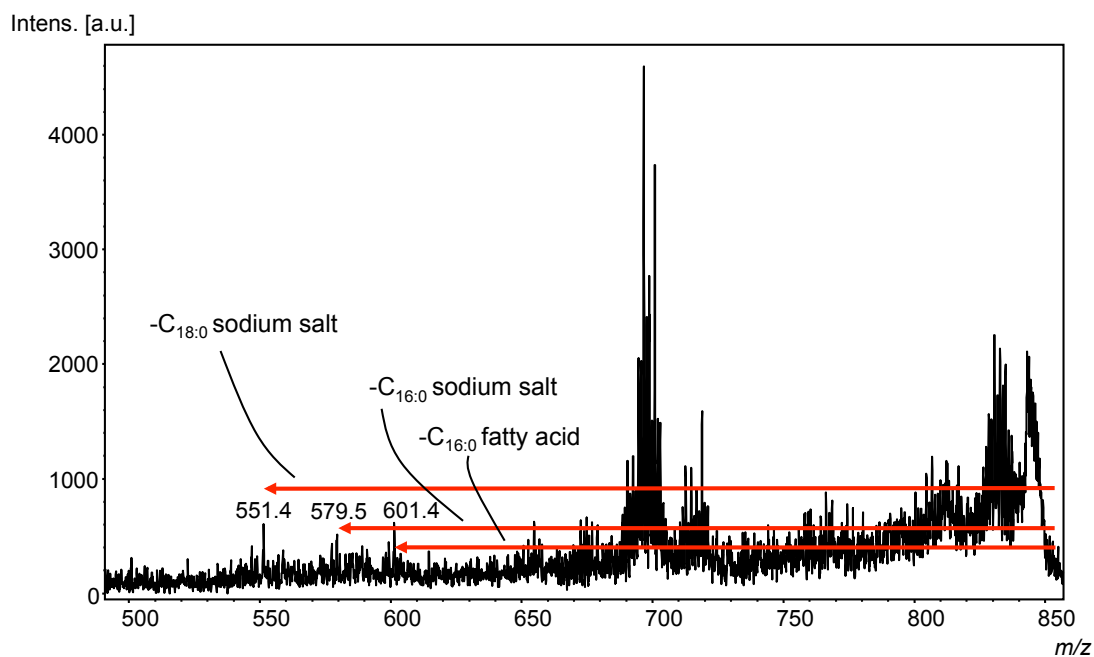
Figure 74. Tandem mass spectrum of m/z 857 ($T_{50:0}$) from extract of PRN 2319, showing loss of $C_{16:0}$ and $C_{18:0}$ fatty acids.
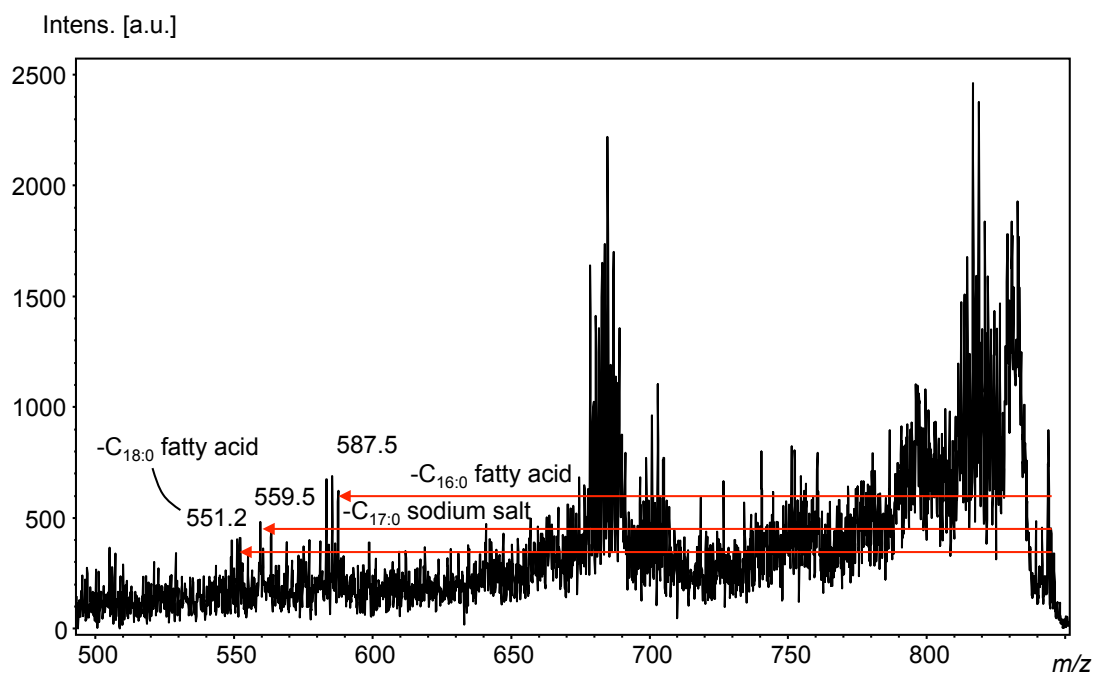
Figure 75. Tandem mass spectrum of m/z 843 ($T_{49:0}$) from extract of PRN 2319, showing loss of $C_{16:0}$, $C_{17:0}$ and $C_{18:0}$ fatty acids or fatty acid sodium salts.

Table 12 shows the range of TAGs detected in the Durrington Walls samples using OCI-HTGC-MS and MALDI-MS. The table shows that a wider range of TAGs was detected by MALDI-MS in almost all cases, showing that MALDI-MS is better able to detect TAGs in archaeological lipid extracts than OCI-HTGC-MS is. As well as being able to detect a wider range of lipids, the MALDI-MS analysis was also able to detect more odd carbon numbered TAGs and more unsaturated TAGs. Odd carbon numbered TAGs are known to be present in animal fats at lower concentrations than even carbon numbered TAGs,[67] so the fact that they are not detected so often when using OCI-HTGC-MS is probably because they are below the LOD in many cases, whereas the higher sensitivity of MALDI-MS for TAGs allows them to be detected. Similarly, since in MALDI-MS unsaturated TAGs can be easily resolved from their saturated counterparts because of the m/z difference of 2 units, it is relatively easy for these unsaturated TAGs to be detected. In OCI-HTGC-MS there were only a few unsaturated TAGs detected. This may be because they are below the LOD, but it is likely to be due at least partly to a lack of resolution between the saturated and unsaturated TAGs meaning that the unsaturated TAGs are not detected. The unsaturated TAGs may also be more heat labile than their saturated counterparts and therefore not survive at the high temperatures required to elute them.

182

Table 12. Range of even carbon numbered TAGs detected in a selection of Durrington Walls samples by both OCI-HTGC-MS and MALDI-MS.

PRN	OCI-HTGC-MS	MALDI-MS
1698	$T_{48} - T_{52}$	Not detected
5051	$T_{48} - T_{52}$	$T_{48} - T_{54}$
2998	$T_{48} - T_{52}$	$T_{48} - T_{54}$
4481	Not detected	$T_{48} - T_{54}$
2062	$T_{50} - T_{52}$	$T_{48} - T_{54}$
2319	$T_{48} - T_{52}$	$T_{46} - T_{54}$
3142	$T_{48} - T_{54}$	$T_{48} - T_{54}$
2175	$T_{48} - T_{54}$	$T_{48} - T_{54}$

5.2.5 Fractionation

The SPE-based fractionation method (chapter 4) was applied to a small selection of Durrington Walls samples to see if it could successfully improve the detection of TAGs in archaeological samples, as had been indicated by the fractionation of the extracts of experimentally buried pots and the ethnographic milk pot. Three samples were chosen, based on them having poor S/N and/or the presence of contaminating peaks on analysis of their total lipid extracts using MALDI-MS. The selected samples were PRN 1301, 3298 and 3323.

PRN 1301, on analysis of its TLE, had shown TAGs but with poor S/N, but there were also many peaks with *m/z* values not corresponding to TAGs in a similar *m/z* range to the TAGs. These were interfering with interpretation of the data (Figure 76a), and it was hoped that fractionation would separate these contaminants and allow better TAG detection. After fractionation, the peaks which did not correspond to TAGs had disappeared and the TAG peaks were better able to be seen (Figure 76b). However, the range of TAGs detected did not increase after fractionation.
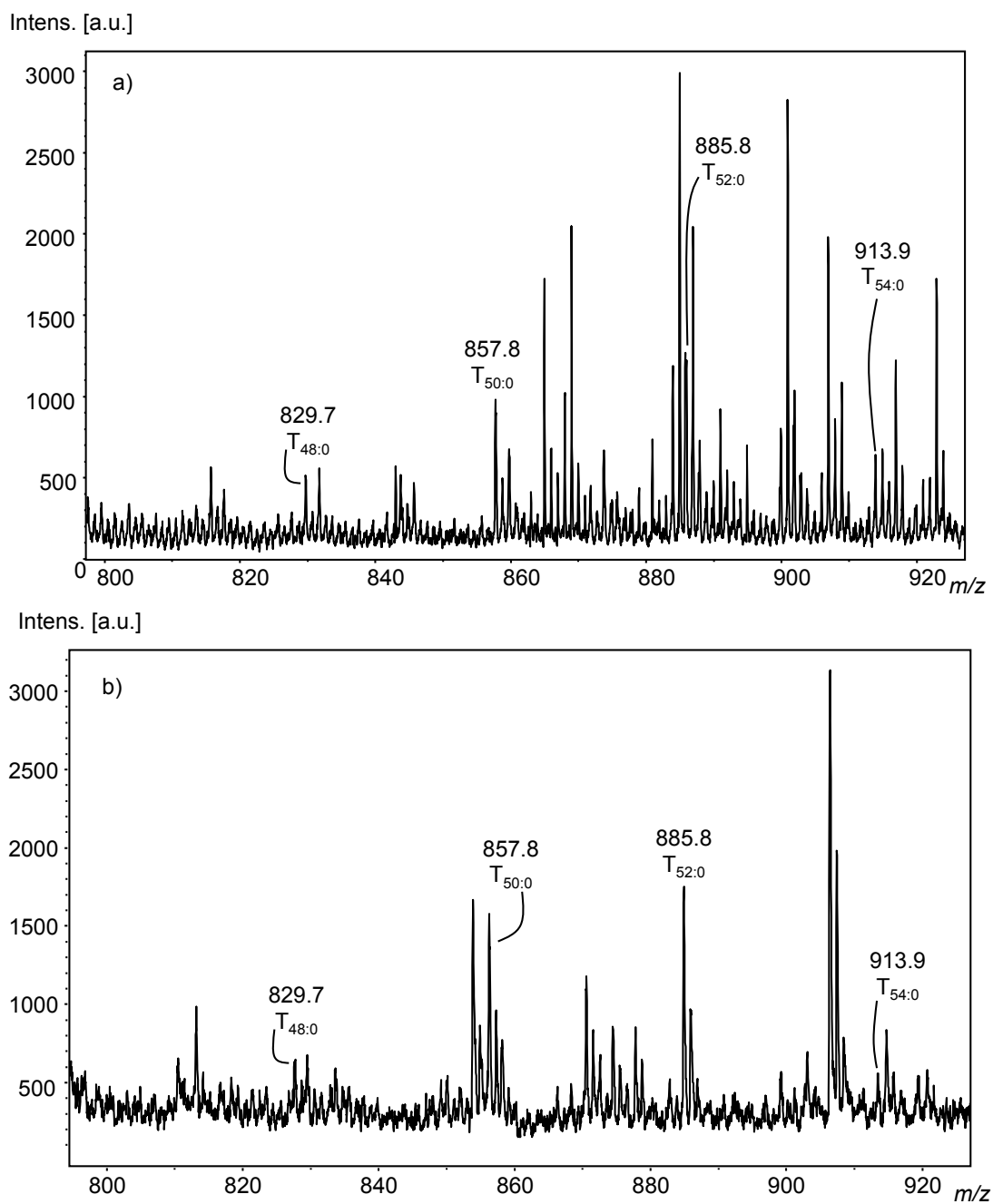
Figure 76. MALDI mass spectra of extract of PRN 1301. a) unfractionated and b) fractionated, showing how the fractionation has removed some of the interfering peaks and made the TAGs easier to detect.

185
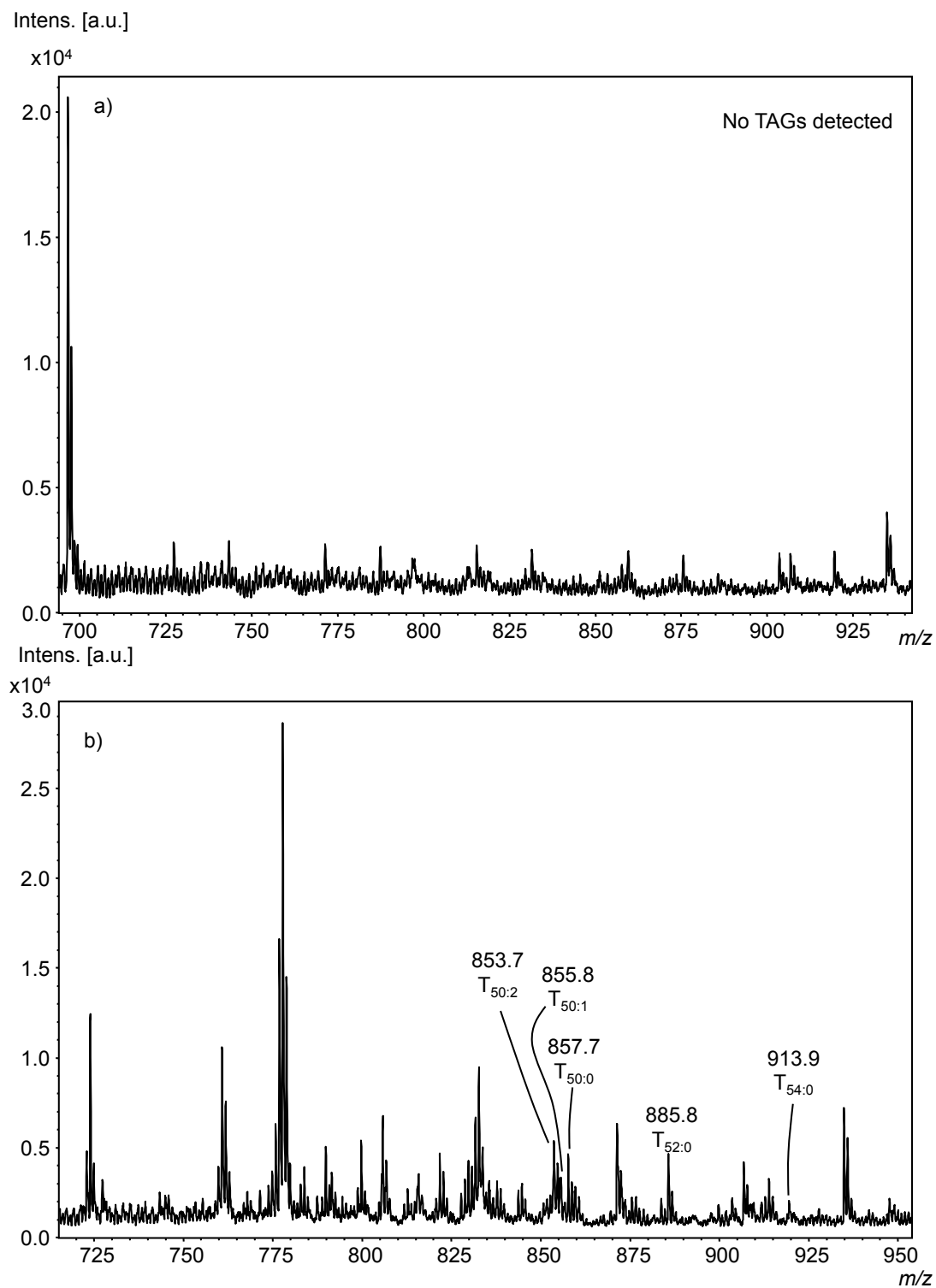
Figure 77. MALDI mass spectra of extract of PRN 3298. a) unfractionated and b) fractionated. Before fractionation no TAGs were detected but after fractionation TAGs from T_{50} to T_{54} were detected.

In the extract of PRN 3298 TAGs were not detected above the noise at all (Figure 77a). However, after fractionation a range of TAGs from $T_{48:0}$ to $T_{54:0}$ were detected (Figure 77b), and the S/N was sufficient to allow isolation of the ions and tandem mass spectrometry to be carried out (Figure 78). This sample is marked in Table 8 with an asterisk because the TAGs were only detected after fractionation.
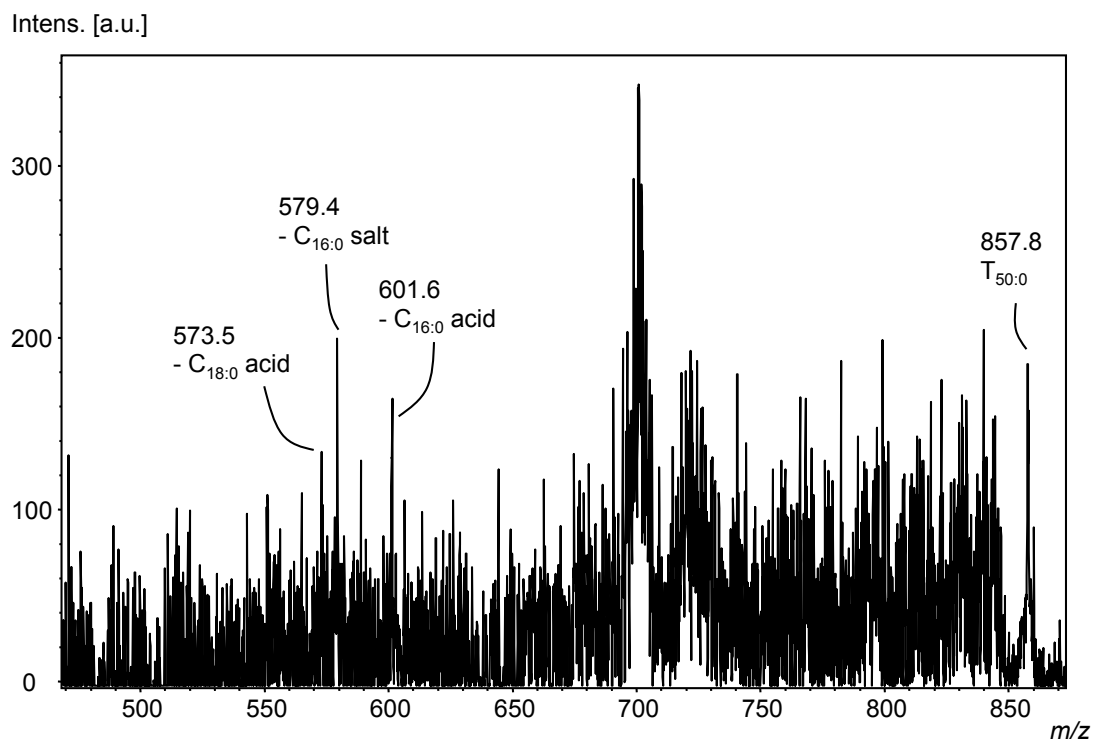
Figure 78. Tandem mass spectrum of the peak at *m/z* 857 ($T_{50:0}$) in extract of PRN 3298 after fractionation, showing how fractionation had improved the S/N sufficiently to allow MS/MS to be carried out.

Fractionation of the extract of PRN 3323 was less successful. Before fractionation, the TAG peaks were of low S/N and there were other peaks present (Figure 79a), but after fractionation there was only a very small increase in S/N (Figure 79b). The spectrum was slightly cleaner after fractionation but it did not make a difference to the detection of TAGs.
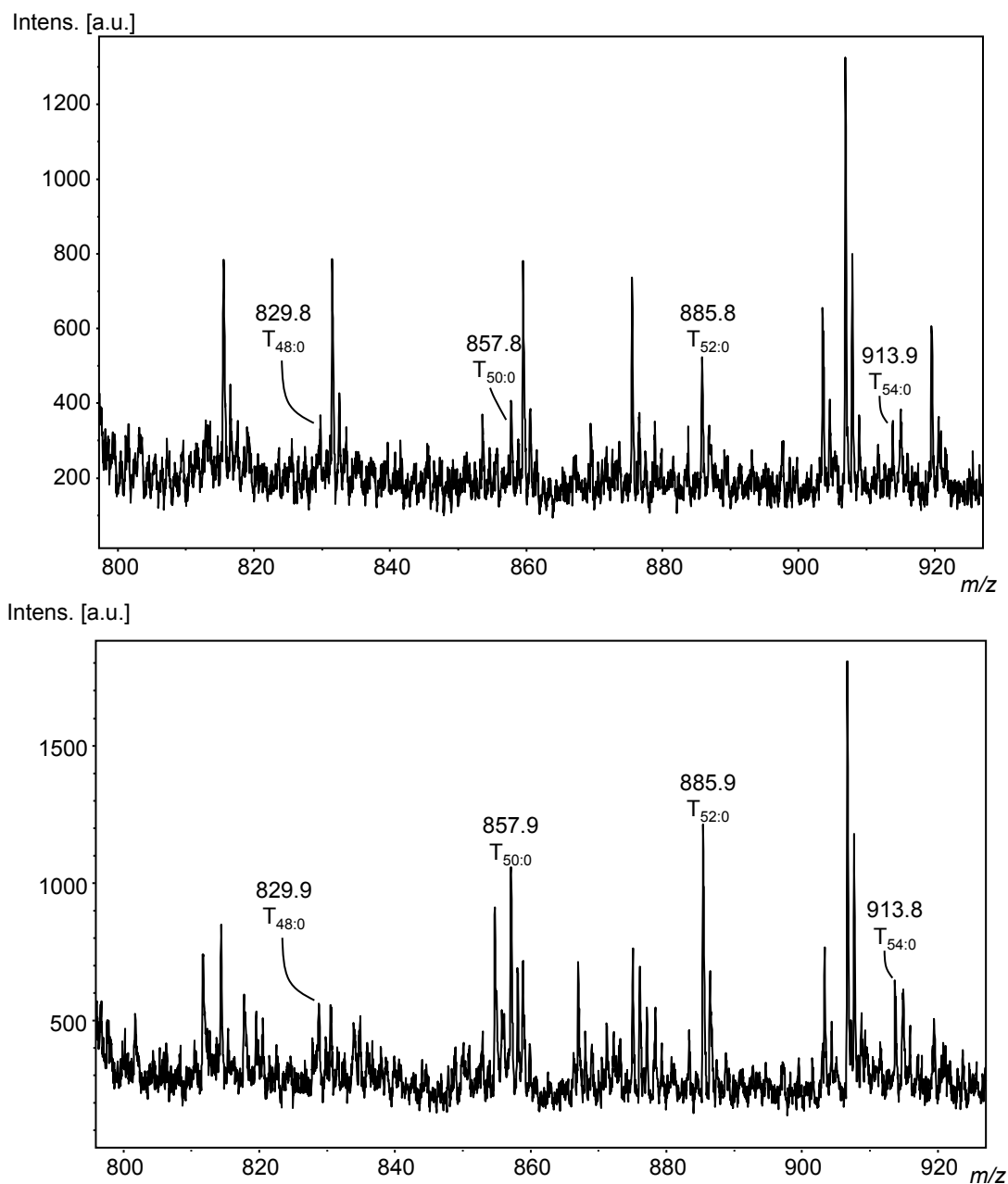
Figure 79. MALDI mass spectra of extract of PRN 3323. a) unfractionated and b) fractionated, showing how the fractionation has not made much difference to TAG detection.

Overall, the results of the fractionation carried out on the archaeological samples reinforced the conclusions made after fractionation of the extracts of the experimentally buried pots and the ethnographic milk pot, which are that fractionation can be used to improve TAG detection in some samples. However, it is not always successful and since it is not required when the crude extracts give good S/N, and takes a significant amount of time, it should only be used after MALDI-MS analysis of TLEs has indicated which samples may benefit from fractionation.

5.3 CONCLUSIONS

The application of the developed MALDI-MS method to samples from Durrington Walls has demonstrated that it is appropriate for TAG detection in lipid extracts of archaeological ceramics. On comparison with OCI-HTGC-MS, the MALDI-MS method performed favourably. It was able to detect a wider carbon number range of TAGs in most cases, and more odd carbon number and unsaturated TAGs.

Unfortunately, the TAG distributions in this set of sample extracts indicated that preservation was not good enough to provide information about the specific animal sources of the lipids. No TAG lighter than T_{46} was detected in any sample, and in order to assign lipid distributions to specific animals a wider range of TAGs than this is required.

The MALDI-MS method has many additional advantages over the conventional HTGC-MS method: it is much faster and so can increase throughput of samples, and is able to provide information about the fatty acids present in each TAG through the use of tandem MS. Sample preparation is also faster with MALDI-MS than with HTGC-MS, because derivatisation does not need to be carried out for MALDI-MS.

In this study, MALDI-MS was carried out after HTGC analysis for validation purposes. However, MALDI-MS has great potential as a medium-throughput screening method for identifying well-preserved samples that would benefit from further in-depth HTGC-MS and GC-c-IRMS analysis. Therefore, its place in the canon of archaeological science analytical techniques is as the first step after extraction.

6 RESULTS: LIPID ANALYSIS OF CHLORITE COOKING VESSELS FROM ANCIENT MERV, TURKMENISTAN

The work reported in this chapter was carried out primarily in the Department of Conservation and Scientific Research at the British Museum whilst on a placement there. OCI-HTGC-MS analysis, as the conventional method for analysis of lipids in archaeological science, was carried out at the British Museum on a selection of stone potsherds from two time periods, $9^{th} – 10^{th}$ century AD and $12^{th} – 13^{th}$ century AD, from the Central Asian city of Merv. This analysis was followed by MALDI-MS analysis of the same samples, carried out on returning to the University of York.

6.1 INTRODUCTION

Merv (37.6628° N, 62.1925° E) was a major city in what is modern-day Turkmenistan, in Central Asia (Figure 80). Founded in the 6th century BC, the city was occupied until the 16th century AD, and there is evidence of occupation in the region dating as far back as the 3rd millennium BC.[179] The site is of great archaeological significance due to its location at the interface between Central Asia and Iran, and it has the ability to provide a wealth of information on the economics and cultural connections of the region, and how these have changed through time.[180,181]

Figure 80. Map showing the location of Turkmenistan, with Merv indicated by the red marker. Map data ©2015 Google, ORION-ME, SK planet, ZENRIN.

The site was first excavated in 1890, but was most recently and extensively excavated in the 1990s by the International Merv Project, a collaboration between the British Museum, University College London and the former Academy of Sciences of Turkmenistan.[182]

Merv was occupied by various people over its history, with different areas occupied at different times. A brief history of the city over the time periods from which the samples in this study were taken is given here.

Islam came to Merv in the 7th century AD.[183] The Sasanian empire had ended abruptly in AD 651 with the murder of the king not far outside the city walls, followed soon afterwards by occupation by an Arab army.[179] The city gradually moved as parts of it were abandoned and occupation moved into surrounding areas, and the previously inhabited areas became industrial suburbs, in which extensive evidence for the production of steel in the Early Islamic period has been uncovered.[179]

The Seljuk dynasty began in Merv in 1037 AD, and from this time Merv was an important city. This ended with the death of Sultan Sanjar in 1157 AD. After this there were various political struggles followed in 1221 by a siege. When the city was surrendered most of the inhabitants were killed. The city never fully recovered from this and went into a gradual decline.[183]

The excavations at Merv produced many finds associated with the occupation of the city. Large numbers of ceramic potsherds were found, as well as smaller numbers of potsherds made from chlorite, a type of stone. Stone pots were widespread from the Early Islamic period onwards, one reason for which is the greater ease with which they could be cleaned compared to ceramic vessels.[184] The chlorite potsherds from Merv, which are held in the British Museum collection, are the subject of the analysis presented here. They are taken from two time-periods in the occupation of Merv: Early Islamic (9th – 10th century AD) and Seljuk dynasty (12th – 13th century AD). The Seljuk dynasty potsherds were excavated from the domestic area of a residential building,[185] and the Early Islamic potsherds from an industrial area in which steel production had taken place.[186]

Other finds at the site which relate to domestic activities include animal bones and botanical remains. The animal bone assemblage is dominated by sheep and goat, with some cow, pig and donkey as well as bird and fish.[184,185] Many of the bones bear the marks of butchery. The range of species to which the animal bones belong does not seem to vary between the two time periods, except for the fact that no pig bones were found in the area occupied during the Seljuk dynasty.[185] Interestingly, the bones of a dog (with butchery marks) were found in the area where the Early Islamic samples were found.[184] This is thought to be an unlikely food source in the Early Islamic period (as is pig), and may imply the presence of non-Muslims.[184] There was not any appreciable variation in the botanical remains between the two time periods. Wheat, barley and millet made up the cereal remains and watermelon and grape the fruit remains.[184] Almond and pistachio remains were found in the Seljuk dynasty excavations,[185] and cotton seeds were found in both time periods.[184,185]

Although ceramic vessels have long been known to preserve traces of the foods cooked and stored in them, and analysis of such residues can be used to gain information about the diets and lifestyles of the people who used the vessels (Chapters 1, 4 and 5 and references therein), there has been much less research into the capacity of stone vessels to preserve such residues. Recent analysis of Seljuk dynasty chlorite potsherds excavated from Merv has shown that such vessels can indeed preserve lipid residues.[32] It was shown that, on heating to 300 °C, the microporosity of the stone increased. This increase in porosity could enable preservation of lipids within the stone fabric, in a similar way to the preservation within the pores of ceramic material, and preliminary analysis by OCI-HTGC-MS indicated that a range of lipids, including intact TAGs, were preserved.[32]

The two types of vessel analysed in this study are considerably different in shape from each other, with the Early Islamic vessels being small bowls with straight sides, and the Seljuk vessels being larger pots with round bottoms. The potsherds from both time periods are notable for the fact that many of them have small circular holes that appear to have been made for repair purposes, with pieces of broken pot held together with wire attached *via* the holes.[184,185] It is, however, unclear how well these vessels would have functioned after their repair, and why it was worth repairing them in this way. Figure 81 is a drawing of one of the Seljuk vessels, and Figure 82

shows photographs of other Seljuk dynasty potsherds. Figure 83 shows photographs of two of the Early Islamic potsherds. The Seljuk dynasty potsherds had blackened outer surfaces[185] and the Early Islamic potsherds had charred black residues on their internal surfaces,[184] indicating that both types of vessel had been used for cooking (rather than simply as table wares).
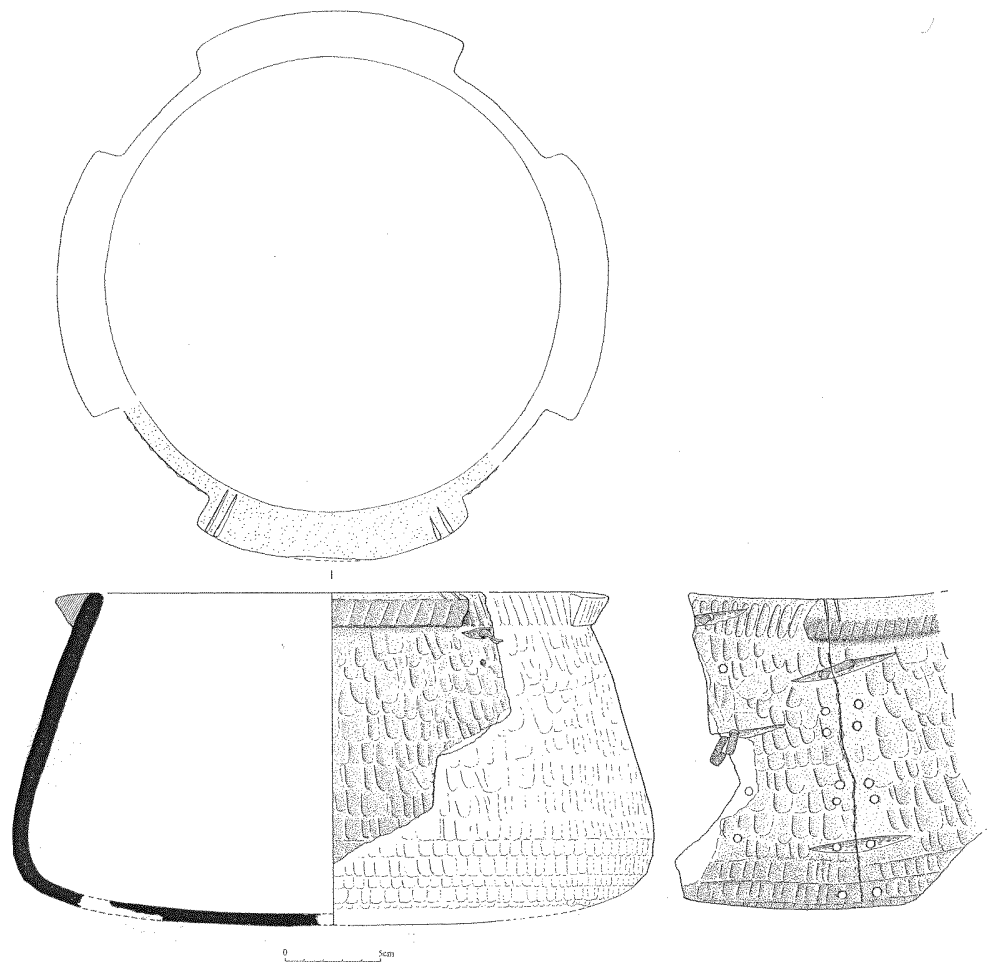
Figure 81. Illustration of a Seljuk dynasty chlorite vessel. Repair holes and the wire threaded through them can be seen in the image. ©Trustees of British Museum.

Figure 82. Photograph of some chlorite potsherds from a Seljuk dynasty chlorite cooking pot. Copper wire from a repair can be seen threaded through a hole in the potsherd at the bottom of the image. ©Trustees of British Museum.

Figure 83. Photographs of two of the Early Islamic chlorite potsherds from Merv. ©Trustees of British Museum.

6.2 AIMS

Preliminary lipid analysis of the Seljuk samples had previously been carried out using OCI-HTGC-MS,[32] and the aims of the work presented here were to investigate the lipid residues in more detail than had been carried out in the previous analysis, and to compare the residues in the two vessel types. The aim of the comparison between the vessel types was to see if the change in vessel shape was reflected in a change in lipid residue that could indicate a change in the foods cooked or in the cooking method. This work was also used as a case study comparison of OCI-HTGC-MS and MALDI-MS. OCI-HTGC-MS was used to detect and identify the range of lipid compounds present in the samples, and MALDI-MS to gain more information about the intact TAGs present in the samples. Tandem mass spectrometry was carried out in order to gain information about the fatty acid compositions of the TAGs. This is where MALDI-MS is particularly useful because sodiated TAGs fragment in tandem mass spectrometry by loss of fatty acids and fatty acid sodium salts (Chapters 4 and 5). This chapter also includes a comparison of the results from the work presented in chapters 5 and 6, and a discussion of the issues in these types of studies.

6.3 SAMPLES

Potsherds from twelve chlorite cooking vessels from the Seljuk dynasty and three from the Early Islamic period were selected, and lipids were extracted following the methods described in section 3.3. Preliminary OCI-HTGC-MS analysis of the Seljuk dynasty samples had been carried out but the data had been interpreted only to determine whether lipid had been preserved, and broadly the classes of lipid present.[32] The selection of samples was based on the results of that preliminary analysis, with the samples chosen to cover a range of levels of lipid preservation. A further Early Islamic chlorite sample, which was thought to be an inkwell and not a cooking bowl, was included as a control. This potsherd was different to the other Early Islamic samples because it came from a square vessel (rather than round) and had different markings on the outside. Table 13 lists the samples, the type of potsherd and their time period. An extraction blank was also carried out, which involved carrying out the extraction process on an empty tube (with no potsherd powder present).

Table 13. Details of the potsherds used in this investigation.

British Museum Reg. Number	Sample number	Potsherd type	Period
2009,6001.3	MCP18	Body	Seljuk
2009,6001.4	MCP19	Body	Seljuk
2009,6001.5	MCP20	Body	Seljuk
2009,6001.6	MCP22	Rim	Seljuk
2009,6001.7	MCP23	Body	Seljuk
2009,6001.10	MCP26	Body	Seljuk
2009,6001.11	MCP27	Rim	Seljuk
2009,6001.12	MCP28	Rim	Seljuk
2009,6001.13	MCP29	Rim	Seljuk
2009,6001.14	MCP30	Body	Seljuk
2009,6001.17	MCP33	Rim	Seljuk
2009,6001.18	MCP34	Rim	Seljuk
2009,6016.267	IMP8220	Base/body	Early Islamic
2009,6016.268	IMP8104	Base/body	Early Islamic
2009,6016.269	IMP8495	Body	Early Islamic
2009,6016.276	64	Control	Early Islamic

6.4   RESULTS

6.4.1   High Temperature Gas Chromatography-Mass Spectrometry

Extracts from each Merv potsherd sample were subjected to OCI-HTGC-MS analysis, following trimethylsilyl derivatisation, in order to detect and identify the lipids in the samples. Based on previously carried out preliminary investigations,[32] the expectation was that a range of lipid species, including intact TAGs and their breakdown products DAGs, MAGs and free fatty acids would be detected.

Lipids were identified using retention times and MS data. Fatty acids were detected as trimethylsilyl (TMS) esters, and MAGs, DAGs and sterols were detected as TMS ethers. The ions used for identification, determined from knowledge of fragmentation patterns,[6] are summarised in Table 14 and described as follows.

Unsaturated lipids elute just before their fully saturated counterparts due to their slightly higher polarity.

Fatty acids were identified by a weak $M^{+\bullet}$ signal and a stronger signal at $[M-15]^+$, due to loss of a methyl radical from the TMS group. Major characteristic fragments for fatty acid TMS esters were observed at *m/z* 73 and 117, along with several other fragments.

MAGs were identified by $[M-15]^+$ sometimes with a weak signal for $M^{+\bullet}$. MAGs can exist as one of two isomers, because the fatty acid can be substituted in the 1- or 2-position of the glycerol moiety, and are given the notation of 1-MAG or 2-MAG respectively. They can be differentiated because the 2-MAG gives a characteristic fragment at *m/z* 218 due to $[(CH_3)_3SiOCH=CHCH_2OSi(CH_3)_3]^{+\bullet}$, whereas the 1-MAG gives a fragment at $[M-CH_2OSi(CH_3)_3]^+$ (at *m/z* $[M-103]^+$).

DAGs were identified by weak signals at $[M-15]^+$ (due to loss of a methyl radical) and $[M-90]^{+\bullet}$ (due to loss of the TMS group), and more prominent peaks at $[RCO]^+$, $[RCO+74]^+$ and $[RCO+90]^+$ for the fatty acid moieties. 1,3-DAGs were distinguished by their base peak at $[M-RCOOCH_2]^+$. Characteristic fragments occurred at *m/z* 129 (for $[CH_2CHCHOSi(CH_3)_3]^+$) and *m/z* 145 (for $[CH(O)CHCH_2OSi(CH_3)_3]^+$). The individual acyl groups on the glycerol backbone can be identified by signals for $[M-RCOO]^+$.

TAGs, lacking protic sites, were not derivatised by TMS. $M^{+\bullet}$ signals were absent, so identification was by the presence of signals for the fragments $[RCO]^+$ and $[RCO+74]^+$. Signals for $[M-RCOO]^+$ were also observed.

Sterols were identified by a characteristic fragment at *m/z* 129, and peaks at $M^{+\bullet}$, $[M-90]^{+\bullet}$, $[M-90-15]^+$ and $[M-129]$ for the specific sterol (although cholesterol was the only sterol detected).

Alkanes are highly fragmented under GC-MS conditions and no $M^{+\bullet}$ peak is observed. Their spectra have a characteristic sequence of peaks with diminishing intensity, separated by 14 *m/z* units.

Phthalate plasticisers were also observed. These are often seen in archaeological lipid extracts and arise from contamination from plastic gloves, pipette tips and

plastic bags (in which samples are sometimes stored). They are characterised by a peak at m/z 149.

Table 14. Characteristic GC-MS ions observed in lipid classes detected in Merv samples.

Compound	Observed Ions
Fatty acid, TMS ester	Characteristic fragments: m/z 73, 75, 117, 129, 132, 145
	Molecule-specific ions: $M^{+\bullet}$, $[M-15]^+$
Monoacylglycerol, TMS ether	Characteristic fragments: m/z 103, 218 (2-MAG only)
	Molecule-specific ions: $[M-103]^+$ (1-MAG only), $M^{+\bullet}$, $[M-15]^+$
Diacylglycerol, TMS ether	Characteristic fragments: m/z 129, 145
	Molecule-specific ions: $[M-15]^+$, $[M-90]^{+\bullet}$, $[RCO]^+$, $[RCO+74]^+$, $[RCO+90]^+$, $[M-RCOO]^+$, $[M-RCOOCH_2]^+$ (1,3-DAG only)
Triacylglycerol	$[RCO]^+$, $[RCO+74]^+$, $[M-RCOO]^+$
Sterol, TMS ether	Characteristic fragment: m/z 129
	Molecule-specific ions: $M^{+\bullet}$, $[M-90]^{+\bullet}$, $[M-90-15]^+$, $[M-129]$
Alkane (C_{34} alkane internal standard)	Sequence of peaks with diminishing intensity and m/z difference of 14 due to CH_2 group loss (m/z 57, 71, 85, 99 etc.)

The chromatogram obtained on HTGC-MS analysis of an extract of a particularly well-preserved sample (MCP30) is shown in Figure 84, and example spectra from each of the compound classes detected (TAGs, DAGs, MAGs, fatty acids, sterols and the C_{34} alkane internal standard) are shown in Figure 85 - Figure 92, respectively, with the assignments of the ions observed.
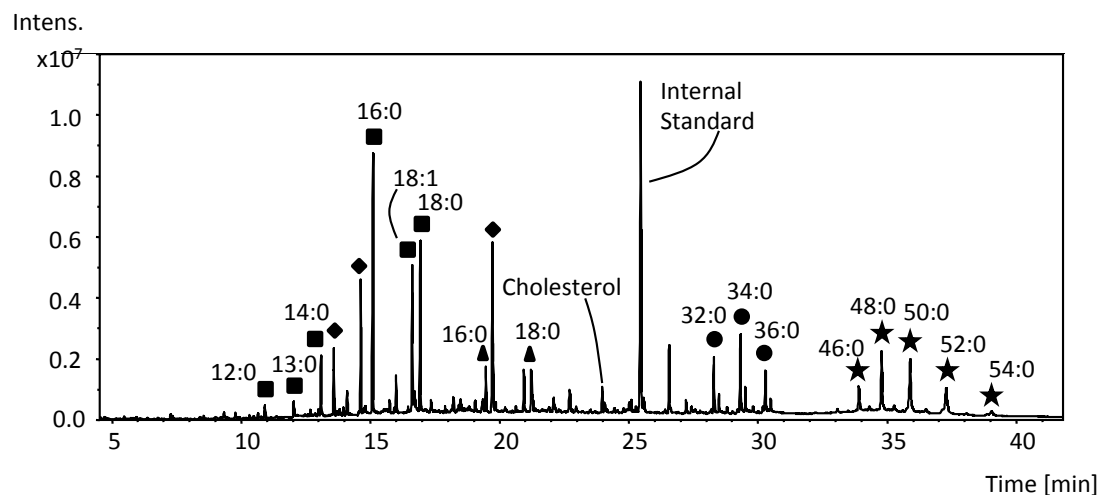
Figure 84. High temperature gas chromatogram of lipid extract of MCP30, showing a range of lipid components with their acyl carbon number. Asterisks represent TAGs; circles represent DAGs; triangles represent MAGs; squares represent free fatty acids; diamonds represent phthalate plasticiser contamination.
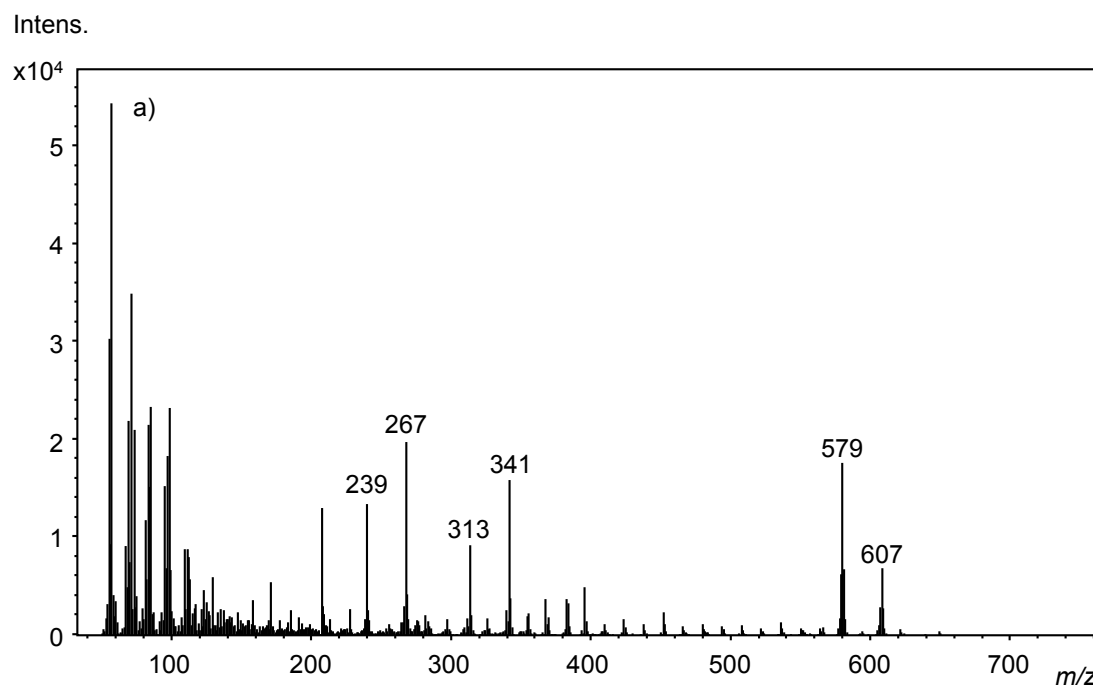
b)	$T_{52:0}$ ($M^{+\bullet} = 862$)	
m/z value	**Assignment**	
607	$[M-C_{15}H_{31}COO]^+$	
579	$[M-C_{17}H_{35}COO]^+$	
341	$[C_{17}H_{35}CO+74]^+$	
313	$[C_{15}H_{31}CO+74]^+$	
267	$[C_{17}H_{35}CO]^+$	
239	$[C_{15}H_{31}CO]^+$	

Figure 85. $T_{52:0}$ TAG ($t_R = 37.2$ min) from extract of MCP30 a) mass spectrum; b) m/z value assignments.

Intens.
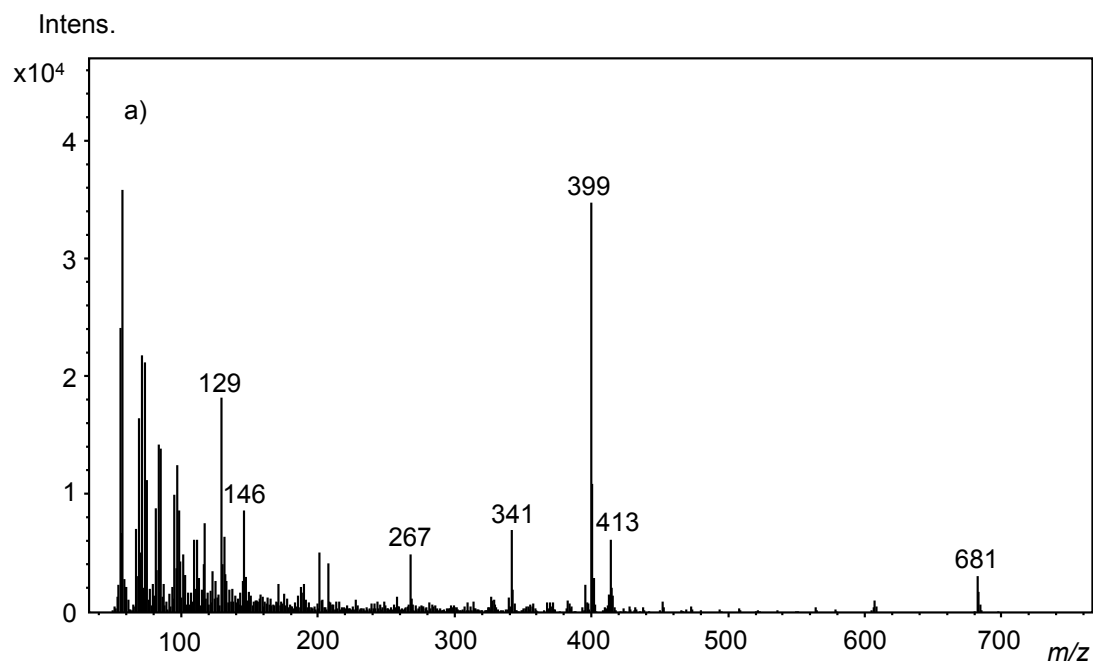
1,3-D$_{36:0}$, TMS (M$^{+\bullet}$ = 696)	
m/z value	**Assignment**
681	[M-15]$^+$
413	[M-C$_{17}$H$_{35}$COO]$^+$
399	[M-C$_{17}$H$_{35}$COOCH$_2$]$^+$
341	[C$_{17}$H$_{35}$CO+74]$^+$
267	[C$_{17}$H$_{35}$CO]$^+$
145*	[CH(O)CHCH$_2$OSi(CH$_3$)$_3$]$^+$
129	[CH$_2$CHCHOSi(CH$_3$)$_3$]$^+$

Figure 86. 1,3-D$_{36:0}$ DAG (t_R = 30.4 min) from extract of MCP30 a) mass spectrum; b) m/z value assignments. *The peak with m/z 146 was of higher intensity than the peak with m/z 145 so m/z 146 is labelled on the spectrum.

m/z value	Assignment
681	$[M-15]^+$
413	$[M-C_{17}H_{35}COO]^+$
357	$[C_{17}H_{35}CO+90]^+$
341	$[C_{17}H_{35}CO+74]^+$
267	$[C_{17}H_{35}CO]^+$
145	$[CH(O)CHCH_2OSi(CH_3)_3]^+$
129	$[CH_2CHCHOSi(CH_3)_3]^+$

b) **1,2-D$_{36:0}$, TMS (M$^{+\bullet}$ = 696)**

Figure 87. 1,2-D$_{36:0}$ DAG (t_R = 30.2 min) from extract of MCP30 a) mass spectrum; b) m/z value assignments.
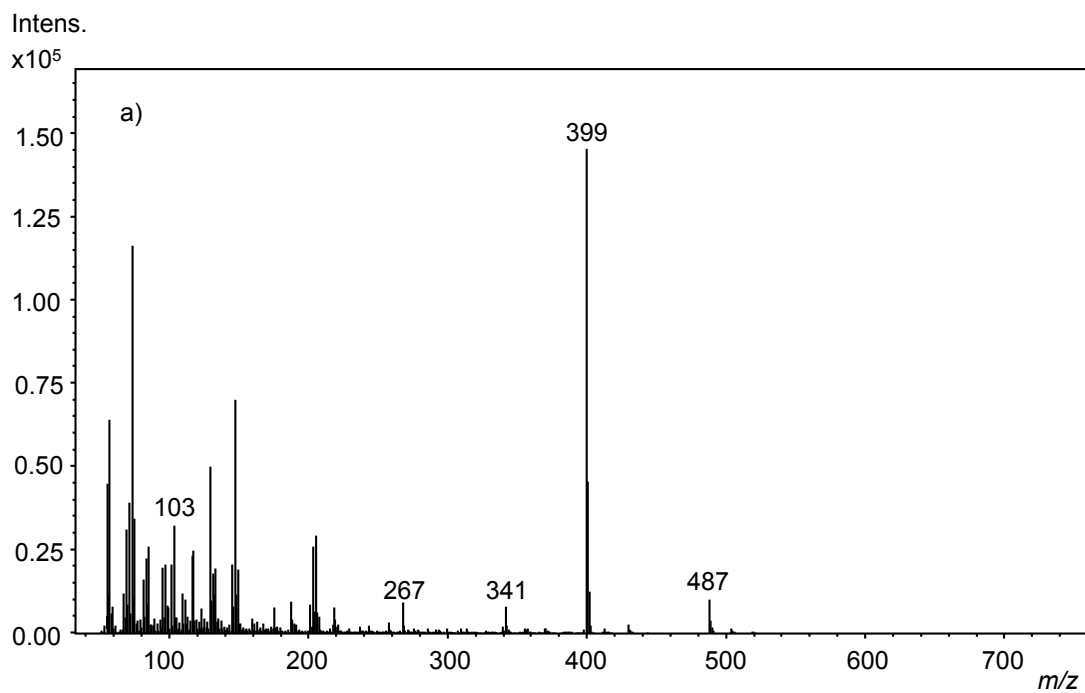
1-$M_{18:0}$, TMS ($M^{+\bullet}$ = 502)	
m/z value	Assignment
487	$[M-15]^+$
399	$[M-CH_2OSi(CH_3)_3]^+$
341	$[C_{17}H_{35}CO+74]^+$
267	$[C_{17}H_{35}CO]^+$
103	$[CH_2OSi(CH_3)_3]^+$

Figure 88. 1-$M_{18:0}$ MAG (t_R = 21.2 min) from extract of MCP30 a) mass spectrum; b) *m/z* value assignments.
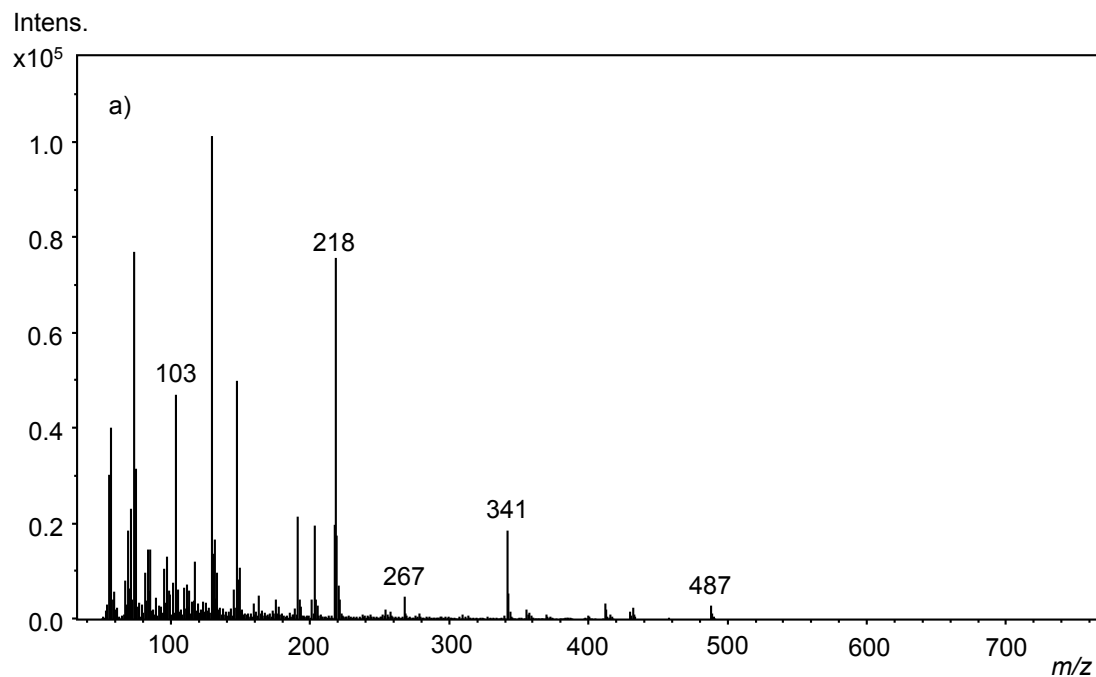
<table>
<tr><td>b)</td><td colspan="2">2-$M_{18:0}$, TMS ($M^{+\bullet} = 502$)</td></tr>
</table>

m/z value	Assignment
487	$[M-15]^+$
341	$[C_{17}H_{35}CO+74]^+$
267	$[C_{17}H_{35}CO]^+$
218	$[(CH_3)_3SiOCHCHCH_2OSi(CH_3)_3]^+$
103	$[CH_2OSi(CH_3)_3]^+$

Figure 89. 2-$M_{18:0}$ MAG ($t_R = 20.9$ min) from extract of MCP30 a) mass spectrum; b) *m/z* value assignments.
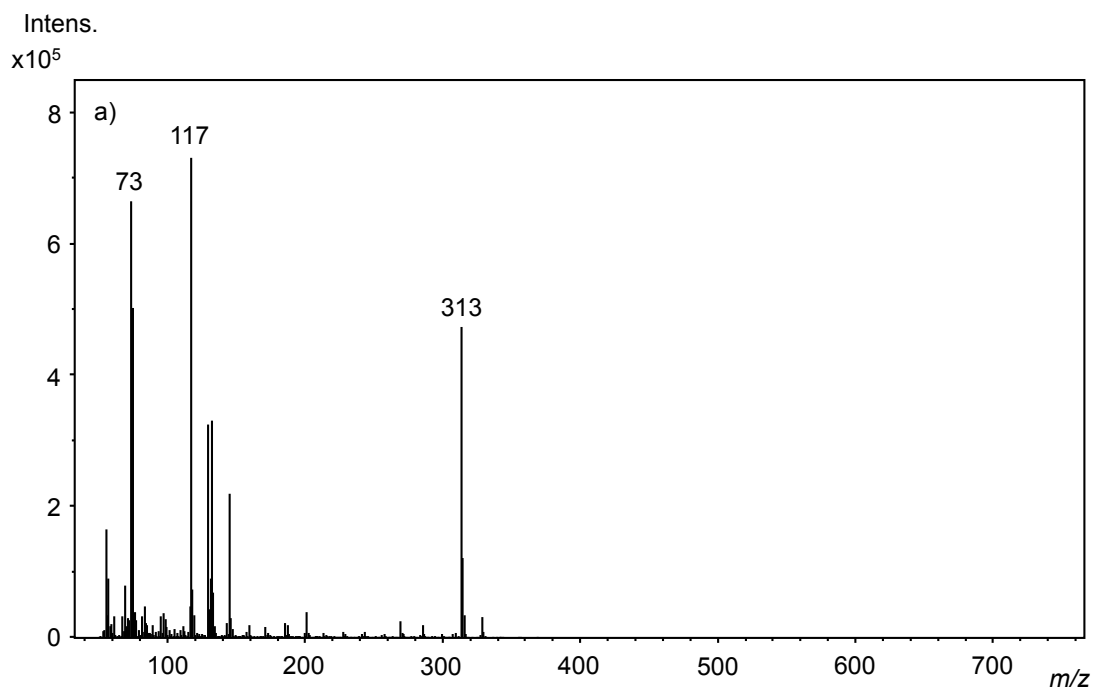
C$_{16:0}$ fatty acid, TMS (M$^{+\bullet}$ = 328)	
m/z value	Assignment
313	[M-15]$^{+}$
117	[COOSi(CH$_3$)$_3$]$^{+}$
73	[Si(CH$_3$)$_3$]$^{+}$

Figure 90. C$_{16:0}$ fatty acid (t_R = 15.1 min) from extract of MCP30 a) mass spectrum; b) *m/z* value assignments.
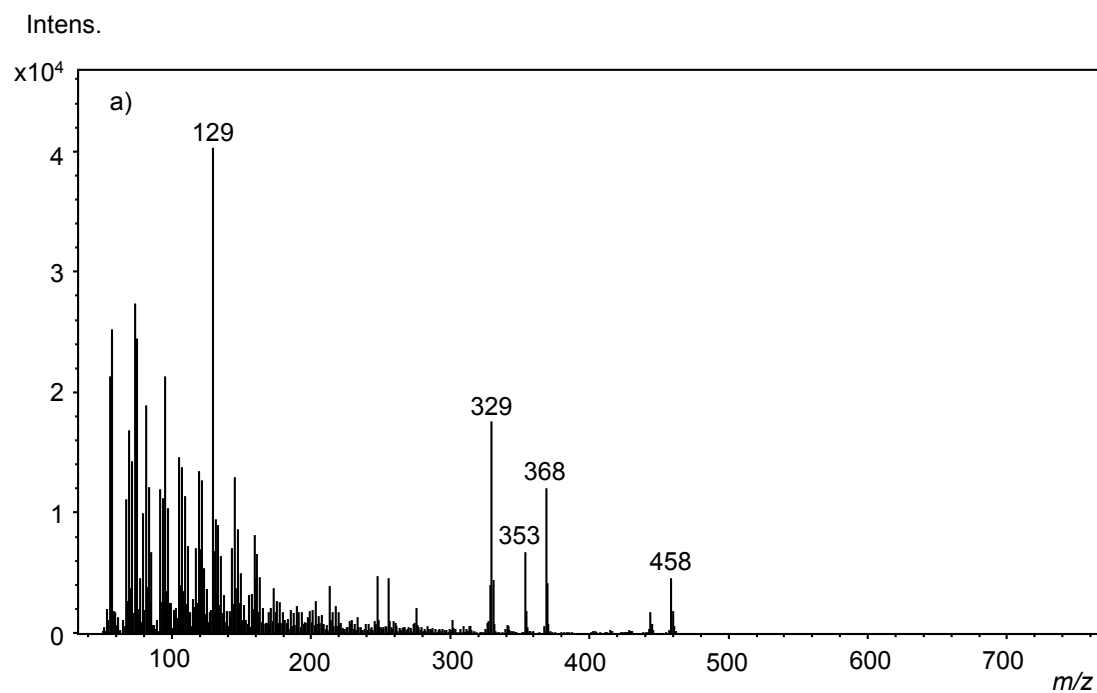
b)	Cholesterol, TMS ($M^{+\bullet}$ = 458)	
m/z value	Assignment	
458	M^+	
368	$[M-90]^+$	
353	$[M-90-15]^+$	
329	$[M-129]^+$	
129	$[CH_2CHCHOSi(CH_3)_3]^+$	

Figure 91. Cholesterol (t_R = 24.0 min) from extract of MCP30 a) mass spectrum; b) *m/z* value assignments.
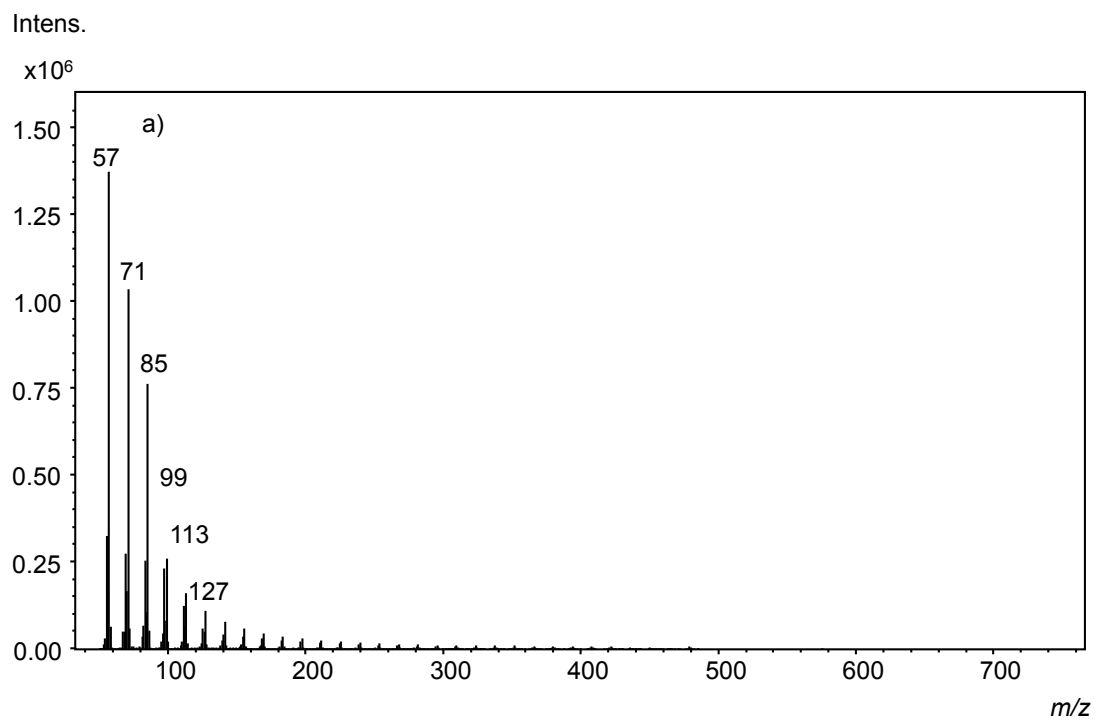
Figure 92. Mass spectrum of the C_{34} alkane (internal standard, $t_R = 25.4$ min) from extract of MCP30.

Table 15 shows the lipid components identified by HTGC-MS in extracts, following TMS derivatisation, of each of the potsherds analysed and the total lipid yield in µg/g of potsherd.

Table 15. Lipids identified by HTGC-MS in extracts of each of the Merv vessels, following trimethylsilylation.

Sample number	Potsherd type	Period	Lipids identified	Total lipid yield / µg/g
MCP18	Body	Seljuk	**FAs:** $C_{11:0} - C_{18:0}$; cholesterol	1
MCP19	Body	Seljuk	**FAs:** $C_{11:0} - C_{18:0}$, $C_{18:1}$; **MAGs:** 1-$M_{16:0}$, 1-$M_{18:0}$, 2-$M_{18:0}$ **branched FAs:** $C_{15:0} - C_{17:0}$; **DAGs:** 1,2-$D_{32:0}$, 1,3-$D_{32:0}$, 1,2-$D_{34:0}$, 1,3-$D_{34:0}$, 1,2-$D_{36:0}$, 1,3-$D_{36:0}$; **TAGs:** $T_{48:0}$, $T_{50:0}$, $T_{52:0}$, $T_{54:0}$; **sterols:** cholesterol	3
MCP20	Body	Seljuk	**FAs:** $C_{9:0} - C_{18:0}$, $C_{16:1}$, $C_{18:1}$; **branched FAs:** $C_{15:0} - C_{17:0}$; **MAGs:** 1-$M_{16:0}$, 2-$M_{16:0}$, 1-$M_{18:0}$, 2-$M_{18:0}$; **DAGs:** 1,2-$D_{32:0}$, 1,3-$D_{32:0}$, 1,2-$D_{34:0}$, 1,3-$D_{34:0}$, 1,2-$D_{36:0}$, 1,3-$D_{36:0}$; **TAGs:** $T_{48:0}$, $T_{50:0}$, $T_{52:0}$; **sterols:** cholesterol	39
MCP22	Rim	Seljuk	**FAs:** $C_{9:0} - C_{18:0}$, $C_{16:1}$, $C_{18:1}$; **branched FAs:** $C_{15:0} - C_{17:0}$; **MAGs:** 1-$M_{16:0}$, $M_{18:0}$, 2-$M_{16:0}$, 2-$M_{18:0}$; **DAGs:** 1,3-$D_{30:0}$, 1,2-$D_{32:0}$, 1,3-$D_{32:0}$, 1,2-$D_{34:0}$, 1,3-$D_{34:0}$, 1,2-$D_{35:0}$, 1,2-$D_{36:0}$, 1,3-$D_{36:0}$, 1,2-$D_{36:1}$, 1,3-$D_{36:1}$; **TAGs:** $T_{46:0}$, $T_{48:0}$, $T_{49:0}$, $T_{50:0}$, $T_{51:0}$, $T_{52:0}$, $T_{54:0}$; **sterols:** cholesterol	13
MCP23	Body	Seljuk	**FAs:** $C_{11:0} - C_{18:0}$, $C_{18:1}$; **branched FAs:** $C_{15:0}$, $C_{17:0}$; **MAGs:** 2-$M_{16:0}$, 1-$M_{18:0}$, 2-$M_{18:0}$; **DAGs:** 1,2-$D_{32:0}$, 1,3-$D_{32:0}$, 1,2-$D_{34:0}$, 1,3-$D_{34:0}$, 1,2-$D_{36:0}$, 1,3-$D_{36:0}$; **TAGs:** $T_{48:0}$, $T_{50:0}$, $T_{52:0}$, $T_{54:0}$; **sterols:** cholesterol	7
MCP26	Body	Seljuk	**FAs:** $C_{11:0} - C_{18:0}$, $C_{18:1}$; **branched FAs:** $C_{15:0}$, $C_{17:0}$; **MAGs:** 1-$M_{16:0}$-$M_{18:0}$, 2-$M_{16:0}$, 2-$M_{18:0}$; **DAGs:** 1,2-$D_{32:0}$, 1,3-$D_{32:0}$, 1,2-$D_{34:0}$, 1,3-$D_{34:0}$, 1,2-$D_{36:0}$, 1,3-$D_{36:0}$; **sterols:** cholesterol	2
MCP27	Rim	Seljuk	**FAs:** $C_{9:0} - C_{18:0}$; **sterols:** cholesterol	2

Sample number	Potsherd type	Period	Lipids identified	Total lipid yield / $\mu g/g$
MCP28	Rim	Seljuk	**FAs:** $C_{9:0} - C_{18:0}$, $C_{18:1}$; **MAGs:** 1-$M_{18:0}$; **sterols:** cholesterol	1
MCP29	Rim	Seljuk	**FAs:** $C_{9:0} - C_{18:0}$, $C_{16:1}$, $C_{18:1}$; **branched FAs:** $C_{15:0} - C_{17:0}$; **MAGs:** 1-$M_{16:0}$, 1-$M_{18:0}$; **TAGs:** $T_{48:0}$, $T_{50:0}$, $T_{52:0}$; **sterols:** cholesterol	6
MCP30	Body	Seljuk	**FAs:** $C_{8:0} - C_{18:0}$, $C_{16:1}$, $C_{18:1}$; **branched FAs:** $C_{15:0} - C_{17:0}$; **MAGs:** 1-$M_{14:0}$, 2-$M_{14:0}$, 1-$M_{16:0}$-$M_{18:0}$, 2-$M_{16:0}$-$M_{18:0}$; **DAGs:** 1,2-$D_{30:0}$, 1,3-$D_{30:0}$, 1,2-$D_{32:0}$, 1,3-$D_{32:0}$, 1,2-$D_{33:0}$, 1,2-$D_{34:0}$, 1,3-$D_{34:0}$, 1,2-$D_{36:0}$, 1,3-$D_{36:0}$, 1,2-$D_{34:1}$, 1,2-$D_{35:0}$, 1,2-$D_{36:1}$, 1,3-$D_{36:1}$; **TAGs:** $T_{44:0}$, $T_{46:0}$, $T_{47:0}$, $T_{48:0}$, $T_{49:0}$, $T_{50:0}$, $T_{51:0}$, $T_{52:0}$, $T_{54:0}$, $T_{52:1}$, $T_{54:1}$; **sterols:** cholesterol	33
MCP33	Rim	Seljuk	**FAs:** $C_{9:0} - C_{18:0}$, $C_{18:1}$; **branched FAs:** $C_{15:0}$, $C_{17:0}$; **sterols:** cholesterol	4
MCP34	Rim	Seljuk	**FAs:** $C_{9:0} - C_{18:0}$, $C_{16:1}$, $C_{18:1}$; **branched FAs:** $C_{15:0}$, $C_{17:0}$; **MAGs:** 1-$M_{16:0}$; **DAGs:** 1,2-$D_{30:0}$, 1,2-$D_{32:0}$, 1,3-$D_{32:0}$, 1,2-$D_{34:0}$, 1,3-$D_{34:0}$, 1,2-$D_{36:0}$, 1,3-$D_{36:0}$, 1,2-$D_{34:1}$, 1,2-$D_{36:1}$, 1,3-$D_{36:1}$; **TAGs:** $T_{42:0}$, $T_{44:0}$, $T_{46:0}$, $T_{48:0}$, $T_{50:0}$, $T_{52:0}$, $T_{54:0}$, $T_{50:1}$, $T_{52:1}$, $T_{54:1}$; **sterols:** cholesterol	9
IMP8220	Base/body	Early Islamic	**FAs:** $C_{9:0} - C_{18:0}$, $C_{18:1}$; **branched FAs:** $C_{15:0}$, $C_{17:0}$; **MAGs:** 1-$M_{16:0}$, 1-$M_{18:0}$; **sterols:** cholesterol	1
IMP8104	Base/body	Early Islamic	**FAs:** $C_{9:0} - C_{18:0}$, $C_{16:1}$, $C_{18:1}$; **branched FAs:** $C_{15:0}$; **MAGs:** 1-$M_{16:0}$; **sterols:** cholesterol	2
IMP8495	Body	Early Islamic	**FAs:** $C_{9:0} - C_{18:0}$, $C_{16:1}$, $C_{18:1}$; **branched FAs:** $C_{15:0}$; **MAGs:** 1-$M_{16:0}$; **sterols:** cholesterol	1
64	Control	Early Islamic	**FAs:** $C_{9:0} - C_{18:0}$, $C_{16:1}$, $C_{18:1}$; **sterols:** cholesterol	3

As can be seen from Table 15, six of the twelve Seljuk samples contained significant lipid residue (i.e. more than 5 $\mu g/g$ of potsherd[18]) whereas none of the Early Islamic samples did. By comparison, the extraction blank was found to contain fatty acids

only ($C_{11:0} - C_{18:0}$ and $C_{18:1}$) at a level equivalent to approximately 2 µg/g, showing that samples with this low level of lipid cannot reliably be interpreted in archaeological terms.

All samples analysed contained detectable free fatty acids, with most of the Seljuk samples also containing intact TAGs and their breakdown products, DAGs and MAGs. The range of fatty acids found in samples from the two time periods does not seem to vary significantly, with fatty acids in the range $C_{9:0} - C_{18:0}$ found in most sample extracts from both periods. The shortest fatty acid was $C_{8:0}$, found in sample MCP30. As can be seen from the presence of a wide range of TAG components identified in this sample (Figure 84) and its relatively high lipid yield, this was a particularly well-preserved sample, which may explain the slightly greater fatty acid range observed. Several samples exhibited a slightly smaller fatty acid range, from $C_{10:0}$ or $C_{11:0}$ to $C_{18:0}$.

The primary fatty acids found in all samples were the $C_{16:0}$ and $C_{18:0}$ acids. $C_{16:1}$ and/or $C_{18:1}$ were observed in most of the samples. The presence of odd carbon-numbered fatty acids, especially $C_{15:0}$ and $C_{17:0}$, and those with branched chains (mainly $C_{15:0}$ and $C_{17:0}$, but also $C_{16:0}$ in some cases) was also noted.

Samples that contained DAGs primarily contained the fully saturated $D_{32:0}$, $D_{34:0}$ and $D_{36:0}$ components, in both the 1,2- and 1,3-substitution patterns. The lipid extracts of only three samples (MCP22, MCP30 and MCP34) contained a DAG as short as $D_{30:0}$, with the extract of MCP22 containing the 1,3-substituted isomer, the extract of MCP34 having 1,2-$D_{30:0}$ and the extract of MCP30 having both. Some samples contained $D_{34:1}$ and $D_{36:1}$, but these were the only unsaturated DAGs detected. Odd carbon-numbered DAGs were also detected in the extracts of MCP22 and MCP30: 1,2-$D_{35:0}$ in both of these samples and 1,2-$D_{33:0}$ in MCP30.

For samples in which MAGs were detected, the most common MAG components were $M_{16:0}$ and $M_{18:0}$, with some samples containing only the 1-MAG and others containing the 2-MAG in addition to the 1-MAG. 1-$M_{17:0}$ was detected in two samples, and one sample also contained 2-$M_{17:0}$ as well as both 1- and 2-$M_{14:0}$. This was the extract of MCP30, which, as is noted above, was the most well-preserved sample analysed.

All of the Early Islamic samples contained essentially the same lipid components as each other, with fatty acids in the range $C_{9:0} - C_{18:0}$ and $C_{18:1}$, and two of the three samples also containing $C_{16:1}$. These samples were clearly less well preserved in general than the Seljuk samples, since intact TAGs were not detected in any of them. MAGs were detected in the Early Islamic samples, though at low levels, which is to be expected based on the fact that complete hydrolysis is understood to occur rapidly after the loss of the first fatty acid. The fact that the Early Islamic samples all had lipid yields lower than 5 µg/g and no intact TAGs is consistent with the lipids in these samples being poorly preserved.

The extract of the control chlorite sample contained only fatty acids and cholesterol. Since this potsherd is thought to have come from an inkwell rather than a vessel used to cook or store food, these analytes are likely to be a result of contamination from the burial environment, rather than absorbed residues indicative of food remains.

6.4.2 Matrix-Assisted Laser Desorption/Ionisation-Mass Spectrometry

MALDI-MS was carried out, using the Bruker ultraflex III TOF/TOF MS, in an attempt to gain more information about the intact TAGs present in the samples. Figure 93 shows an example MALDI mass spectrum, from the extract of MCP30. A continuous range of TAGs from $T_{44:0}$ to $T_{54:0}$, including both even and odd carbon number TAGs and several unsaturated ones, was observed. Samples were spotted in duplicate for MALDI-MS analysis, since it is known that variation occurs within and between MALDI spots.[97,187,188]
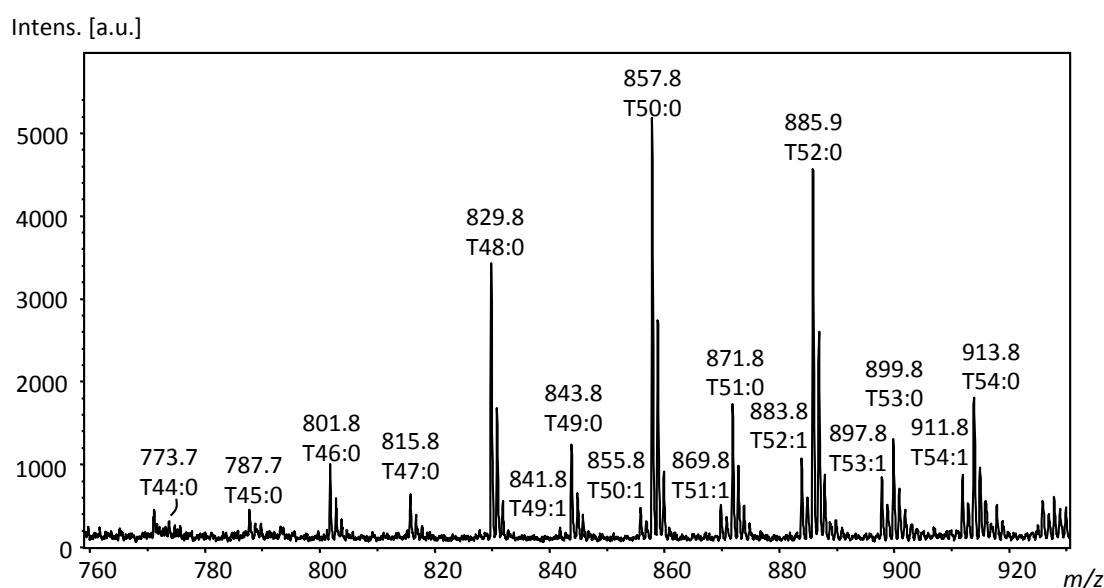
Figure 93. MALDI mass spectrum of the extract of MCP30.

Figure 94 presents an overview of the TAGs that were detected on MALDI-MS analysis of the lipid extracts from the Merv samples, with the range of saturated TAGs detected indicated by the length of the top bar for each sample (purple), and the presence of singly unsaturated TAGs by the second bar (grey). No TAGs with more than one double bond were detected.

Acyl carbon number / Sample number	T$_{44}$	T$_{45}$	T$_{46}$	T$_{47}$	T$_{48}$	T$_{49}$	T$_{50}$	T$_{51}$	T$_{52}$	T$_{53}$	T$_{54}$
MCP18	No TAGs detected										
MCP19											
MCP20											
MCP22											
MCP23											
MCP26											
MCP27	No TAGs detected										
MCP28	No TAGs detected										
MCP29	No TAGs detected										
MCP30											
MCP33	No TAGs detected										
MCP34											
IMP8220	No TAGs detected										
IMP8104	No TAGs detected										
IMP8495	No TAGs detected										
64	No TAGs detected										

Figure 94. TAGs detected by MALDI-MS in each of the samples. The upper bar (purple) in each case represents fully saturated TAGs, whilst the lower bar (grey) indicates singly unsaturated TAGs.

Table 16 gives a summary of the results of the TAG analysis in each of the Merv samples using HTGC-MS and MALDI-MS. In general, the results uphold the conclusion from previous chapters that MALDI-MS has a better sensitivity for TAGs than HTGC-MS does, as it is able to detect TAGs that are not detected by HTGC-MS. This is particularly apparent with the odd carbon-numbered TAGs, which are usually minor components (because of the fact that animal fats are composed primarily of even carbon chain fatty acids). As can be seen from Figure 94, in the sample extracts in which TAGs were detected, a continuous range of both even and odd carbon-numbered TAGs was detected. In contrast, odd carbon-numbered TAGs were detected by HTGC-MS in only two of the samples (MCP22 and MCP30), and the range of these was not as great as the range detected by MALDI-MS. However, MALDI-MS was not always able to detect as wide a range of TAGs as HTGC-MS did. For example, the lightest TAG detected in any sample was $T_{42:0}$, in sample MCP34 by HTGC-MS. MALDI-MS was only able to detect down to $T_{44:0}$ in this sample. The reason for this may be the fact that some of the MALDI mass spectra have a fairly high noise level, meaning that a relatively high signal is required to give an acceptable S/N ratio for identification. Therefore, the analytes may be present but give peaks that are too weak to be identified.

There was one sample (MCP26) in which MALDI-MS was much more successful than HTGC-MS. In this case, a fairly wide range of TAGs ($T_{45:0} - T_{54:0}$, plus some unsaturated TAGs) was detected by MALDI-MS with good S/N, whilst they were not detected at all by HTGC-MS. On HTGC-MS analysis of this sample a range of fatty acids, MAGs and DAGs, as well as cholesterol, were detected, showing that the HTGC-MS analysis did work and there were no problems with injection.

Table 16. Summary of the TAGs detected in each Merv sample by HTGC-MS and MALDI-MS.

Sample number	HTGC-MS	MALDI-MS
MCP18	No TAGs	No TAGs
MCP19	$T_{48:0} - T_{54:0}$ (even only)	$T_{47:0} - T_{54:0}$, $T_{54:1}$
MCP20	$T_{48:0} - T_{52:0}$ (even only)	$T_{47:0} - T_{54:0}$
MCP22	$T_{46:0} - T_{54:0}$ (even), $T_{49:0}$, $T_{51:0}$	$T_{45:0} - T_{54:0}$, $T_{50:1}$, $T_{52:1}$, $T_{54:1}$
MCP23	$T_{48:0} - T_{54:0}$ (even only)	$T_{46:0} - T_{54:0}$, $T_{52:1}$, $T_{54:1}$
MCP26	No TAGs	$T_{45:0} - T_{54:0}$, $T_{50:1}$, $T_{52:1}$, $T_{54:1}$
MCP27	No TAGs	No TAGs
MCP28	No TAGs	No TAGs
MCP29	$T_{48:0} - T_{52:0}$ (even only)	No TAGs
MCP30	$T_{44:0} - T_{54:0}$ (even), $T_{47:0}$, $T_{49:0}$, $T_{51:0}$, $T_{52:1}$, $T_{54:1}$	$T_{44:0} - T_{54:0}$, $T_{49:1} - T_{54:1}$
MCP33	No TAGs	No TAGs
MCP34	$T_{42:0} - T_{54:0}$ (even only), $T_{50:1}$, $T_{52:1}$, $T_{54:1}$	$T_{44:0} - T_{51:0}$, $T_{50:1}$
IMP8220	No TAGs	No TAGs
IMP8104	No TAGs	No TAGs
IMP8495	No TAGs	No TAGs
64	No TAGs	No TAGs

Tandem MS was carried out on the TAGs in some of the samples that gave good TAG signals on MALDI-MS, to gain information about the fatty acid composition of the TAGs, and the fatty acids losses observed are shown in Table 17. Figure 95 shows an example product ion spectrum, from MCP22.

Table 17. Ions deriving from fatty acid losses on tandem MS of intact TAGs detected in the sample extracts by MALDI-MS.

Sample	TAG	m/z	Product ion m/z	Neutral loss	Sample	TAG	m/z	Product ion m/z	Neutral loss
MCP19	$T_{54:0}$	913	629	$C_{18:0}$ acid	MCP22	$T_{54:0}$	913	629	$C_{18:0}$ acid
			607	$C_{18:0}$ salt				607	$C_{18:0}$ salt
	$T_{52:0}$	885	629	$C_{16:0}$ acid				657	$C_{16:0}$ acid
			607	$C_{16:0}$ salt		$T_{52:0}$	885	629	$C_{16:0}$ acid
			601	$C_{18:0}$ acid				607	$C_{16:0}$ salt
			579	$C_{18:0}$ salt				601	$C_{18:0}$ acid
	$T_{50:0}$	857	601	$C_{16:0}$ acid				579	$C_{18:0}$ salt
			579	$C_{16:0}$ salt		$T_{50:0}$	857	629	$C_{14:0}$ acid
			573	$C_{18:0}$ acid				607	$C_{14:0}$ salt
			551	$C_{18:0}$ salt				601	$C_{16:0}$ acid
	$T_{48:0}$	829	573	$C_{16:0}$ acid				579	$C_{16:0}$ salt
			551	$C_{16:0}$ salt				573	$C_{18:0}$ acid
MCP20	$T_{54:0}$	913	629	$C_{18:0}$ acid				551	$C_{18:0}$ salt
			607	$C_{18:0}$ salt		$T_{48:0}$	829	601	$C_{14:0}$ acid
	$T_{52:0}$	885	629	$C_{16:0}$ acid				579	$C_{14:0}$ salt
			607	$C_{16:0}$ salt				573	$C_{16:0}$ acid
			601	$C_{18:0}$ acid				551	$C_{16:0}$ salt
			579	$C_{18:0}$ salt				523	$C_{18:0}$ salt
	$T_{50:0}$	857	601	$C_{16:0}$ acid		$T_{46:0}$	801	523	$C_{16:0}$ salt
			579	$C_{16:0}$ salt					
			573	$C_{18:0}$ acid					
			551	$C_{18:0}$ salt					
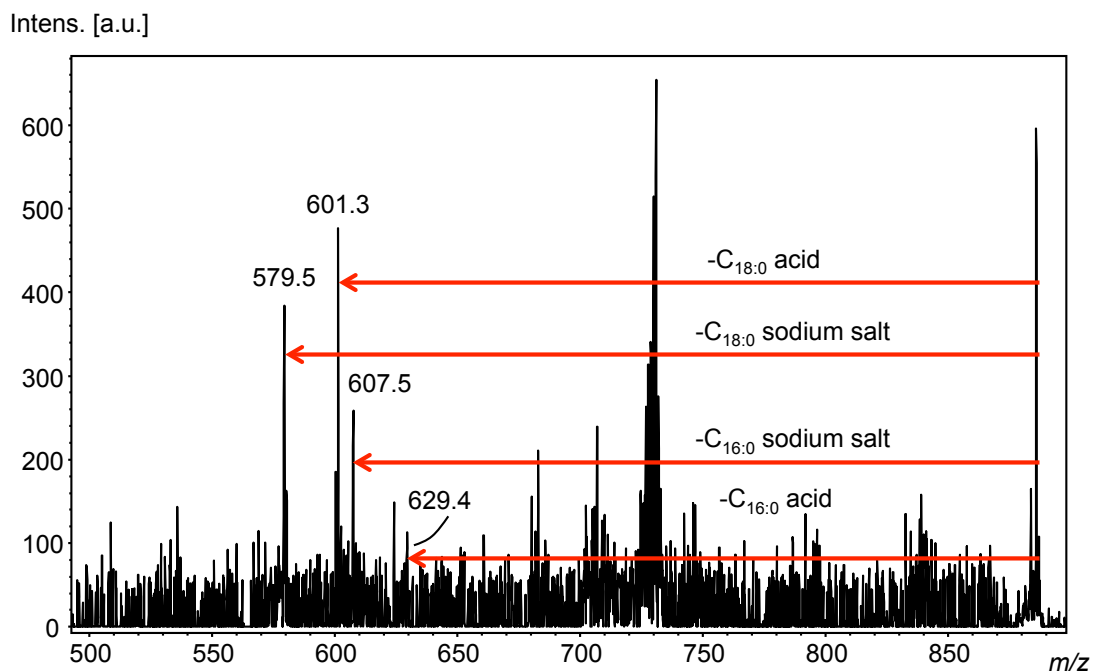
Figure 95. Product ion spectrum of the species with *m/z* 885 from the extract of MCP22, corresponding to $[T_{52:0} + Na]^+$, showing neutral losses of $C_{16:0}$ and $C_{18:0}$ fatty acids and fatty acid sodium salts.

As can be seen from Table 17, the neutral losses observed all correspond to even carbon-numbered fatty acids and fatty acid sodium salts, mainly $C_{16:0}$ and $C_{18:0}$, with some $C_{14:0}$. The TAGs all gave expected neutral losses, consistent with fairly simple mixtures of TAG molecular species. For example, the vast majority of $T_{54:0}$ molecules would be expected to be composed of three $C_{18:0}$ fatty acids, which is what the tandem MS data indicate. There may be a small number of molecules with some $C_{16:0}$ and $C_{20:0}$ but losses of these fatty acids may not be detected in product ion spectra due to the low number of molecules of this type. A similar situation occurs for $T_{48:0}$, where the expectation would be of three $C_{16:0}$ fatty acids. In sample MCP19 this is observed, but in sample MCP22 there is also evidence of $C_{14:0}$ and $C_{18:0}$. Sample MCP22 gives an unusual result for the $T_{54:0}$ TAG, which would be expected to show neutral losses corresponding to $C_{18:0}$ fatty acids. This does indeed occur, but there is also a peak for the neutral loss of the $C_{16:0}$ fatty acid at *m/z* 657 (though not for the sodium salt). For there to be a $C_{16:0}$ fatty acid in a $T_{54:0}$ TAG molecule, $C_{20:0}$ would also need to be present. This is not observed, though the peak at *m/z* 657 was weak so it may be that peaks corresponding to loss of $C_{20:0}$ are too weak to be detected.

217

The lightest TAG on which tandem MS was carried out was $T_{46:0}$. This did not give particularly satisfactory results, with only the neutral loss of a $C_{16:0}$ sodium salt observed. However, the S/N of the precursor ion (m/z 801) was not very high, which is likely to be the explanation.

Tandem MS was not carried out on any of the unsaturated or odd carbon number TAGs, as the signals for these were not of sufficient S/N to allow the ions to be isolated and fragmented.

6.5 DISCUSSION

Analysis of the lipids extracted from the potsherds has revealed fairly well-preserved residues consistent with the presence of absorbed food remains, and therefore supports the initial conclusion, based on the presence of blackened residues on the pots, that they were used for cooking rather than just for storage. It also further illustrates the previously published observation that chlorite is capable of preserving lipid residues in a similar fashion to ceramic.[32]

The lipid yields, as determined from HTGC-MS analysis, do not seem to follow any pattern that correlates with the potsherd type. The range of lipids observed also does not seem to correlate with potsherd type. Lipids are known to accumulate in ceramic vessels to different extents in different parts of the vessel, with higher lipid yields usually found in the rim, followed by the base and then the body.[189] However, this is not observed in the stone samples from Merv. Only rim and body stone potsherds have been found from the Seljuk dynasty, and although the two highest lipid yields observed were both from body potsherds, the lower lipid yields come from both rim and body potsherds. Although lipids accumulate to different extents in different parts of ceramic vessels,[189] it does not necessarily follow that the same will be true for stone vessels, or that the places where lipid accumulates most will be the same between these vessel types. Because the ability of stone to entrap and preserve lipids is thought to be linked to its porosity, which is affected by heating during cooking, the porosity of the stone is likely to vary across the area of the vessel. Different parts of the vessel will have been in direct contact with the heat source and/or with the food inside, and will therefore be likely to reach different temperatures during cooking. In the case of stone vessels, it could be that the rim does not reach such

high temperatures as the rest of the vessel, meaning that its porosity does not increase sufficiently to allow large amounts of lipid to be preserved. All of the Early Islamic potsherds had similar lipid yields and range of lipids. However, they were also all base/body or body potsherds, and so no conclusions about lipids accumulating in different parts of the vessels can be drawn from these samples.

Two of the Seljuk dynasty samples and all of the Early Islamic samples contained MAGs but no DAGs or TAGs. This indicates an intermediate level of preservation between those samples that contain only fatty acids and those that contain intact TAGs, but is interesting because experiments have shown that complete hydrolysis of TAGs appears to occur rapidly after the loss of the first fatty acid and that MAGs and DAGs do not build up to an appreciable extent.[64] Two possible explanations could account for the detection of MAGs but not DAGs in these samples. One is the fact that these MAGs were present at very low levels, so it may be that there were also small amounts of DAG in these samples which were not detected because they were just below the LOD. The second is that the studies of lipid degradation in archaeological artefacts have all been carried out on ceramics, and it could be that the degradation and preservation processes that occur in stone artefacts are slightly different to those in ceramics.

Since almost all of the work on lipids preserved in archaeological artefacts has been carried out on ceramic, it is impossible to know whether the degradative processes might be the same in stone potsherds compared to ceramics. Because it is thought that the lipids are protected from microbial decay by the fact that they are trapped in pores that are too small for microbes, pore size is clearly important. Previously reported analysis of the pore size in archaeological ceramic potsherds from Merv and in Seljuk dynasty stone potsherds has shown that the pores in the stone potsherds are much more variable in size than in the ceramic.[32] The stone potsherds also included many much larger pores that are probably not suitable for lipid preservation. This could indicate that the stone potsherds may not be able to preserve lipids to as great an extent as ceramic, although this was not found to be the case in the previous work.[32] However, other factors such as the stone material being less suitable for microbial life than ceramic material may account for this. This might affect the type

of degradation that occurs, as well as the extent of it, and is something that would benefit from further study.

On HTGC-MS analysis, all samples showed a range of free fatty acids, with the longest fatty acids detected in any sample being $C_{18:0}$. This fatty acid was, along with $C_{16:0}$, the most prominent component of the samples. These observations, along with the absence of compounds such as long-chain alcohols which are associated with plant waxes,[40] are highly consistent with the residues being those of degraded animal fat, since $C_{16:0}$ and $C_{18:0}$ are the most common fatty acids found in animal fats. The presence of relatively high levels of free fatty acids compared to intact TAGs is typical for archaeological residues and illustrates the inherent state of degradation of the samples, since fatty acids are produced by hydrolysis of TAGs, which are the primary components of undegraded animal fats. The range of fatty acids extended down to $C_{11:0}$ in all cases, but some samples contained a wider range of fatty acids, down to $C_{8:0}$ in one case and $C_{9:0}$ in several others. These short chain TAGs could indicate a dairy source for the lipids. However, the lack of short chain TAGs makes it impossible to draw this conclusion with any certainty.

The fact that the range of fatty acids varies slightly may just be a result of variation in preservation rather than a difference in the lipids originally deposited in the samples, since it is known that short chain fatty acids are lost more easily than longer chain fatty acids (both in terms of their hydrolysis from the glycerol backbone of TAGs to produce free fatty acids, and the subsequent loss of the fatty acids from the sample).[64] This proposed variation in levels of preservation is supported by the presence or absence of TAGs in the samples, because there does seem to be some correlation between the presence of intact TAGs (and therefore the level of preservation) and the range of fatty acids observed, with the samples with the smaller fatty acid ranges tending to show lower levels of preservation based on TAG content. This does not hold in all cases, but it is certainly true that the most well-preserved sample (MCP30) showed the widest range of fatty acids. The samples with relatively high lipid yields (MCP20, MCP22 and MCP30) all had wide fatty acid ranges, further supporting the theory. However, many of the samples with low lipid yields also contained fatty acids down to $C_{9:0}$. The presence of branched and odd carbon-numbered fatty acids, especially $C_{15:0}$ and $C_{17:0,}$ may indicate a ruminant source for

220

the lipids.[31] This fits with the faunal evidence from the site, with the animal bone assemblage being dominated by sheep and goat.[185]

The acyl lipids (MAGs, DAGs and TAGs) observed are of carbon numbers consistent with the fatty acids, though the range of carbon numbers is not so great as that found in the free fatty acids. This is to be expected because short-chain fatty acids are more easily hydrolysed from the glycerol backbone than their longer-chain counterparts.[64] Despite this, a wide range of TAGs was detected in some samples, from $T_{42:0}$ in one case, up to $T_{54:0}$.

HTGC-MS is a very commonly used technique for the analysis of lipids extracted from archaeological potsherds and it is able to detect a wide range of lipid species. However, work presented in this thesis has shown that MALDI-MS has the potential to detect intact TAGs with greater sensitivity than HTGC-MS can (chapters 4 and 5). The results presented in this chapter support the work presented earlier, showing that in some cases MALDI-MS can detect TAGs in samples in which HTGC-MS was not able to at all (sample MCP26). In almost all samples in which TAGs were detected, HTGC-MS failed to detect any odd carbon-numbered TAGs, but on MALDI-MS analysis all samples containing TAGs were shown to have a continuous range of odd and even carbon-numbered TAGs. The other area in which MALDI-MS showed greater sensitivity was the detection of unsaturated TAGs. Only two samples showed unsaturated TAGs on HTGC-MS, but MALDI-MS allowed detection of such TAGs in all but one of the cases where TAGs were detected.

Tandem mass spectrometry was also carried out on the TAGs detected by MALDI-MS. On this analysis, neutral losses of fatty acids and fatty acid sodium salts are observed. Tandem MS was carried out on TAGs detected in a selection of samples, and neutral losses corresponding to $C_{14:0}$, $C_{16:0}$ and $C_{18:0}$ were observed. This is consistent with the TAGs being of animal fat origin, since $C_{16:0}$ and $C_{18:0}$ are the most common fatty acids in animal fats.

One of the aims of this work was to analyse residues from different types of vessel from two time periods in the occupation of Merv: small straight-sided bowls from the Early Islamic period, and larger round-bottomed pots from the Seljuk dynasty. The question being investigated was whether this change in vessel shape and size

was concomitant with a change in the foods being cooked or in the cooking methods employed.

Analysis of the lipid residues and comparison of the residues from the two types of vessel shows that there is no great difference in the lipids in the two vessel types, with the fatty acid ranges being comparable, indicating that there was no marked difference in the types of foods that were being cooked in the two time periods. The most striking difference between the residues was the greater state of degradation of the residues in the Early Islamic vessels, with no TAGs or DAGs detected in any of these samples, and only minimal MAGs. In addition, the lipid yields in the Early Islamic potsherds were only either 1 μg/g of potsherd or 2 μg/g, much lower than most of the Seljuk dynasty samples. This difference in state of degradation could be taken as evidence of a different cooking method being employed, since previous work into the capacity of chlorite potsherds to preserve lipid residues has shown that heating of the vessels is necessary to increase the porosity of the material and allow absorption of lipid.[32] It was shown that heating to temperatures of 300 °C increased the microporosity of the material, but heating to 600 °C caused cracking of the stone. If a different cooking method was used for the two different vessel types, exposing the stone to different cooking temperatures, this could have had an effect on the abilities of the different pots to absorb lipid residues. A difference in cooking method can be envisaged based on the differences in shape and size of the vessels: the larger vessels could have been used to cook for more people over a potentially larger and hotter fire than the small bowls, meaning that the microporosity of the Seljuk vessels would have changed more than that of the Early Islamic vessels. Porosimetry analysis of the two vessel types could be carried out to see if a difference in their microporosity can be detected. Another factor is that, although analysis to determine the exact mineral composition of the Seljuk dynasty samples has been carried out,[32] such analysis has not been carried out on the Early Islamic samples. Therefore, it could be that the chlorite is slightly different between the two vessel types, which may affect the ability of the different samples to preserve lipid or affect the way they respond to thermal stress. In addition, the Early Islamic samples are older than those from the Seljuk dynasty and therefore the greater state of degradation may just be a result of a longer burial time, and with possible changes in

222

the environmental conditions over time which may also affect the state of degradation.

6.6   COMPARISON OF THE RESULTS FROM CHAPTERS 5 AND 6

The work carried out in chapters 5 and 6 involved the application of HTGC-MS and MALDI-MS to lipid extracts from potsherds from two different archaeological sites (Durrington Walls and Merv, respectively). There are several differences between the samples and the sites involved: age, geographical location and material from which the potsherds were made. Durrington Walls is located in southern Britain and is approximately 4500 years old.[143] In contrast, Merv is located in Central Asia and, although the site itself was in use for over two thousand years, the samples used in this study were between around 800 and 1200 years old (section 6.1). Because of the difference in geographical location between the two sites their environmental conditions are very different, and this has implications for the preservation of lipids in potsherds from each of the sites.[11] The difference in age is also expected to affect levels of preservation, with the older samples having been subject to a longer period of degradation than the more recent samples, although the temperatures to which the objects were exposed during burial are also key factors. This difference in age presents another issue: Durrington Walls is a prehistoric site and therefore no written records exist from it, whereas there are historical reports, including recipe books, from the medieval period from which the Merv samples date. This means that there is documentary information about the foods that were consumed in the medieval period, which can be used as further evidence to support conclusions made based on the scientific evidence. Such evidence does not exist for prehistoric periods. The difference in the material from which the Durrington Walls and Merv samples were made (ceramic and stone, respectively) may be a significant factor affecting the potential for lipid preservation between the two sample sets, but because of the lack of research into the ability of stone pots to preserve lipids, this cannot be said for certain.

Comparison of the lipids detected in the two sample sets shows that, in general, the same types of components were detected in the samples from the two sites: a range of lipids including free fatty acids, MAGs, DAGs and TAGs. However, the carbon number range of lipids detected varied between samples from the two sites, with the

223

Merv samples in general showing a wider carbon number range than the samples from Durrington Walls. The lightest TAG detected in the Durrington Walls samples was $T_{46:0}$, whereas $T_{44:0}$ was detected in some of the Merv Samples. In the Merv samples, the smallest TAG range detected in any of the samples had $T_{47:0}$ as the lightest TAG, whereas most of the Durrington Walls samples had $T_{48:0}$ as the lightest and there were several cases where the lightest was $T_{50:0}$. These results could suggest that the Merv samples are better preserved than the samples from Durrington Walls, an interpretation that fits with the age of the samples. In contrast to this, there was a much greater range of unsaturated TAGs detected in the Durrington Walls samples than in those from Merv. It is also notable that a much greater proportion of Durrington Walls samples contained detectable TAGs than did Merv samples: 70% versus 47%, respectively. These two factors indicate better preservation in the Durrington Walls samples. Another notable difference was the fact that there seemed to be more odd carbon numbered TAGs detected in the Merv samples. This may indicate a greater ruminant contribution to the lipids at Merv than at Durrington Walls.[31]

The fact that different aspects of the detected lipids indicate different relative levels of preservation between the two sample sets demonstrates the complexity of interpreting these types of samples. The aim in studies of lipids absorbed in archaeological potsherds is to try and provide a link between the preserved lipids and their animal/plant sources, in order to determine the types of foods that past populations were consuming. However, this is difficult because it is impossible to know whether components that are absent were never present, or if they have degraded to the point of undetectability. This is a specific, if not unique, problem with archaeological analysis, because in other fields of analysis steps are taken to ensure that samples are stored under conditions that minimise degradation (e.g. low temperatures, controlled humidity etc.) or are analysed before much degradation can occur. In archaeological analysis there is no control over the conditions until after excavation. Because of this inherent difficulty, it is necessary to draw on all possible sources of information to aid the interpretation of the samples. These include the various analytical methods such as HTGC(-MS) and GC-c-IRMS, but the results must also be put into the context of other finds at the archaeological site, such as animal and plant remains. Research into new methods that may be able to improve

lipid detection, such as MALDI-MS as demonstrated here, can therefore contribute to the archaeological science field by improving detection of low-abundance lipid components, or those that are not well detected by other methods, and hence mitigate the effects of degradation making certain components undetectable.

6.7 CONCLUSIONS

The work presented here involved the application of HTGC-MS and MALDI-MS (including tandem mass spectrometry) to lipid extracts from chlorite cooking vessels from two time periods in the occupation of Merv, with the aim of discovering if there was any difference in the detectable food residues which could perhaps be linked to the fact that the vessels from the two time periods were significantly different in both size and shape. The two techniques were used because HTGC-MS can provide information about the range of lipids present, but MALDI-MS has a higher sensitivity for intact TAGs and is therefore able to provide more information about the TAGs. Analysis of the lipid residues has shown that there does not seem to be a marked difference in the residues detected in the extracts of the two vessel types, providing no evidence that the foods being cooked in the two time periods were markedly different. The residues seem to indicate the cooking of meat, perhaps of ruminant origin. The most significant difference between the residues was their levels of preservation, with those from the Seljuk dynasty samples being significantly better preserved than those from the Early Islamic period. It has been suggested that this could be attributed to a possible difference in cooking method resulting in different levels of absorption into the chlorite material, and therefore difference in the ability of that material to preserve the lipids.

225

7 RESULTS: DETECTION OF OPIUM ALKALOIDS IN A CYPRIOT BASE-RING JUGLET

The work presented in this chapter was a subproject related to the other work carried out in the PhD because it was concerned with the analysis by MS of an archaeological vessel. However, in this case it was the contents, rather than the vessel itself, that were analysed. The object is a Bronze Age vessel from Cyprus, called a base-ring juglet, whose contents were analysed by HPLC-MS for the presence of opium alkaloids.

7.1 INTRODUCTION

The opium poppy, *Papaver somniferum*, has been cultivated since at least the early Neolithic period and there are many examples of *P. somniferum* seeds at European Neolithic sites.[190] For example, seeds of *P. somniferum* have been found at the 6th millennium BC site of La Marmotta in Italy. However, it is impossible to tell from the archaeological evidence what exactly the plants were used for, and whether people were aware of and made use of the narcotic effects of opium. Since the seeds are edible and are the source of poppyseed oil, which is also edible, their use for culinary purposes at least seems logical. It has been suggested that there may have been ritual use of opium at La Marmotta, due to the presence of what looks like a religious room at the site,[190] but the evidence for this use of *P. somniferum* is not strong.

The latex obtained from the capsule of *P. somniferum* is the source of the psychoactive compounds that give opium its narcotic effects. Opium is obtained by scoring unripe poppy capsules and allowing the latex to ooze out.[191] Once dry this is scraped off and processed to produce opium. Because it is the capsule that is the source of opium, rather than the seeds, representations of poppy capsules have been interpreted by archaeologists as evidence of the narcotic use of *P. somniferum*.

There are a large number of artefacts from the eastern Mediterranean region in the Late Bronze Age (ca. 1650 – 1350 BC) which seem to resemble poppy capsules. In 1962, R. S. Merrillees proposed that a form of pottery known as base-ring juglets may have been used as opium containers due to their shape, which bears a striking resemblance to the inverted opium poppy capsule.[192] Figure 96 shows the base-ring

juglet that is the subject of the work reported in this chapter, along with an inverted poppy capsule. Base-ring juglets are characterised by their ring-shaped bases which give them their name, and they have thin walls usually with a highly polished brown coating (known as a slip). The juglets have an ovoid body and a narrow neck, with a handle from the shoulder to near the top of the neck. The juglet base is thought to reflect the stigma on the top of the capsule, and the neck the stalk. On some examples of base-ring juglets there are two rings on the neck at the point where the handle attaches, resembling the thalamus of the poppy.
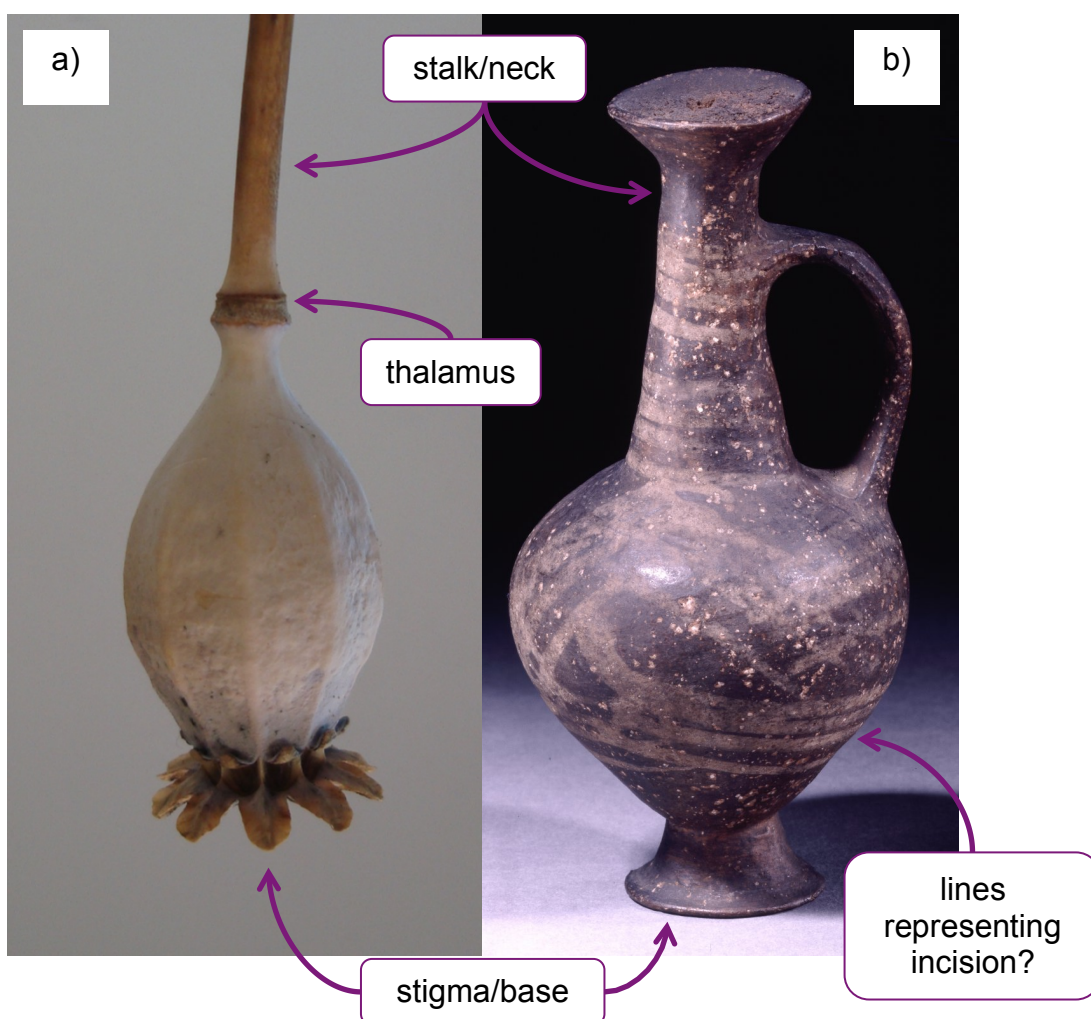
Figure 96. (a) Inverted poppy capsule compared to (b) a base-ring juglet from the British Museum collection (BM Reg. No.: 1981,1218.53, image ©Trustees of British Museum).

Base-ring juglets were produced in Cyprus and widely traded in the eastern Mediterranean in the Late Bronze Age. Merrillees' theory was that, since the vessels were imported into Egypt from Cyprus, it would be sensible for their shape to

directly represent their contents because it is unlikely that there would have been a common language between the traders and consumers. Added to this is the fact that the vessels hold only a small volume, which implies that their contents were precious and valuable.

There are two distinct types of base-ring juglet, type I and type II. Type II developed gradually from type I, with the main change being the addition of decoration in the form of parallel lines painted onto the body of the vessels. These were proposed by Merrillees to represent the score lines on the poppy head which are made to allow the latex to exude from the poppy capsule, providing further evidence for the idea that they were designed to visually represent the opium poppy because they contained opium. The example analysed in this work (Figure 96b) is a type II base-ring juglet, with the parallel lines painted on.

Due to Merrillees' hypothesis, base-ring juglets are of great interest for tracing the spread of the opium trade in the Mediterranean region during the Bronze Age. Numerous attempts have been made to detect opiates in base-ring juglet potsherds and vessels, with limited success.

Over 40 alkaloids are produced by *P. somniferum* but the five primary alkaloids are the phenanthrenes morphine, codeine and thebaine, and the benzylisoquinolines papaverine and noscapine (Figure 97).[193,194] Of these, morphine is the most abundant and is also the main source of opium's narcotic effects. This abundance makes morphine the obvious target for chemical analysis of residues in base-ring juglets, and, indeed, most previous studies have attempted to detect morphine. However, work carried out on the artificial ageing of opium, with analysis by GC-MS, has shown that morphine does not survive well, and that papaverine, thebaine and the breakdown products of noscapine (cotarnine, hydrocotarnine, meconic acid and opianic acid) are the most well preserved, making them much more likely targets for detection of opiates in base-ring juglets.[195] As well as being a breakdown product of noscapine, meconic acid is a significant component of raw opium, comprising 5% of its weight.[196] In fact, in the early part of the 20th century its presence in urine was used to identify opium smokers (tested for by adding $FeCl_3$ to the urine, which would turn red if meconic acid was present).[196]

228

Morphine   Codeine   Thebaine

Papaverine   Noscapine
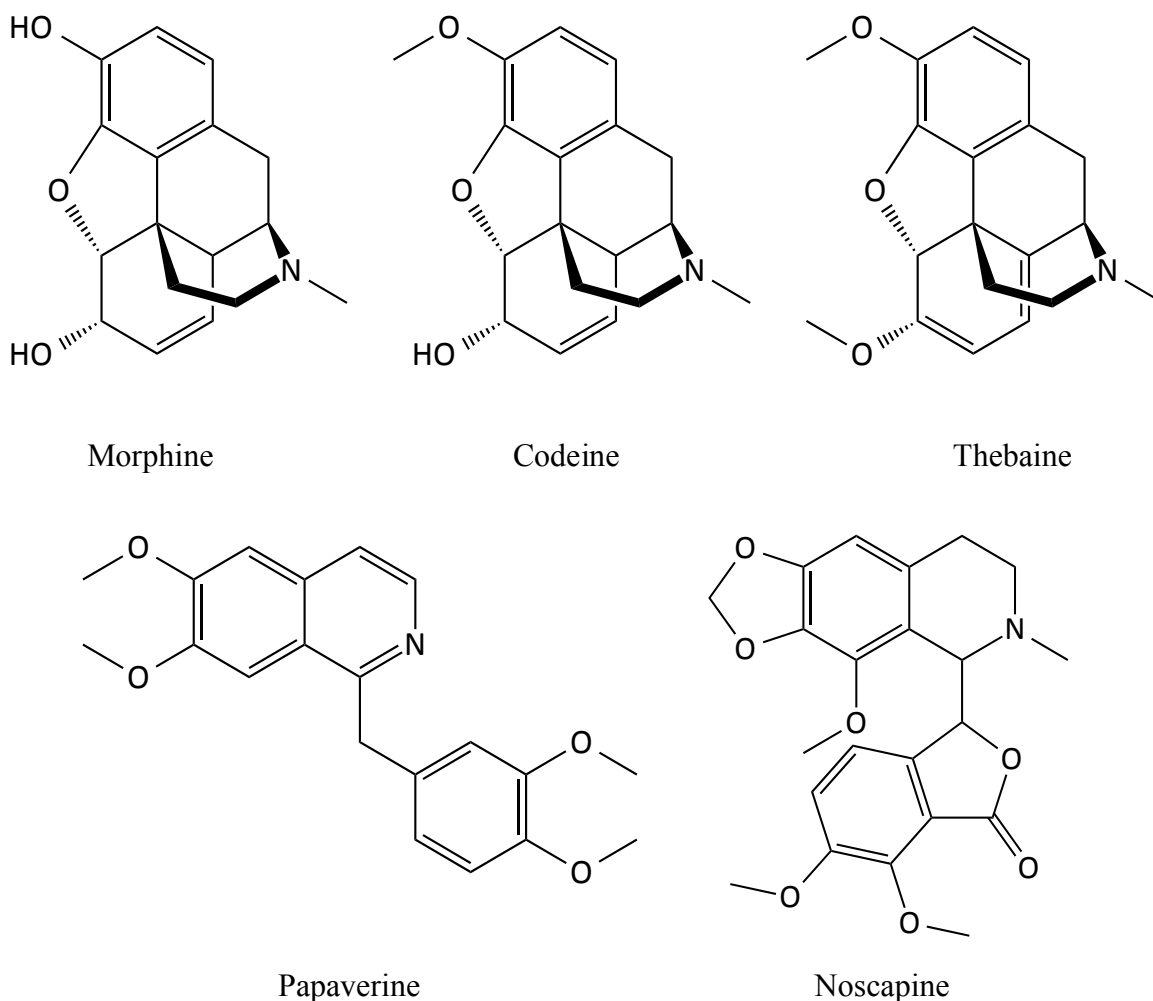
Figure 97. Structures of the five primary opium alkaloids.

The only report of a positive result for opium alkaloids in a base-ring juglet was published in 1996 and describes 'a yellowish-brown amorphic resine like residue mixed with quartz sand grains' taken from inside a base-ring juglet from Egypt. It was analysed using thin-layer chromatography (TLC) and GC-MS,[197] and immunoassay methods specific for morphine.[198] These analyses found that opium alkaloids were present in the vessel – primarily morphine, with codeine and noscapine also present. However, these results do not seem to fit with the more recently published opium artificial ageing study which indicates that morphine, codeine and noscapine are relatively unstable and unlikely to survive over long periods. In the 1996 juglet analysis paper an authentic standard for stable thebaine was available and used to determine its retention time and retention factor and the paper reports its detection in a sample of crude opium using both GC-MS and TLC. The authors also report the detection of papaverine in the crude opium sample using

TLC (though it is unclear how they were able to assign the TLC spot as papaverine), but surprisingly, given the stability of these latter two alkaloids, they do not report the detection of either in their juglet residue.

The vessel analysed in the work reported here is held in the British Museum collection and is a sealed type II base-ring juglet (BM reg. number 1981,1218.53, Figure 96b), which radiography has revealed to be partially filled with residue (Figure 98). The vessel is 14.6 cm tall. Examples of complete, sealed base-ring juglets with residue inside are extremely rare so this object provides an exceptional opportunity to study the contents of such a vessel in order to examine chemical evidence for their association with opium.

Analysis by GC-MS and pyrolysis-GC-MS (pyGC-MS) of the residue has been carried out at the museum (Rebecca Stacey, personal communication). GC-MS analysis of solvent extracts of the residue showed the bulk of the material to be degraded oil. PyGC-MS analysis was able to provide tantalising evidence that papaverine may be present, but the result was unable to be repeated and there were problems with carryover. Due to these problems, an alternative analytical method was required to determine whether papaverine really is present.

Figure 98. Radiograph of the base-ring juglet, showing the presence of residue inside. ©Trustees of British Museum.

230

7.2   AIMS

The aims of the work reported in this chapter were to develop methods for the extraction and analysis of alkaloids from the oily contents of the base-ring juglet. Based on the work carried out at the British Museum using pyGC-MS, it was thought that opium alkaloids were present in the vessel contents, so the ultimate aim of this work was to provide the first rigorous chemical evidence for a link between base-ring juglets and opium.

7.3   RESULTS AND DISCUSSION

7.3.1   Sample Appearance

The content of the vessel was a dark brown, thick, oily material. When removed from the juglet it had to be smeared on the inside of glass vials in order to transfer it from the microprobe. Figure 99 shows one such vial, with the contents. This is in contrast to the material analysed in the only other published report of opium alkaloids from a base-ring juglet, where the contents were described as 'a yellowish-brown amorphic resine like residue mixed with quartz sand grains'.[197] This implies that the material in these two vessels may not be the same. However, it is unclear from the published report whether that vessel was sealed or not. If the contents of the British Museum vessel, which was sealed, had been exposed to the air for a long period, or buried, then its texture would undoubtedly have changed.

Figure 99. Juglet contents smeared on the inside of a glass vial (vial height 3 cm).

7.3.2   Poppyseed Oil Analysis

Since analysis of the contents of the vessel by GC-MS had shown it to be primarily plant-based oil, it was necessary to produce test samples that were oil-based and to develop a method for extraction of alkaloids from the oily matrix.

Poppyseed oil was chosen as the first test sample, since the fact that the contents of the vessel had already been shown to be oil meant that it was essential to consider the possibility that it was poppyseed oil. Although Merrillees' original theory had proposed that the contents could be opium, the GC-MS results could point to it in fact being poppyseed oil rather than opium, which would still support a relationship between vessel shape and use.

The method used for extraction and purification of papaverine was modified from that published by Guo *et al*[144] for the extraction of poppy alkaloids from Chinese hot pot broth (a type of soup), and is reported in section 3.4.3. The method was chosen because it was designed for extracting alkaloids from an oily matrix, which was also the aim of the work presented here. Briefly, 0.1 M HCl was added to the samples to protonate the alkaloids, facilitating extraction into the aqueous phase. Following ultrasonication of the mixture, hexane was added and the mixture centrifuged to separate the phases, and alkaloids extracted from the aqueous phase using SPE.

Two different examples of poppyseed oil (Oshadhi and Fandler) were purchased for analysis. Both oils were analysed using SRM on the triple quadrupole MS and showed the presence of each of the four alkaloids for which standards were purchased, although the Fandler poppyseed oil had higher concentrations of all four than the Oshadhi poppyseed oil. Figure 100 shows the SRM chromatograms of each of the alkaloids in Fandler poppyseed oil.
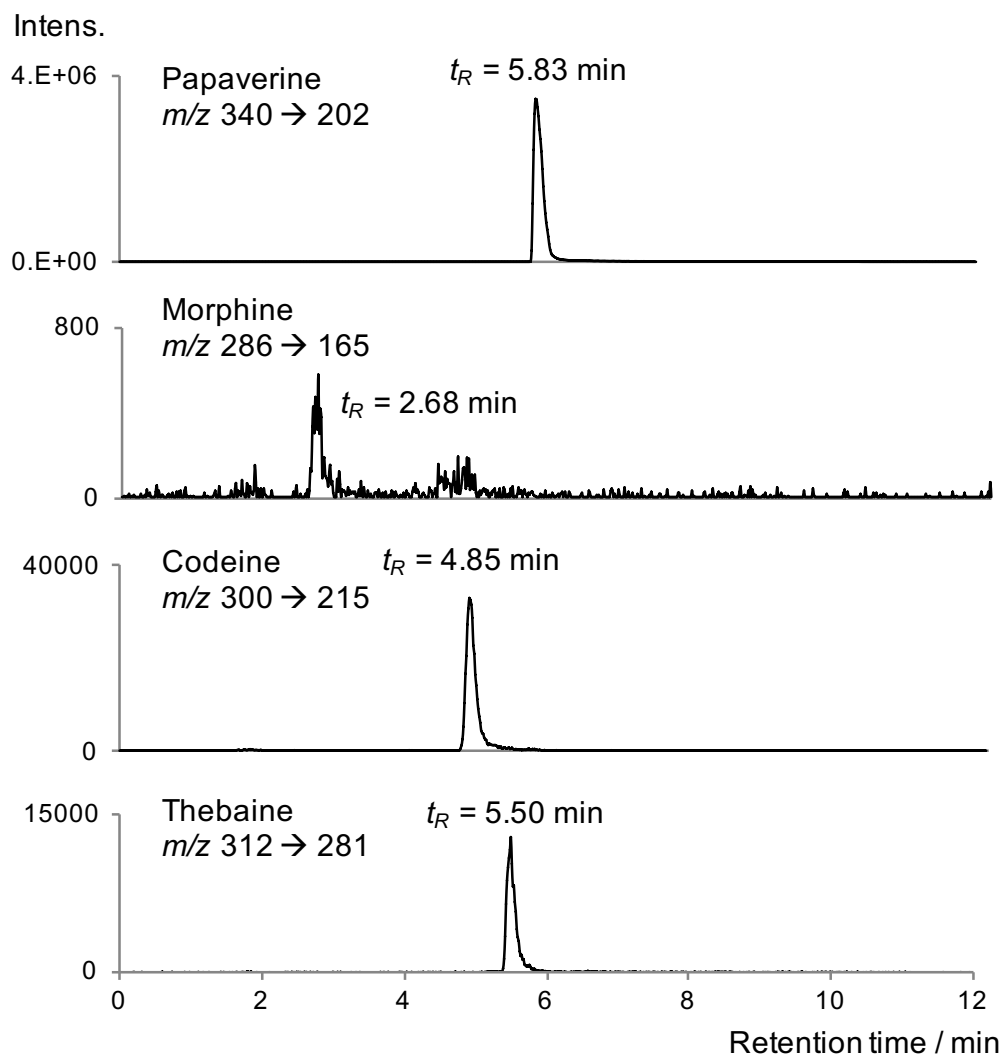
Figure 100. SRM chromatograms for each of the four alkaloids in the extract of Fandler poppyseed oil.

The extracts were also analysed using the FTICR MS in order to look for opium-related compounds for which standards could not be obtained. Extracted ion chromatograms (EICs) were produced of the *m/z* values (measured to 3 decimal places) for noscapine and its breakdown products cotarnine, hydrocotarnine, meconic acid and opianic acid, and for the four alkaloids already detected using SRM (see Table 18 for the *m/z* values). As well as peaks in the EICs for codeine, thebaine and papaverine, noscapine was detected with good S/N in both types of poppyseed oil. Morphine was not detected in either, but this is probably due to the lower sensitivity of full scan analysis on the FTICR MS compared with SRM on the triple quadrupole MS. Meconic acid was also not detected in the extracts of the oils. Cotarnine, hydrocotarnine and opianic acid were, however, detected in the Fandler

poppyseed oil, and cotarnine and hydrocotarnine were detected in the Oshadhi poppyseed oil. Figure 101 shows the EICs for noscapine, cotarnine, hydrocotarnine and opianic acid in Fandler poppyseed oil. There were two peaks for the hydrocotarnine *m/z* value, both present at low S/N compared to the other analytes.

Table 18. Formulae and $[M+H]^+$ *m/z* values for selected opium alkaloids and breakdown products.

Analyte	Formula	$[M+H]^+$ *m/z*
Meconic acid	$C_7H_4O_7$	201.003
Opianic acid	$C_{10}H_{10}O_5$	211.060
Cotarnine	$C_{12}H_{13}NO_3$	220.097
Hydrocotarnine	$C_{12}H_{15}NO_3$	222.112
Morphine	$C_{17}H_{19}NO_3$	286.144
Codeine	$C_{18}H_{21}NO_3$	300.159
Thebaine	$C_{19}H_{21}NO_3$	312.159
Papaverine	$C_{20}H_{21}NO_4$	340.154
Noscapine	$C_{22}H_{23}NO_7$	414.155
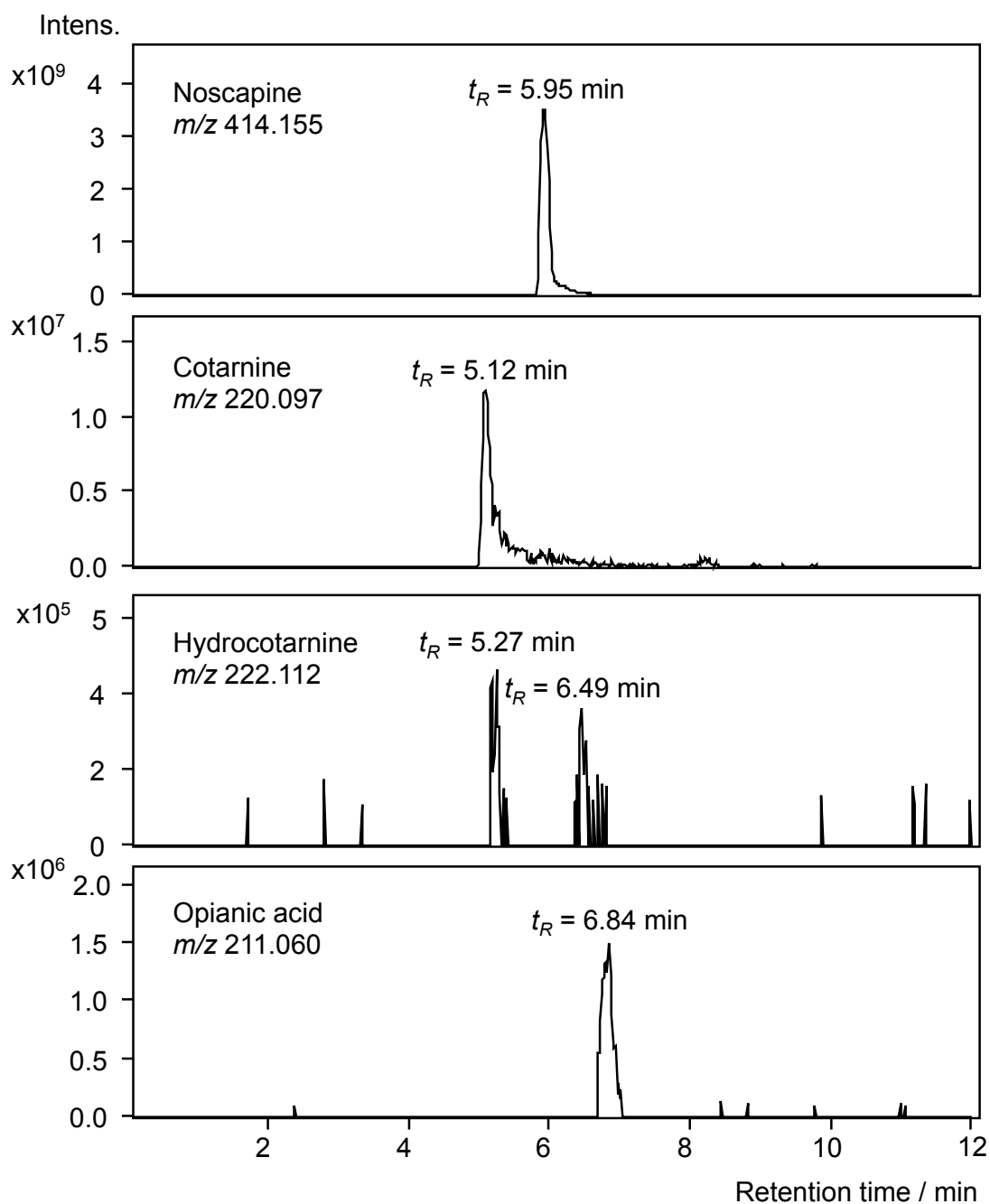
Figure 101. EICs for noscapine, cotarnine, hydrocotarnine and opianic acid analysed using HPLC-FTICR-MS.

The fact that the alkaloids were found in poppyseed oil is not a surprising result since it would be expected that poppyseed oil might contain small amounts of poppy alkaloids, though most of the alkaloids are found in the latex. Published analysis, by GC-MS, of the alkaloid content of poppy seeds gave values of between 41 μg/g and 230 μg/g for the different alkaloids in Indian poppy seeds and between 0.17 μg/g and 39 μg/g in Dutch poppy seeds.[199] No information on the alkaloid content of

poppyseed oil could be found, but since the oil is pressed from the seeds the values for the seeds give an indication of what the values in poppyseed oil might be.

The detection of opium alkaloids in poppyseed oil using this method is an encouraging finding, demonstrating that the method can be used to extract opium alkaloids successfully from fresh poppyseed oil. This is a requirement if the juglet contents are indeed poppyseed oil because there will have been some degradation in the archaeological sample, so if the method is not able to detect papaverine in fresh, undegraded oil it is very unlikely to work for an archaeological, presumably degraded sample.

7.3.3   Artificial Ageing Experiments

Fandler poppyseed oil was artificially aged with the purpose of determining what the degradation products are and to assess whether opiates can still be detected after a period of ageing, to see how viable the method is likely to be for the archaeological sample. Published work on the artificial ageing of opium alkaloids using similar ageing methods to those used here, but applied to raw opium rather than poppyseed oil, has shown that papaverine and thebaine are the most stable opium alkaloids and are therefore good targets for analysis.[195] In addition, the pyGC-MS analysis of the juglet contents carried out at the British Museum had provided tentative evidence for papaverine but no other opium alkaloids (Rebecca Stacey, personal communication).

To carry out artificial ageing of poppyseed oil, 100 µL samples of oil were prepared in different ways, sealed inside glass Kilner® jars and heated in a GC oven at 60 °C to accelerate ageing of the oil (see section 3.4.5).

Because the ageing process is likely to change the material properties of the oil, e.g. its viscosity, it was anticipated that the extraction method may need some further development in order for it to be applicable to aged samples. To test this, ten samples of poppyseed oil were aged, as pools at ambient humidity with no ceramic added, for 17 days. The samples became more viscous during the heating and could not be transferred using a pipette. In order to allow proper mixing of the sample with the acid it was necessary first to solubilise or at least suspend the samples. Three solvents were tested for this purpose: hexane, DCM and acetone. The oil samples dissolved in all three solvents, though none of them produced a completely clear

solution. However, it was possible to transfer the oil into the extraction vessel using the solvent as a carrier. After addition of the acid, the two phases mixed on ultrasonication when using all three of the solvents. For the samples in DCM or acetone, hexane was then added (as it had been for the original method for fresh poppyseed oil) and the samples were centrifuged to separate the layers. The alkaloids were extracted from the aqueous layer using SPE and analysed by HPLC-MS using the triple quadrupole MS. The samples in hexane and acetone did not give peaks corresponding to any of the alkaloids. However, the samples dissolved in dichloromethane gave peaks corresponding to papaverine. In the thebaine SRM chromatogram there was a peak at $t_R = 5.89$ min, but it was not at the correct retention time for thebaine ($t_R = 5.50$ min). Figure 102 shows the SRM chromatograms for papaverine and thebaine extracted from the aged poppyseed oil.
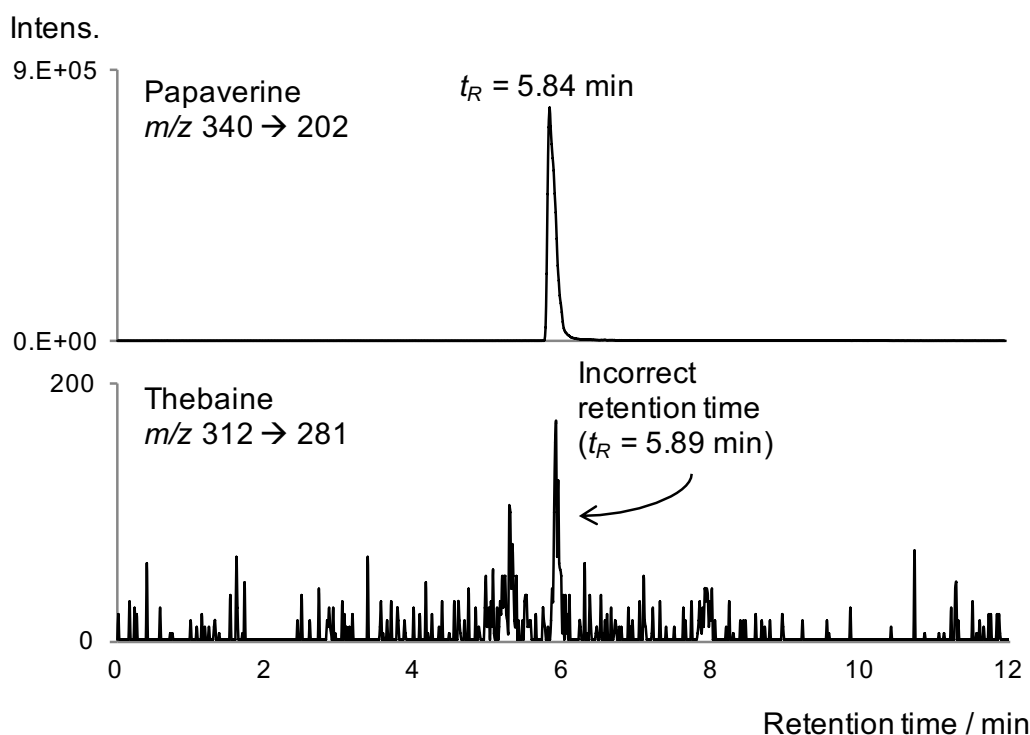
Figure 102. SRM chromatograms of papaverine and thebaine in Fandler poppyseed oil aged for 17 days at 60 °C and dissolved in DCM before extraction.

Opiates other than papaverine and thebaine were not detected in the 17 day aged samples. However, since the extraction method had been shown to be appropriate for all four of the alkaloids in fresh poppyseed oil samples, and it was known that morphine and codeine are less stable than papaverine and thebaine, it was proposed

that morphine, codeine and thebaine had degraded to the extent that they were no longer detectable rather than that they had not been extracted (despite thebaine's higher stability it will still be subject to some degradation). Therefore, while bearing in mind that the archaeological sample may behave differently compared to aged poppyseed oil, it was decided that dichloromethane was suitable for use as the carrier solvent and was employed for handling all subsequent samples.

Further poppyseed oil samples were prepared for artificial ageing in the following ways: spread out thinly on a glass slide or as a pool of oil inside an open 1 mL vial; with or without addition of crushed ceramic pot to simulate interaction with a ceramic surface, as will have been the case in the archaeological sample; in 100 % relative humidity (achieved by adding a small open vial of deionised water to the jar) or at ambient humidity. As well as the samples aged for 17 days, samples were prepared for analysis after heating for 8.5 months, 10.5 months and 11 months. In total, 16 samples were prepared (in addition to the 17 day samples) to cover various combinations of the different conditions (Table 3 in section 3.4.5). However, during the ageing experiments two of the thin layers of oil were lost by sliding off the glass slide on which they were being heated. These were the 8.5 and 10.5 month humid samples with no ceramic added, and are marked on Table 3.

During the heating, particularly for the longer heating times, the oil darkened from a pale yellow colour to amber. Its viscosity increased to the extent that it did not flow (and therefore the samples that were lost must have slid off the glass slide relatively early in the heating process). In addition, the samples with added ceramic set solid. There were consequently some difficulties in transferring the aged samples from the vials/glass slides to the extraction vials. For the pools, DCM was added to the vials to loosen the oil so that it could be removed to the extraction vials by pipetting, and the thin layers were scraped off into extraction vials before DCM was added.

After heating, morphine and codeine were not detected in any of the samples. This is, of course, not surprising, since they have already been shown to degrade under similar conditions to those used here,[195] and they were not detected in the samples which were aged for only 17 days.

Papaverine was detected in some of the samples, particularly those aged for the shorter time periods. In the 17 day samples papaverine was detected at concentrations ranging from 79 pg/mg of fresh poppyseed oil to 307 pg/mL. In the 8.5 month samples (of which the humid, thin layer sample with no ceramic added was lost by slipping off the slide during heating) the detected concentrations had reduced to between 2.2 pg/mg and 3.2 pg/mg of fresh poppyseed oil, with the conditions under which they were heated not making much difference to the amount of papaverine detected. However, after 10.5 months of heating papaverine was no longer detected in most of the samples, although the ambient humidity pools did contain detectable amounts. Some of the 11 month samples, which were all heated at ambient humidity, also contained detectable amounts of papaverine. Overall, the levels of papaverine detected were variable, probably because of difficulties in getting the samples into the extraction vials after heating. However, there did seem to be a reduction over time, as would be expected, particularly between 17 days and 8.5 months.

Thebaine was not detected in any of the aged samples, except for its tentative detection in the 17 day samples, but in each of the aged samples there was a peak (t_R = approx. 5.9 min) in the SRM chromatogram for thebaine but with the wrong retention time. This peak had very good S/N in some of the aged samples, and had the same retention time as papaverine. The peak was also observed in the archaeological sample, and is discussed in more detail below.

Analysis on the FTICR MS did not give peaks in EICs for noscapine or its breakdown products in any of the aged samples.

7.3.4 Extraction Efficiency and Limits of Detection

Although poppyseed oil was used for the artificial ageing tests, since it contains opium alkaloids, in order to test the extraction efficiency of the method it was necessary to use a matrix in which there are no opium alkaloids already present and to spike the alkaloids into it. Olive oil was extracted and analysed and, as expected, was found to contain no detectable alkaloids and was thus a suitable oily matrix for spiking experiments to test extraction efficiency.

239

7.3.4.1 Extraction Efficiency

As part of the extraction method development, the extraction efficiency was calculated. This was carried out using papaverine as the only alkaloid. Papaverine was spiked into olive oil and extracted using the method as developed. Papaverine extracted from spiked oil was analysed on the ion trap MS alongside papaverine standard dissolved directly into the injection solvent, with 5 µL injected onto the HPLC column. Papaverine spiked at 10 ng/mL (two replicates) and 5 ng/mL (one replicate) of olive oil (i.e. 50 pg and 25 pg injected onto the column) gave extraction efficiencies of 89% and 87%, respectively, using peak areas for quantification. This was deemed to be an acceptable extraction efficiency. Figure 103 shows the EICs for 10 ng/mL extracted spiked papaverine (50 pg injected), and the corresponding standard.
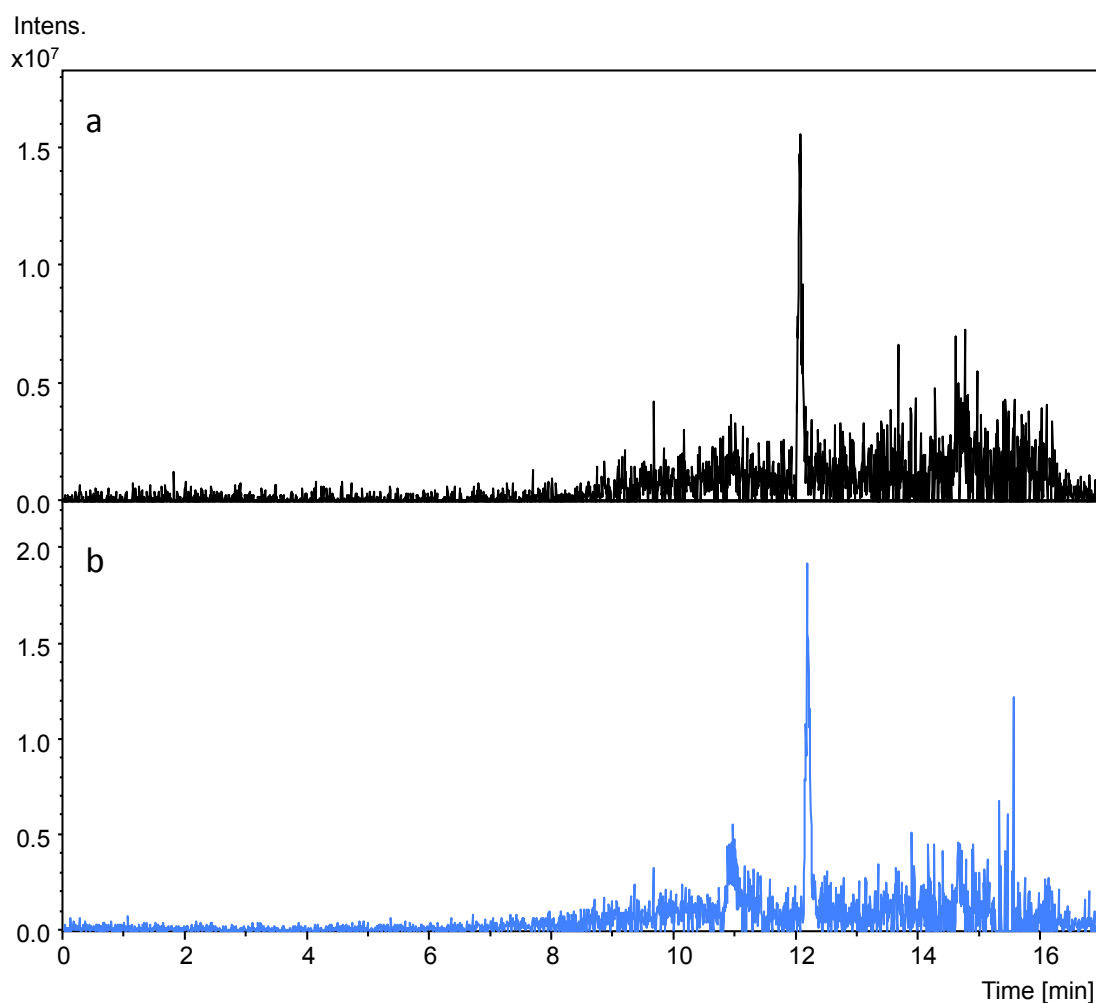
Figure 103. EICs of 50 pg papaverine. a) extracted from spiked oil; b) standard dissolved in injection solvent. Analysis was by HPLC-MS on the ion trap MS.

The method was developed on fresh olive oil, which was liquid enough to mix with the aqueous extraction solvent. However, the aged poppyseed oil and the archaeological sample were too viscous to allow mixing with the extraction solvent without using another solvent (i.e. DCM, because this was found to be the most effective solvent) for solubilisation/suspension of the very viscous samples. Extraction of aged poppyseed oil was tried without the addition of the extra solvent and no papaverine was detected. Because of the introduction of DCM into the extraction method, the extraction efficiency was calculated again. All four alkaloids were spiked into olive oil at concentrations of 5 ng/mL and 50 ng/mL each (i.e. 25 pg and 250 pg injected), in triplicate. DCM was added and the mixtures were extracted. On analysis, these gave widely varying extraction efficiencies, between almost as low as 0% and as high as 100%. Since the only difference between these extraction experiments and the first set of extraction experiments was the addition of DCM, the explanation must be that the DCM undermined the reproducibility of the extraction. This is unfortunate because it means that quantitation of the alkaloids in the archaeological sample cannot be accurately carried out (because the extraction efficiency cannot be allowed for). However, it was the only way to analyse the viscous samples, and does not at all detract from the very clear qualitative detection of the alkaloids.

7.3.4.2   Limits of Detection and Quantitation

Because of problems with carryover in the papaverine analysis (discussed later), the limits of detection and quantitation (LOD and LOQ) were determined by comparison with solvent injection blanks, according to the definition given in the IUPAC Gold Book:[200]

$$x_L = \bar{x}_{bi} + k s_{bi}$$

where:

x_L is the limit

$\bar{x}_{bi}$ is the mean of blank measures

k is the confidence level required (i.e. 3 for LOD and 10 for LOQ)

s_{bi} is the standard deviation of blank measures

Carryover meant that, when standards were analysed in order to construct a calibration plot for quantitation of papaverine, the size of the peak for papaverine in the blanks became progressively greater. The standards were injected in triplicate sets, each set starting from the lowest concentration to the highest. One or two solvent blank injections were interspersed between each standard injection and after each sequence from low to high concentration there were four injections of solvent blank. The solvent reservoir from which the blank was sampled was replaced at the start of each sequence. Because of the increase in size of the papaverine peak in the blank over the course of each set of calibration standards, the standard deviation would be artificially large if all of the blanks were used in determining the LOD and LOQ. Therefore, $\bar{x}_{bi}$ and s_{bi} for each set of calibration standards were calculated based on the peak areas of the four blank injections at the end of each set. For each blank injection (or pair of blank injections) earlier in the run, a scaled s_{bi} value was produced, based on a comparison of the peak area (or mean of a pair of peak areas) of the blank(s) with the mean of the four blanks from which the original s_{bi} was calculated. This was done as follows:

$$\text{scaled } s_{bi} = \left(\frac{\text{(mean) peak area of blank(s)}}{\text{mean peak area of final four blanks}} \right) s_{bi}$$

LODs and LOQs were calculated based on each blank's peak area (or mean of a pair of peak areas) and its associated scaled s_{bi} value; whether a standard peak area was above the limits was assessed based on the calculated values for the blank(s) immediately following it. For each of the three sequences of calibration standards, standards from 15 pg injected onto the column were all above the LOD. One of the 5 pg standards was just above the LOD and two were just below. All of the 50 pg standards were above the LOQ and two of the 15 pg standards were above the LOQ, whilst the third 15 pg standard was very slightly below the LOQ.

For thebaine, the same process was carried out. There were not the problems of carryover for thebaine that there were for papaverine, so fewer blank injections were carried out and one value of $\bar{x}_{bi}$ and one of s_{bi} were calculated for each sequence to give LOD and LOQ values. The lowest injected amount of thebaine that was above the LOD in all three standard runs was 25 pg and for LOQ it was 100 pg.

As can be seen from the analysis of a mixture of 25 pg each of papaverine, thebaine, morphine and codeine standards (Figure 104), the signal level was different for each of the analytes, with papaverine giving by far the best signal and morphine the worst. Because morphine and codeine were not quantified, their LODs have not been calculated.
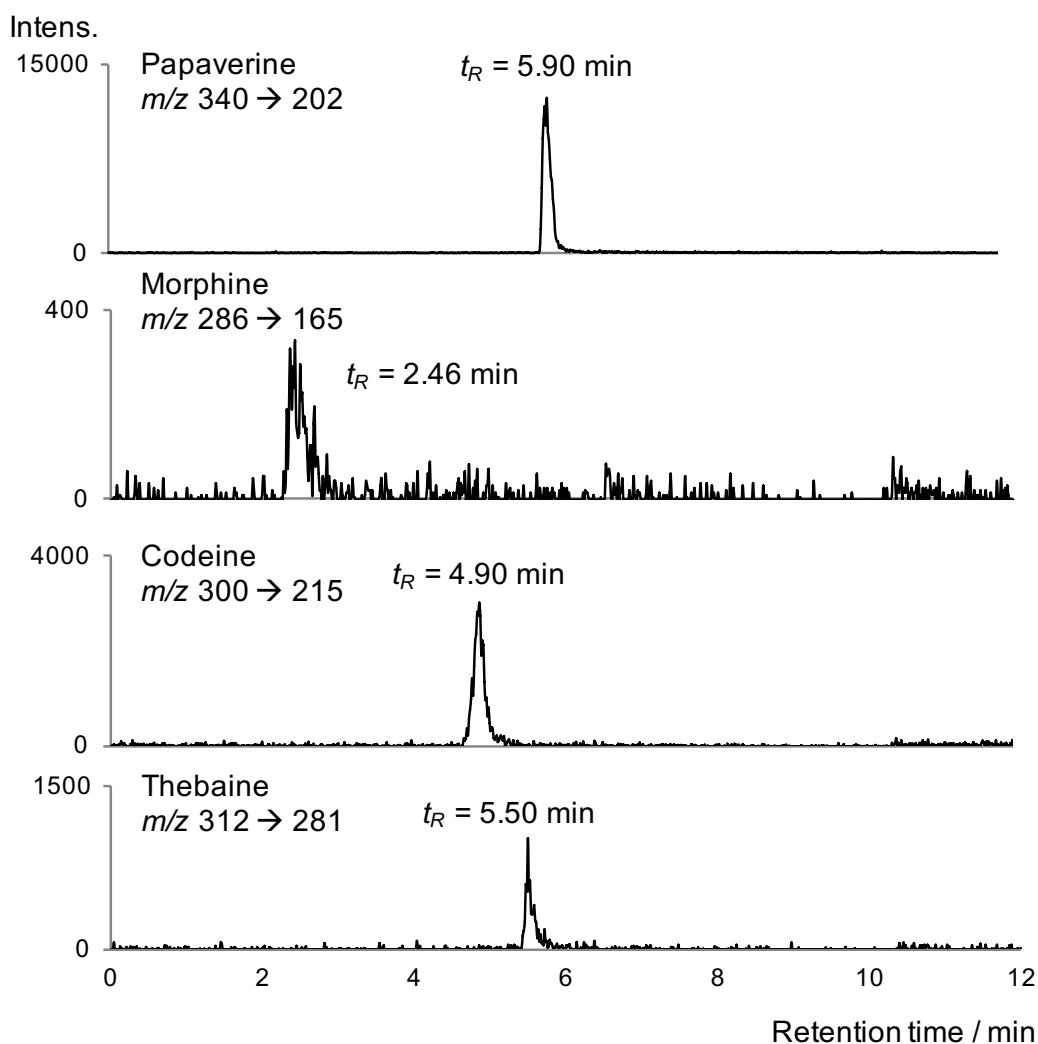
Figure 104. SRM chromatograms of 25 pg of each of the four opiate standards.

For samples, the LOD and LOQ were calculated in a similar way to those for the quantitation standards, with peak areas of blank injections carried out during the sequence used as the blank values. There was not the same problem of the blank peak area increasing in size because increasing concentrations of papaverine were not used, and the levels analysed were typically fairly low, and therefore one value of $\bar{x}_{bi}$ and one of s_{bi} were calculated for each sequence to give LOD and LOQ values.

7.3.5   Archaeological Sample

Portions of the contents of the vessel were extracted using the method developed on artificially aged poppyseed oil. Three portions of DCM were successively added to the vials containing the juglet contents to remove all of the residue and transfer it to the extraction vessel, followed by extraction and SPE. The extracts were analysed using SRM on the triple quadrupole MS and the FTICR MS to obtain full scan data.

Papaverine and thebaine were both detected in each of the portions of extract. No morphine or codeine were detected. Figure 105 shows the SRM chromatograms of papaverine and thebaine in one of the juglet portions. Papaverine concentrations in the extracts varied between 0.4 pg/mg of residue and 2.6 pg/mg (though, because of the problems with extraction efficiency, these values cannot be accurately converted into concentrations in the juglet contents). As can be seen from Figure 105, there are two peaks in the papaverine transition chromatogram and they are not fully resolved. The larger, later-eluting, peak (t_R = 5.91 min) has a retention time corresponding to that for papaverine. It is proposed that the other peak (t_R = 5.67 min) may be due to a breakdown product of one of the alkaloids, and since it has the same transition as papaverine is perhaps an isomer of papaverine. Thebaine concentrations varied between 2 pg/mg and 12 pg/mg. In addition to a peak at t_R = 5.51 min for thebaine, there was a significantly larger peak at t_R = 5.91 min observed with the same SRM transition, as can be seen in Figure 105. This was observed for each of the juglet extract portions and at the same retention time as the additional peak in the thebaine chromatogram obtained from the artificially aged samples. Like the additional peak in the papaverine chromatogram, this is proposed to be due to a breakdown product of one of the alkaloids. However, in order to check that it was not due to thebaine, standard thebaine was spiked into a portion of one of the extracts (Figure 106). This caused the peak with t_R = 5.51 to increase in size but caused no change in the size of the other peak (t_R ≈ 6 min), showing that the t_R ≈ 6 min peak is due to an analyte other than thebaine. Since the peak with t_R ≈ 6 min has the same retention time as papaverine, it could be due to an in-source fragment of papaverine. However, the product ion scan of papaverine does not give any fragments with the *m/z* values used for the thebaine transition so this seems unlikely.

244
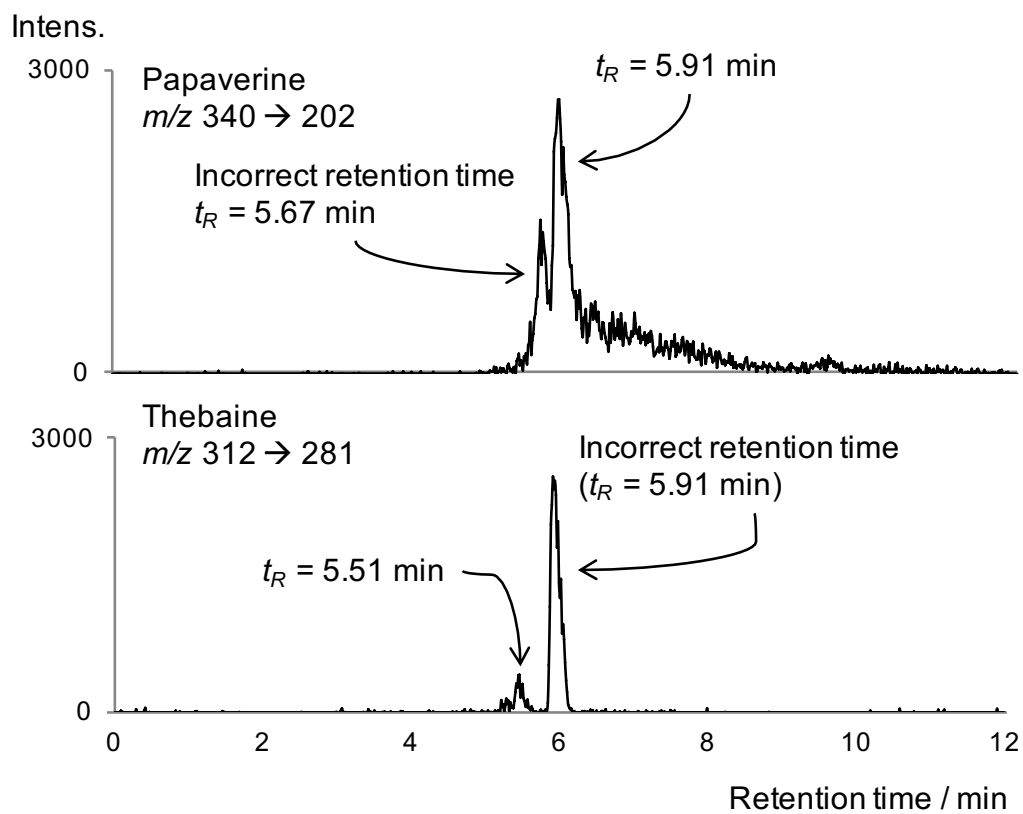
Figure 105. SRM chromatograms for papaverine and thebaine in the extract of one of the portions of juglet contents.
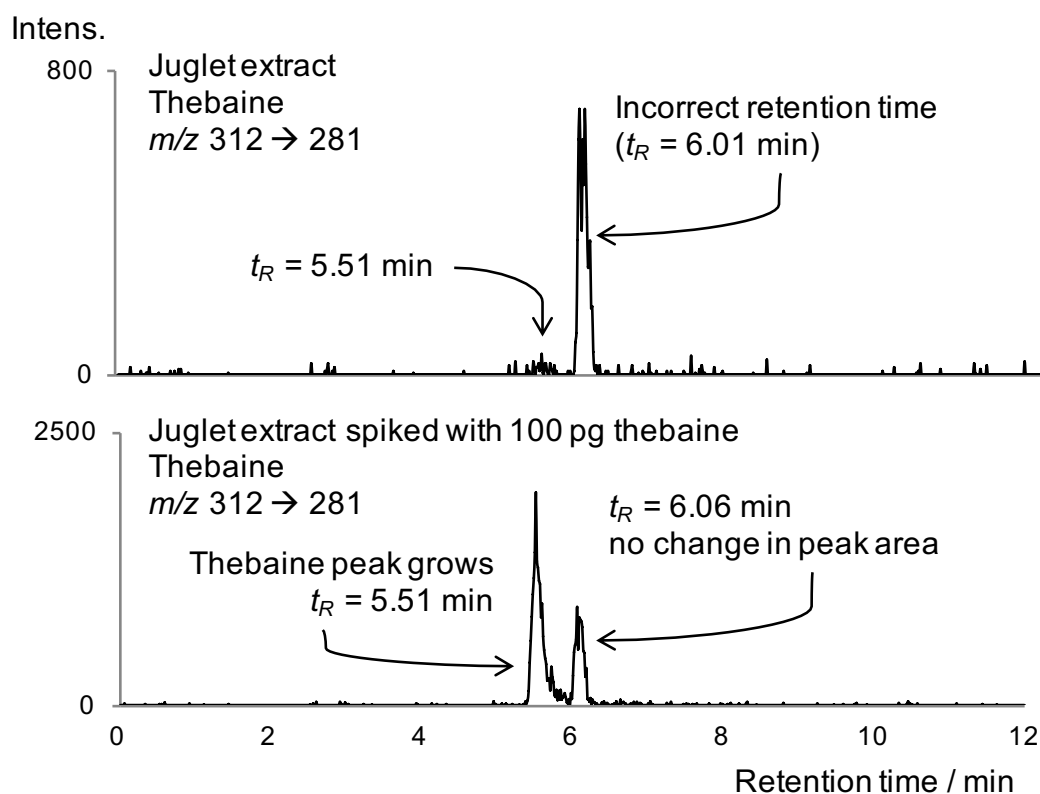
Figure 106. SRM chromatograms for the thebaine transition in the extract of one of the juglet portions and the same portion spiked with 100 pg thebaine.

The failure to detect morphine and codeine in the juglet contents extract is not unexpected, since these have been shown to be more liable to degradation than papaverine and thebaine[195] and the experiments on the artificial ageing of poppyseed presented here have shown the same results. Consequently, the detection of papaverine and thebaine in a base-ring juglet are extremely important findings.

Base-ring juglets have long been associated with the opium poppy, but this is the first rigorous demonstration of chemical evidence to support the proposed link between base-ring juglets and poppies. In contrast with previous attempts the results are fully consistent with the known ageing behaviour of opium alkaloids and the findings of earlier studies ought now to be reconsidered.

However, these results also raise further questions about the use of these vessels. For its use as a narcotic, opium would not be expected to be prepared or stored in an oil. Opium itself is the latex from the poppy capsule, and when it dries it forms a sticky residue. It is not an oil, and the GC-MS analysis has, as already discussed, shown that the bulk of the residue from the sample is oil. The usual methods for taking

246

opium as a drug are either to smoke it or to ingest it, usually dissolved in alcohol. The presence of oil could indicate that the vessel was used for poppyseed oil rather than opium. This certainly raises questions about the link between the vessel and opium, because although it could prove a link to the poppy, there is not necessarily evidence that this was through opium itself. Alternatively, it could imply that the vessel was reused in ancient times, and that the oil was a second use after the opium had been removed. Merrillees' hypothesis was partly based on the fact that the vessels were small so their contents may have been valuable, but if the contents were poppyseed oil, which was presumably less precious than opium, this sheds some doubt on that part of the argument. In addition, the fact that thebaine was observed in the fresh poppyseed oil and the archaeological sample but not in artificially aged poppyseed oil, even after a short time of ageing, implies that the source of the thebaine in the juglet contents may not be poppyseed oil. The thebaine concentrations in the juglet extracts were in fact higher than the papaverine concentrations. However, the fact that thebaine has a higher LOD than papaverine, and that the thebaine levels detected in the juglet contents are close to the LOD, means that it may be that the amounts of thebaine remaining in the aged poppyseed oils are only just below the LoD and are not much lower than that in the juglet contents.

Ideally, in order to draw general conclusions, many base-ring juglets would be sampled and analysed. However, although they were traded widely at the time of their production, there are few surviving sealed examples of them complete with contents, which is what makes the specimen at the British Museum so interesting and valuable to the debate about the use of such vessels. In the past there have been unsuccessful attempts to detect opium alkaloids in base-ring juglet potsherds, as residues absorbed in a similar way to how lipids are absorbed into cooking pots. However, alkaloids are chemically very different from lipids, being water soluble. One of the factors thought to contribute to the preservation of lipids in archaeological potsherds is their hydrophobicity, which means they are resistant to leaching by water when the potsherds are buried.[36] Since this is not the case with alkaloids they are unlikely to be preserved as absorbed residues to the same extent as lipids, which are typically detected at levels of μg per g of potsherd powder.[18] Given the findings reported here, where only ng of alkaloid per g of extracted juglet

contents were detected (notwithstanding the extraction efficiency issues), it seems indeed unlikely that alkaloids can be preserved as absorbed residues to any appreciable extent in potsherds. There is a second sealed base-ring juglet, with contents, in the British Museum collection (BM Reg. No.: 1999,0802.1) which has so far not been chemically investigated. Further work should be carried out to analyse the contents of this vessel to see if it is similar to the vessel analysed here.

7.3.6 Papaverine Analysis

The published work on artificial ageing of opium reveals that papaverine is one of the most stable opium alkaloids,[195] so it was one of the primary analytical targets for this work. There are many publications which describe HPLC-MS analysis of papaverine,[144,201,146,202] including the use of papaverine as an internal standard.[145,203] However, in the work presented here, many problems with carryover were encountered when analysing papaverine, with papaverine eluting in blanks run after samples/standards. This happened with both pyGC-MS and HPLC-MS.

PyGC-MS was the first analytical method to be applied to the contents of the vessel in an attempt to detect papaverine, and the analyte was tentatively detected in the juglet contents using this method. However, papaverine was also observed in blank runs following sample injections. For this reason, a different analytical method was sought and HPLC-MS was chosen, since it is well-reported in the literature to be an appropriately sensitive method for detecting the relevant alkaloids.

When using HPLC-MS similar problems with carryover were observed. To rule out accidental contamination of the mobile phase, the glass reservoirs were washed with 5% nitric acid solution, the lines were washed with 1% formic acid solution and, additionally, the injection system rinsed with 1% formic acid. This acidic washing regime was used with the intent to protonate any contaminating papaverine and increase its solubility in water to try to help wash it away. The mobile phase reservoirs were then rinsed three times with HPLC-MS grade solvent (each bottle being rinsed with the solvent it was to hold) and refilled with HPLC-MS grade solvent. After carrying out these measures, on injection of a solvent blank no papaverine peak was observed.

In addition to the possible contamination of the mobile phase, when the first portion of juglet contents was extracted, the extraction blank prepared alongside it also gave a peak for papaverine. The extract of the juglet contents gave a papaverine peak that had an area 18 times the size of the extraction blank peak area, so it was persuasive evidence that the juglet did contain papaverine. However, the peak area of the extraction blank was not negligible and so before further portions of juglet contents were extracted it was necessary to understand and to eradicate the problem. Great care had been taken to ensure that all glassware was clean and solvent was fresh from the bottles to rule out contamination of the solvents or glassware used for the extractions.

Importantly, there were problems with carryover when a high concentration standard was analysed, when the blanks run afterwards had significant papaverine peaks which would reduce in intensity with the injection of subsequent blanks but only to a point, after which it would not reduce any further. The problem started to occur with 1.5 ng injected onto the column and became significant with 5 ng injected, resulting in levels of papaverine in the blanks equivalent to approximately 5 pg of papaverine being injected. The high papaverine level standards were required to construct a calibration curve of the appropriate range, to allow quantitation for example of the fresh poppyseed oil. It was supposed that the papaverine may have contaminated the injection system. However, carrying out extra washes of the injection system using 1% formic acid did not solve the problem. Only after washing the glassware with 5% nitric acid and replacing the solvent was the problem solved. It is unclear how it might be possible to contaminate the solvent reservoirs during an automated sample injection series, so carryover in the analytical system seems the most credible explanation for the observations.

No published reports of the problem of contamination by and carryover of papaverine could be found. However, since during the analysis of the vessel reported in this work the problem was encountered with two different analytical methods in three different labs (work was carried out at the University of York and the British Museum as well as at the National Gallery), it seems to be a real concern for handling and measuring this analyte. Although it remains unclear exactly where the problem is occurring, it would appear that papaverine sticks to the HPLC system and

is not rinsed out fully, even at high organic mobile phase compositions. It was observed that the problem is more marked after running the HPLC system at low organic mobile phase compositions, as might be expected, and high organic compositions do remove some of the papaverine. However, it seems that when a relatively large amount of papaverine is injected it contaminates the whole system and the only way to remove the contamination is to clean all of the lines and glassware and replace the solvent.

Having encountered these problems, in order to carry out the extraction and analysis effectively and produce convincing results, it was necessary to take the utmost care to exclude cross-contamination. This involved using HPLC-MS grade solvents rather than lower grade HPLC grade solvents, and making sure the solvents used for extraction and purification were taken fresh from the bottle daily, as well as replacing the solvent blank reservoirs daily. With these measures it was possible to produce extraction blanks that were almost completely blank, giving confidence in the results obtained from the replicate aliquots of the archaeological sample that we extracted and analysed.

The difficulties with papaverine were not observed with any of the other alkaloids analysed.

7.4   CONCLUSIONS

A method for extracting opium alkaloids from oily substances has been developed and applied to poppy-related samples including fresh and artificially aged poppyseed oil and the contents of a Bronze Age Cypriot base-ring juglet. The extracts have been analysed by HPLC coupled to a triple quadrupole MS for SRM and an FTICR MS to obtain high mass resolution full scan data in order to look for alkaloids for which standards could not be obtained. The five primary opium alkaloids were detected in fresh poppyseed oil, and papaverine was detected in most of the aged samples. The archaeological sample extracts were found to contain papaverine and thebaine, at concentrations of between 0.4 pg/mg of residue and 2.6 pg/mg for papaverine and between 2 pg/mg and 12 pg/mg for thebaine (although these quantities cannot be converted to quantities in the juglet contents due to uncertainty over the extraction efficiency).

Problems with carryover were encountered when analysing papaverine, using both HPLC-MS and pyGC-MS. No other reports of this problem could be found, but since during the course of this work it was encountered with two different techniques (with two different operators in three different labs) it seem to be a fundamental problem for this analyte and should be borne in mind in future analyses.

The detection of opium alkaloids in the contents of a base-ring juglet is a very important finding, shedding light on the use of such vessels in antiquity. However, this is not the end of the story – the implications of the detection of papaverine in an oily matrix from one of these vessels is likely to prompt further debate amongst archaeologists on the purpose of these vessels and why they were traded so widely.

8 SUMMARY OF RESULTS, OVERALL CONCLUSIONS AND FURTHER WORK

The primary aim of this thesis was to develop mass spectrometric methods for the analysis of archaeological samples. This was split into two branches, the first being the development of a method to improve the detection of TAGs in lipid extracts (from food residues) from archaeological pots, and the second being the development of a method to detect opium alkaloids, as biomarkers of opium, contained in one particular object.

The method developed for TAG detection was MALDI-MS. This technique has been extensively reported in the literature as being suitable for the analysis of TAGs, but it had not been applied to archaeological lipid samples before. The rationale for its application to archaeological samples was that the conventional method used for analysis of such samples, HTGC, is not ideal for the detection of TAGs. Therefore, in archaeological studies these important constituents of lipid extracts may not always be detected even when they are present. Another consideration was that HTGC analysis is time-consuming but that not all potsherds contain detectable levels of lipid, so much analytical and instrument time is currently wasted on the analysis of samples that yield no useful information. Since TAGs are the undegraded remains of the originally deposited fats, detection of these analytes can give a measure of the overall level of preservation of the samples and indicate which samples may be suitable for HTGC analysis. MALDI-MS was chosen because it is a rapid analytical method, making it suitable as a medium-throughput screening method for TAGs in archaeological lipid extracts.

In the work described in chapter 4, a MALDI-MS method was developed using authentic lipid standards, lipid extracts of modern animal fats and lipid extracts of modern pots that had been used to cook milk and then buried for a few years. The optimised method was found to be suitable for the detection of TAGs from all three of the standard/sample types, and comparison with HTGC showed that MALDI-MS was superior to HTGC in its ability to detect TAGs. The MALDI-MS method had the added advantage that, using tandem MS, the fatty acid composition of the TAGs could be determined. Sample preparation and analysis using MALDI-MS was quicker than that using HTGC, and the spectra obtained were easily interpreted

because the identities of the TAGs could be determined simply from the *m/z* values, because TAGs were detected as sodiated molecules. In contrast, determination of TAG identity from HTGC-MS data is more time-consuming because in electron ionisation of TAGs there is generally no molecular ion peak, and so retention times obtained from authentic standards must be used in conjunction with MS data.

Chapters 5 and 6 describe the results of application of the MALDI-MS method to archaeological samples. In the work described in chapter 5, the samples were from the British Neolithic site of Durrington Walls in Wiltshire. These samples had been analysed using HTGC by another researcher but the number of samples found to contain TAGs was disappointingly low. This made them ideal candidates for testing the MALDI-MS method on archaeological samples. Using MALDI-MS, TAGs were detected in 70% of the samples, whereas only 17% had detectable TAGs on HTGC analysis, showing that the MALDI-MS method is better able to detect TAGs than HTGC.

In the work described in chapter 6, the samples were from two medieval time periods (separated by around 300 years), from the Central Asian city of Merv. These samples are particularly interesting because they are made from stone, and previous analysis had shown that, unexpectedly, these stone vessels can preserve lipid residues in a similar way to ceramic.[32] As well as being used as a set of samples on which to test the MALDI-MS method, there was a specific archaeological question: whether the lipid residues differed between the two time periods and if they did, whether this could indicate a change in the foods being cooked. Comparison of the results of MALDI-MS with those of HTGC-MS for these samples showed that MALDI-MS was better able to detect TAGs, although the difference was less marked than with the Durrington Walls samples. TAGs were detected in the same proportion of samples (47%) using both methods, though a greater range of TAGs was detected using MALDI-MS than HTGC-MS. This difference between the Durrington Walls samples and the Merv samples is likely to be due to the level of preservation. The Merv samples in general seemed to be less well preserved than the Durrington Walls samples in spite of their being more modern, and so in samples where TAGs were not detected it was because they had degraded to the extent that they were below the LOD of both methods. In the Durrington Walls samples, the general level of TAG

preservation was such that TAGs were below the LOD for HTGC but above that of MALDI-MS. This illustrates one of the important factors in archaeological analysis, that significant levels of preservation are crucial in order to be able to obtain useful data from such archaeological samples.

In terms of whether there was a difference in the lipids detected between the samples from the two Merv time periods, the most significant difference was that the lipids from the earlier time period were much less well preserved than the later samples, though the fatty acid ranges detected did not seem to vary between the two sets of samples. This could be due to a difference in cooking methods used.

For both of the sample sets (Durrington Walls and Merv) to which MALDI-MS has been applied in the studies described in this thesis, the MALDI-MS analysis was done after HTGC analysis. However, in order for MALDI-MS to be used as a screening method, it should be carried out before HTGC analysis. In both of the case studies, if TAG detection by MALDI-MS had been carried out first, it would have shown very quickly that the lipids were well preserved enough to make HTGC analysis worthwhile. Use of MALDI-MS in this way can allow a prioritisation of other resources.

MALDI-MS is already used by archaeological scientists for analysis of collagen for species identification of archaeological bone. So called zooarchaeology by Mass Spectrometry (ZooMS)[204] was developed in BioArCh at the University of York and is now used extensively, so MALDI-MS is not new to the archaeological science community. Its wider adoption for lipid analysis could help to improve throughput of these samples, and thus potentially reduce costs.

In the future, MALDI-MS could potentially be used as a screening method to direct archaeological excavations. Samples could be sent from the site during excavations and rapidly analysed to determine whether samples from different parts of the site contain better preserved lipids, and are therefore more worth spending time and resources on excavating, than samples from other parts.

MALDI-MS could also be used for more in-depth studies of TAG fatty acid composition than have been carried out in this thesis. Because the aim of the work reported here was mainly to develop the MALDI-MS method and show that it is

suitable for the analysis of archaeological samples, the amount of tandem MS carried out was limited. If MALDI-MS is used in future as an integral part of archaeological lipid analysis, tandem MS of all of the TAGs detected should be carried out, to gain a full picture of the fatty acid compositions of the preserved TAGs from all samples.

Another group of MS methods that could contribute to archaeological science are the ambient MS methods.[112] First introduced in 2004 with desorption ESI (DESI),[109] these methods allow rapid detection of analytes from a surface, with very little sample preparation and under ambient conditions. This would be ideal for the analysis of archaeological lipids, because many samples could be analysed very quickly for screening purposes. Although MALDI-MS analysis is rapid, sample preparation for ambient methods is easier because there is no need for a matrix or for the sample plate to be placed under vacuum. One can imagine spotting lipid extracts onto a multi-well plate and analysing each well to screen the samples. Various ambient methods have been reported for TAG analysis: DESI for edible oils, margarine and chocolate,[205] easy ambient sonic-spray ionisation (EASI) for oils[206] and meats[207] and direct analysis in real time (DART) for milk products.[208]

A good deal of work investigating the development of DESI and other ambient methods for archaeological lipid samples has been carried out during this PhD. However, this work did not progress as hoped, due to the difficulties of obtaining a stable signal, lack of robustness of the DESI and other experimental sources investigated, and the poor LODs, all of which made it disappointingly difficult to progress this strand of research.

It is tempting to imagine carrying out ambient MS straight from the surface of a potsherd. This would greatly increase throughput because, even with fast analytical methods, one of the most time-consuming aspects of lipid analysis from archaeological potsherds is the lipid extraction. However, because the lipids are thought to be absorbed into the ceramic material and not preserved on the surface, the aim of analysing directly from the potsherd surface may not be achievable.

The application of MALDI-MS has shown that there are established analytical methods that can contribute to archaeology. As is often the case with analytical work, MALDI-MS is complementary to other methods already in use; whereas

MALDI-MS can detect TAGs it does not detect the other lipid constituents of archaeological lipid extracts. In contrast, most of the lipid classes can be detected using HTGC, but it is not ideal for TAG detection. Therefore, the use of MALDI-MS and HTGC, along with other methods such as GC-c-IRMS and consideration of the floral and faunal assemblage excavated from a site (e.g. bone) can all be used together to gain information about the diets of people in the past.

The second branch of this thesis concerned the analysis of the contents of one archaeological vessel. This was a Cypriot base-ring juglet, which is a type of vessel produced in the Late Bronze Age and widely traded in the eastern Mediterranean at the time. They have been associated with opium due to their shape, which resembles an inverted poppy capsule. Chemical analysis supporting this association has so far been rare, partly because of the fact that examples of these vessels surviving intact with contents are extremely rare. As a result, the British Museum collection contains only two such vessels. Chapter 7 describes the development of methods to extract opium alkaloids from the contents of one of the vessels and to detect the alkaloids using HPLC-MS. This was successful, with two such alkaloids, papaverine and thebaine, being detected. These findings are extremely important because they provide the first robust chemical evidence for a link between these vessels and their use, that has so far been only supposition. There was a problem with the reproducibility of the extraction efficiency, meaning that accurate quantitation could not be carried out. Further work should be undertaken to try and solve this problem. The second vessel has yet to be analysed, but should be investigated to see if the results are similar.

List of Abbreviations

ac	Alternating current
APCI	Atmospheric pressure chemical ionisation
BSTFA	bis(trimethylsilyl)trifluoroacetamide
CHCA	α-cyano-4-hydroxycinnamic acid
CID	Collision-induced dissociation
CRM	Charged residue model
DAG	Diacylglycerol
dc	Direct current
DCM	Dichloromethane
DHB	2,5-dihydroxybenzoic acid
EI	Electron ionisation
EIC	Extracted ion chromatogram
EM	Electron multiplier (detector)
ESI	Electrospray ionisation
FA	Fatty acid
FID	Flame ionisation detection
FTICR-MS	Fourier transform ion cyclotron resonance mass spectrometry
GC	Gas chromatography
GC-c-IRMS	Gas chromatography-combustion-isotope ratio mass spectrometry
HPLC	High-performance liquid chromatography
HTGC	High-temperature gas chromatography
IEM	Ion evaporation model
ISD	In-source decay
LD	Laser desorption
LID	Laser-induced dissociation
LOD	limit of detection
MAG	Monoacylglycerol
MALDI-MS	Matrix-assisted laser desorption/ionisation mass spectrometry
MCP	Microchannel plate (detector)
MRM	Multiple reaction monitoring
MS	Mass spectrometry
NP	Normal phase
OCI	On-column injection

257

PC	Phosphatidylcholine
PCIS	Precursor ion selector
PLMS	Post lift metastable suppressor
PRN	Pottery residue number
PSD	Post-source decay
pyGC	pyrolysis-gas chromatography
r.f.	Radiofrequency
RP	Reversed phase
S/N	signal-to-noise
SPE	Solid-phase extraction
SRM	Single reaction monitoring
SWIFT	Stored waveform inverse Fourier transform
TAG	Triacylglycerol
TLE	Total lipid extract
TMS	Trimethylsilyl
UHPLC	Ultra-high performance liquid chromatography

List of References

1. P. M. Rice, *Pottery Analysis: A Sourcebook*, The University of Chicago Press, 1987.

2. M. Regert, *Mass Spectrometry Reviews*, 2011, **30**, 177– 220.

3. D. A. Skoog, D. M. West, F. J. Holler, and S. R. Crouch, *Fundamentals of Analytical Chemistry*, Thomson Brooks/Cole, 8th ed., 2004.

4. D. C. Harris, *Quantitative Chemical Analysis*, W. H. Freeman and Company, 8th ed., 2010.

5. E. J. Guthrie and D. L. Vassilaros, *Frequently Asked Questions About Chromatographic Gases: A Practical Primer*, Air Products and Chemicals, Inc., 2003.

6. M. Pollard, C. Batt, B. Stern, and S. M. M. Young, *Analytical Chemistry in Archaeology*, Cambridge University Press, 2007.

7. R. Dandeneau and E. Zerenner, *Journal of High Resolution Chromatography & Chromatography Communications*, 1979, **2**, 351–356.

8. G. W. Ewing, *Analytical Instrumentation Handbook*, Marcel Dekker, 2nd ed., 1997.

9. M. Klee, *GC Inlets: An Introduction*, Agilent Technologies, 2005.

10. G. Schomburg, H. Behlau, R. Dielmann, F. Weeke, and H. Husmann, *Journal of Chromatography*, 1977, **142**, 87–102.

11. R. P. Evershed, *Archaeometry*, 2008, **50**, 895–924.

12. T. F. M. Oudemans and J. J. Boon, *Journal of Analytical and Applied Pyrolysis*, 1991, **20**, 197–227.

13. O. E. Craig, H. Saul, A. Lucquin, Y. Nishida, K. Taché, L. Clarke, A. Thompson, D. T. Altoft, J. Uchiyama, M. Ajimoto, K. Gibbs, S. Isaksson, C. P. Heron, and P. Jordan, *Nature*, 2013, **496**, 351–354.

14. R. P. Evershed, K. Jerman, and G. Eglinton, *Nature*, 1985, **314**, 528–530.

15. B. Stern, C. Heron, L. Corr, M. Serpico, and J. Bourriau, *Archaeometry*, 2003, **45**, 457–469.

16.   A. Lucquin, R. J. March, and S. Cassen, *Journal of Archaeological Science*, 2007, **34**, 704–710.

17.   I. D. Bull, P. F. van Bergen, P. R. Poulton, and R. P. Evershed, *Organic Geochemistry*, 1998, **28**, 11–26.

18.   R. P. Evershed, *World Archaeology*, 2008, **40**, 26–47.

19.   M. I. Gurr and J. L. Harwood, *Lipid Biochemistry: An Introduction*, Chapman & Hall, 4th ed., 1991.

20.   IUPAC-IUB Commission on Biochemical Nomenclature, *Journal of Lipid Research*, 1978, **19**, 114–128.

21.   J. Condamin, F. Formenti, M. O. Metais, M. Michel, and P. Blond, *Archaeometry*, 1976, **18**, 195–201.

22.   C. Heron, R. P. Evershed, and L. J. Goad, *Journal of Archaeological Science*, 1991, **18**, 641–659.

23.   R. P. Evershed, C. Heron, and L. Goad, *The Analyst*, 1990, **115**, 1339–1342.

24.   S. Mirabaud, C. Rolando, and M. Regert, *Analytical Chemistry*, 2007, **79**, 6182–6192.

25.   O. E. Craig, V. J. Steele, A. Fischer, S. Hartz, S. H. Andersen, P. Donohoe, A. Glykou, H. Saul, D. M. Jones, E. Koch, and C. P. Heron, *Proceedings of the National Academy of Sciences*, 2011, **108**, 17910–17915.

26.   M. Patrick, A. J. de Koning, and A. B. Smith, *Archaeometry*, 1985, **27**, 231–236.

27.   K. Grob, G. Grob, and K. J. Grob, *Journal of High Resolution Chromatography & Chromatography Communications*, 1979, **2**, 31–35.

28.   K. Grob and K. J. Grob, *Journal of Chromatography*, 1978, **151**, 311–320.

29.   K. Grob and G. Grob, *Journal of High Resolution Chromatography & Chromatography Communications*, 1979, **2**, 109–117.

30.   P. P. Schmid, M. D. Müller, and W. Simon, *Journal of High Resolution Chromatography & Chromatography Communications*, 1979, **2**, 675–676.

31.   R. P. Evershed, S. N. Dudd, M. S. Copley, R. Berstan, A. W. Stott, H. R. Mottram, S. A. Buckley, and Z. Crossman, *Accounts of Chemical Research*,

2002, **35**, 660–668.

32. D. Namdar, R. J. Stacey, and S. J. Simpson, *Journal of Archaeological Science*, 2009, **36**, 2507–2516.

33. K. Kimpe, P. A. Jacobs, and M. Waelkens, *Journal of Chromatography A*, 2002, **968**, 151–160.

34. K. Grob Jr, *Journal of Chromatography*, 1979, **178**, 387–392.

35. M. Buchgraber, F. Ulberth, and E. Anklam, *Journal of Chromatography A*, 2004, **1036**, 197–203.

36. R. P. Evershed, *World Archaeology*, 1993, **25**, 74–93.

37. G. Eglinton and G. A. Logan, *Philosophical Transactions of the Royal Society of London Series B - Biological Sciences*, 1991, **333**, 315–328.

38. M. Regert, H. A. Bland, S. N. Dudd, P. F. van Bergen, and R. P. Evershed, *Proceedings of the Royal Society B - Biological Sciences*, 1998, **265**, 2027–2032.

39. R. P. Evershed, C. Heron, and L. J. Goad, *Antiquity*, 1991, **65**, 540–544.

40. S. Charters, R. P. Evershed, A. Quye, P. W. Blinkhorn, and V. Reeves, *Journal of Archaeological Science*, 1997, **24**, 1–7.

41. R. P. Evershed, K. I. Arnot, J. Collister, G. Eglinton, and S. Charters, *The Analyst*, 1994, **119**, 909–914.

42. R. P. Evershed, S. N. Dudd, S. Charters, H. R. Mottram, A. W. Stott, A. Raven, P. F. van Bergen, and H. A. Bland, *Philosophical Transactions of the Royal Society B - Biological Sciences*, 1999, **354**, 19–31.

43. R. P. Evershed, A. W. Stott, A. Raven, S. N. Dudd, S. Charters, and A. Leyden, *Tetrahedron Letters*, 1995, **36**, 8875–8878.

44. F. A. Hansel, M. S. Copley, L. A. S. Madureira, and R. P. Evershed, *Tetrahedron Letters*, 2004, **45**, 2999–3002.

45. M. S. Copley, F. A. Hansel, K. Sadr, and R. P. Evershed, *South African Journal of Science*, 2004, **100**, 279–283.

46. O. E. Craig, M. Forster, S. H. Andersen, E. Koch, P. Crombé, N. J. Milner, B. Stern, G. N. Bailey, and C. P. Heron, *Archaeometry*, 2007, **1**, 135–152.

47. R. G. Ackman and S. N. Hooper, *Comparative Biochemistry and Physiology*, 1968, **24**, 549–565.

48. S. Passi, S. Cataudella, P. di Marco, F. de Simone, and L. Rastrelli, *Journal of Agricultural and Food Chemistry*, 2002, **50**, 7314–7322.

49. J. Matikainen, S. Kaltia, M. Ala-Peijari, N. Petit-Gras, K. Harju, J. Heikkilä, R. Yksjärvi, and T. Hase, *Tetrahedron*, 2003, **59**, 567–573.

50. R. P. Evershed, M. S. Copley, L. Dickson, and F. A. Hansel, *Archaeometry*, 2008, **50**, 101–113.

51. B. Hjulström, S. Isaksson, and C. Karlsson, *Acta Archaeologica*, 2008, **79**, 62–78.

52. I. A. Simpson, P. F. van Bergen, V. Perret, M. M. Elhmmali, D. J. Roberts, and R. P. Evershed, *The Holocene*, 1999, **9**, 223–230.

53. B. Hjulström and S. Isaksson, *Journal of Archaeological Science*, 2009, **36**, 174–183.

54. N. Robinson, R. P. Evershed, W. J. Higgs, K. Jerman, and G. Eglinton, *The Analyst*, 1987, **112**, 637–644.

55. S. Charters, R. P. Evershed, L. J. Goad, C. Heron, and P. W. Blinkhorn, *Archaeometry*, 1993, **35**, 91–101.

56. M. Regert, N. Garnier, O. Decavallas, C. Cren-Olivé, and C. Rolando, *Measurement Science and Technology*, 2003, **14**, 1620–1630.

57. A. P. Tulloch, *Chemistry and Physics of Lipids*, 1971, **6**, 235–265.

58. S. B. Hawthorne and D. J. Miller, *Journal of Chromatography*, 1987, **388**, 397–409.

59. C. Heron, N. Nemcek, K. M. Bonfield, D. Dixon, and B. S. Ottaway, *Naturwissenschaften*, 1994, **81**, 266–269.

60. R. J. Stacey, *Analytical and Bioanalytical Chemistry*, 2011, **401**, 1749–1759.

61. R. P. Evershed and S. N. Dudd, *Journal of Archaeological Science*, 2003, **30**, 1–12.

62. S. Charters, R. P. Evershed, P. W. Blinkhorn, and V. Denham, *Archaeometry*, 1995, **37**, 113–127.

63. T. Coultate and J. Davies, *Food: The Chemistry of its Components*, The Royal Society of Chemistry, 4th ed., 2002.

64. S. N. Dudd, M. Regert, and R. P. Evershed, *Organic Geochemistry*, 1998, **29**, 1345–1354.

65. S. N. Dudd and R. P. Evershed, *Science*, 1998, **282**, 1478–1481.

66. R. P. Evershed, H. R. Mottram, S. N. Dudd, S. Charters, A. W. Stott, G. J. Lawrence, A. M. Gibson, A. Conner, P. W. Blinkhorn, and V. Reeves, *Naturwissenschaften*, 1997, **84**, 402–406.

67. W. W. Christie, *Progress in Lipid Research*, 1978, **17**, 111–205.

68. S. N. Dudd, R. P. Evershed, and A. Gibson, *Journal of Archaeological Science*, 1999, **26**, 1473–1482.

69. M. Salque, P. I. Bogucki, J. Pyzel, I. Sobkowiak-Tabaka, R. Grygiel, M. Szmyt, and R. P. Evershed, *Nature*, 2013, **493**, 522–525.

70. R. G. Vernon, *Progress in Lipid Research*, 1980, **19**, 23–106.

71. J. H. Moore and W. W. Christie, *Progress in Lipid Research*, 1979, **17**, 347–395.

72. O. E. Craig, R. B. Allen, A. Thompson, R. E. Stevens, V. J. Steele, and C. Heron, *Rapid Communications in Mass Spectrometry*, 2012, **26**, 2359–2364.

73. R. P. Evershed, S. N. Dudd, M. S. Copley, and A. J. Mukherjee, *Documenta Praehistorica*, 2002, **29**, 73–96.

74. D. E. Matthews and J. M. Hayes, *Analytical Chemistry*, 1978, **50**, 1465–1473.

75. K. Freeman, J. Hayes, J. Trendel, and P. Albrecht, *Nature*, 1990, **343**, 254–256.

76. M. S. Copley, R. Berstan, S. N. Dudd, G. Docherty, A. J. Mukherjee, V. Straker, S. Payne, and R. P. Evershed, *Proceedings of the National Academy of Sciences*, 2003, **100**, 1524–1529.

77. S. Woodbury, R. P. Evershed, J. B. Rossell, R. E. Griffith, and P. Farnell, *Analytical Chemistry*, 1995, **67**, 2685–2690.

78. A. J. Mukherjee, M. S. Copley, R. Berstan, K. A. Clark, and R. P. Evershed, in *The Zooarchaeology of Fats, Oils, Milk and Dairying*, eds. J. Mulville and

A. K. Outram, Oxbow Books, 2005, pp. 77–93.

79. S. Passi, M. C. Rothschild-Boros, P. Fasella, M. Nazzaro-Porro, and D. Whitehouse, *Journal of Lipid Research*, 1981, **22**, 778–784.

80. H. R. Mottram and R. P. Evershed, *Tetrahedron Letters*, 1996, **37**, 8593–8596.

81. H. R. Mottram, S. E. Woodbury, and R. P. Evershed, *Rapid Communications in Mass Spectrometry*, 1997, **11**, 1240–1252.

82. H. R. Mottram and R. P. Evershed, *Journal of Chromatography A*, 2001, **926**, 239–253.

83. H. R. Mottram, Z. M. Crossman, and R. P. Evershed, *The Analyst*, 2001, **126**, 1018–1024.

84. K. Kimpe, P. A. Jacobs, and M. Waelkens, *Journal of Chromatography A*, 2001, **937**, 87–95.

85. K. Kimpe, C. Drybooms, E. Schrevens, P. A. Jacobs, R. Degeest, and M. Waelkens, *Journal of Archaeological Science*, 2004, **31**, 1503–1510.

86. K. Romanus, J. Poblome, K. Verbeke, A. Luypaerts, P. Jacobs, D. de Vos, and M. Waelkens, *Archaeometry*, 2007, **49**, 729–747.

87. F. Saliu, I. Degano, and M. P. Colombini, *Journal of Chromatography A*, 2014, **1346**, 78–87.

88. E. de Hoffman and V. Stroobant, *Mass Spectrometry: Principles and Applications*, John Wiley & Sons Ltd., 3rd ed., 2007.

89. K. R. Jennings, *International Journal of Mass Spectrometry and Ion Physics*, 1968, **1**, 227–235.

90. A. J. Dempster, *Physical Review*, 1918, **11**, 316–325.

91. M. Karas, D. Bachmann, and F. Hillenkamp, *Analytical Chemistry*, 1985, **57**, 2935–2939.

92. M. Karas, D. Bachmann, U. Bahr, and F. Hillenkamp, *International Journal of Mass Spectrometry and Ion Processes*, 1987, **78**, 53–68.

93. M. Karas and F. Hillenkamp, *Analytical Chemistry*, 1988, **60**, 2299–2301.

94. K. Tanaka, H. Waki, Y. Ido, S. Akita, Y. Yoshida, and T. Yoshida, *Rapid*

Communications in Mass Spectrometry, 1988, **2**, 151–153.

95. K. Dreisewerd, *Chemical Reviews*, 2003, **103**, 395–425.

96. M. Karas and R. Krüger, *Chemical Reviews*, 2003, **103**, 427–439.

97. R. W. Garden and J. V. Sweedler, *Analytical Chemistry*, 2000, **72**, 30–36.

98. S. L. Cohen and B. T. Chait, *Analytical Chemistry*, 1996, **68**, 31–37.

99. M. Kussmann, E. Nordhoff, H. Rahbek-Nielsen, S. Haebel, M. Rossel-Larsen, L. Jakobsen, J. Gobom, E. Mirgorodskaya, A. Kroll-Kristensen, L. Palm, and P. Roepstorff, *Journal of Mass Spectrometry*, 1997, **32**, 593–601.

100. Y. Dai, R. M. Whittal, and L. Li, *Analytical Chemistry*, 1999, **71**, 1087–1091.

101. A. Walch, S. Rauser, S. O. Deininger, and H. Höfler, *Histochemistry and Cell Biology*, 2008, **130**, 421–434.

102. D. S. Cornett, M. L. Reyzer, P. Chaurand, and R. M. Caprioli, *Nature Methods*, 2007, **4**, 828–833.

103. S. J. Gabriel, C. Schwarzinger, B. Schwarzinger, U. Panne, and S. M. Weidner, *Journal of the American Society for Mass Spectrometry*, 2014, **25**, 1356–1363.

104. S. Abdul Rahman, E. Bergström, C. J. Watson, K. M. Wilson, D. A. Ashford, J. R. Thomas, D. Ungar, and J. E. Thomas-Oates, *Journal of Proteome Research*, 2014, **13**, 1167–1176.

105. M. Dole, L. L. Mack, R. L. Hines, R. C. Mobley, L. D. Ferguson, and M. B. Alice, *Journal of Chemical Physics*, 1968, **49**, 2240–2249.

106. M. Yamashita and J. B. Fenn, *Journal of Physical Chemistry*, 1984, **88**, 4451–4459.

107. J. B. Fenn, M. Mann, C. K. Meng, S. F. Wong, and C. M. Whitehouse, *Science*, 1989, **246**, 64–71.

108. J. V. Iribarne and B. A. Thomson, *Journal of Chemical Physics*, 1976, **64**, 2287–2294.

109. Z. Takáts, J. M. Wiseman, B. Gologan, and R. G. Cooks, *Science*, 2004, **306**, 471–473.

110. Z. Takáts, J. M. Wiseman, and R. G. Cooks, *Journal of Mass Spectrometry*,

2005, **40**, 1261–1275.

111. A. Venter, M. Nefliu, and R. G. Cooks, *Trends in Analytical Chemistry*, 2008, **27**, 284–290.

112. G. A. Harris, A. S. Galhena, and F. M. Fernández, *Analytical Chemistry*, 2011, **83**, 4508–4538.

113. W. Paul, *Reviews of Modern Physics*, 1990, **62**, 531–540.

114. R. E. March, *International Journal of Mass Spectrometry*, 2000, **200**, 285–312.

115. R. E. March, *Journal of Mass Spectrometry*, 1997, **32**, 351–369.

116. K. R. Jonscher and J. R. Yates, *Analytical Biochemistry*, 1997, **244**, 1–15.

117. G. C. Stafford Jr., P. E. Kelley, J. E. P. Syka, W. E. Reynolds, and J. F. J. Todd, *International Journal of Mass Spectrometry and Ion Processes*, 1984, **60**, 85–98.

118. M. Nappi, C. Weil, C. D. Cleven, L. A. Horn, H. Wollnik, and R. G. Cooks, *International Journal of Mass Spectrometry and Ion Processes*, 1997, **161**, 77–85.

119. R. E. Kaiser, R. G. Cooks, G. C. Stafford Jr., J. E. P. Syka, and P. H. Hemberger, *International Journal of Mass Spectrometry and Ion Processes*, 1991, **106**, 79–115.

120. J. N. Louris, J. S. Brodbelt-Lustig, R. G. Cooks, G. L. Glish, G. J. van Berkel, and S. A. McLuckey, *International Journal of Mass Spectrometry and Ion Processes*, 1990, **96**, 117–137.

121. M. H. Soni and R. G. Cooks, *Analytical Chemistry*, 1994, **66**, 2488–2496.

122. J. N. Louris, R. G. Cooks, J. E. P. Syka, P. E. Kelley, G. C. Stafford Jr., and J. F. J. Todd, *Analytical Chemistry*, 1987, **59**, 1677–1685.

123. E. Mathieson and T. J. Harris, *American Journal of Physics*, 1969, **37**, 1054–1059.

124. W. E. Stephens, *Physical Review*, 1946, **69**, 691–691.

125. W. C. Wiley and I. H. McLaren, *Review of Scientific Instruments*, 1955, **26**, 1150–1157.

126. R. J. Cotter, *Analytical Chemistry*, 1999, **71**, 445A–451A.

127. M. Guilhaus, *Journal of Mass Spectrometry*, 1995, **30**, 1519– 1532.

128. B. A. Mamyrin, V. I. Karataev, D. V Shmikk, and V. A. Zagulin, *Soviet Physics - JETP*, 1973, **37**, 45–48.

129. R. S. Brown and J. J. Lennon, *Analytical Chemistry*, 1995, **67**, 1998–2003.

130. R. M. Whittal and L. Li, *Analytical Chemistry*, 1995, **67**, 1950–1954.

131. R. S. Brown and J. J. Lennon, *Analytical Chemistry*, 1995, **67**, 3990–3999.

132. R. Kaufmann, D. Kirsch, and B. Spengler, *International Journal of Mass Spectrometry and Ion Processes*, 1994, **131**, 355–385.

133. *ultraflex III User Manual*, Bruker Daltonik GmbH, 2006.

134. D. Suckau, A. Resemann, M. Schuerenberg, P. Hufnagel, J. Franzen, and A. Holle, *Analytical and Bioanalytical Chemistry*, 2003, **376**, 952–965.

135. M. B. Comisarow and A. G. Marshall, *Chemical Physics Letters*, 1974, **25**, 282–283.

136. M. B. Comisarow and A. G. Marshall, *Chemical Physics Letters*, 1974, **26**, 489–490.

137. A. G. Marshall, C. L. Hendrickson, and G. S. Jackson, *Mass Spectrometry Reviews*, 1998, **17**, 1–35.

138. I. J. Amster, *Journal of Mass Spectrometry*, 1996, **31**, 1325–1337.

139. G. R. Asbury, K. Al-Saad, W. F. Siems, R. M. Hannan, and H. H. Hill, *Journal of the American Society for Mass Spectrometry*, 1999, **10**, 983–991.

140. F. O. Ayorinde, B. E. Eribo, K. V. Balan, J. H. Johnson Jr., and L. W. Wan, *Rapid Communications in Mass Spectrometry*, 1999, **13**, 937–942.

141. J. S. Garcia, G. B. Sanvido, S. A. Saraiva, J. J. Zacca, R. G. Cosso, and M. N. Eberlin, *Food Chemistry*, 2012, **131**, 722–726.

142. G. Picariello, R. Sacchi, and F. Addeo, *European Journal of Lipid Science and Technology*, 2007, **109**, 511–524.

143. O. E. Craig, L.-M. Shillito, U. Albarella, S. Viner-Daniels, B. Chan, R. Cleal, R. Ixer, M. Jay, P. Marshall, E. Simmons, E. Wright, and M. Parker Pearson,

Antiquity, 2015, **89**, 1096–1109.

144. Q. Guo, J. Zhang, S. Zhao, and B. Shao, *Food Analytical Methods*, 2012, **6**, 698–704.

145. P. Gu, Y. Ding, D. Sun, T. Hang, W. Liu, and L. Ding, *Biomedical Chromatography*, 2010, **24**, 420–425.

146. K. Taylor and S. Elliott, *Forensic Science International*, 2009, **187**, 34–41.

147. E. L. Øiestad, U. Johansen, Å. M. L. Øiestad, and A. S. Christophersen, *Journal of Analytical Toxicology*, 2011, **35**, 280–293.

148. T. Berg, E. Lundanes, A. S. Christophersen, and D. H. Strand, *Journal of Chromatography B*, 2009, **877**, 421–432.

149. E. Gustavsson, M. Andersson, N. Stephanson, and O. Beck, *Journal of Mass Spectrometry*, 2007, **42**, 881–889.

150. H.-R. Lin, C.-C. Liao, and T.-C. Lin, *Rapid Communications in Mass Spectrometry*, 2014, **28**, 2043–2053.

151. P. Mareš, *Progress in Lipid Research*, 1988, **27**, 107–133.

152. *Bruker Guide to MALDI Sample Preparation*, Bruker Daltonik GmbH, Revision 2., 2012.

153. C. H. Le, J. Han, and C. H. Borchers, *Analytical Chemistry*, 2012, **84**, 8391–8398.

154. F. O. Ayorinde, K. Garvin, and K. Saeed, *Rapid Communications in Mass Spectrometry*, 2000, **14**, 608–615.

155. H. Yu, E. Lopez, S. W. Young, J. Luo, H. Tian, and P. Cao, *Analytical Biochemistry*, 2006, **354**, 182–191.

156. J. Schiller, R. Süß, M. Petković, and K. Arnold, *Journal of Food Lipids*, 2002, **9**, 185–200.

157. B. Fuchs, R. Süß, and J. Schiller, *Progress in Lipid Research*, 2010, **49**, 450–475.

158. R. Shroff, A. Muck, and A. Svatoš, *Rapid Communications in Mass Spectrometry*, 2007, **21**, 3295–3300.

159. S. Benard, J. Arnhold, M. Lehnert, J. Schiller, and K. Arnold, *Chemistry and*

Physics of Lipids, 1999, **100**, 115–125.

160. S. Vichi, A. Lazzez, N. Grati-Kamoun, and J. Caixach, *LWT - Food Science and Technology*, 2012, **48**, 24–29.

161. E. Pittenauer and G. Allmaier, *Journal of the American Society for Mass Spectrometry*, 2009, **20**, 1037–1047.

162. C. Debono Spiteri, *PhD Thesis, University of York*, 2012.

163. B. Emerson, J. Gidden, J. O. Lay Jr., and B. Durham, *Journal of Lipid Research*, 2010, **51**, 2428–2434.

164. H. Brockerhoff, *Comparative Biochemistry and Physiology*, 1966, **19**, 1–12.

165. F. Guyon, C. Absalon, A. Eloy, M. H. Salagoity, M. Esclapez, and B. Medina, *Rapid Communications in Mass Spectrometry*, 2003, **17**, 2317–2322.

166. W. C. Breckenridge and A. Kuksis, *Journal of Lipid Research*, 1967, **8**, 473–478.

167. H. Devle, I. Vetti, C. F. Naess-Andresen, E. O. Rukke, G. Vegarud, and D. Ekeberg, *European Journal of Lipid Science and Technology*, 2012, **114**, 1036–1043.

168. M. Parker Pearson, J. Pollard, C. Richards, J. Thomas, C. Tilley, and K. Welham, *Documenta Praehistorica*, 2008, **35**, 153–166.

169. M. Parker Pearson, R. Cleal, P. Marshall, S. Needham, J. Pollard, C. Richards, C. Ruggles, A. Sheridan, J. Thomas, and C. Tilley, *Antiquity*, 2007, **81**, 617–639.

170. G. J. Wainwright, *Antiquity*, 1968, **42**, 20–26.

171. O. G. S. Crawford, *Antiquity*, 1929, **3**, 49–59.

172. S. Piggott, *Antiquity*, 1959, **33**, 289–290.

173. H. Case, in *Bell Beakers Today: Pottery, People, Culture, Symbols in Prehistoric Europe*, ed. F. Nicolis, Provincia Autonoma di Trento, Servizio Beni Culturali, Ufficio Beni Archeologici, 2001, pp. 361–377.

174. T. Darvill, P. Marshall, M. Parker Pearson, and G. Wainwright, *Antiquity*, 2012, **86**, 1021 – 1040.

175. M. Parker Pearson and Ramilisonina, *Antiquity*, 1998, **72**, 308–326.

176. U. Albarella and D. Serjeantson, in *Consuming Patterns and Patterns of Consumption*, eds. P. Miracle and N. Milner, McDonald Institute for Archaeological Research, 2002, pp. 33–49.

177. R. Cleal and A. MacSween, *Grooved Ware in Britain and Ireland*, Oxbow Books, 1999.

178. A. J. Mukherjee, A. M. Gibson, and R. P. Evershed, *Journal of Archaeological Science*, 2008, **35**, 2059–2073.

179. S. J. Simpson, *Institute for Archaeo-Metallurgical Studies*, 2001, **21**, 14–15.

180. G. Herrmann and K. Kurbansakhatov, *Iran*, 1994, **32**, 53–75.

181. S. J. Simpson, in *The Turkmen Land as a Centre of Ancient Cultures and Civilizations: Materials of the International Scientific Conference*, Ashgabat: Ministry of Culture, 2008, pp. 247–255.

182. G. Herrmann, V. M. Masson, and K. Kurbansakhatov, *Iran*, 1993, **31**, 39–62.

183. T. Williams, in *Cities in the Pre-Modern Islamic World: The Urban Impact of Religion, State and Society*, eds. A. K. Bennison and A. L. Gascoigne, Routledge, 2007, pp. 42–62.

184. G. Herrmann, K. Kurbansakhatov, and S. J. Simpson, *Iran*, 1997, **35**, 1–33.

185. G. Herrmann, K. Kurbansakhatov, and S. J. Simpson, *Iran*, 1998, **36**, 53–75.

186. G. Herrmann and K. Kurbansakhatov, *Iran*, 1995, **33**, 31–60.

187. W. Bouschen and B. Spengler, *International Journal of Mass Spectrometry*, 2007, **266**, 129–137.

188. H. Qiao, G. Piyadasa, V. Spicer, and W. Ens, *International Journal of Mass Spectrometry*, 2009, **281**, 41–51.

189. S. Charters, R. P. Evershed, L. J. Goad, A. Leyden, P. W. Blinkhorn, and V. Denham, *Archaeometry*, 1993, **35**, 211–223.

190. M. Merlin, *Economic Botany*, 2003, **57**, 295–323.

191. M. Julyan and M. Dircksen, *Akroterion*, 2011, **56**, 75–90.

192. R. Merrillees, *Antiquity*, 1962, **36**, 287–292.

193. A. Dittbrenner, H. Mock, A. Borner, and U. Lohwasser, *Journal of Applied*

Botany and Food Quality, 2009, **82**, 103–107.

194. T. Reisine and G. Pasternak, in *Goodman & Gilman's The Pharmacological Basis of of Therapeutics*, eds. L. S. Goodman, A. Gilman, and J. G. Hardman, McGraw Hill, 9th ed., 1995, pp. 521–555.

195. Z. Chovanec, S. Rafferty, and S. Swiny, *Ethnoarchaeology*, 2012, **4**, 5–36.

196. S. Lovell, P. Subramony, and B. Kahr, *Journal of the American Chemical Society*, 1999, **121**, 7020–7025.

197. K. Koschel, *Egypt and the Levant*, 1996, **6**, 159–166.

198. N. G. Bisset, J. G. Bruhn, and M. H. Zenk, *Egypt and the Levant*, 1996, **6**, 203–204.

199. B. Paul, C. Dreka, E. Knight, and M. Smith, *Planta Medica*, 1996, **62**, 544–547.

200. *IUPAC. Compendium of Chemical Terminology, 2nd ed. (the 'Gold Book')*, Blackwell Scientific Publications, Oxford (1997). XML on-line corrected version: http://goldbook.iupac.org (2006-) created by M. Nic, J. Jirat, B. Kosata; updates compiled by A. Jenkins. ISBN 0-9678550-9-8. doi:10.1351/goldbook.

201. Z. Peng, W. Song, F. Han, H. Chen, M. Zhu, and Y. Chen, *International Journal of Mass Spectrometry*, 2007, **266**, 114–121.

202. R. Kikura-Hanajiri, N. Kaniwa, M. Ishibashi, Y. Makino, and S. Kojima, *Journal of Chromatography B*, 2003, **789**, 139–150.

203. C. R. Mallet, J. R. Mazzeo, and U. Neue, *Rapid Communications in Mass Spectrometry*, 2001, **15**, 1075–1083.

204. M. Buckley, S. Whitcher Kansa, S. Howard, S. Campbell, J. Thomas-Oates, and M. Collins, *Journal of Archaeological Science*, 2010, **37**, 13–20.

205. S. Gerbig and Z. Takáts, *Rapid Communications in Mass Spectrometry*, 2010, **24**, 2186–2192.

206. K. C. Cardoso, M. J. Da Silva, R. Grimaldi, M. Stahl, R. C. Simas, I. B. S. Cunha, M. N. Eberlin, and R. M. Alberici, *Journal of the American Oil Chemists' Society*, 2011, **89**, 67–71.

207. A. M. Porcari, N. V. Schwab, R. M. Alberici, E. C. Cabral, D. R. de Moraes, P. F. Montanher, C. R. Ferreira, M. N. Eberlin, and J. V. Visentainer, *Analytical Methods*, 2012, **4**, 3551–3557.

208. V. Hrbek, L. Vaclavik, O. Elich, and J. Hajslova, *Food Control*, 2014, **36**, 138–145.